UNIVERSIDADE DE LISBOA
FACULDADE DE CIÊNCIAS

Atmospheric circulation and climate of the Euro-Atlantic sector since 1685 based on new directional flow indices

" Documento Definitivo"

Doutoramento em Ciências Geofísicas e da Geoinformação
Especialidade de Meteorologia

Javier Mellado-Cano

Tese orientada por:
Dr. Ricardo Machado Trigo
Dr. David Barriopedro

Documento especialmente elaborado para a obtenção do grau de doutor

2019

UNIVERSIDADE DE LISBOA
FACULDADE DE CIÊNCIAS

Ciências
ULisboa

Atmospheric circulation and climate of the Euro-Atlantic sector since 1685 based on new directional flow indices

Doutoramento em Ciências Geofísicas e da Geoinformaçao

Especialidade de Meteorologia

Javier Mellado-Cano

Tese orientada por:

Dr. Ricardo Machado Trigo

Dr. David Barriopedro

Júri:

Presidente:

- João Manuel de Almeida Serra, Professor catedrático e Presidente do Departamento de Engenharia Geográfica, Geofísica e Energía da Faculdade de Ciências da Universidade de Lisboa

Vogais:

- Doutor David Barriopedro Cepero, Research Scientist do Instituto de Geociencias da Universidad Complutense de Madrid, Espanha
- Doutor José Manuel Vaquero Mártinez, Professor Titular do Centro Universitario de Mérida da Universidad de Extremadura, Espanha
- Doutor David Gallego Puyol, Professor Titular da Facultad de Ciencias Experimentales da Universidad Pablo de Olavide, Sevilha.
- Doutor Pedro Miguel Ribeiro Sousa, Investigador Pós Doutoramento no Instituto Dom Luiz da Universidade de Lisboa

Documento especialmente elaborado para a obtenção do grau de doutor

Trabalho Financiado pela Fundação para a Ciência e a Tecnologia (PD/BD/106028/2014)

2019

Acknowledgements

I would like to thank all people involved in this thesis.

First of all, I would like to acknowledge Dr. Ricardo Machado Trigo for giving me the opportunity to live this adventure in Lisbon and write this PhD thesis in the University of Lisbon. He was always a supporting supervisor of this thesis and a great leader of the Climate variability and Climate Change Group at Instituto Dom Luiz.

A good deal of the research themes in this work is due to Dr. David Barriopedro. He was first the advisor of my master and now also PhD thesis. Thank you for all the critical examinations, discussions, corrections and endless things that are impossible to express in words. Today I am finishing a PhD thanks to everything you have taught me. You have always been, and you will always be a scientific' model for me.

In fact, the person who started this adventure was Ricardo Garcia-Herrera. Among many things, he showed me that I have to believe in my results and that all the results can always be put in a sexier way. Thank you for your experience and support throughout this long ride.

A special thanks goes to the STREAM group, although throughout this process I have never been an official part of it, unofficially you made me feel like part of this big family. I would also like to express my gratitude to the Climate change, atmosphere-land-ocean processes and extremes group from IDL that accommodated me during these years. A little part of this adventure took place in Germany; I would like to thank the Climatology, Climate Dynamics and Climate Change group from the University of Giessen, in particular Professor Jürg Luterbacher, for opening the doors of their castle and give me the opportunity to live and work for some months in Giessen.

I am especially grateful to the *Oompa Loompas* (Antonio, Fernando, Froila, Jose and Maddalen) at the 220 office, for their friendly shoulder when I needed it. Big thanks goes to my PhD colleagues Rodrigo and Ana. Living in a foreign country, far for home, is not always easy. In my case, you are the people who have made Lisbon a home for me. Very special thanks goes to my friends near and far. They know who they are, and I am very thankful for all your time and support.

I would have not gotten this far if it was not for my family. During this long journey many of you have passed away, although you never understood very well what I was doing so far from you. I know that wherever you are, you are proud of me as much as I am of being your grandson and nephew. You will live as much as my memories do.

The greatest of the thanks to my sister and parents for all their love, support and distraction. All three of you are my idols. I have become who I am thanks to you.

Last but not least, my most sincere thanks goes to the serendipity of this journey. Esther, you observed and lived this ride of emotions with me, thanks for giving me the peace and balance that I need. Thank you for believing in me and for seeing always the best part of me. You are and you will always be a source of inspiration to me, without you I would not have made it.

Abstract

Knowledge of atmospheric circulation beyond the mid-18th century is hampered by the scarcity of instrumental records, particularly over the Ocean. In this regard, wind direction observations kept in ships' logbooks are a consolidated but underexploited instrumental source of climatic information.

In this Thesis we present four monthly indices of wind persistence, one for each cardinal direction, based on daily wind direction observations taken aboard ships over the English Channel. These Directional Indices (DIs) are the longest observational record of atmospheric circulation to date, covering the 1685-2014 period. DIs anomalies are associated with near-surface climatic signals over large areas of Europe in all seasons, being excellent benchmarks for proxy calibrations.

DIs series are dominated by large interannual-to-interdecadal variability and provide all year-round observational evidences of atmospheric circulation responses to external forcings (tropical volcanic eruptions) or the role of the atmospheric circulation in anomalous periods such as the Late Maunder Minimum (LMM, 1675-1715). In both cases, the results emphasize complex patterns that are more heterogeneous than previously thought, with contrasting spatial signals in both circulation and temperature.

When considered together, DIs explain a considerable amount of European climate variability, improving that accounted for by single modes of variability. This allows us to yield the longest instrumental-based series of the winter North Atlantic Oscillation (NAO) and East Atlantic (EA). The results highlight the role of EA in shaping the North Atlantic action centers and the NAO's European climate responses. Transitions in the NAO/EA phase space have been recurrent and explain non-stationary NAO signatures and anomalous periods. NAO and EA have additive effects on the jet speed but opposite impacts on the jet latitude, allowing us to derive the first instrumental reconstruction of the North Atlantic eddy-driven jet stream for the last three centuries.

Keywords: Ships' logbooks, Euro-Atlantic atmospheric circulation, North Atlantic Oscillation, Jet Stream, Past European Climate.

Resumo

O conhecimento relativo à circulação atmosférica antes de meados do século XIX está condicionado pela escassez de registos instrumentais, em particular sobre os oceanos. Os diários de bordo de navios representam uma fonte privilegiada de observações meteorológicas sobre os oceanos e mares relativamente a este período pré-instrumental. Em particular, os registros de direção do vento são uma fonte consolidada, mas sub-explorada, de informação climática homogénea, medida com uma bússola ao longo de vários séculos. Algumas regiões com intensa actividade marítima, como o Canal da Mancha (English Channel) podem proporcionar observações contínuas relativamente às condições atmosféricas em áreas estratégicas, nomeadamente as latitudes médias do oceano Atlântico, desempenhando um papel importante na definição das condições climáticas da Europa.

Nesta tese apresenta-se uma metodologia robusta de forma a obter quatro índices mensais de persistência do vento, um para cada direção cardinal: Norte, Este, Sul e Oeste, baseados em observações diárias de direção do vento registadas em embarcações que navegavam o Canal da Mancha. Até à data, estes índices direcionais representam o registo observacional mais longo da circulação atmosférica, cobrindo o período 1685-2014. As anomalias destes índices refletem sinais climáticos sobre áreas extensas da Europa em todas as estações do ano. Em geral, valores anómalos dos índices zonais (de Oeste e Leste) e meridionais (de Norte e de Sul) afetam diferentes regiões da Europa. Os sinais de precipitação são fortemente controlados pela advecção da humidade, principalmente influída pelos índices zonais, e apresentam uma resposta robusta e coerente ao longo do ano. De maneira distinta, a resposta espacial da temperatura é explicada pela advecção da temperatura e processos radiativos. Consequentemente, o sinal de temperatura associado aos índices zonais inverte durante o verão.

Modelos estatísticos que incluam como preditores todos os índices direcionais são capazes de explicar uma boa fração da variabilidade climática europeia, melhorando em muitos casos aqueles baseados apenas na Oscilação do Atlântico Norte (NAO, *North Atlantic Oscillation)*. Alem disso, os índices direcionais mostram potencial para constringir a resposta da circulação atmosférica a forçamentos externos e as anomalias climáticas associadas. Em particular, são fornecidas evidências instrumentais de sinais de circulação atmosférica ao longo de todo o ano na sequência de fortes erupções vulcânicas tropicais ocorridas nos últimos três séculos.

Estas respostas sugerem que o testemunhado aquecimento invernal, bem como o arrefecimento do verão depois de uma erupção, podem ser detetados com vários meses de antecedência.

O início dos registos utilizados neste trabalho (1685-1715) coincide com as últimas décadas do Mínimo de Maunder (ca., 1645-1715), um dos períodos mais frios na Europa que persistiu por várias décadas. Uma análise baseada nos índices direcionais demonstrou que a circulação de inverno foi a que mais contribuiu para as condições generalizadas de frio que caracterizaram as três últimas décadas desse período. No entanto, o período na Europa foi mais heterogéneo do que anteriormente se pensava, exibindo padrões espaciais contrastantes tanto na circulação atmosférica como nas anomalias do campo da temperatura e uma considerável variabilidade decadal. Em particular, é demonstrado um aumento dos ventos de Norte na primeira metade do período (1685-1700) que favoreceram invernos mais frios, enquanto na segunda metade (1700-1715) a predominância dos ventos de Sul contribuíram para condições mais amenas.

Os índices direcionais permitiram a obtenção de um novo e completo catálogo com as características dinâmicas de todos os invernos para o período 1685-1715. Neste contexto, a temperatura inferida a partir da circulação atmosférica confirma a maioria dos invernos extremamente frios bem testemunhados na literatura existente para este período. No entanto esta análise cuidada também permitiu revelar outros invernos bastante frios mas pouco descritos como tal na literatura, bem como uma quantidade substancial de invernos amenos que passaram desapercebidos até agora. Os resultados sugerem uma não estacionariadade do padrão da NAO dentro do período considerado (1685-1715) explicando as discrepâncias entre o comportamento extremo ou ameno, em termos de temperatura, de alguns dos invernos.

Outro resultado central deste trabalho foi a possibilidade de, com base nos índices direcionais, construir a mais longa reconstrução observacional dos dois modos principais de variabilidade atmosférica no inverno no setor Euro-Atlântico, isto é da *North Atlantic Oscillation* (NAO) e o da *East Atlantic pattern* (EA). A identificação de tipologias de invernos através de combinações da NAO e da EA durante o século XX sublinham o papel da EA na alteração de centros de ação no Atlântico Norte e na influência que exerce nas respostas climáticas da NAO. A modulação do impacto climático da NAO, em função da fase e intensidade da EA, é verificada de uma forma mais intensa no campo da precipitação do que no da temperatura, afetando de forma significativa áreas extensas com respostas fortes à NAO, tais como a Gronelândia e algumas regiões no Mediterrâneo. Isto impede o uso de relações simplistas

estabelecidas entre *proxies* naturais da NAO provenientes da Gronelândia, Ibéria, Balcãs ou Turquia.

Além disso, os resultados para o século XX indicam que a NAO e a EA têm um sinal forte na corrente de jato do Atlântico Norte: a NAO e a EA têm efeitos aditivos na velocidade do jato, sendo maior o sinal da NAO, e efeitos opostos comparavelmente importantes na latitude preferencial do jato. Portanto, as maiores anomalias na velocidade do jato tendem a ocorrer em invernos com fases de igual fase para ambos os modos, enquanto as maiores divergências na latitude do jato ocorrem em invernos com fases opostas. Estas relações recentes são exploradas para reconstruir a evolução das principais características do jato ao longo dos três últimos séculos. Os resultados mostram uma variabilidade substancial na corrente de jato do Atlântico Norte tanto à escala inter-anual como à escala inter-decadal, fornecendo novas evidências das dinâmicas por detrás de alguns períodos anómalos. Esta variabilidade asocia-se a períodos dominados por combinações específicas da NAO e a EA. Transições entre diferentes combinações de fase de ambos os modos têm sido recorrentes e explicam as assinaturas não-estacionárias da NAO, tal como o deslocamento dos seus centros de ação no final do século XX e também algumas divergências observadas entre índices históricos da NAO.

Em resumo, este conjunto de resultados promissores evidenciam o valor acrescido dos índices direcionais construídos através de registros instrumentais de bordo de embarcações. No contexto de trabalho futuro, a sua natureza instrumental, elevada resolução temporal e origem marítima faz com que sejam uma excelente referência para compreender a variabilidade da circulação atmosférica e melhorar reconstruções atuais do clima europeu nos últimos séculos.

Palavras-chave: Diários de bordo de embarcações, circulação atmosférica Euro-Atlântica, North Atlantic Oscillation, Corrente de jato, Clima Europeu passado.

Contents

List of Acronyms and Abbreviations

20CR	20th century: the Twenty Century Reanalysis
AH	Azores High
ASM	Australian Summer Monsoon
BARCAST	Bayesian Algorithm for Reconstructing Climate Anomalies in Space and Time
CET	Central England Temperature
CLIWOC	Climatological Database for the World's Oceans
CMIP	Coupled Model Intercomparison Project
CMIP5	Coupled Model Intercomparison Project (phase 5)
CPC	Climate Prediction Center
CRU	Climate Research Unit
DIs	Directional Indices
DJF	December, January, February
EA	East Atlantic pattern
ECMWF	European Centre for Medium Range Weather Forecast
EI	Easterly Index
GPCC	Global Precipitation Climatology Center
HadISST	Hadley Centre Global Sea Ice and Sea Surface
HLUK	Historical Logbooks from United Kingdom
ICOADS	International Comprehensive Ocean-Atmosphere Data set
IL	Iceland Low
INCITE	Instrumental Climatic Indexes Application to the study of the monsoon Mediterranean Teleconnection
ISM	Indian Summer Monsoon
ISPD	International Surface Pressure Databank
IVMFC	Vertically Integrated Moisture Flux Convergence
JJA	June, July, August
LIA	Little Ice Age
LMM	Late Maunder Minimum
MAM	March, April, May
MCA	Medieval Climate Anomaly
MM	Maunder Minimum
MSE	Mean Squared Errors

MSEC	Mean Squared Errors of Climatology
MSSS	Mean-Squared Skill Score
NAO	North Atlantic Oscillation
NCAR	National Center for Atmospheric Research
NCEP	National Centers for Environmental Prediction
NGDC	National Geophysical Data Center
NI	Northerly Index
NOAA	National Oceanic and Atmospheric Administration
NWI	Northerly Wind Index
RECLAIM	RECovery of Logbooks And International Marine data
RMSD	Root Mean Square Difference
SCA	Scandinavian pattern
SEA	Superposed Epoch Analyses
SI	Southerly Index
SLP	Sea Level Pressure
SNAO	High-summer North Atlantic Oscillation
SON	September, October, November
SRM	Stepwise Regression Model
SVD	Singular Value Decomposition
VEI	Volcanic Explosivity Index
WAM	West African Monsoon
WI	Westerly Index
WI	Westerly Index
WNPDI	Western North Pacific Directional Index
WNPSM	Western North Pacific Summer Monsoon

List of Figures

List of Tables

Chapter 1

1. Introduction

1.1 Climate variability and change

Current climate conditions can be viewed as the result of different processes interacting at a wide range of timescales under certain boundary conditions. Climate variability arises from internal dynamics and feedbacks in the climate system (Delworth and Zeng, 2012) or as a response to changes in natural or anthropogenic external forcings (Otterå et al. 2010; Myhre et al. 2013). External forcings include natural (e.g., volcanic eruptions, solar variability) and anthropogenic (e.g., changing concentrations of greenhouse gases, land cover and use changes produced by human activities, etc.) factors. Regarding the atmospheric circulation, much of its variations are related to internal mechanisms, but there is growing evidence of a role of external forcings (Fischer et al. 2007; Woollings and Blackburn, 2012; Mbengue and Schneider, 2013; Barnes and Polvani, 2013; Xu et al. 2018).

In the context of the ongoing climate change, the forced responses in some parts of the climate system, particularly the atmospheric circulation, are complex and characterized by non-additive effects that result from a combination of feedbacks and non-linear processes (Cubasch et al. 2013). This complexity contributes to the large uncertainty in the climate change projections of atmospheric circulation among models from the CMIP (Coupled Model Intercomparison Project), particularly on regional scales (Shepherd 2014). The detection and attribution of climate change signals is further complicated by the fact that the forced responses often project onto the internal modes of atmospheric variability (Gillet and Fyfe, 2013). Another source of uncertainty arises from the non-robust response of the models (Flato et al. 2013) to the same external forcings (Figure 1.1). For example, regional circulation changes to a CO_2 doubling perturbation depend on the parametrized orographic wave drag (Sigmond and Scinocca, 2010) or the simulated changes in the stratospheric circulation (Manzini et al. 2014). The considerable spread of climate change projections for the end of the 21st century under a given scenario is partly due to model-dependent projections in the degree of upper-troposphere tropical warming and lower-troposphere Arctic warming, which have competing effects on the atmospheric circulation (Woollings and Blackburn, 2012;

Francis and Vavrus, 2012; Barnes and Polvani, 2013; Zappa and Shepherd, 2017; Peings et al., 2018).

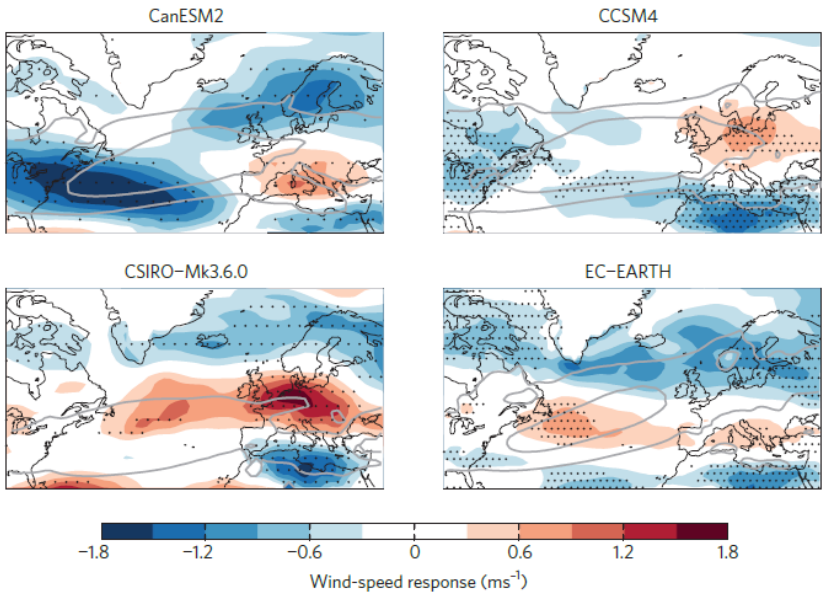

Figure 1.1. Non-robustness of the predicted circulation response to climate change. Lower tropospheric (850 hPa) wintertime zonal wind speed (grey contours, 5 ms−1 spacing) over the North Atlantic, and the predicted response to climate change over the twenty-first century under the Representative Concentration Pathway 8.5 scenario (color shading), from four different CMIP5 models, averaged over five members from each model ensemble. Stippling (density is proportional to grid spacing) indicates regions where the climate change response is significant at the 95% level based on the five ensemble members. From Shepherd 2014

On near-term horizons (middle of the 21st century), internal climate variability is the dominant source of uncertainty in the simulated climate response of atmospheric circulation, accounting for more than half of the inter-model spread (Deser et al. 2012). Internal variability occurs at a variety of time scales (from daily to at least multidecadal time scales), some of which are poorly characterized due to the short observational record and the transient influence of anthropogenic signals in the industrial era (Masson-Delmotte et al. 2013). Thus, an extension of the instrumental record back to periods when the footprint of the anthropogenic forcing is negligible is required to better constrain the range of internal variability, characterize the forced responses and overall understand the climate system. This backward extension allows studying the climate system on a wide range of time scales and puts present and future climate change in a better context, helping to disentangle natural and anthropogenic forcing signals and potentially improving the predictions of future climate change (Marcos and Amores, 2014; Allen et al. 2018).

1.2 Past climate beyond the industrial period

There are several approaches to study past climate beyond the industrial period, such as the analysis of indirect (proxy) sources of climate information, the use of climate models or the recovery of historical records found in different kinds of documents. Despite their different advantages and caveats all of these approaches can help to expand the knowledge gained from instrumental records alone to multidecadal and longer time-scales (Jones et al., 2009; Masson-Delmotte et al., 2013).

Proxy records (mostly natural archives) testimony past climate conditions in very different ways (biological, chemical, physical processes), being able to record climate-related phenomena (e.g., Jones et al. 2001; Mann 2002; Jones and Mann; 2004; Figure 1.2). These data are used in statistical models that are calibrated with instrumental data to provide estimates of the past evolution of a particular climatic variable of interest (e.g., Mann et al. 2007). They may extend back continuously from the present, or provide discrete windows of the past, shedding light on climate conditions in earlier times (Hughes et al. 2011; Michel et al. 2019). Some proxy indicators, including most sediment cores, low accumulation ice cores, and preserved pollen, have low (decadal to centennial) resolution, sometimes even impeding validation against instrumental data (Mann 2002; Jones et al. 2009). Therefore, high-resolution reconstructions are often based on specific climate records such as growth and density from tree rings, corals or historical documents that can describe past climate fluctuations on interannual timescales (Moberg et al. 2005; Crowley and Unterman, 2013; Morrill et al. 2013; Pages 2k consortium 2013). Despite their potential to provide useful past climate information, multi-proxy reconstructions present different problems (McShane and Wyner, 2011): 1) merging proxies from different sources and areas contributes to larger uncertainties and noise (e.g., Li et al. 2010); 2) it is not always clear the spatial (local or regional) and temporal (seasonal or annual means) representativeness of the proxy signal (e.g., Neuwirth et al. 2007; Neukom et al. 2018); 3) quite often proxies reflect the influence of more than one meteorological variable, making the interpretation difficult (e.g., Mann et al. 2005; McShane and Wyner, 2011); 4) due to non-linear and non-stationary relationships between proxies and the climate variable (e.g., Emile-Geay and Tingley, 2016; Schultz et al. 2015) multiproxy reconstruction methods have problems in preserving the variance in all frequencies (e.g., Masson-Delmotte et al., 2013). Although most studies have focused on the reconstruction of past temperature and hydrological-related fields (i.e., the typical variables

recorded by proxies), proxy signals have also been used to infer regional atmospheric circulation by assuming stationary impacts of the latter on surface climate (e.g., Pauling et al. 2006; Trouet et al., 2009; Ortega et al., 2015).

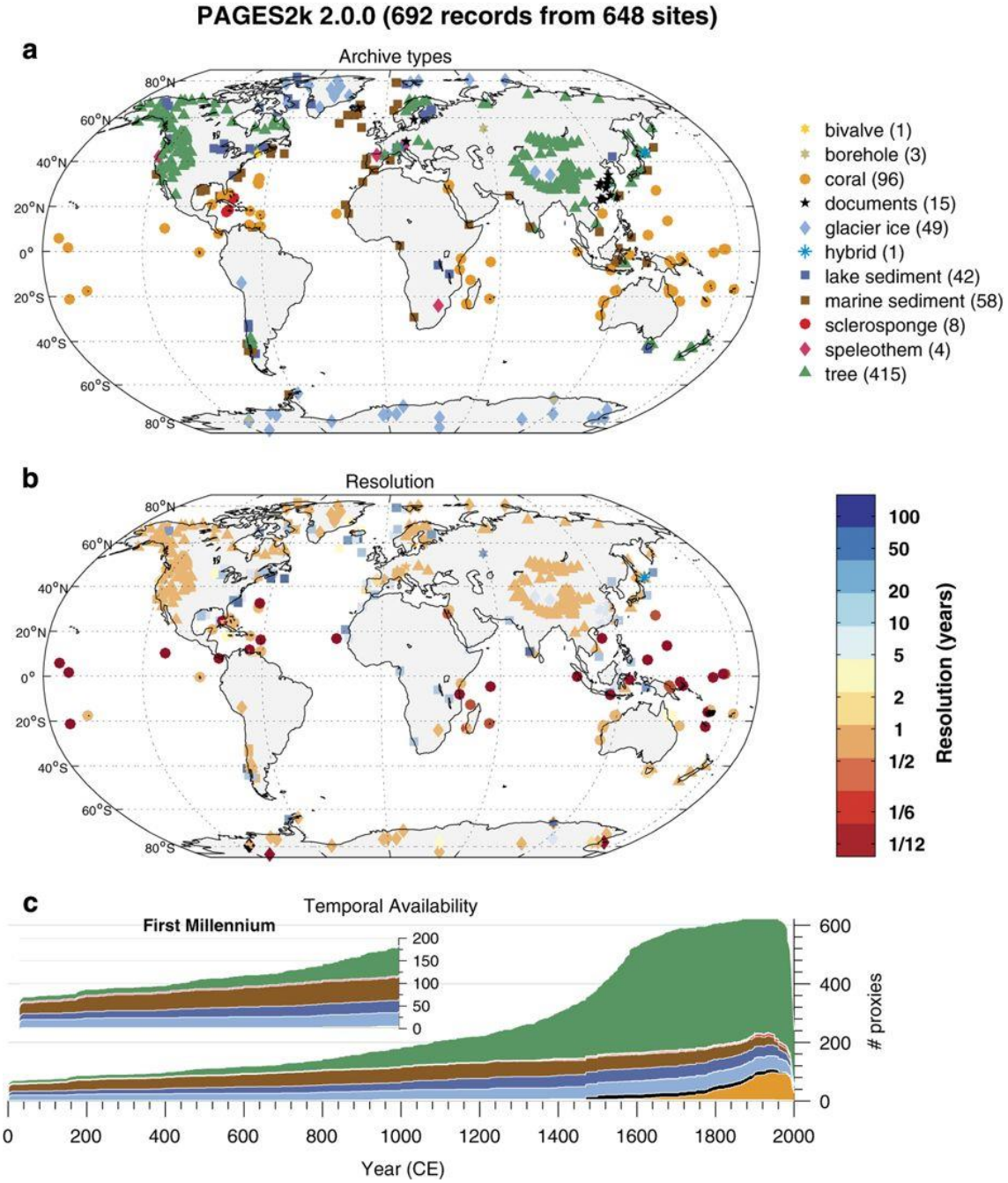

Figure 1.2. Spatiotemporal data availability in the PAGES2k database. (a) Geographical distribution, by archive type, coded by color and shape. (b) Temporal resolution in the PAGES2k database, defined here as the median of the spacing between consecutive observations. Shapes as in (a), colors encode the resolution in years (see colorbar). (c) Temporal availability, coded by color as in (a).

On the other hand, climate models offer a surrogated reality of the climate system compatible with some boundary conditions (external forcings) in which different hypotheses can be tested (e.g., Smerdon 2012). The models range from simple energy balance models (e.g., Crowley et al. 2001; Hegerl et al. 2007) to complex Earth System models which include a more realistic representation of some components, such as the carbon cycle (e.g., Lehner et al. 2015). Idealized and forced transient climate experiments for the past, present and future (Flato 2011, Braconnot et al. 2012) allow us to: 1) evaluate the range of internal variability and the forced responses to external forcings as well as the mechanisms involved (Jerome et al. 2010; Hegerl et al. 2011); 2) validate the statistical methodologies applied in reconstructions (Smerdon 2012); 3) narrow the ranges of climate sensitivity (Hegerl et al. 2007). Although models provide the most comprehensive and exhaustive representation of the climate system, they also contain their own sources of uncertainty, (e.g., limited knowledge of boundary conditions, complexity and spatial resolution, parametrizations and different model formulations (e.g., Hawkins and Sutton, 2009; Knutti et al., 2010). As a consequence, differences arise from the intercomparison of models, with no one emerging as "the best" overall (Flato et al. 2013). Even if models largely capture the main large-scale signatures of the observed climate and its evolution through the 20th century (Figure 1.3), one cannot be sure that they will also provide realistic outputs for all initial and boundary conditions (i.e., under other climate conditions representative of paleoclimate or future states; AchutaRao and Sperber, 2006; Knutti 2008; Stott and Forest, 2007; Winton 2011; Williams et al. 2012). In this sense, it can be said that models cannot be "verified", since it is a non-trivial problem to prove that a response of a model to a certain forcing is "right" because of the "right reasons" (Von Storch 2010).

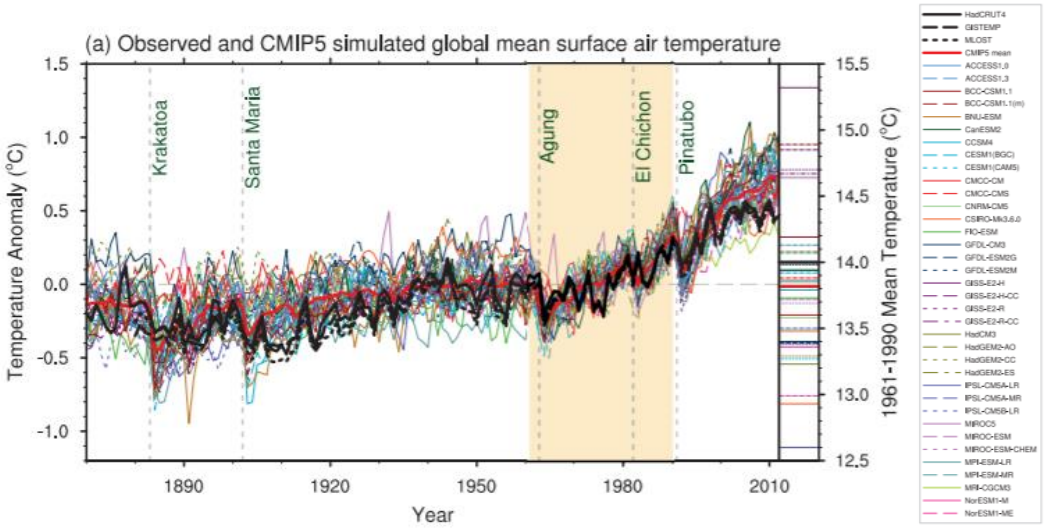

Figure 1.3. Observed and simulated time series of the anomalies in annual and global mean surface temperature. All anomalies are differences from the 1961–1990 time-mean of each individual time series. The reference period 1961–1990 is indicated by yellow shading; vertical dashed grey lines represent times of major volcanic eruptions. Single simulations for CMIP5 models (thin lines); multi-model mean (thick red line); different observations (thick black lines). Adapted from Flato et al. 2013

Increasing computing resources have allowed model improvement and the performance of large ensembles of simulations, which can be used to estimate the range of internal variability, detect the fingerprints of external forcings and attribute observed or reconstructed climate changes to forced responses. Although models may reproduce well the observed level of internal variability and the involved phenomenon (e.g., the El Niño-Southern Oscillation, ENSO, Flato et al. 2013), they are not expected to simulate accurately the observed evolution of internal fluctuations (Goosse et al. 2012). Therefore, if an observed anomalous period was internally forced by a given phenomenon or combination of phenomena, model simulations would fail to unambiguously detect and attribute it to the right causes. In this context, recent studies concluded that the reported agreement between model simulations and reconstructions of the last millennium has been overstated (Fernández-Donado et al. 2013). Assuming that current reconstructions are sufficiently reliable, the model-data disagreement for some anomalous periods of the past (such as the Medieval Climate Anomaly, MCA, 950-1250 CE) suggests that either models failed to capture the forced responses, or that these periods largely resulted from internal (and unknown) phenomena. Other recent multi-ensemble exercises have also reported substantial uncertainty in the simulated responses to external forcings, even across the members of the same model (Figure 1.4), suggesting that the forced responses may depend on the background state and/or interact with internal variability (Deser et al. 2012; Otto-Bliesner et al. 2016).

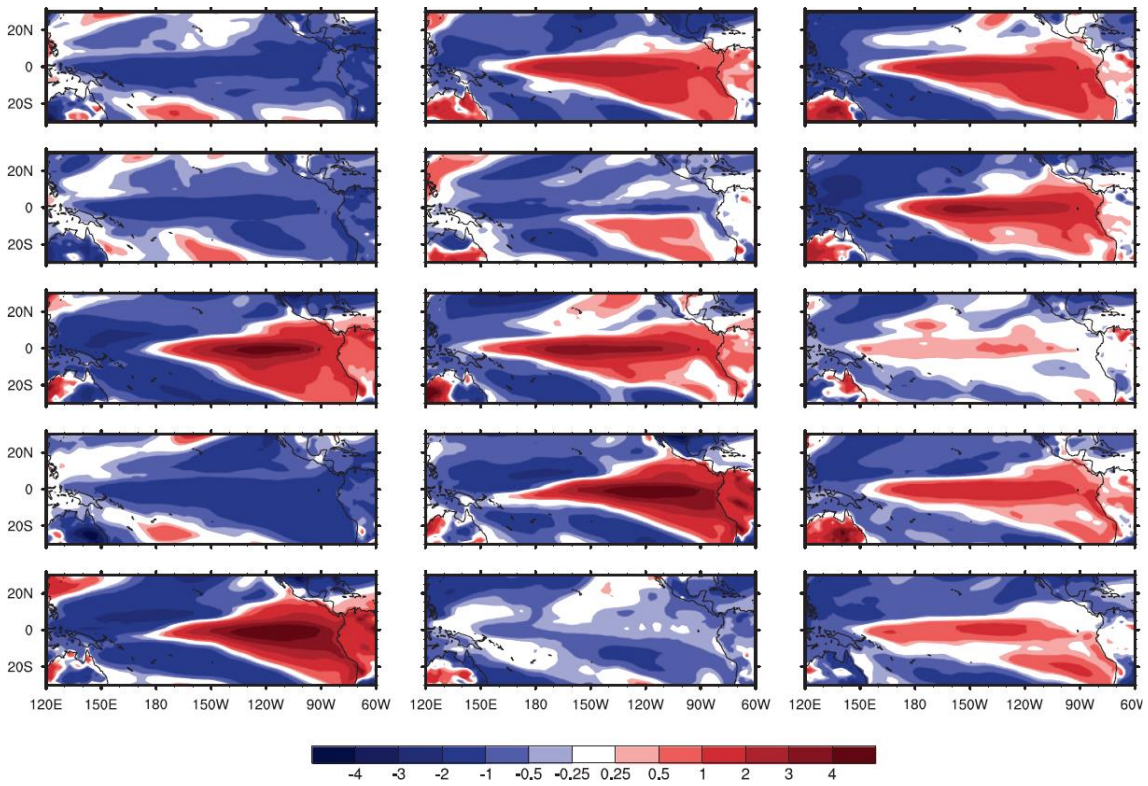

Figure 1.4 Tambora eruption (Apr 1815) and the simulated tropical Pacific surface temperature anomalies (°C) during winter 1816 for the 15 CESM-LME simulations that include volcanic forcing. The Dec–Feb (DJF) seasonal surface temperature anomalies for each simulation with volcanic forcing shown here are computed relative to each simulation's long-term annual cycle. Taken from Otto-Bliesner et al. (2016).

Finally, a third option can be found in historical records, including early instrumental data (Jones et al. 1997; Slonosky et al. 2001; Cornes et al. 2013), weather reports (Wheeler 1996, 2005), letters with weather information (Garcia et al. 2001; Fernández-Fernández et al. 2015) and other types of historical documents such as newspapers, civil and ecclesiastical records or agricultural returns (e.g., Barriendos 1997; Domínguez-Castro et al. 2012; Fernandez-Fernandez et al. 2015; Domínguez-Castro et al. 2015). In any case, these historical records contain always some kind of direct observations of past meteorological conditions. As an example, the left panel of Figure 1.5 shows a printed page of a meteorological diary for February 1785 from the earliest known eight-year meteorological record of instrumental observations for the Southern Hemisphere (Farrona et al. 2012). The right panel of Figure 1.5 shows a description of the solar eclipse on February 9th of 1785 that was published within a much longer report of meteorological and astronomical observations made in Rio de Janeiro during 1785 (Vaquero et al. 2005).

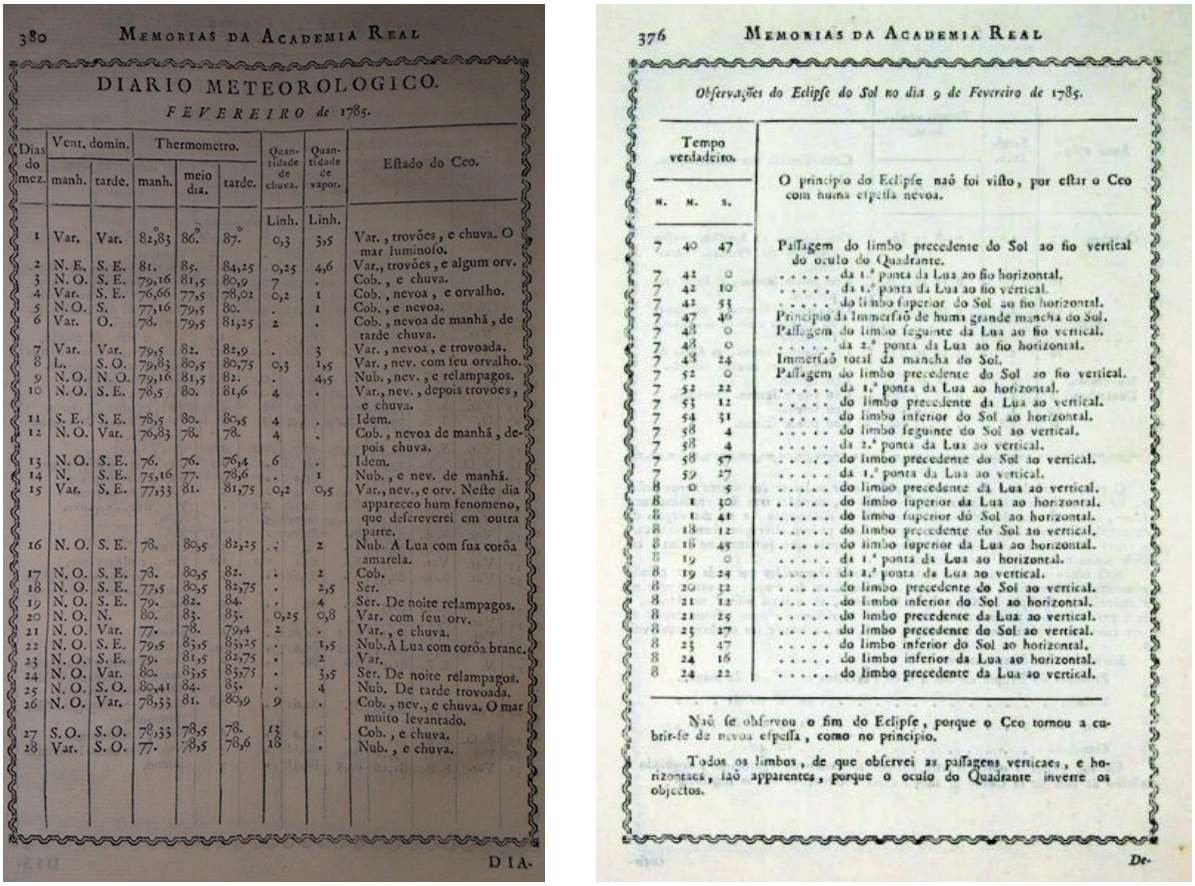

380 MEMORIAS DA ACADEMIA REAL

DIARIO METEOROLOGICO.

FEVEREIRO de 1785.

Dias do mez.	Vent. domin. manh.	Vent. domin. tarde.	Thermometro. manh.	Thermometro. meio dia.	Thermometro. tarde.	Quantidade de chuva.	Quantidade de vapor.	Estado do Ceo.
						Linh.	Linh.	
1	Var.	Var.	82,83	86.	87.	0,3	3,5	Var., trovões, e chuva. O mar luminoso.
2	N. E.	S. E.	81.	85.	84,25	0,25	4,6	Var., trovões, e algum orv.
3	N. O.	S. E.	79,16	81,5	80,9	7	.	Cob., e chuva.
4	Var.	S. E.	76,66	77,5	78,02	0,2	1	Cob., nevoa, e orvalho.
5	N. O.	S.	77,16	79,5	80.	.	1	Cob., e nevoa.
6	Var.	O.	78.	79,5	81,25	2	.	Cob., nevoa de manhã, de tarde chuva.
7	Var.	Var.	79,5	82.	82,9	.	3	Var., nevoa, e trovoada.
8	L.	S. O.	79,83	80,5	80,75	0,3	1,5	Var., nev. com seu orvalho.
9	N. O.	N. O.	79,16	81,5	82.	.	4,5	Nub., nev., e relampagos.
10	N. O.	S. E.	78,5	80.	81,6	4	.	Var., nev., depois trovões, e chuva.
11	S. E.	S. E.	78,5	80.	80,5	4	.	Idem.
12	N. O.	Var.	76,83	78.	78.	4	.	Cob., nevoa de manhã, depois chuva.
13	N. O.	S. E.	76.	76.	76,4	6	.	Idem.
14	N.	S. E.	75,16	77.	78,6	.	1	Nub., e nev. de manhã.
15	Var.	S. E.	77,33	81.	81,75	0,2	0,5	Var., nev., e orv. Neste dia appareceo hum fenomeno, que descreverei em outra parte.
16	N. O.	S. E.	78.	80,5	82,25	.	2	Nub. A Lua com sua corôa amarela.
17	N. O.	S. E.	78.	80,5	82.	.	2	Cob.
18	N. O.	S. E.	77,5	80,5	82,75	.	2,5	Ser.
19	N. O.	S. E.	79.	82.	84.	.	4	Ser. De noite relampagos.
20	N. O.	N.	80.	83.	83.	0,25	0,8	Var. com seu orv.
21	N. O.	Var.	77.	78.	79,4	2	.	Var., e chuva.
22	N. O.	S. E.	79,5	83,5	83,25	.	1,5	Nub. A Lua com corôa branc.
23	N. O.	S. E.	79.	81,5	82,75	.	2	Var.
24	N. O.	Var.	80.	83,5	83,75	.	3,5	Ser. De noite relampagos.
25	N. O.	S. O.	80,41	84.	83.	.	4	Nub. De tarde trovoada.
26	N. O.	Var.	78,33	81.	80,9	9	.	Cob., nev., e chuva. O mar muito levantado.
27	S. O.	S. O.	78,33	78,5	78.	13	.	Cob., e chuva.
28	Var.	S. O.	77.	78,5	78,6	18	.	Nub., e chuva.

DIA-

376 MEMORIAS DA ACADEMIA REAL

Observações do Eclipse do Sol no dia 9 de Fevereiro de 1785.

Tempo verdadeiro. H.	M.	S.	
			O principio do Eclipse naõ foi visto, por estar o Ceo com huma espessa nevoa.
7	40	47	Passagem do limbo precedente do Sol ao fio vertical do oculo do Quadrante.
7	42	0	. . . . . da 1.ª ponta da Lua ao fio horizontal.
7	42	10	. . . . . da 1.ª ponta da Lua ao fio vertical.
7	42	53	. . . . . do limbo superior do Sol ao fio horizontal.
7	47	40	Principio da Immersaõ de huma grande mancha do Sol.
7	48	0	Passagem do limbo seguinte da Lua ao fio vertical.
7	48	0	. . . . . da 2.ª ponta da Lua ao fio horizontal.
7	48	24	Immersaõ total da mancha do Sol.
7	52	0	Passagem do limbo precedente do Sol ao fio vertical.
7	52	22	. . . . . da 1.ª ponta da Lua ao horizontal.
7	53	12	. . . . . do limbo precedente da Lua ao vertical.
7	54	31	. . . . . do limbo inferior do Sol ao horizontal.
7	58	4	. . . . . do limbo seguinte do Sol ao vertical.
7	58	4	. . . . . da 2.ª ponta da Lua ao vertical.
7	58	57	. . . . . do limbo precedente do Sol ao vertical.
7	59	27	. . . . . da 1.ª ponta da Lua ao vertical.
8	0	5	. . . . . do limbo precedente da Lua ao vertical.
8	1	30	. . . . . do limbo superior da Lua ao horizontal.
8	1	41	. . . . . do limbo superior do Sol ao horizontal.
8	18	12	. . . . . do limbo precedente do Sol ao vertical.
8	18	48	. . . . . do limbo superior da Lua ao horizontal.
8	19	0	. . . . . da 1.ª ponta da Lua ao horizontal.
8	19	24	. . . . . da 2.ª ponta da Lua ao vertical.
8	20	32	. . . . . do limbo precedente do Sol ao vertical.
8	21	12	. . . . . do limbo inferior do Sol ao horizontal.
8	21	25	. . . . . do limbo precedente da Lua ao vertical.
8	23	27	. . . . . do limbo precedente do Sol ao vertical.
8	23	47	. . . . . do limbo inferior do Sol ao horizontal.
8	24	16	. . . . . do limbo inferior da Lua ao horizontal.
8	24	22	. . . . . do limbo precedente da Lua ao vertical.

Naõ se observou o fim do Eclipse, porque o Ceo tornou a cubrir-se de nevoa espessa, como no principio.

Todos os limbos, de que observei as passagens verticaes, e horizontaes, saõ apparentes, porque o oculo do Quadrante inverte os objectos.

De-

Figure 1.5 Left panel: printed page of Bento Sanches Dorta weather observations of February 1785 in Rio de Janeiro (Brazil) (Sanches Dorta 1799b, p. 380) (Farrona et al. 2012); Right panel: complete description of the solar eclipse observation sequence realized by Dorta on February 9th of 1785 in Rio de Janeiro (Brazil). From Vaquero et al. 2005

Although historical data most often provide direct observations, this kind of information is only continuously available at the global scale since the late 19th century, and in very few places since the 18th century (Figure 1.6). Besides, these records were always taken over land and most of the them cover short periods or have been poorly preserved. Consequently, continuous records are mainly confined to specific and scarce places around the world, such as Europe and east Asia (e.g., Mann et al. 2002; Zang 2004; Bradley et al. 2011; Alcoforado et al. 2012; Brázdil 2018). Europe is also the region where these records start further back in time, reaching the mid-18th century (Figure 1.6; Bradley et al. 2011). Instrumental data from mainland Europe have been used to develop temperature, precipitation or sea level pressure reconstructions (e.g., Jones et al. 1999; Pauling et al. 2006).

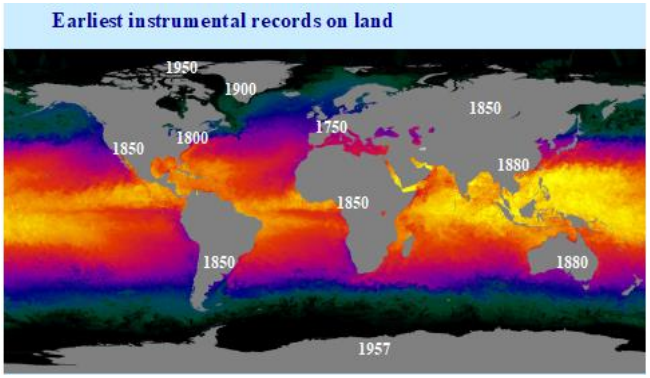

Figure 1.6. Approximate earliest date of continuous instrumental records. From Bradley 2011

1.3 Ships' logbooks as source of climatic information

During the last decades much more attention has been devoted to recover historical observations over the ocean, a region poorly covered by instrumental meteorological measurements until the 19th century (e.g., Wheeler 2014; García-Herrera et al. 2017; García-Herrera et al. 2018). These observations are mostly related to a unique type of documents which are ships' logbooks. Logbooks are a reliable source of climate information, less exploited than observations in land (García-Herrera et al. 2018). They contain information related to the conditions that the ships experienced along their routes across the world oceans. In addition to a variety of non-climatic information, ship's logbooks provide temperature, pressure and wind data, the midday position and a description of sea and weather state. The two first only begin to appear frequently towards the end of the 19th century. On the other hand, wind information goes much further back in time, since it was the most important variable for navigation, being regularly measured and preserved in logbooks. As an example, Figure 1.7 illustrates two different logbooks separated by more than two hundred years. The high degree of similarity between them stresses the long-term homogeneity of standard observational procedures. The logbook content also offers a homogeneous data source irrespective of the country of origin (García-Herrera et al. 2005a; Wheeler and García-Herrera 2008; Wheeler et al. 2010). Thanks to projects such as CLIWOC (García-Herrera et al. 2005b; Können and Koek 2005) or RECLAIM (Wilkinson et al. 2011), ships' logbooks are already a crucial piece to reconstruct past climate (García-Herrera et al. 2018 and references therein). Most of the data collected in these projects are now included in the International Comprehensive Ocean-Atmosphere Data set (ICOADS, http://icoads.noaa.gov/), which

includes meteorological observations over the oceans from different platforms (ships, buoys, etc.).

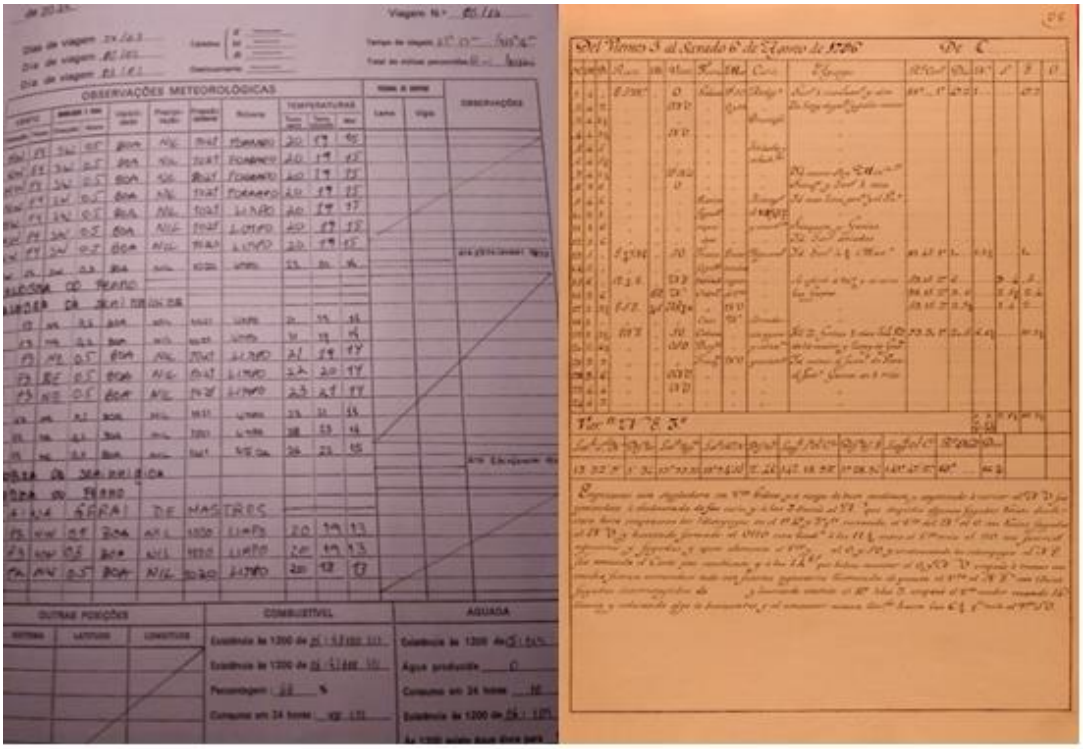

Figure 1.7. Left column: logbook' page from the Creoula, a training ship of the Portuguese Navy, of the year 2015. Right column: logbook' page from the Spanish Brig S. Francisco Javier (La suerte) of the year 1796.

Previous studies have demonstrated that wind records from ships' logbooks provide consistent and robust instrumental measurements that can be used as a reliable source of meteorological information. On the one hand, wind strength was recorded through descriptions of the state of the sea, the effects of wind on the sails, cloud observations or using the ship speed calculated with a rope with knots. The latter was the maritime speed unit (equivalent to one nautical mile per hour). Most of these descriptions could be directly related to the current Beaufort scale (García-Herrera et al. 2005a). Thus, in recent years, the wind force derived from ships' logbooks has been widely employed to recover long climatic series (e.g., Wheeler and Wilkinson 2005; Jones and Salmon 2005; Küttel et al. 2010). Nevertheless, the re-expression of wind force terms to Beaufort scale equivalents can be problematic due to the evolution of nautical vocabulary used in the descriptive information of the wind force (Wheeler and Wilkinson 2005; Gallego et al. 2007). On the other hand, wind direction does not suffer from such a problem since it has been measured with a ship's compass for centuries. Therefore, wind direction can be considered an instrumental measure, with the

additional advantage of not requiring subjective judgments or re-scaling to modern quantitative standards (Jackson et al. 2000; Jones and Salmon 2005; Wheeler et al. 2010). As compass reading is made with respect to the magnetic north, wind direction only requires a correction to true north by taking into account the known spatial and temporal patterns of variations in the geomagnetic field (Wheeler and García-Herrera 2008). In short, ships' logbooks contain first-hand and well-dated daily (sometimes sub-daily) weather information beyond the instrumental era, providing a unique source of early meteorological observations over an area of the globe poorly covered in the past (García Herrera et al. 2018 and references therein).

1.4 Wind directional indices

Ships' logbooks offer the possibility of collecting long and continuous records of wind direction over regions frequently sailed by ships (main routes of navigation) around the world (García-Herrera et al. 2005b; García-Herrera et al. 2017; García-Herrera et al. 2018). Figure 1.8 shows the number of wind direction observations from ICOADS over the oceans for the 1800-2014 period. They provide a considerable amount of meteorological observations in many parts of the world. As such, during the last decade, wind direction observations have been used to construct climate indices to characterize the regional atmospheric circulation and its variability in the past. The common strategy is to compute monthly indices over a specific area based on the percentage of days in the month with prevailing wind blowing from a specific direction. These wind directional indices have been derived for different areas that range from subtropical to subpolar regions, characterizing the regional atmospheric circulation and key global phenomena (García-Herrera et al. 2018 and references therein).

As an example of wind directional indices, here we illustrate recent developments and applications to characterize monsoonal subsystems, which are key drivers of regional climates over the tropics and mid-latitudes, with large socio-economic impacts in areas such as Africa, India, Australia or China. Their study has traditionally been carried out using monthly precipitation series because these were the longest instrumental observations for most of these areas, sometimes extending back to the early 20^{th} century (Wang and LinHo, 2002).

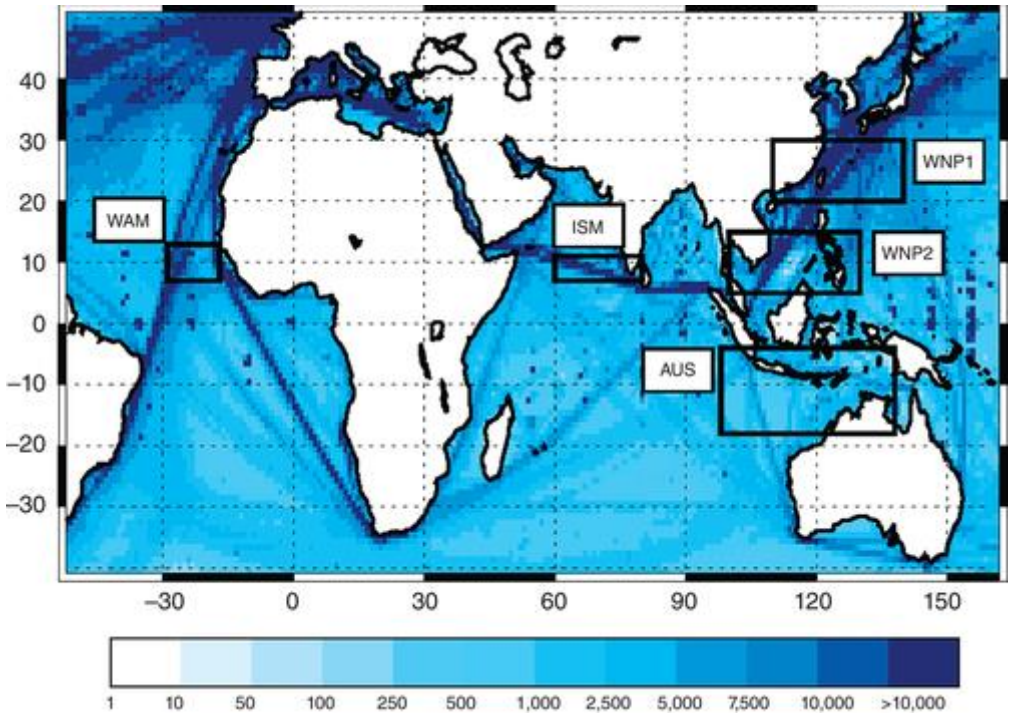

Figure 1.8. Number of wind direction observations in a 1 × 1 grid for the 1800–2014 period available in ICOADS 3.0. Black rectangles (labeled by white boxes) indicate the areas selected to compute monsoonal indices. From García-Herrera et al. 2018

In the framework of the INCITE project ("Instrumental Climatic Indexes Application to the study of the monsoon Mediterranean Teleconnection"), new monsoonal indices going back to the beginning of the 19th century were developed in different areas of the world. They are based on wind directional indices constructed from the ICOADS dataset, taking into account that the most salient feature of monsoons is the change in the dominant wind direction. Figure 1.8 confirms that a sufficiently large number of meteorological observations is available over strategic areas to capture the major monsoon subsystems (boxes from Figure 1.8). Figure 1.9 shows the long-term variability of the wind directional indices for the: a) West African Monsoon (WAM; Gallego et al. 2015); b) the Australian Summer Monsoon (ASM; Gallego et al. 2017); c) the Western North Pacific Summer Monsoon (WNPSM; Vega et al. (2018) and d) the Indian Summer Monsoon (ISM; Ordoñez et al. 2015). These indices are the longest instrumental monsoonal indices of their respective areas, providing a wider temporal context to interpret recent changes. For example, the African Southwesterly Index (ASWI, Figure 1.9 a) indicates that the anomalous behavior of the WAM since 1970s has no precedents in the last 170 years (Gallego et al. 2015). Figure 1.9b shows the intensification of the ASM in the 20th century, in agreement with previous studies (e.g., Smith 2004; Taschetto

and England 2009) and also indicates that it was noticeably weaker before 1900 (Gallego et al. 2017). On the other hand, the Western North Pacific Directional Index (WNPDI, Figure 1.9c) unveiled non-stationary relationships between the WNPSM and ENSO on multidecadal timescales (Vega et al. 2018). Similarly, Ordoñez et al. (2015) reported multidecadal fluctuations in the onset of the ISM since the 19th century (Figure 1.9d), and a good agreement with the official ISM onset dates developed by the India Meteorological Department, which rely on satellite data and cannot be applied before the 1970s.

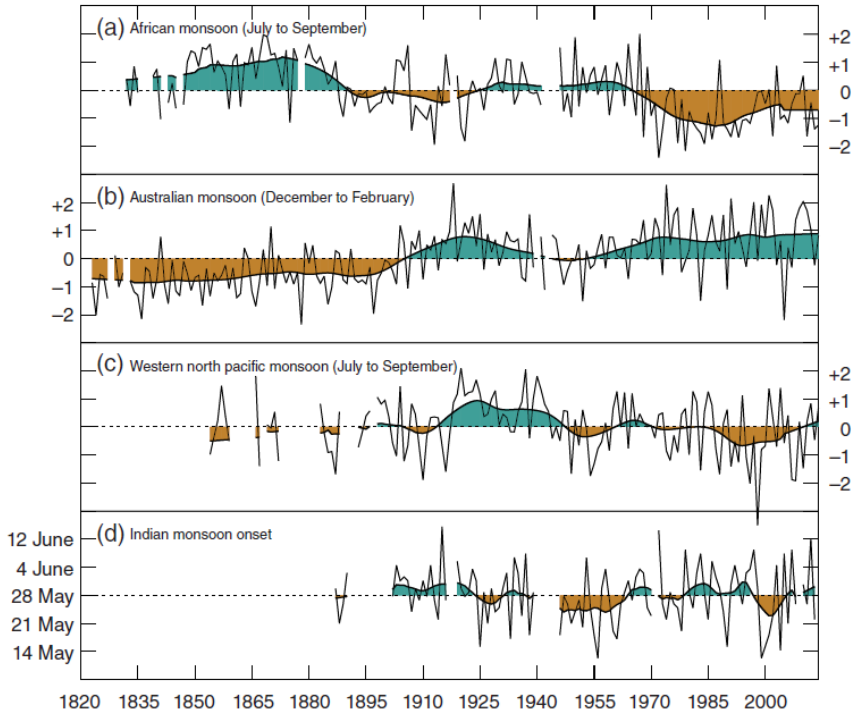

Figure 1.9. Monsoon Instrumental Climatic Indexes developed in the context of the INCITE project using ICOADS 3.0 for a) the African Summer Monsoon (AMS), b) The Australian Summer Monsoon, c) the Western North Pacific Summer Monsoon and, d) date of the Indian Summer Monsoon onset. Shaded smoothed curves are computed as a robust locally weighted regression with a 21-year window width (Cleveland, 1979). From García-Herrera et al. 2018.

Wind directional indices have also proven to be powerful tools to characterize the atmospheric circulation in mid-latitude regions. For example, Gomez-Delgado et al. (2018) developed the Northerly Wind Index (NWI), which captures the persistence of the summertime northerly winds over the eastern Mediterranean (the so-called Etesian winds) since the opening of the Suez Canal in 1869 (Bunel et al., 2017). They show that Etesian winds have become less frequent in the second half of the 20th century. As for the extratropical regions, Ayre et al. (2015) collected a significant number of logbooks for the

Artic latitudes beyond the instrumental period with observations of sea ice coverage and iceberg sightings. Arctic logbooks were used to build climate indices of the wind direction and force, and snow cover extension over the Arctic since the end of the 18th century, providing a unique and valuable source of climatic information for this area of scarcity of observations.

1.5 Euro-Atlantic atmospheric circulation

There are regions in Figure 1.8 with large density of observations, such as the North Atlantic, making them suitable to build climate indices that can help to improve our current understanding of the Euro-Atlantic atmospheric circulation. The atmospheric circulation in this sector largely determines the European surface climate variability and is dictated by the North Atlantic jet stream and its wave-like distortions generated by eddy-mean flow interactions (e.g., Woollings et al. 2010). Anomalies in wind speed, latitudinal location, waviness and/or tilt of the jet reflect the variability of mid-latitude weather systems and the action centers of the Euro-Atlantic atmospheric circulation (i.e., the Azores High (AH) and Iceland Low (IL)), which ultimately determine European climate anomalies. For example, in observational and model studies the jet is strongly related to the occurrence of mid-latitude weather extremes (e.g., Mahlstein et al. 2012; Röthlisberger et al. 2016), the location of the storm tracks (e.g., Athanasiadis et al., 2010) and the occurrence of atmospheric blocking (e.g., Trigo et al., 2004; Barnes and Hartmann, 2010). Indeed, future regional changes in European climate strongly depend on the responses of the jet-stream to climate change, which are subject to large uncertainties (e.g., Zappa and Shepherd 2017; Peings et al. 2018).

On longer time scales, the North Atlantic jet connects the regional climates to the main modes of atmospheric circulation variability in the Euro-Atlantic sector (Christensen et al., 2013). The latter are largely driven by internal dynamics (i.e., eddy-mean flow interaction) and therefore summarize preferred states of the jet stream. Figure 1.10 shows the three first modes of atmospheric circulation variability and their explained variance for each season. The first one is the well-known North Atlantic Oscillation (NAO; e.g., Hurrell 2003; Luterbacher et al. 2002; Cornes et al. 2013; Ortega et al. 2015), a meridional dipole involving a large-scale pressure seesaw between the AH and IL that was first described by Teisserenc de Bort (1883), albeit the name was coined by Sir Gilbert Walker in 1924 (Walker 1924). Positive phases of the NAO are associated with warm conditions in central and northern Europe and below-

normal temperatures in Greenland, the Middle East and southern Europe, as well as precipitation deficits in central and southern Europe and above-normal precipitation over northern Europe. The opposite pattern is observed during negative phases (e.g., Trigo et al. 2002). The NAO is observed all year-round, but its canonical pattern experiences changes throughout the year, particularly during summer, when the dipole shifts poleward and is spatially more confined (the so-called high-summer NAO, SNAO; Figure 1.10; Folland et al. 2009, Bladé et al. 2012).

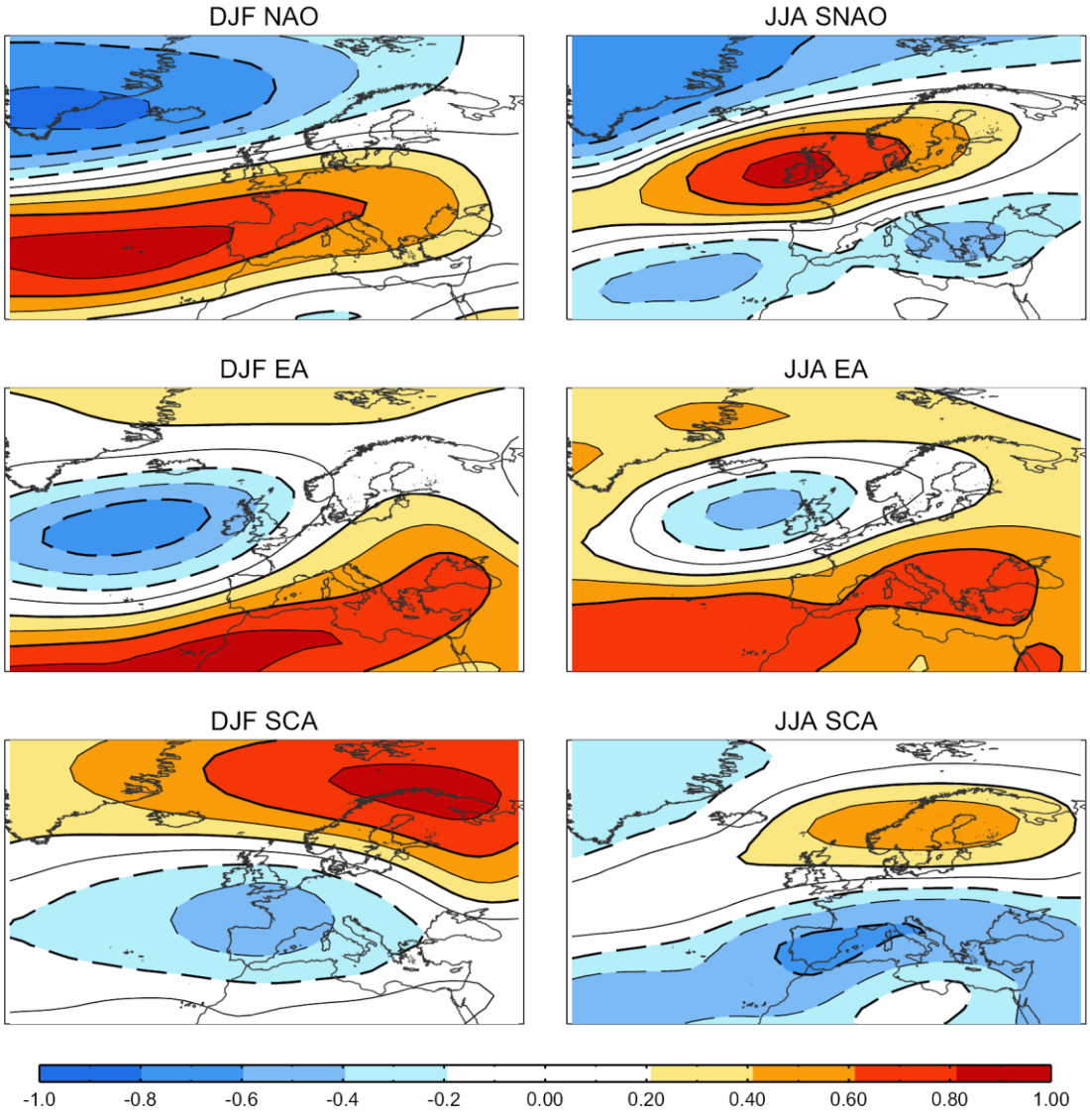

Figure 1.10. Main modes of atmospheric variability over the Euro-Atlantic sector for winter (December-to-February, left panels) and summer (June-to-August, right panels), as shown by correlation maps between the seasonal time series of the indices and geopotential height at 500 hPa for the 1951-2018 period.

Climatic anomalies in other European regions are not properly accounted for by the NAO (Figure 1.11; e.g., García-Herrera and Barriopedro 2018 and references therein). In particular, the East Atlantic (EA, Figure 1.10) and the Scandinavian (SCA, Figure 1.10) patterns (Wallace and Gutzler, 1981) explain a significant amount of climate variability throughout the year (e.g., Comas-Bru and McDermott, 2014; Jerez and Trigo, 2013; Trigo et al. 2008). The influence of these teleconnection patterns on European surface climate is stronger in winter, when the atmospheric circulation is dynamically more active and plays a major control on near-surface conditions (Vautard and Yiou 2009). Accordingly, most studies addressing the main modes of Euro-Atlantic atmospheric variability and their associated impacts are biased towards the winter (Trigo et al. 2004; Casado et al. 2009, Comas-Bru and McDermott 2014; Bastos et al. 2015; Comas-Bru et al. 2016; Stryhal and Huth 2017).

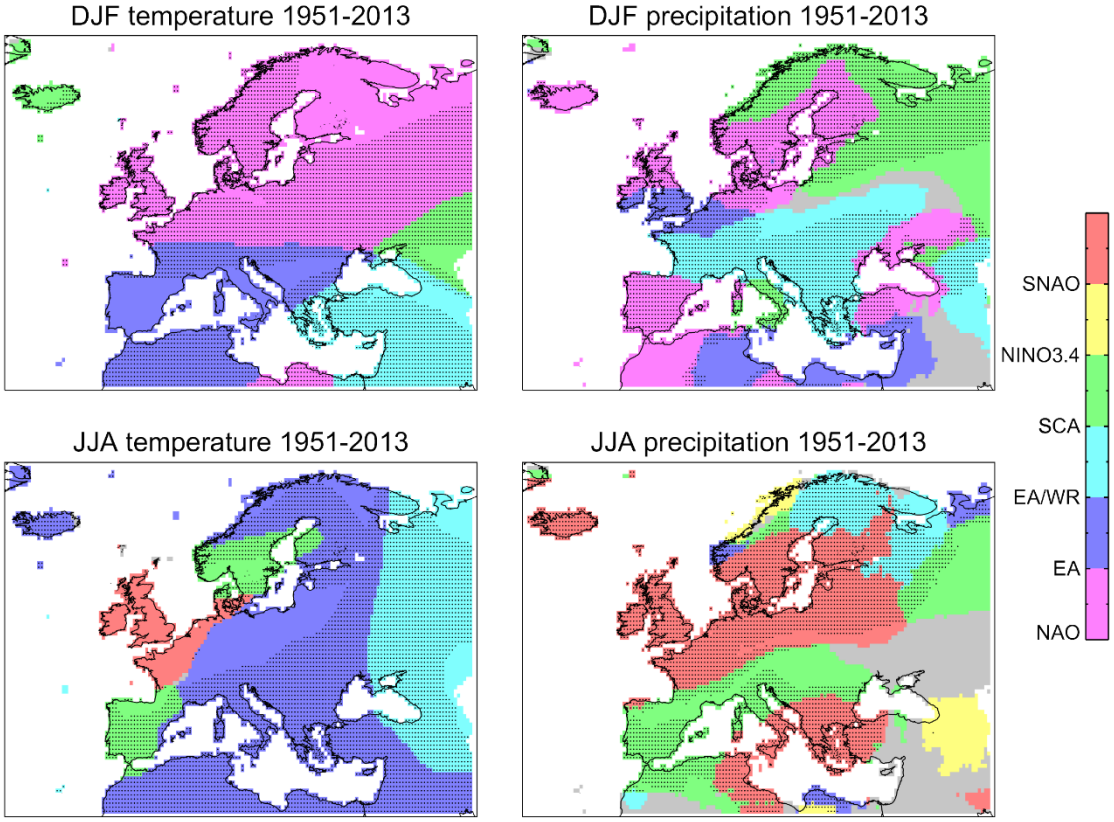

Figure 1.11 Spatial distribution of the dominant modes of atmospheric variability influencing temperature (left panels) and precipitation (right panels) interannual variations during winter (DJF, top panels) and summer (JJA, bottom panels) seasons of the 1950–2014 period. Colors identify the teleconnection pattern with the largest Pearson (Spearman) correlation coefficient with seasonal-mean temperature (precipitation) data. Dotted (grey shaded) regions identify areas where more than one (none) mode of variability displays significant correlations at the 95% confidence level. The following: NAO, EA, East Atlantic/Western Russian pattern (EA/WR), SCA, ENSO and the high-summer NAO (SNAO). Adapted from García-Herrera and Barriopedro (2018).

As the NAO is the main driver of climate variability in the Euro-Atlantic region, special emphasis has been given to extend its record back in time as a first attempt to assess the long-term variability of the atmospheric circulation and improve our understanding of European past climate (e.g., Jones et al. 1997; Hurrell et al. 1995; Luterbacher et al. 2002; Trouet et al. 2009; Pinto and Raible 2012; Cornes et al. 2013). Indices from historical instrumental series only reach the 18th century (e.g., Jones et al. 1997; Cornes et al. 2013) while NAO reconstructions based on proxy records extend further back in time (e.g., Luterbacher et al. 2002; Ortega et al. 2015 and references therein) but tend to show notable discrepancies in the pre-industrial period (Schmutz et al. 2000; Cook et al. 2002; Cornes et al. 2013). As a consequence, the variability of the NAO in the past remains only partially answered. Comparatively to the NAO, less efforts have been made to extend the records of other modes of climate variability beyond the instrumental period. For example, the longest EA index has recently been developed and only reaches the mid-19th century (Comas-Bru and Hernandez 2018). Similarly, the impact assessment of the atmospheric circulation on the surface climate has most often been confined to the second half of the 20th century using reanalysis products (e.g., Hurrell et al. 2003; Trigo et al. 2002). However, recent studies addressing the whole 20th century have shown that the NAO influence on the European climate cannot be considered stationary (e.g., Vicente-Serrano and Lopez-Moreno, 2008; Raible et al. 2014). Sources of non-stationary signals include migrations and intensity changes in the North Atlantic action centers (e.g., Barriopedro et al. 2014; Comas-Bru and McDermott 2014). Non-stationary issues can be addressed by complementing NAO indices with other indicators of the atmospheric circulation or targeting reconstructions of the full Sea Level Pressure (SLP) field over the Euro-Atlantic sector (Luterbacher et al. 2002; Casty et al. 2005). In this sense, recent works have indicated that the EA modulates the location of the North Atlantic action centers, thus partially explaining the non-stationary NAO signals (e.g., Moore et al. 2013; Comas-Bru and McDermott, 2014; Comas-Bru and Hernández, 2018). For example, the EA played a key role in shaping the NAO's centers during the outstanding negative NAO episodes associated with the extremely cold European events of December 2010 and winter 2006/07 (Moore et al. 2011; Moore and Renfrew 2012). Besides, Bastos et al. (2015) showed that both modes influence European land CO_2 sinks, underscoring the necessity of a better characterization of these atmospheric circulation patterns in coupled carbon-climate models.

Instrumental records of these leading modes of variability are short, hampering a proper characterization of the atmospheric circulation beyond the mid-19th century. Irrespective of

the approach adopted (either SLP fields or simplified circulation indices based on pressure differences between two fixed locations), the current knowledge of past atmospheric circulation mainly relies on series taken over land. This yields limited information, biased to regions of the Euro-Atlantic sector where the pressure gradients are the lowest and largely influenced by local factors. This is supported by Figure 1.10, which shows that most of the governing centers of the main modes of Euro-Atlantic atmospheric circulation variability mainly lay over the oceans. Therefore, as a major limitation, previous studies have not been able to fully capture the key driver of the Euro-Atlantic circulation, namely the eddy-driven jet stream (e.g., Slonosky et al. 2001; Jacobeit et al. 2003, 2017). A substantial step forward was made by incorporating observations from the Atlantic Ocean to previous land-based SLP reconstructions (Küttel et al. 2010). This brought a significant improvement in the skill of the SLP reconstruction and the characterization of the European climate, since the 18th century.

1.6 Use of logbooks over the Euro-Atlantic sector

The English Channel has been a region of intense marine activity from the 17th century (Figure 1.8). Over this region, Royal Navy logbooks are sufficient in number to provide a near daily record since 1685 (Wheeler et al. 2010). Furthermore, this area is located in a strategic area (the exit zone of the eddy-driven jet stream), making it representative of the Euro-Atlantic atmospheric circulation and consequently a good indicator of the European climate (e.g., Wheeler et al. 2010; Barriopedro et al. 2014; Kidston et al. 2015; Vicente-Serrano et al. 2016). Taking advantage of this, Barriopedro et al. (2014) developed the Westerly Index (WI), which measures the frequency of days with westerly wind over the English Channel since 1685 until 2008. WI exhibits significant robust signals in European temperature and precipitation throughout the year. Figure 1.12 shows a schematic of the main climatic signals of the WI during the cold (top panel) and warm (bottom panel) seasons, being able to capture the seasonally-varying signatures of NAO. Despite their similarities, both indices are different and should be considered as complementary. As an example, Vicente-Serrano et al. (2016) found that when NAO and WI are considered jointly, other modes of atmospheric circulation do not add significant information to explain the variability of drought severity in most of Europe.

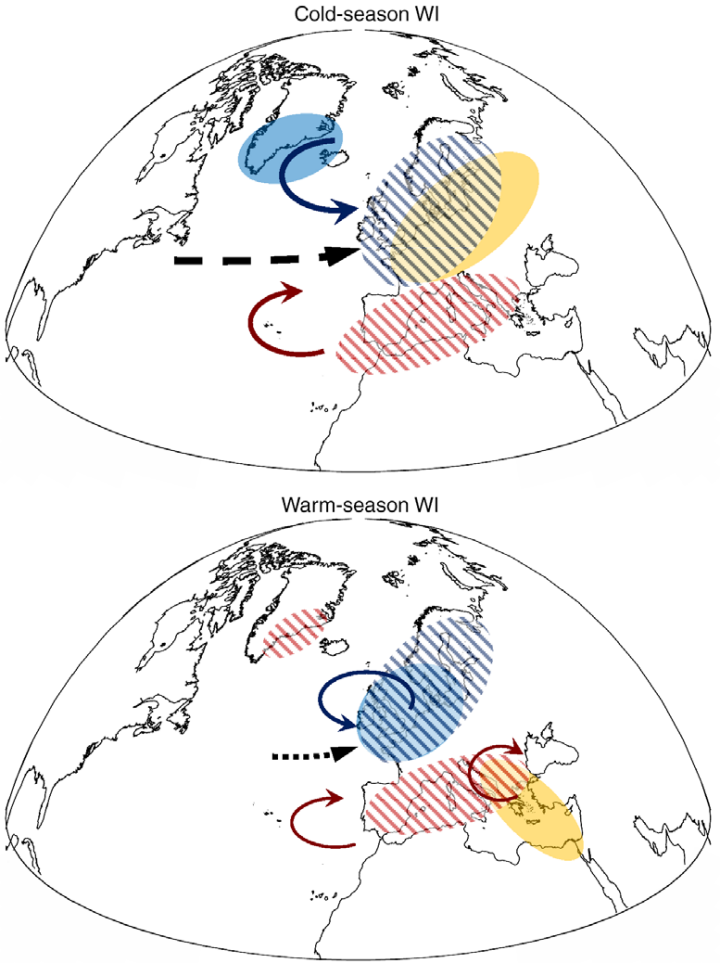

Figure 1.12. Schematic displaying the main signatures in atmospheric circulation (arrows), temperature (filled shading) and precipitation (hatching) associated with positive phases of the Westerly Index in: top) cold seasons (herein referred to all seasons, except for summer); bottom) warm season (June-to-august). Solid arrows denote enhanced cyclonic (in blue) and anticyclonic (in red) circulation, with dashed arrows indicating the intensity of the westerlies. Orange/blue shading denotes anomalously warm / cold temperatures. Red/blue hatching indicates regions with reduced/increased precipitation. From García-Herrera et al. 2018

Still, WI and NAO are insufficient to fully capture the atmospheric circulation over the Euro-Atlantic sector (Trigo et al. 2008; Barriopedro et al. 2014). Similarly to the NAO, the skill of the WI to reproduce the plethora of atmospheric circulation patterns is limited, partially because it disregards the information contained in other wind directions. Indeed, a decline in the frequency of westerlies should be compensated by increases in other wind directions, each one reflecting different weather systems and jet anomalies with very different impacts on Europe. This highlights the need of complementing the WI information with other wind directions that may provide a better characterization of the atmospheric circulation and consequently of the European past climate and its variability.

1.7 Objectives

The main aim of this work is to build instrumental directional indices for all wind directions based on ships' observations of the last centuries in order to better characterize the Euro-Atlantic atmospheric circulation and improve our understanding of past European climate. More specifically, the four main objectives of this Thesis are:

1. To exploit ships' logbooks and wind direction records of ICOADS to extend the WI to other wind directions, by designing a novel methodology that provides robust estimates of the monthly persistence of the wind in the main four cardinal directions: Northerly, Southerly, Easterly and Westerly.

2. Using these wind Directional Indices (DIs) over the eastern Atlantic for the period 1685-2014 to provide new evidences and first-ever instrumental-based insights of the Euro-Atlantic atmospheric circulation through the last 330 years and their associated impacts on the European surface climate.

3. To exploit the DIs to characterize the atmospheric circulation during specific anomalous periods of the past European climate and to quantify the role played by the atmospheric circulation. To this end, the last part of the Late Maunder Minimum (LMM, 1675-1715 CE) will be used as a test study because it was one of the coldest decadal-long periods in recent history, whose causes are still subject to debate.

4. To derive instrumental-based reconstructions of the winter NAO, EA and eddy-driven jet stream for the period 1685-2014 based on the DIs, therefore providing the most complete picture of the Euro-Atlantic atmospheric circulation variability and first-ever observational estimates of the North Atlantic jet stream for the last three centuries.

This Thesis is structured in six additional Chapters, the first one describing the Data and Methods employed in the four following Chapters, which provide a detailed description of the results associated with each objective, respectively. The last Chapter is devoted to summarize and discuss the main conclusions and future outlook. Three submitted or published papers support the four Chapters of results.

Chapter 2

2. Data and methods

2.1 Data

2.1.1 Wind direction observations

To achieve the main objectives of this Thesis two different sources of wind direction observations have been used: the International Comprehensive Ocean Atmosphere Data set (ICOADS, version 3.0; Freeman et al. 2017) for the 1870-2014 period and archival ships' logbooks (1685-1870) not included in the ICOADS dataset. The oceanic region chosen for this study was (10°W-5°E, 48°N-52°N; Figure 2.1), which allowed us to build quasi-continuous series spanning the period 1685-2014. The area includes the English Channel and the ocean area south of Ireland, but for simplicity, it will be referred to as English Channel throughout this Thesis.

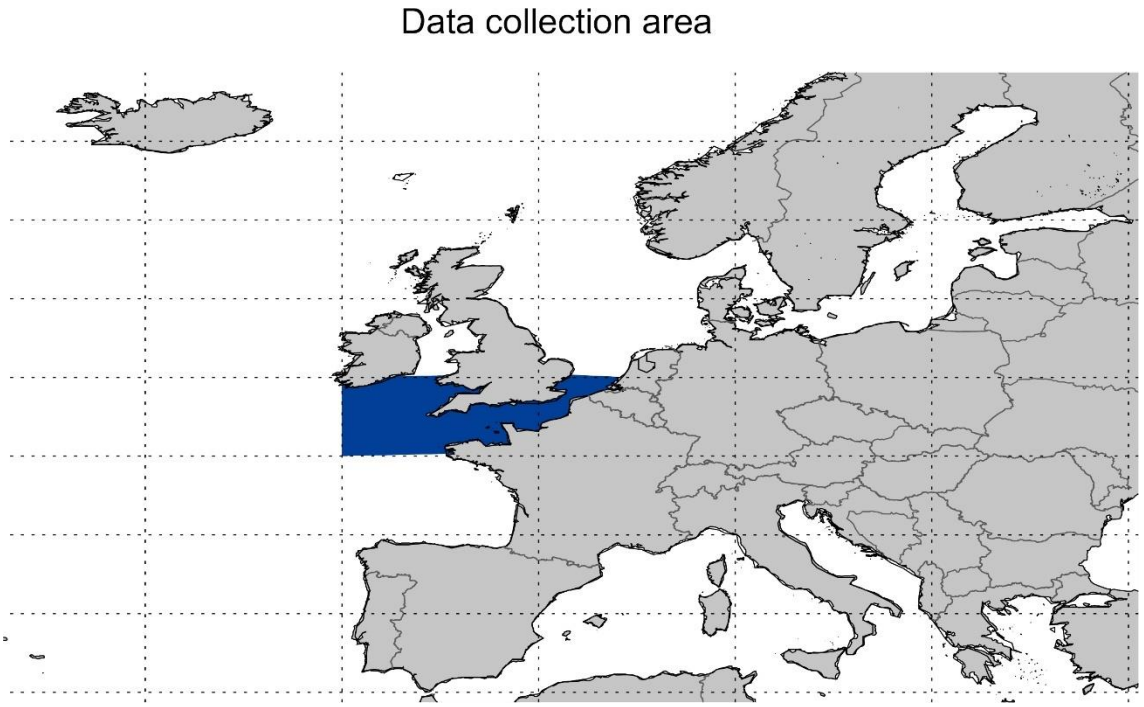

Figure 2.1. Area of analysis. Blue shading shows the selected region for the collection of wind direction observations during the period 1685-2014

A total of 74.363 daily wind records were abstracted for the period 1685 to 1870 from Royal Navy ships' logbooks kept in the National Maritime Museum and the United Kingdom (UK) National Archives (Historical Logbooks from United Kingdom; HLUK hereinafter). There are more than 25000 Royal Navy ships' logbooks of all types well-preserved that constitute an immense amount of information. This vast quantity of documents requires an efficient procedure of data identification and abstraction. In this sense, it is important to know which of the logbooks derive from ships within the study area. To assist in this respect, there are fleet list with information of vessels arranged geographically and by month that allow the identification of ships within the study area. The logbook search was optimized giving priority to ships in the open sea and securing at least one wind observations per day (the midday) Most of these data were already scrutinized and employed in Wheeler et al. (2009) and Barriopedro et al. (2014). However, as compared to Barriopedro et al. (2014), additional ships' logbooks were searched by Dennis Wheeler from 1850 to 1870, since this was a period of relatively frequent missing data therein. After the classification of these new data, there is an improvement on the temporal coverage of wind observations to 97.9% of the days in the 1685-1870 period.

Similar to modern standards, the wind direction was measured with a 32-point compass (i.e. ~11º resolution) in degrees with respect to the magnetic north. Calm and variable wind situations were also annotated in the logbooks. When only one observation was made by a vessel, it can be assumed with high confidence that it corresponds to the midday observation, since it was the mandatory observation of each day. If several sub-daily observations were available, only the midday record was abstracted. When a range of wind directions was provided with no indication about the time of observation, which occurs very rarely, the median was taken instead.

Wind direction observations from logbooks only require very minor corrections: 1) the change from Julian to Gregorian calendar before 1753 and from nautical to civil day (a 12 hour lag); 2) the correction by magnetic variation. The latter was applied by using monthly magnetic declination data with 1ºx1º longitude-latitude resolution over the English Channel from the National Geophysical Data Center (NGDC). These data provide estimated values of magnetic declination (in degrees from true north) based on historical records (Jackson et al. 2000) up to 1900 and on the International Geomagnetic Reference Field (IGRF; Thébault et al. 2015) since 1900, with a smooth transition between them. The correction was applied by

simply adding the magnetic declination of the given year and month to all daily compass readings available for that time, with the exception of calm and variable winds. As the precise location of the vessel was not always available, the spatial average of the magnetic declination over the English Channel was used instead (Figure 2.2a). Observational station data for London and Paris have been included in Figure 2.2.a . The magnetic declination has a range of -29.36º during the study period in the English Channel, while the standard deviation (SD) within the English Channel has a value of 2.11º. Thus, differently to its long-term variations, spatial changes in magnetic declination within a limited area such as the English Channel are small and can be considered negligible, particularly when compared to the resolution of wind direction observations. As such, similar results were obtained using the declination from the nearest gridpoint relative to each available ship location (not shown). During 1685-1870, the magnetic correction affected to 1%, 5%, 2% and 2% of the total days that were formerly classified as easterlies, southerlies, westerlies and northerlies, respectively.

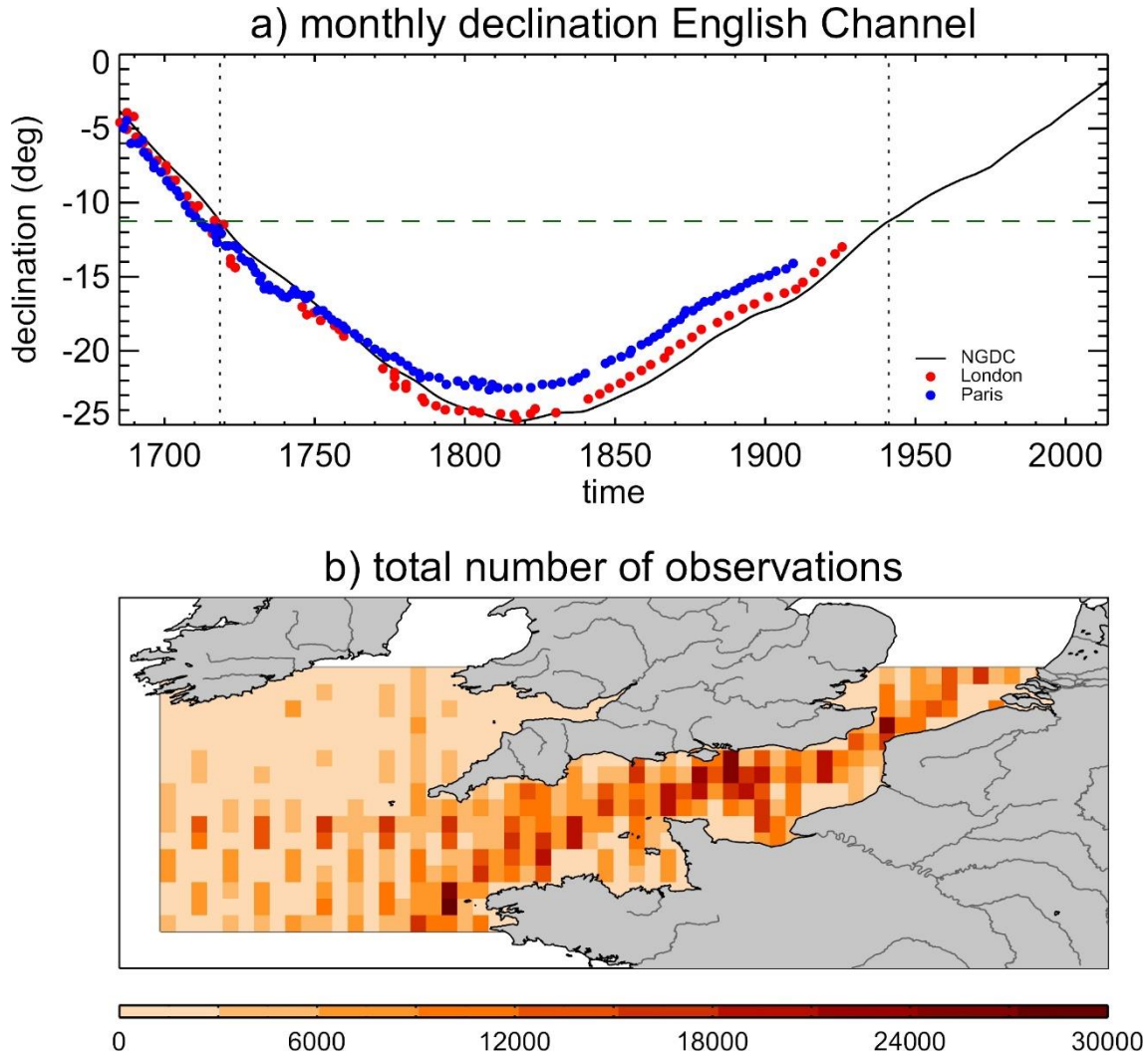

Figure 2.2. (a) Monthly time series of the areal-average magnetic declination (in º from true north) over the English Channel (solid line). Dots indicate historical monthly observations of the magnetic declination from London (red; Malin and Bullard 1891)) and Paris (blue; Hartmann et al. 2013); (b)Total number of daily windy observations retained (1662-2014) over a regular grid of 0.25ºx0.25º in longitude-latitude in English Channel

Since 1662 onwards to 2014, the ICOADS v3.0 release (Freeman et al. 2016) contains 453 million records over the globe, with 4.318.330 observations for the English Channel alone, although most of them (99.4%) were confined to the period after 1870. This source contains observations that have already been processed after exhaustive analysis and interpretation of the information. ICOADS provides surface marine data from different sources, mainly ships (69.2%), with wind direction being provided in degrees with respect to true north (calm and variable winds are also labeled). The compass resolution of the wind direction measurements is often detailed in the files, being in most cases of 32-point, as in the case of the logbooks. The frequency of daily ICOADS observations within the English Channel increases with time, showing an abrupt growth in the last part of the record, largely due to wind observations

taken at different times of the day over the same geographical locations. For coherence with HLUK observations of the 1685-1870 period, we only selected the ICOADS wind direction observations taken by ships over the open sea. To avoid biases towards oversampled points, we only picked one record for each location with wind observations in a given day, giving preference to those that were close to 12:00 UTC. Using this procedure, the final number of wind direction observations from ICOADS decreased to 2.091.946 but displayed a more homogeneous temporal distribution (not shown). The spatial distribution of the remaining ICOADS observations shows a maximum over the open sea (Figure 2.2b), and this pattern remains with time regardless of the total number of daily records (not shown), thus highlighting the preferred routes of navigation.

Finally, we merged the ICOADS and HLUK records. However, if only two records were available for a given day we only kept one of them, giving priority to HLUK, with the aim of avoiding conflicting wind directions, as described in Section 3.1 of Chapter 3. Recall that ICOADS already includes ships' logbooks data collected by previous projects (e.g., CLIWOC) and the coherence between both sources of information has largely been proven (Brohan et al. 2009; Freeman et al. 2016). After merging, the resulting database usually has one record per day up to ~1870, and high spatial density of observations (more than 37 records per day, on average) from 1870 onwards (Figure 2.3a). The database displays good temporal coverage, except for years around 1875 and the WWII period (Figure 2.3b), with 96.0% of the days in the 1685-2014 period containing at least one wind observation.

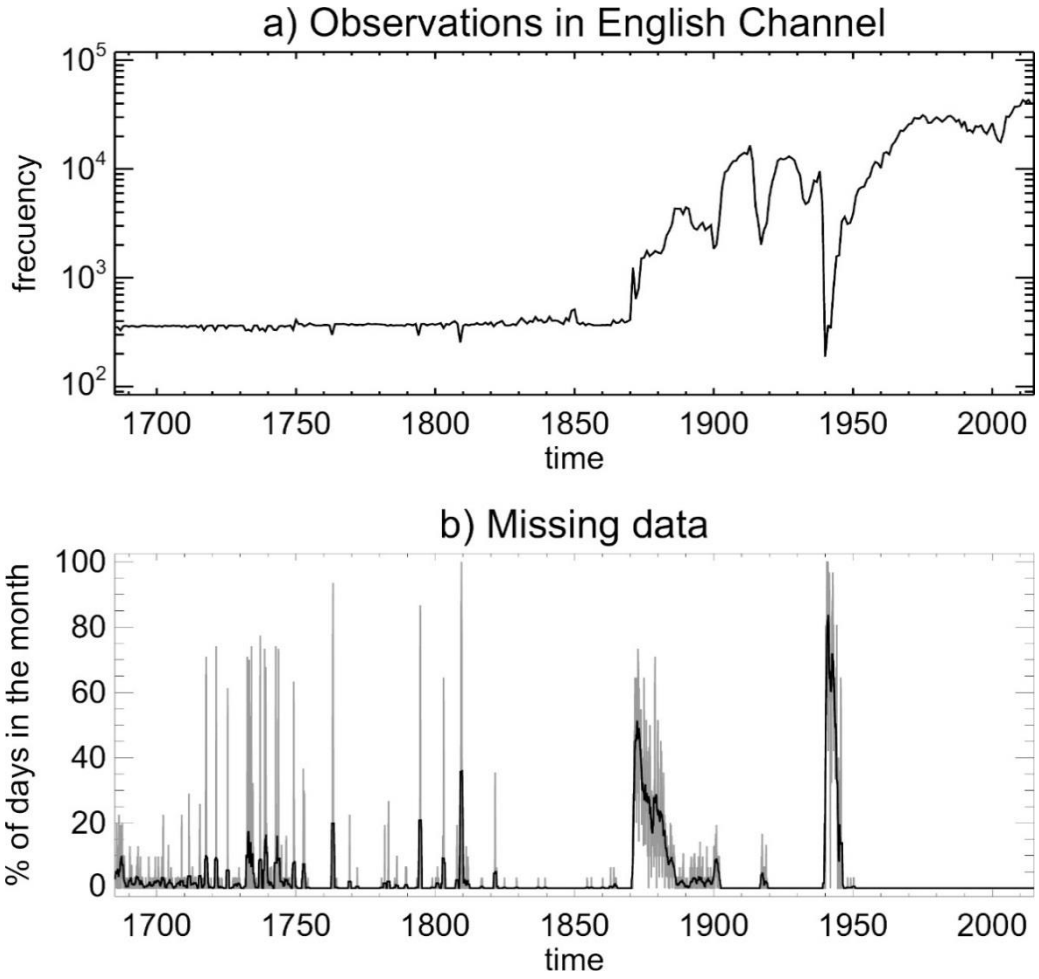

Figure 2.3. (a) Annual time series with the daily mean frequency of wind direction observations over the English Channel (in # per year) from Royal Navy Ships' logbooks and ICOADS V3.0; b) Monthly time series showing the percentage of days with missing data (grey line) along the 1685–2014 period. The black line depicts a 12-month running average.

2.1.2 Observational and Reanalysis products

2.1.2.1 Observational products

Monthly 2 m temperature data was obtained from the Climate Research Unit version TSv3.23 (CRU; Harris et al. 2014) on a 0.5°x0.5° spatial resolution grid. This version covers all land areas (60°S and 80°N; excluding Antarctica) and the period 1901-2015. This dataset is derived from climate observatories and has been subject to extensive manual and semi-automated quality control measures.

Monthly precipitation totals were retrieved from the Global Precipitation Climatology Center for the period 1901-2014 (GPCC, Schamm et al. 2014). This product provides an

estimate of the global precipitation over land on daily and monthly basis and different spatial resolutions. Several products are available (full data, monitoring and first guess), each using different input and procedures. Here, we used the Full Data version 6.0 on 1ºx1º spatial resolution, which covers the 1891-2016 period. This product is the most accurate in situ precipitation dataset of GPCC, being based on interpolated rain gauge data of ~80,000 stations world-wide, although the number of stations decreases back in time up to ~6,000 before 1900.

2.1.2.2 Reanalyses datasets

We have used meteorological fields provided by two recently released reanalyses for the 20th century: the Twenty Century Reanalysis (20CR version 2c, Compo et al. 2011) of the National Oceanic and Atmospheric Administration (NOAA) for 1851-2014, and the ERA-20C reanalysis (Poli et al. 2016) of the European Centre for Medium Range Weather Forecast (ECMWF) for 1901-2010. 20CR uses a modified version of the atmospheric component of operational climate forecast system model (T62, 28 vertical levels) from the National Centers for Environmental Prediction (NCEP), assimilating surface pressure from the International Surface Pressure Databank (ISPDv2) and ICOADS, and using observed monthly sea-surface temperature and sea-ice distributions from the Hadley Centre Global Sea Ice and Sea Surface Temperature (HadISST1.1) as boundary conditions. ERA-20C was produced with the coupled atmosphere/land-surface/ocean model of the ECWMF Integrated Forecast System (T159, 91 model levels), which assimilates surface and mean sea level pressures from ISPDv3.2.6 and ICOADSv2.5.1, and surface marine winds from ICOADSv2.5.1. Due to subtle differences in the input data and the assimilation schemes, ERA-20C may perform better than 20CR in relatively well observed regions such as western Europe, while 20CR may take better advantage of sparse observations in poorly covered regions (Poli et al. 2016 and references therein).

The 20CR was launched first, and was the only 20th century reanalysis available at the beginning of this Thesis, having been used in the supporting papers of the Chapters 3-5. In this case, we used daily geopotential height at 500 hPa and sea level pressure at 2ºx2º resolution for the period 1901-2014. Furthermore, the following variables were computed using daily mean fields of geopotential height, temperature, humidity, and zonal and meridional wind at different pressure levels:

(1) The vertically integrated moisture flux through the 1000–500 hPa layer that can be calculated following Equation 2.1

$$\vec{Q}_T = \frac{1}{g}\int_{500}^{1000} (q\vec{V})\, dp \tag{2.1}$$

where q represent the specific humidity, g is the gravity acceleration, p is the pressure and $\vec{V}$ is the horizontal wind vector.

(2) The moisture convergence between 1000 and 500 hPa, also known as Vertically Integrated Moisture Flux Convergence (IVMFC), that can be calculated following the Equation 2.2:

$$IVMFC \equiv \nabla \cdot \vec{Q}_T = \frac{1}{g}\int_{500}^{1000} \left(\frac{\partial uq}{\partial x} + \frac{\partial vq}{\partial y}\right) dp \tag{2.2}$$

where u, v are the components of the wind velocity at each pressure level.

(3) Temperature advection at different pressure levels following Equation 2.3

$$-\vec{V} \cdot \nabla T = -\left(\frac{\partial T}{\partial x}u + \frac{\partial T}{\partial y}v\right) \tag{2.3}$$

where T represents the temperature.

(4) The storm-tracks, defined as the standard deviation of the high-pass filtered (2–7 days) geopotential height at 500 hPa.

On the other hand, the last Chapter already uses daily mean zonal wind at different pressure levels as well as monthly SLP and geopotential height at 500 hPa from the ERA-20C for the period 1901-2010 and at 2.5°x2.5° spatial resolution.

2.1.2.3 NAO and EA indices

During this Thesis several NAO and EA indices are employed for the historical period. Regarding the NAO, we used the Principal Component (PC) NAO index of Hurrell et al. (1995) and the station-based indices of Jones et al. (1997) and Luterbacher et al. (2001), all derived from SLP data. As for the EA index, we used the index of Comas-Bru and Hernández (2018), derived from a multi-reanalysis PC-based approach, and the EA index defined as the second Empricial Ortoghonal Function (EOF) of the SLP field from the ERA-20C reanalysis. In addition, we employed the NAO and EA indices provided by the Climate Prediction Center (CPC) of the NOAA (https://www.cpc.ncep.noaa.gov/data/teledoc/telecontents.shtml) for the 1950-present period, which are based on a rotated PC analysis of monthly geopotential height at 500 hPa from the NCEP and National Center for Atmospheric Research (NCAR) reanalysis (Kalnay et al. 1996). A summarized description of these indices is provided in Table 2.1.

Table 2.1. Description of the NAO and EA indices employed in this Thesis.

Source	Period	Resolution	Definition
NAO			
CPC NOAA	1950-2014	Monthly	Rotated PC analysis of monthly geopotential height at 500 hPa
Hurrell et al. 1995	1901-2014	Seasonal	First EOF of SLP anomalies over the Atlantic sector [20-80°N, 90°W-40°E].
Jones et al. 1997	1824-2014	Monthly	Normalized pressure difference between Azores (Ponta Delgada, 37.7 º N, 25.7 º W) and Iceland (Akureyri , 65.7 º N, 18.1 º W and Stykkisholmur, 65.0 º N, 22.8º W)
Luterbacher et al. 2001	1685-2001	Seasonal	Standardized (1901-1980) SLP difference between Azores and Iceland, each region defined as the mean of four grid-points on a 5ºx5º longitude-latitude grid
EA			
CPC NOAA	1950-2014	Monthly	Rotated PC analysis of monthly geopotential height at 500 hPa
2nd EOF SLP ERA-20C	1901-2010	Seasonal	Second PC of the monthly standardized area-weighted SLP anomaly over [10-80ºN, 100ºW-40ºE]
Comas-Bru	1852-2014	Monthly	Composite of EA time series built using two

and Hernández (2018)			historical records (i.e. Bergen Florida and Valentia) and five reanalysis data sets

2.1.2.4 Eddy-driven jet stream

The latitude and speed of the eddy-driven jet stream are identified from daily ERA-20C wind data over the period 1900-2010 following a modified version of the algorithm developed by Woollings et al. 2010:

- For each grid point, the daily mean zonal wind is averaged for the 700, 825 and 925 hPa pressure levels and then low-pass filtered (>10-day) to remove the features associated with individual synoptic systems.
- The resulting field is then zonally averaged over the Atlantic sector [0-60ºW], neglecting winds poleward of 75ºN and equatorward of 15ºN.
- The jet speed is defined as the maximum westerly wind speed of the resulting latitudinal profile, while the latitude is defined by the location of this maximum

2.2 Methods

2.2.1 Composites

Composite analysis is herein used as a simple and effective tool to identify common signatures observed during specific states of the climate or atmospheric circulation signatures. Compared to other statistical methods (e.g., correlations), it has the advantage of taking into account non-linear relationships and their asymmetries. In Chapter 4, seasonal scaled composites were calculated by scaling the mean by the squared root of the sample size and dividing by the standard deviation of the composited sample (Brown and Hall, 1999). This kind of composites is more robust to outliers than the simple mean composites since the associated variance of the members is also included (Küttel et al. 2011; Barriopedro et al. 2014).

2.2.2 Correlation analysis

The Pearson coefficient has also been used to measure the linear correlation between two variables (Wilks 2011). Given variables x and y, the Pearson correlation is defined in Equation 2.4 as the ratio of the sample covariance of the two variables to the product of the two standard deviations.

$$r_{xy} = \frac{cov(x,y)}{s_x s_y} = \frac{n\sum x_i y_i - \sum x_i \sum y_i}{\sqrt{(n\sum x_i^2 - (\sum x_i)^2)(n\sum y_i^2 - (\sum y_i)^2)}} \quad (2.4)$$

2.2.3 Stepwise Regression Model

A Stepwise Regression Model (SRM) is a method of fitting regression where the choice of predictive variables is carried out by an automatic procedure (Bruce and Bruce 2017). SRM finds the combination of predictors that best explains the dependent variable (the predictand). There are three different approaches of stepwise regression (Bruce and Bruce 2017): 1) Forward selection, which starts with no predictors in the model and iteratively adds new predictors until the improvement is no longer significant; 2) Backward selection or backward elimination which on the contrary starts with all the predictors and iteratively removes the least contributive predictors; 3) Stepwise selection or sequential replacement, which is a combination of the other two, and is the strategy selected in this Thesis. Thus, the optimal combination of predictors is generated step by step, proceeding forwards and backwards (i.e., adding and removing explanatory variables) and retaining only those that increase the explained variance of the predictand by a significant amount. The resulting model was tested with a Fischer's test (Wilks 2011) at the 90% confidence level based on the sum of the residual squares.

2.2.4 K-means clustering analysis

Cluster analysis deals with separating data into groups whose identities are not known in advance. In particular, *K*-means clustering is a type of unsupervised learning, which is used to partition data into a given number of categories or groups, so-called clusters. It belongs to the nonhierarchical clustering methods (i.e., that allow reassignment). The goal of the method is to find groups in the data based on a metric of similarity, using a predefined number of

clusters N. The algorithm starts from a random seed of N clusters and works iteratively to assign each point to one of the N groups (Wilks 2011). Here, we use the Euclidean distance in the phase space as a measure of similarity. The algorithm moves iteratively items between clusters looking for minimizing the distance among points of the same cluster and maximize the distance among clusters. The K-means clustering algorithm yields: 1) The centroids of the N clusters (as inferred from the composited feature for all cases of the same cluster); 2) Labels for the data (all points are classified, and each point is assigned to only one cluster) (Wilks 2011).

2.2.5 Singular value decomposition

Given a rectangular matrix $[M]_{(n\,x\,m)}$ with at least as many rows as columns ($n \geq m$), the Singular Value Decomposition (SVD; Bretherton et al. 1992) of $[M]$ is the factorization (Jordan decomposition) of $[M]$ into the product of three matrices:

$$[M]_{(n\,x\,m)} = [L]_{(n\,x\,m)}\,[\Omega]_{(m\,x\,m)}[R]^{T}_{(m\,x\,m)} \tag{2.5}$$

where the m columns of $[L]$ are called the left singular vectors, and the m columns of [R] are called the right singular vectors. Hence both set of vectors are orthonormal ($[R][R]^T = [I] = [L]^T[L]$). The matrix $[\Omega]$ is diagonal, with only positive real elements that are called the singular values (eigenvalues) of $[M]$, herein the spatial structure in the n-space, while the product $[L][R]$ is equivalent to the associated time series (the projection onto the eigenvectors).

This method is often used to detect coupled patterns between two fields (e.g., sea level pressure and precipitation) and their temporal variation, with each pattern explaining a fraction of the covariance between the fields. Here, we have applied the SVD to the time series of four circulation indices with the aim of identifying coupled patterns among them.

2.2.6 Analogue method

The analogue method has been applied in weather forecasting (Lorenz 1969; Kruizinga and Murphy 1983), short-term climate prediction (Barnett and Preisendorfer 1978; van den Dool 1994, Vautard and Yiou 2012), detection and attribution of climate extremes to climate change (e.g., Stott et al. 2016 and references therein) and climate reconstruction (Howe and

Webb, 1983; Overpeck et al., 1985; Jackson and Williams, 2004; Wilmshurst et al., 2007; Guiot et al., 2008). The method identifies cases across space (i.e., between locations) and/or time (e.g., between temporal windows) with statistically similar ('analogous') features. Analogues are identified by minimizing a given distance metric. The method requires sufficiently long observations so that reasonably close analogues can be found. We have used "temporal analogues" to infer the near surface conditions during past events by searching for similar events in the present, in terms of the atmospheric circulation. In particular, we aim to reconstruct European climate anomalies (temperature, precipitation) by searching for flow analogues of past events in the 20th century. This approach provides the climate anomalies due to the dynamics, which in turn may have been internally or externally forced, but it does not account for changes associated to other factors (e.g., feedbacks).

The Root Mean Square Difference (RMSD; Equation 2.6) of the detrended seasonal mean geopotential height at 500 hPa over the Euro-Atlantic sector is used as a distance metric. Flow analogues are those that minimize the RMSD with respect to the target field. As similar atmospheric circulation can trigger different signatures in the surface climate, we pick the N best flow analogues, and their associated near-surface climate anomalies are then averaged.

$$RMSD = \sqrt{\frac{\sum_{i=1}^{i=ndir}(x_i - y_i)^2}{ndir}} \tag{2.6}$$

The validation of the analogue method is assessed by the Mean-Squared Skill Score (MSSS, Equation 2.7), which measures the improvement of the forecast as compared to a climatological prediction (Wilks 2011):

$$\mathrm{MSSS} = \left(1 - \frac{\mathrm{MSE}}{\mathrm{MSEC}}\right) * 100 \tag{2.7}$$

where MSE and MSEC represent the Mean Squared Errors based on the selected analogue and the climatological predictions, respectively.

2.2.7 Statistical significance

In this Thesis the statistical significance of the results was calculated with parametric and non-parametric tests. Bootstrapping is a statistical method for deriving the sampling distribution of an estimator from the full available dataset. The method was introduced in Efron (1979) and allow us to estimate quantities of a population by averaging estimates from multiple small data samples. For example, to assess the significance of a certain seasonal composite formed by n winters, random groups, with the same number of winters as those included in the composites that we want to test, are selected from the entire period and composited afterwards to generate a random distribution. The statistical significance (when indicated) has been assessed with a bootstrap test of 5000 random subsamples without replacement. The tested estimator is statically significant at the 90% (95%) confidence level whenever its value is below the 5th (2.5th) or above the 95th (97.5th) percentile of the resulting random distribution.

On the other hand, the Student's t-test is a parametric test based on the null hypothesis that two univariate random variables X and Y have equal means (von Storch and Zwiers 2003) The optimal test statistic is given by Equation 2.8:

$$t = \frac{\hat{\mu}_x - \hat{\mu}_y}{S_p \sqrt{\frac{1}{n_x} + \frac{1}{n_y}}} \tag{2.8}$$

where n_x and n_y are the sizes of the X and Y samples, $\hat{\mu}_x$ and $\hat{\mu}_y$ are the sample means, and S_p is the pooled estimate of the common standard deviation given by Equation 2.9:

$$S_p^2 = \frac{\sum_{i=1}^{n_x}(x_i - \hat{\mu}_x)^2 + \sum_{i=1}^{n_y}\left(y_i - \hat{\mu}_y\right)^2}{n_x + n_y - 2} \tag{2.9}$$

The null hypothesis is accepted if Equation 2.9 is less or equal than $t_{\alpha/2, n_x+n_y-2}$.

Finally, the statistical significance of the correlation between two time series is assessed using a Student's t-test (Equation 2.10). The null hypothesis is that the two samples are

independent, and it is accepted when the statistic *t* (Equation 2.10), is outside an interval defined by n-2 degrees of freedom:

$$t = \frac{|r|\sqrt{n-2}}{1-r^2} \tag{2.10}$$

Chapter 3

3. Directional Indices

This chapter describes to the methodology employed in the construction of indices of wind direction persistence over the English Channel for the 1685-2014 period and the quantification of their uncertainties.

3.1 Definition

This section aims to construct monthly wind Directional Indices (DIs) for the four cardinal directions (East, South, West, North) over the English Channel. They are defined as the persistence (in % of days) of each wind direction in a given month. The monthly percentage values of the DIs series are computed with respect to the total number of days of each month with at least one wind observation (calm and variable winds are included). However, we did not derive similar indices for calm and variable wind situations, since their relative frequency is too low (<1% of all wind records) to derive meaningful series.

The first step is to assign the prevalent direction of each day to one of the 45º-wide half quadrants, with easterly days corresponding to wind direction in the sector [45, 135)º from the true north in a wind rose. Bearing in mind that there are often several wind observations per day, we adapted the "unidirectional" procedure described in Barriopedro et al. (2014) in order to classify each day in one wind direction. Thus, when only one daily observation was available, the day was classified taking the wind direction of that single observation. If several observations per day were available, a minimum percentage p_d of the total number of observations of that day with *d* wind direction was demanded to classify it as a *d*-wind day (with *d* denoting northerly, easterly, southerly or westerly).

To determine the optimum p_d thresholds, we obtained for each wind direction two types of DIs series, both defined as the percentage of *d*-wind days in the month but based on different thresholds and number of observations. Thus, for each *d* direction, we first derived a suite of *d*-wind series (DI_p), each one based on a different p_d threshold among those ranging between 5% and 95%. For example, a p_d threshold of 50% would mean that a day would be classified as a *d*-wind day if at least 50% of the wind observations of that day over the English

Channel exhibit a d direction. Note that the same day can be classified in several different directions (more likely for low thresholds) or unclassified (if too demanding thresholds are adopted). Second, 1000 "degraded" d-wind series (DI_r) were constructed for each d direction by taking randomly only one of the wind observations available each day. Note that DI_p series are obtained using all observations but variable thresholds, whereas DI_r series are all based on only one wind observation per day and hence do not require any p_d threshold. Finally, each DI_p series was correlated with the 1000 DI_r series to determine the optimal thresholds (those that maximize the correlation with the series constructed from one observation per day). In addition to providing objective criteria for the definition of the DIs, this approach aims at minimizing the effects of the increasing number of daily observations over the English Channel (Figures 2-2b. 2.3a in Chapter 2). As the period 1685-1850 displays only one wind observation per day (as abstracted from the ships' logbooks), the correlation analysis has been applied to the period 1851-2014, which has a high frequency of multiple daily observations, as well as to different chunks of that period in order to check the sensitivity of the derived thresholds to the number of observations.

Figure 3.1 shows the ensemble of correlations as a function of p_d for each d direction. The correlations are statistically significant ($p<0.01$) for all directions and p_d thresholds but they reach a maximum within an ample interval of p_d values that ranges between 25 and 50%, depending on the wind direction. The results are similar (albeit with slightly different magnitudes) if the correlations are computed over periods with different number of daily observations in the English Channel (colored shading in Figure 3.1). The highest correlations are observed for the 1851-1900 sub-period due to the lower number of observations available, which reduces the variability across the randomized series. As a consequence, the resulting series are not sensitive to a small change in the p_d thresholds, which, in turn, do not strongly depend on the total number of daily observations within the English Channel. In spite of this, Figure 3.1 suggests slightly different optimal thresholds for different wind directions, with higher (lower) thresholds for zonal (meridional) wind indices. Thus, different but close p_d thresholds have been adopted for each wind direction, namely 36%, 44%, 37% and 45% for northerly, easterly, southerly and westerly, respectively.

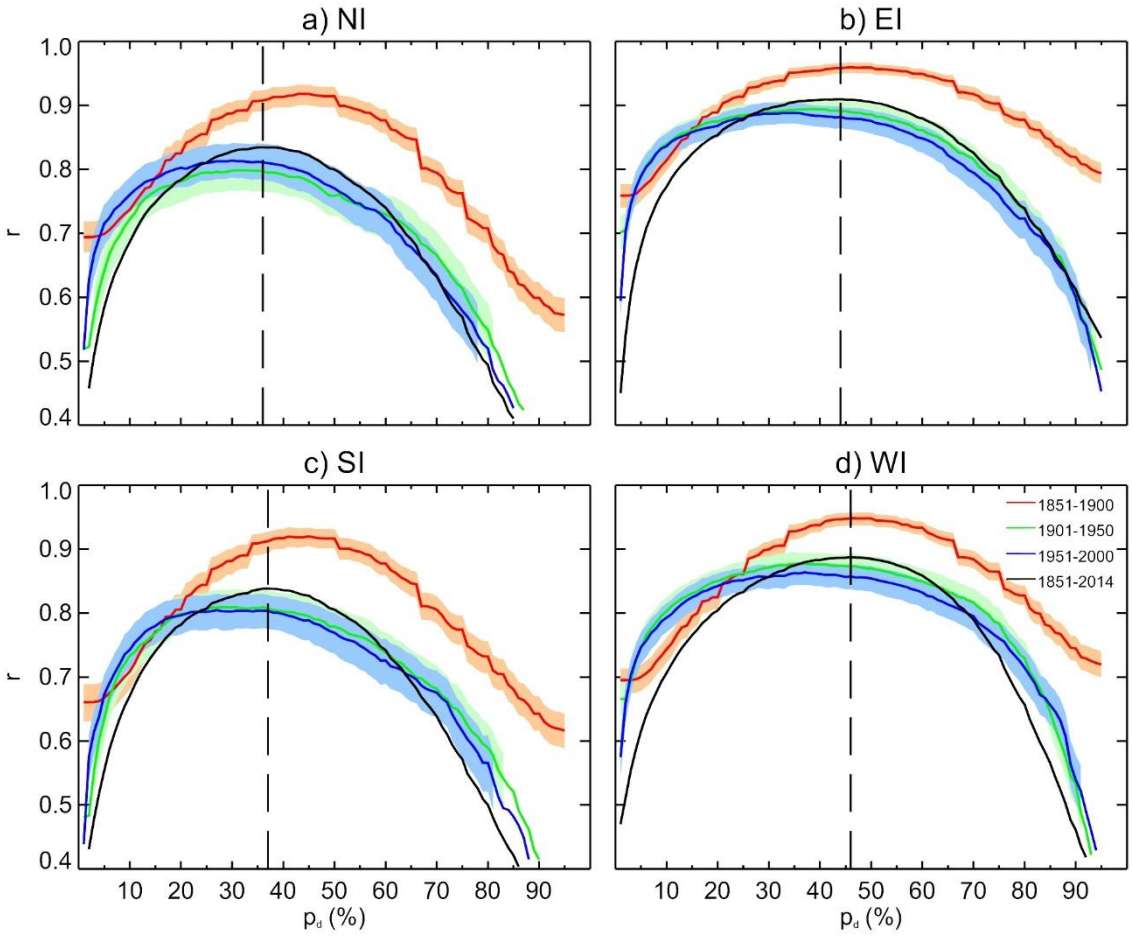

Figure 3.1 Averaged correlations between 1000 randomly degraded DI_r series computed with only one wind record per day and the DI_p series computed from a minimum percentage p_d (x-axis, ranging from 1 to 95%) of wind records with a d-wind direction over the English Channel: a) NI; b) EI; c) SI and; d) WI. Lines (shading) indicate the mean correlation (full range of correlations) obtained from the 1000 random DI_r series for different sub-periods (see legend). The vertical dotted line identifies the p_d threshold value adopted for each DI.

Note that establishing minimum p_d thresholds can lead to undefined days (those that are not classified in any wind direction) and conflicting days (if the thresholds of two wind directions are both exceeded) (Figure 3.2). However, undefined and conflicting situations are relatively uncommon, both occurring roughly 6.0% of the days for the full period. The cumulative frequency of these days growths steadily after 1850 (when multiple wind direction observations are available), being zero before. Recurrent conflicts involve the westerlies (in particular days classified simultaneously as westerlies and southerlies, which occur 2.2% of the time on average, dark yellow line in Figure 3.2), as expected from the dominant south-westerly wind direction in the English Channel (Barriopedro et al. 2014). In order to solve conflicting days, we relied on the amount of exceedance of the d-wind relative frequency above its p_d threshold. Accordingly, if one day is classified in several wind directions, the

following sequence of criteria was established: i) the day is assigned to the wind direction with the largest exceedance value (i.e., the one whose percentage of occurrence for that day exceeds by the largest amount its respective threshold p_d); ii) if two wind directions display the same exceedance value, the day is classified in the wind direction with the largest absolute frequency. The above criteria efficiently disentangle all types of conflicts between two directions, leaving only 1.2% from total number of days unclassified. Other approaches (e.g., using the same p_d thresholds for all wind directions) led to a less efficient treatment of conflicts always remaining conflict days after its application (~ >2% from the total number of days; not shown).

Note that criterion i) might not assign the day to the most frequent wind direction of that day, although this situation was rare given that $p_d$values are pretty close for all directional indices. While the above implication might be counterintuitive, it is supported by Figure 3.1, which displays decreasing correlations when thresholds exceed ~50%. As a consequence, percentages of occurrence that would still be optimal for some wind directions (e.g., zonal winds) would result too demanding for others (e.g., meridional winds). On the other hand, we stress that the possibility of having only two observations in a day with discording wind directions has already been addressed when merging the ICOADS and logbooks series (Chapter 2). If this situation would have occurred (i.e. 50% of wind observations in each wind direction), criterion i) would systematically classify the day in the wind direction with the lowest threshold, artificially biasing the frequency series of the zonal (meridional) winds towards lower (higher) values. That problem would not be solved by using wind-invariant thresholds, either.

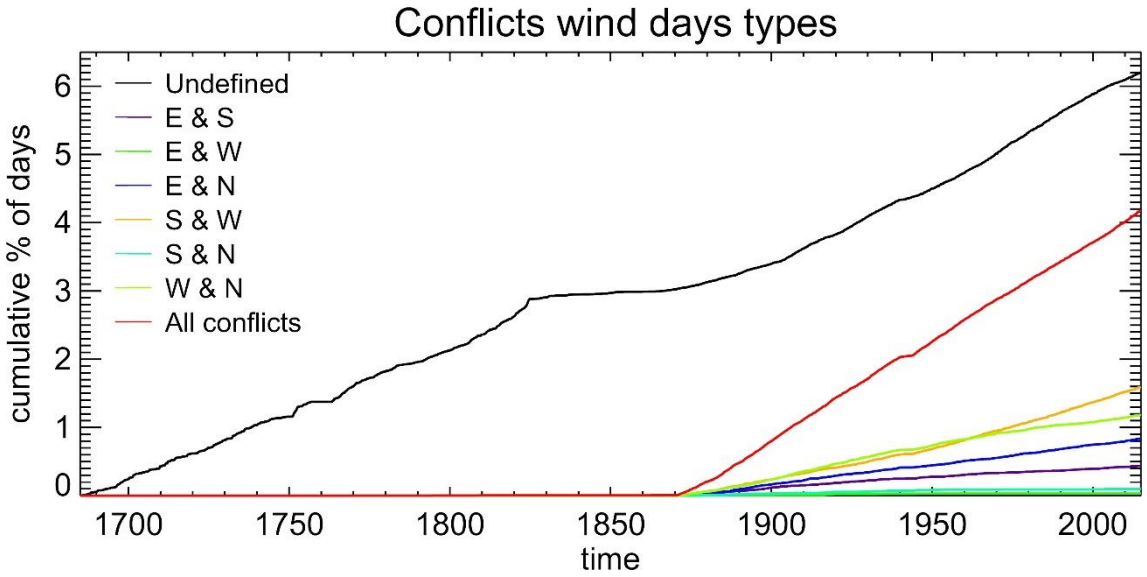

Figure 3.2 Annual time series of the accumulated frequency of different types of conflicts and undefined wind days (in % with respect to the total number of days of the analyzed period).

The resulting monthly series of wind persistence will collectively be referred to as DIs, or as NI, EI, SI and WI (northerly, easterly, southerly and westerly index, respectively) when we refer to a given wind direction. The monthly time series of the DIs are considered meaningful when at least two thirds of the days in the month had at least one wind observation (otherwise, the month was labelled as missing). Similarly, seasonal mean time series are computed from the monthly time series only when the three months had non-missing values.

3.2 Uncertainty

In the construction of the DIs, we also quantified the uncertainty associated with each DI due to the limited number and spatial coverage of observations. The algorithm is based on the total number of wind records available in the month and performs iteratively over 1965-2014, which is the period with the largest number of observations:

1. For the calendar month $\boldsymbol{m}$ and year $\boldsymbol{y}$ of the 1965-2014 period we pick an initial random seed of $\boldsymbol{n = n_i = 10}$ observations among those available at that time. Note that this subset is randomly distributed both in time (i.e. through the entire month) and space (i.e., across the English Channel). Subsequently, the DIs series are computed from the selected observations, as explained in Section 3.1.

2. In a next step, one new random observation is added to the original subset, and the DIs series are computed with the new sample of $\boldsymbol{n = n_i + 1}$ observations. This step is repeated until $\boldsymbol{n = n_f = 500}$.

3. The process (steps 1 and 2) starts again with a new seed of $\boldsymbol{n_i}$ observations for that month and year, repeating the whole procedure until 500 different initial samples of $\boldsymbol{n_i}$ observations have been created and seeded up to $\boldsymbol{n = n_f = 500}$.

4. For each number n of monthly observations, we compute the standard deviation $\boldsymbol{\sigma_d}$ of the 500-trial DIs values of that month and year.

5. To avoid biasing the uncertainties to the chosen year, the algorithm then moves to the next year y+1 of the calendar month m and so on until all years have been selected. In that way, the estimated uncertainty of the DIs series varies with time as a function of the number n of observations of the month m:

$$s_d(n, m) = \pm\sqrt{\sum \sigma_d^2/N} \tag{3.1}$$

where s is the population variance over the 1965-2014 period and N the number of years.

Figure 3.3 shows the distribution of the uncertainty associated with the DIs series for each season (colored lines) as a function of the total number of monthly observations. The magnitude of the uncertainties is similar for all DIs series and seasons and decreases with n to minimum values of about 11%, which are easily reached with a relatively low number of observations (about three observations per day throughout the month on average). The asymptotic behavior of the distributions indicates an unavoidable uncertainty in the exact DIs values due to the spatial variability of the wind direction across the English Channel.

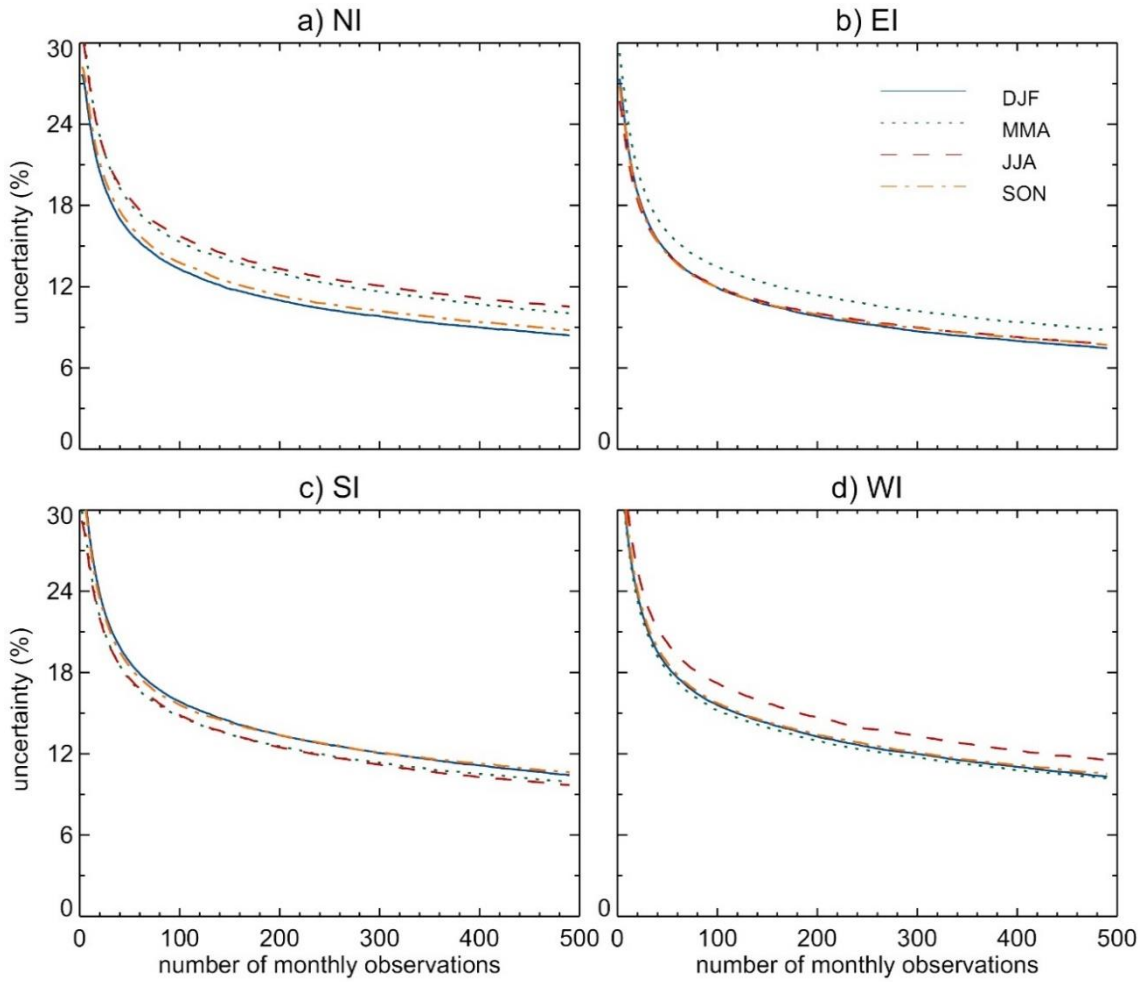

Figure 3.3. Distribution of estimated uncertainties of the DIs as a function of the total number of monthly observations (in percentage of days in the month): a) NI; b) EI; c) SI and; d) WI. Colored lines represent the four seasons (see legend in panel b).

3.3 Homogeneity

Figure 3.4 shows the seasonal series of the four DIs for the 1685-2014 period, along with the estimated uncertainty. A homogeneous climate time series is defined as that where variability is only caused by changes in weather or climate (Freitas et al. 2013). Hence, once the DIs series were constructed, a homogeneity test was performed. The objective here is to validate the robustness of the methodology against changes in the underlying data, rather than adjusting (correcting) the detected shifts. There are several methods to evaluate the homogeneity of climatic time series (Peterson et al. 1998; Li et al. 2003; Costa and Soares 2009; Cao and Yan 2012). Two groups of testing techniques can be distinguished and are usually referred to as “absolute” and “relative” methods; in the former, statistical tests are

applied to each series separately, whereas the latter use records from neighbor references, which are assumed to be homogeneous. Herein, relative testing is not possible and hence we use absolute tests (which use only the single series to be tested).

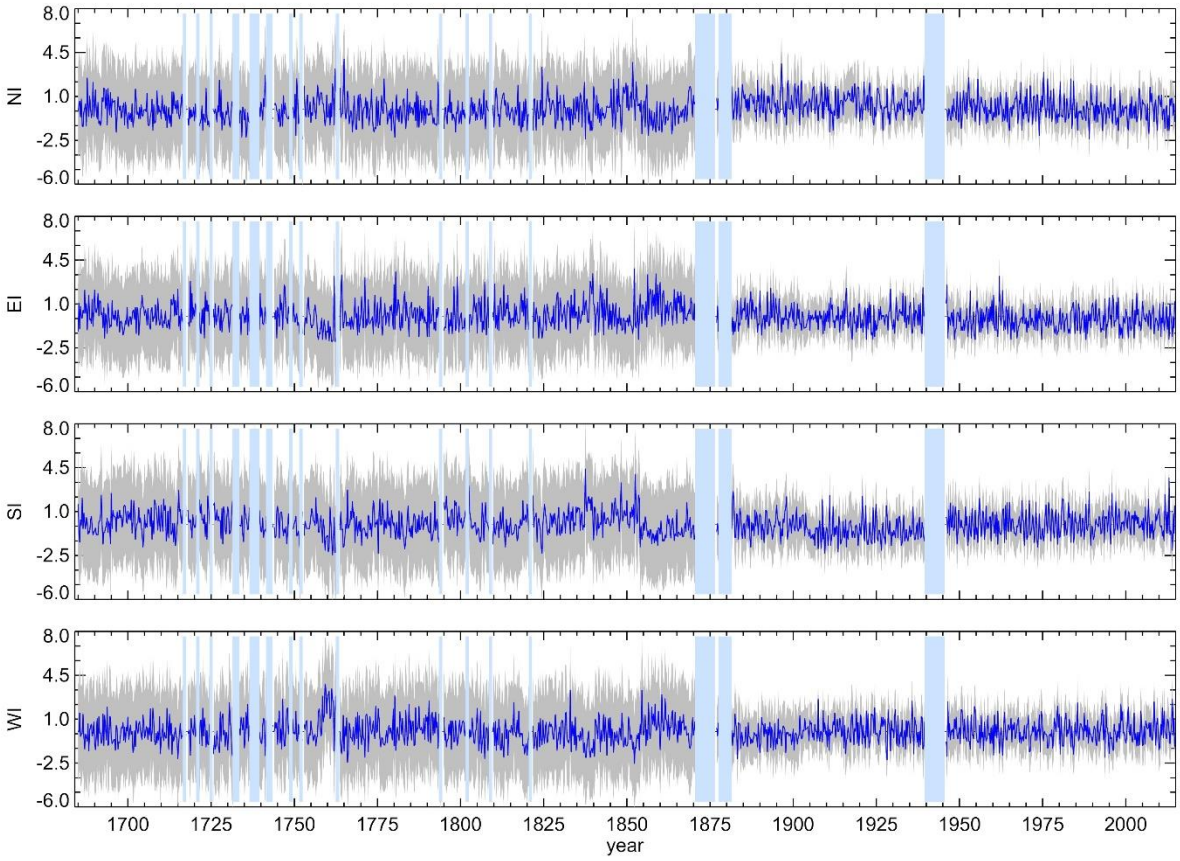

Figure 3.4. Standardized seasonal series of DIs for 1685-2014 (blue line) with the associated uncertainty (grey shading, ± sigma). Vertical blue bars indicate years with at least one missing month**.**

There are not many statistical procedures for dating a discontinuity in isolated series (e.g., Rhoades and Salinger 1993; Zurbenco et al. 1996; Tomé and Miranda 2004), and some of them assume that suspicious breakpoints are known *a priori*. In absolute methods, inhomogeneities are difficult to distinguish from real climate variations, and hence any adjustment would involve large uncertainty and a degree of subjectivity. In particular, such an approach might accidentally remove real long-term trends in the series. Despite this, in the case of the DIs, absolute testing has the advantage of detecting and dating potential inhomogeneities for each DI series separately. If some of the detected change points are common to all DIs, confidence must be given that they identify inhomogeneities in the data sources (changes in the type, number or characteristics of wind observations). For that reason,

potential inhomogeneities detected in the DIs will not be corrected, unless they are robust across all DI series.

We have applied a modified version of the statistical test from Zurbenco et al. (1996) for detecting stepwise shifts in the mean. The test does not require a prior knowledge of the number and location of breakpoint candidates, so one can estimate later if changes in the underlying data are amongst the detected shifts. The algorithm uses intervals of different length in running windows with the aim of identifying the most prominent change points (potential breakpoints) in the series. The method assumes that there is at least one shift present in the series and is able to determine the more likely number of breaks and to allocate their timing (i.e., it is a location-specific test). To find the most prominent *k* change-points, the algorithm performs as follows:

- We seek a random partitioning set of the series with break locations at $\boldsymbol{t_1 < t_2 < \cdots < t_k}$ $\boldsymbol{(1 < t_1, t_k < N}$, with N being the length of the series), which determine k+1 periods with mean values $\boldsymbol{\mu_1, \mu_2, \ldots, \mu_{k+1}}$. We demanded a minimum separation of 10 years between a change point and the next to avoid detecting extreme interannual variations (Peterson et al. 1998). Then, the residuals are created by subtracting the $\boldsymbol{k + 1}$ means to the series over the corresponding period.

- For a given *k* value, the optimal partitioning set (i.e., the break locations) is that minimizing $\boldsymbol{SC}$ (Equation 3.2), as determined by the Schwarz Criterion (Schwarz 1978):

$$SC(k) = \frac{N}{2} \ln \sigma_k^2 + k \ln N \tag{3.2}$$

where k is the number of breakpoints, N is the sample size of the series, and σ_k^2 (Equation 3.3) is the variance of the residuals (i.e., the residual sum of squares, RSS):

$$\sigma_k^2 = \sum_{t=1}^{t_1} (x_t - \mu_1)^2 + \sum_{t=t_1+1}^{t_2} (x_t - \mu_2)^2 + \cdots + \sum_{t=t_{k+1}}^{n} (x_t - \mu_{k+1})^2 \tag{3.3}$$

- **SC** is computed for a range of $\mathbf{k = 1, \dots, K}$ change points, with the minimum of the resulting $\mathbf{SC(k)}$ distribution (i.e., $\mathbf{\min_{k=1,\dots,K} SC(k)}$) determining the optimal number of breaks. Due to the time-consuming computations required to determine all possible combinations of the k break positions in our series ($\mathbf{N = 330 \times 12}$), we assumed that the potential number of discontinuities in the DIs series does not exceed $\mathbf{K = 10}$.

Figure 3.5 shows the distribution of $SC(k)$ for each DIs series. The minima are often reached for two-to-three potential change points, depending on the wind direction, and the corresponding locations are displayed in the respective panels. Potential breakpoints tend to be homogenously distributed throughout the study period. Only the EI and SI present common shifts around ~1854 and ~1853 respectively.

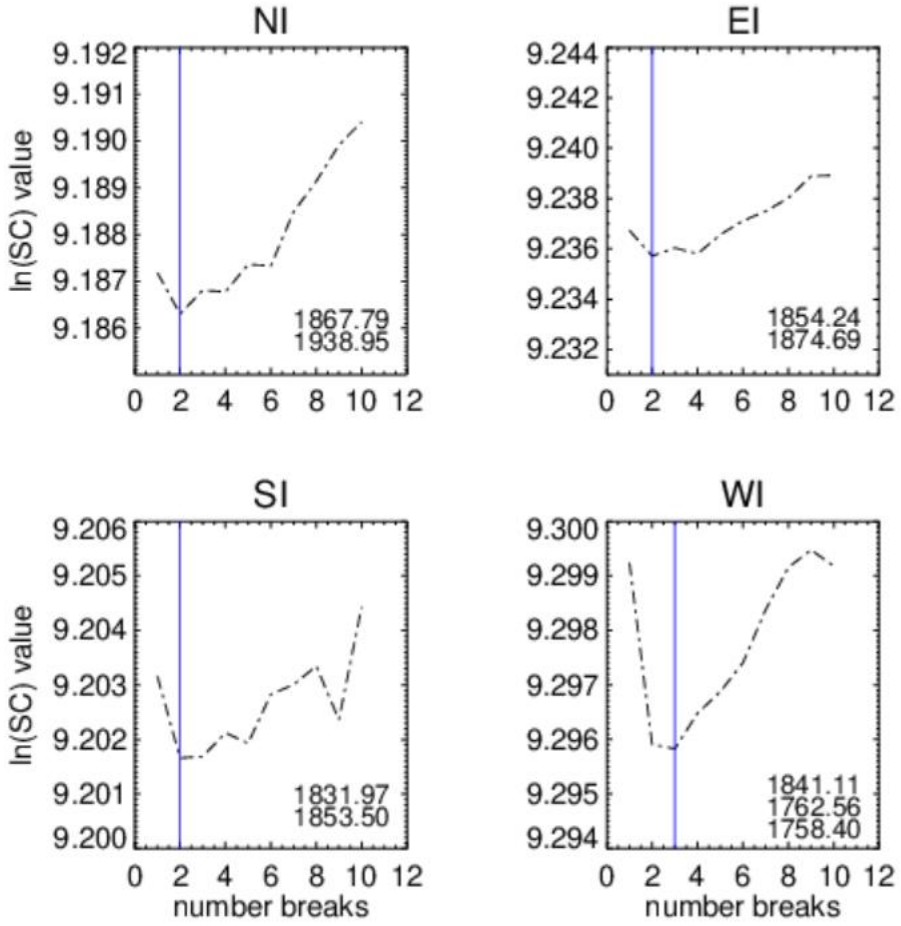

Figure 3.5. Distribution of the SC parameter value as a function of the number of breakpoints in the monthly DIs time series for the 1685-2014 period. The vertical blue line denotes the optimal number of breakpoints in the corresponding DI series, with their locations shown in the lower right corner of each panel.

Nonetheless, there are no apparent reasons to suspect that these shifts correspond to artificial changes in the series because: i) the same standards were used in the abstraction of logbooks through the 1685-1870, and the number of ICOADS observations by that time was negligible; 2) The closest shifts in the other DIs (WI and NI) occur more than 10 years before and after the mid-1850s, and with a 26-year lag between them (1841 and 1867, respectively). Although these potential breakpoints are close to the end of the logbooks input record and to the beginning of a strong presence of ICOADS in the full series, they could be related to the high frequency of missing data (Figure 2.3b), to an unavoidable bias of ships observations to specific spatial locations, or simply to decadal variability. Concerning the latter, previous studies have argued that the mid-19th century was a period of profound atmospheric circulation changes (Jacobeit. et al. 2003; Slonosky et al. 2001; Küttel et al. 2011), and hence the breakpoints might simply reflect a real climate shift.

3.4 Conclusions

By combining daily wind direction observations from ships over the English Channel, four instrumental indices of the North Atlantic atmospheric circulation have been derived for the 1685-2014 period. The main conclusions are listed next:

- A comprehensive methodology has been developed in order to abstract information from ships' logbooks and merge it with ships observations from ICOADS, taking into account the change in the number of daily observations with time. They provide an almost continuous record of wind direction observations over the English Channel through the 1685-2014 period.

- All wind direction data have been subject to an exhaustive statistical treatment to obtain the representative wind direction over the English Channel in a four quadrant for each day of the analyzed period, as well as to avoid the classification of the same day in two different directions.

- The resulting time series provide the monthly persistence of the wind in the four main directions: northerly, easterly, southerly and westerly. These DIs are not critically sensitive to the number of daily observations in the English Channel or the specific thresholds and criteria adopted in the methodology.

- A methodology to quantify the uncertainty due to the number of available observations was performed. All DIs exhibit similar uncertainties all-year round, which decrease from ~20% to ~10% through the analyzed period.

- Finally, a homogeneity test to detect possible shifts in the time series related to changes in the underlying data has been designed. There are no potential discontinuities common to all DIs. The DIs can thus be considered a homogeneous record of wind direction persistence over the English Channel.

The DIs developed following this methodology are the longest and highest resolution instrumental indices of atmospheric circulation over the North Atlantic currently available. These series do not require calibrations or corrections, nor do they suffer from the uncertainties associated with proxy reconstructions, providing an excellent framework to study the European climate from monthly to centennial time scales.

Chapter 4

4. Atmospheric circulation over the Euro-Atlantic sector since 1685

The DIs are the longest observational record of atmospheric circulation to date, and provide high-resolution (monthly) information of the atmospheric circulation over the eastern Atlantic Ocean all year-round. This allows us providing new instrumental-based insights into the Euro-Atlantic climate variability for the last three centuries. This Chapter is devoted to characterize the DIs' signals in the Euro-Atlantic atmospheric circulation and the European surface climate, and to exploit this information to better understand the past climate and its evolution since the 17th century, including the response to some external forcings of the pre-industrial period and the characterization of anomalous periods on different time scales (from monthly-seasonal extreme events to long-term trends). The main results can be found in Mellado-Cano et al. (2019a) (under review).

4.1 Climatological signatures

The climatological (1685-2014) annual mean values of the DIs are 19.1%, 18.7%, 21.5% and 34.6% for NI, EI, SI and WI, respectively. The predominance in the region of westerly and southerly winds is due to the geographical location of the atmospheric action centers (AH and IL) in the North Atlantic, which are aligned through a SE-NW direction throughout most of the year. This imprints a characteristic SW-NE tilt in the eddy-driven jet stream (e.g., Woollings et al. 2010) and favors south-westerly winds over the English Channel. The dominance of westerly and southerly winds is also observed throughout the year, on monthly (Figure 4.1a) and seasonal scales (Figure 4.1b). However, there are differences in the seasonal progression of zonal (i.e., WI and EI) and meridional (i.e., NI and SI) indices. Figure 4.1 displays the annual cycle of the DIs for the period 1685-2014. Zonal indices present a more pronounced annual cycle than meridional indices, with a maximum (minimum) in July for the WI (EI). This is due to a seasonal shift in the location of the North Atlantic action centers in summer, when they become located along the same meridian, inducing a westerly veering of the winds over the English Channel. The resulting increase of the WI (i.e., enhanced

persistence of the westerlies) is compensated by declines in the frequency of the other DIs, particularly in the SI and EI, which reach a minimum in this season.

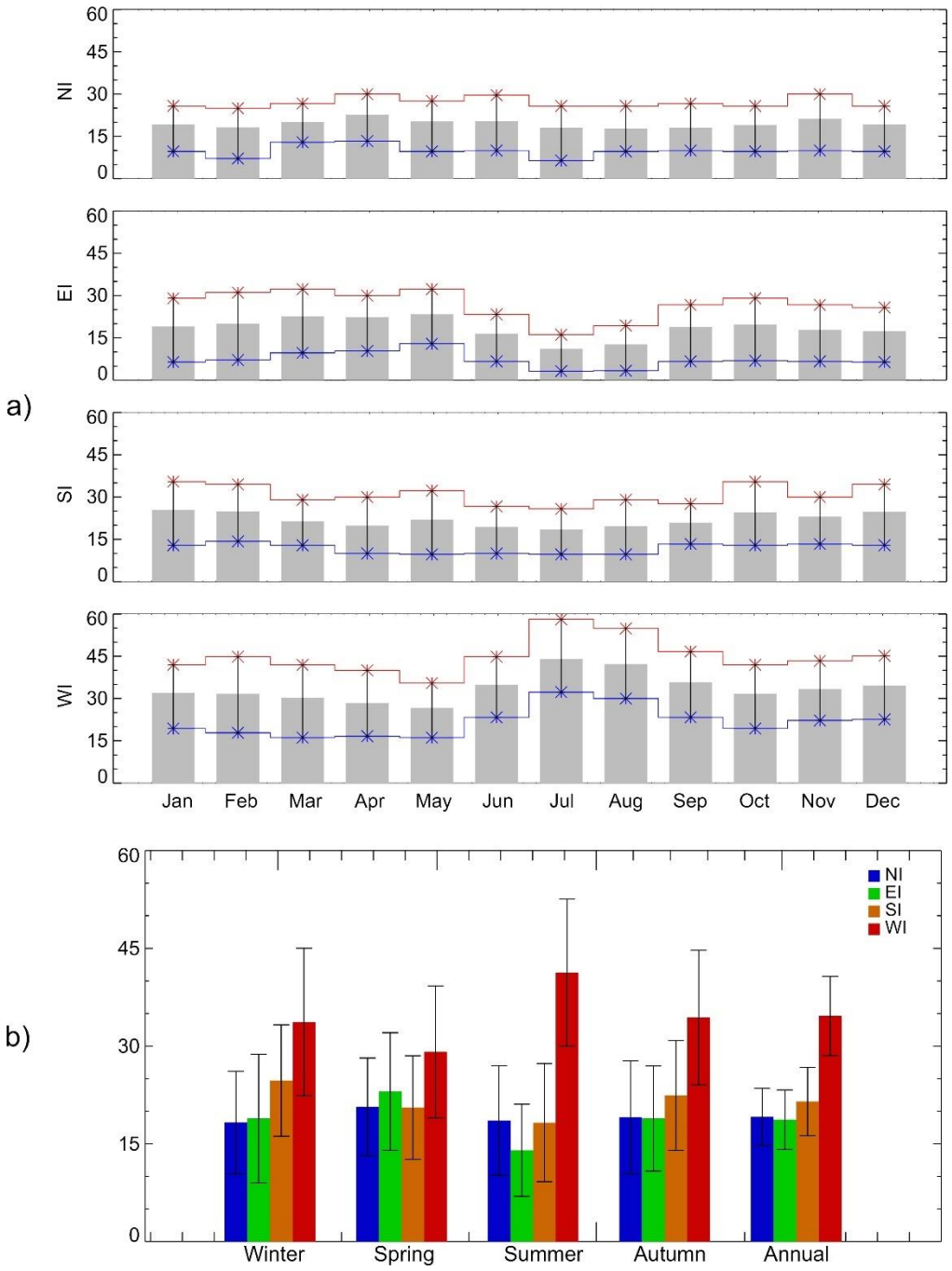

Figure 4.1. a) Annual cycle of the DIs for 1685-2014, expressed in percentage of days of each month with wind blowing from that direction. Red (Blue) lines indicate the 75th (25th) percentile; b) Seasonal and annual mean values of the DIs for 1685-2014, expressed in percentage of days of the month with wind blowing from that direction: NI (blue), EI (green), SI (orange) and WI (red) with error bars indicating the ± 1 sigma interval.

4.2 The impact of the DIs on the European climate

Before exploring the DIs series for the 1685-2014 period, we have analyzed their signatures on the Euro-Atlantic climate variability to better understand the climate implications during periods of anomalous DIs, which will be described in Section 4.3. We have used monthly near surface temperature from the CRU TS v3.23 (Harris et al. 2014) and total monthly precipitation from the GPCC (Schamm et al. 2014) on a grid of 1ºx1º longitude-latitude over land and for the period 1901-2014, as described in Section 2.1.2.1. To interpret the temperature and precipitation anomalies, the following meteorological fields were computed at 2ºx2º resolution from the 20CR V2c (Compo et al. 2011; Section 2.1.2.2): (1) the vertically integrated moisture transport through the 1000–500 hPa layer; (2) the moisture convergence between 1000 and 500 hPa; (3) temperature advection at different pressure levels and; (4) the storm-tracks, as defined in Chapter 2.

The relationship of DIs with the Euro-Atlantic climate variability has been assessed on seasonal scales for the period 1901-2014, with winter and summer denoting December-to-February and June-to-August, respectively. For each season and DI we identified the years with positive and negative phases, defined from seasonal-mean DI values above 1 and below -1 SD, respectively. This provides a balanced and sufficient number of cases, from which we constructed DI-based composites for each phase, and their difference. The composited fields have been scaled, so that they are dimensionless (see Section 2.2.1 in Chapter 2). The significance of the composite difference was calculated at the 90% confidence level for each grid point using a bootstrap test (Section 2.2.7) with 1000 iterations, in which the same number of years as in the composites was selected randomly from the 1901-2014 period.

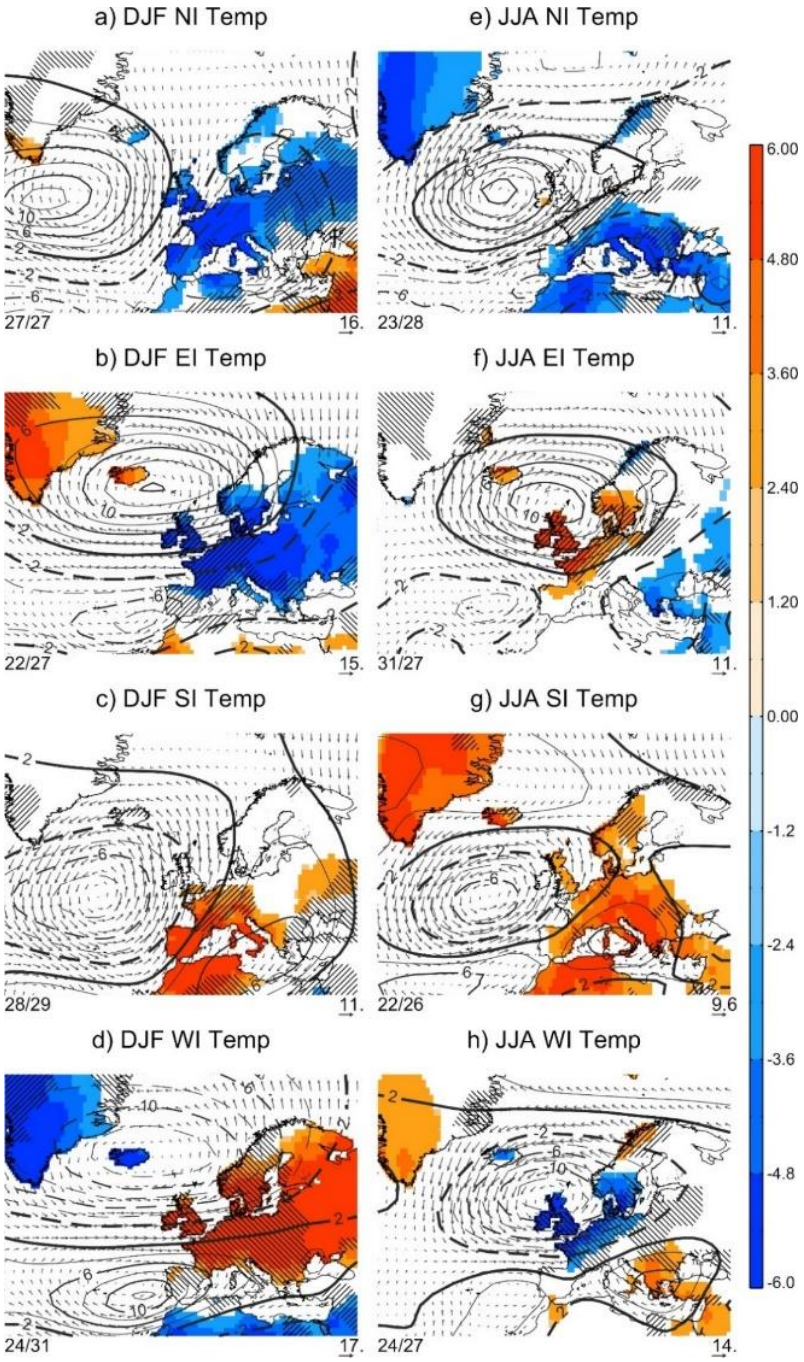

Figure 4.2. Winter (a-d) and summer (e-h) differences between scaled anomaly composites for high (>1 SD) and low (< -1 SD) DIs. The following variables are shown: geopotential height at 500 hPa (Z500, contours), land near-surface temperature (shading), 500 hPa wind (arrows) and 500 hPa temperature advection (hatching). All units are dimensionless. Solid (dashed) contours represent positive (negative) values, with thick lines indicating significant differences from climatology at $p<0.1$. Only temperature differences that are significant at $p<0.1$ are shown. Cross-hatched areas with lines orientated 45º/-45º from the east indicate significant ($p<0.1$) warm/cold temperature advection. The size of the arrows is proportional to the magnitude of the 500 hPa wind anomaly (a reference value is shown in the bottom right corner of each panel). For better readability, hatched areas (arrows) are only displayed over land (ocean). Numbers in the left bottom corner of each panel represent the number of cases employed in the composite for high / low DIs. Significance is assessed with a 1000-trial bootstrap test.

Figures 4.2 and 4.3 show the scaled composite differences of temperature-related and precipitation-related variables, respectively, along with the associated atmospheric circulation for each DI for winter and summer. Figures 4.4 and 4.5 displays spring and autumn season. The results reveal nearly opposite signals for the zonal indices (WI and EI) in both temperature and precipitation, and the same behavior is observed for the meridional indices (SI and NI). Overall, zonal DIs tend to show larger anomalies and/or affect larger areas of northern and central Europe than meridional DIs, due to their more prominent effect on temperature and moisture advection (shown by arrows and hatching in Figures 4.2-5). More importantly, the signatures of zonal and meridional DIs are spatially complementary all year-round.

Regarding the seasonal impacts, the largest signals are obtained in winter (Figures. 4.2a-d and 4.3a-d), when near-surface responses are strongly controlled by the dynamics (Vautard and Yiou 2009). The temperature responses vary seasonally, being qualitatively similar within the cold (winter and autumn, Figures. 4.2a-d and Figures. 4.4e-h) and warm (spring and summer, Figures. 4.4a-d and Figures. 4.2e-h) half of the year. In particular, the temperature signal associated with anomalous zonal winds in winter (Figures 4.2b, d) reverses in summer (Figs. 4.2f, h), despite the smaller spatial scale anomalies observed in the latter. These temperature responses cannot be fully interpreted by the small changes in thermal advection (arrows in Figs. 4.2f, h), suggesting an additional role of other processes (e.g., radiative fluxes; see Barriopedro et al. 2014). On the contrary, the precipitation responses show a more similar spatial pattern in all seasons (compare left and right panels in Figure 4.3 and Figure 4.5), indicating a major role of the wind direction in modulating moisture advection and convergence throughout the year.

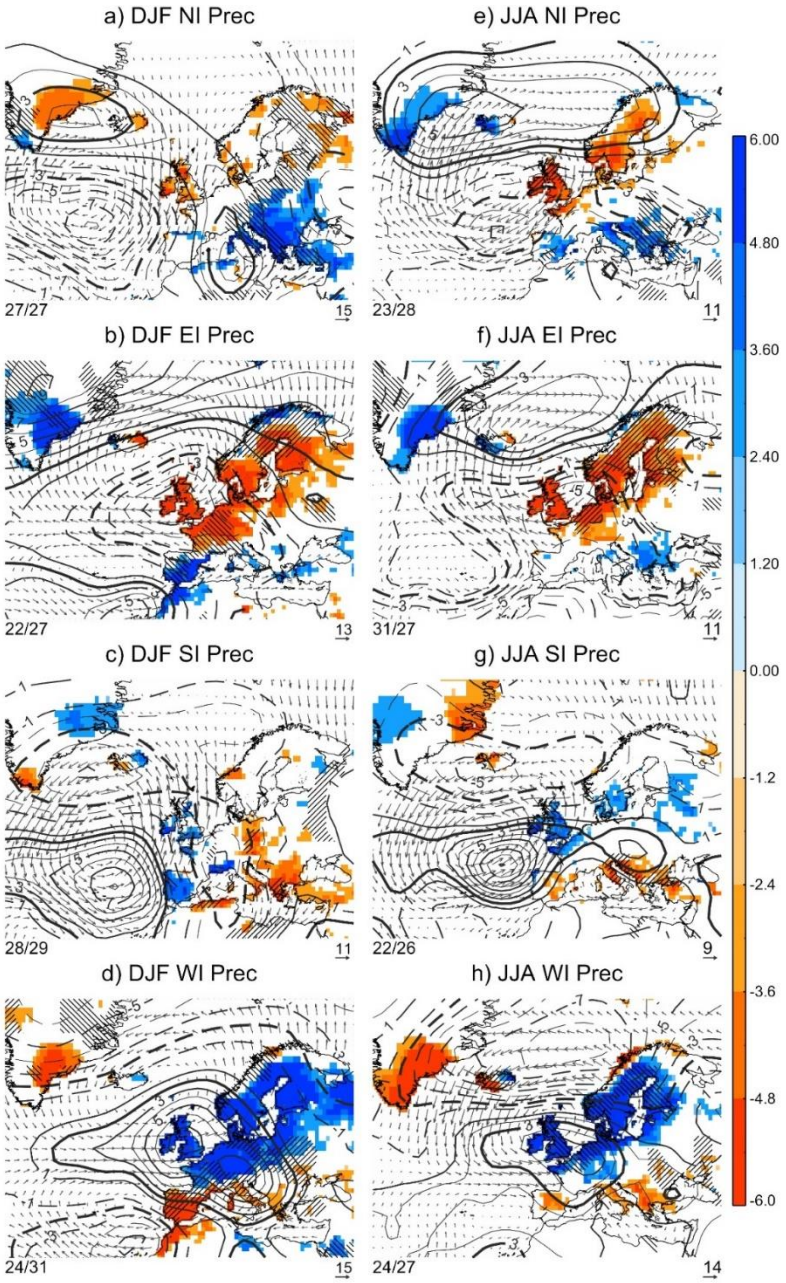

Figure 4.3. As Figure 2 but for the following variables: storm tracks (2–5 high pass filtered Z500 variance, contours), land precipitation (shading), 1000–500 hPa vertically integrated moisture transport (arrows) and 1000–500 hPa moisture convergence (hatching). All units are dimensionless. Solid (dashed) contours represent positive (negative) values, with thick lines indicating significant differences from climatology at $p<0.1$. Only precipitation differences that are significant at $p<0.1$ are shown and gridpoints with climatological mean precipitation below 10 mm are omitted. Cross-hatched areas with lines orientated 45º/-45º from the east indicate significant ($p<0.1$) moisture divergence/convergence. The size of the arrows is proportional to the magnitude of the moisture transport anomaly (a reference value is shown in the bottom right corner of each panel). For better readability, hatched areas (arrows) are only displayed over land (ocean). Numbers in the left bottom corner of each panel represent the number of cases employed in the composite for high / low DIs. Significance is assessed with a 1000-trial bootstrap test.

Focusing now on the atmospheric circulation, the results show that the DIs anomalies reflect a reorganization of air masses on large spatial scales, embracing the whole Euro-Atlantic sector (contours in Figures 4.2 and 4.3), which explains their associated impacts over large areas of Europe. Enhanced westerlies show a meridional dipolar pattern in geopotential height, with negative anomalies at higher latitudes and positive ones in subtropical regions (Figure 4.2d, contours) as well as increased storm-track activity affecting most of northwestern and central Europe (Figure 4.3d, contours). These patterns resemble the positive phase of the NAO (Trigo et al. 2002) and are nearly opposite to those found for persistent easterlies (Figures 4.2b, 4.3b). In summer, the anomaly centers in geopotential height associated with WI and EI tend to shift equatorward and become spatially more confined (Figures 4.2f, h), still resembling the high-summer NAO (Bladé et al. 2012). In fact, WI and EI are significantly correlated with the NAO index of Jones et al. (1997) in winter (r_{WI} = 0.73 and r_{EI} = -0.60, both $p<0.01$), and with the summer NAO index of Folland et al. (2009) (r_{WI} = 0.63 and r_{EI} =-0.43, both $p<0.01$) for the period 1901-2014. In spite of this, the DIs and the NAO measure different aspects of the circulation (wind direction vs wind speed) and therefore their associated impacts and skills as predictors are different, as will be shown later. On the other hand, the meridional wind indices are associated with a zonally oriented dipolar pattern in geopotential height, largely dominated by an anomaly center over the mid latitudes of the Atlantic Ocean (i.e., south of the main axis of the storm tracks, Figures 4.2a, c). As such, their largest impacts are recorded in temperature, with enhanced northerlies (southerlies) being associated to high (low) pressure systems over the Atlantic that cause widespread cooling (warming) over Europe. During summer (Figures 4.2e, g), the dominant anomaly center in geopotential height shifts towards Europe and stretches meridionally, affecting the spatial extension of the surface anomalies.

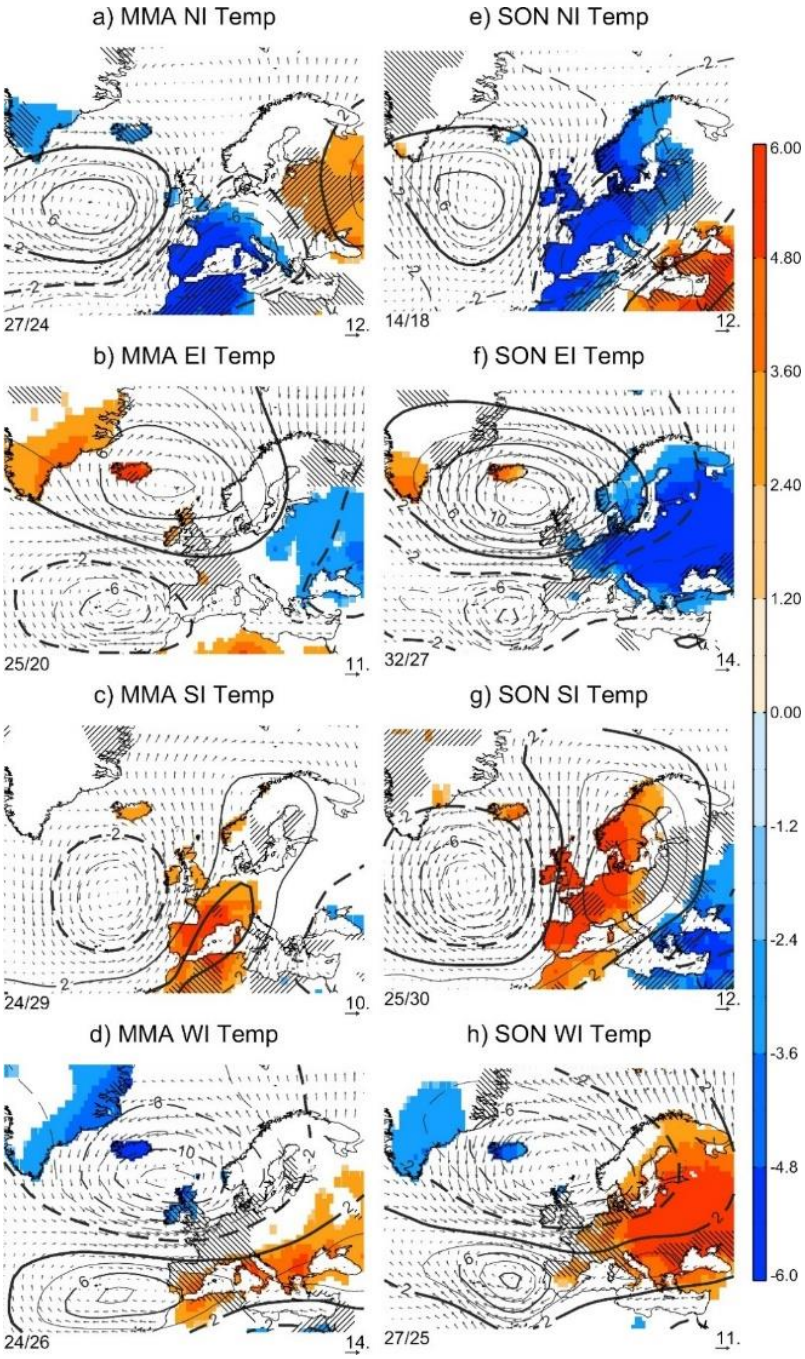

Figure 4.4. As Figure 4.2 but for spring (a-d) and autumn (e-h).

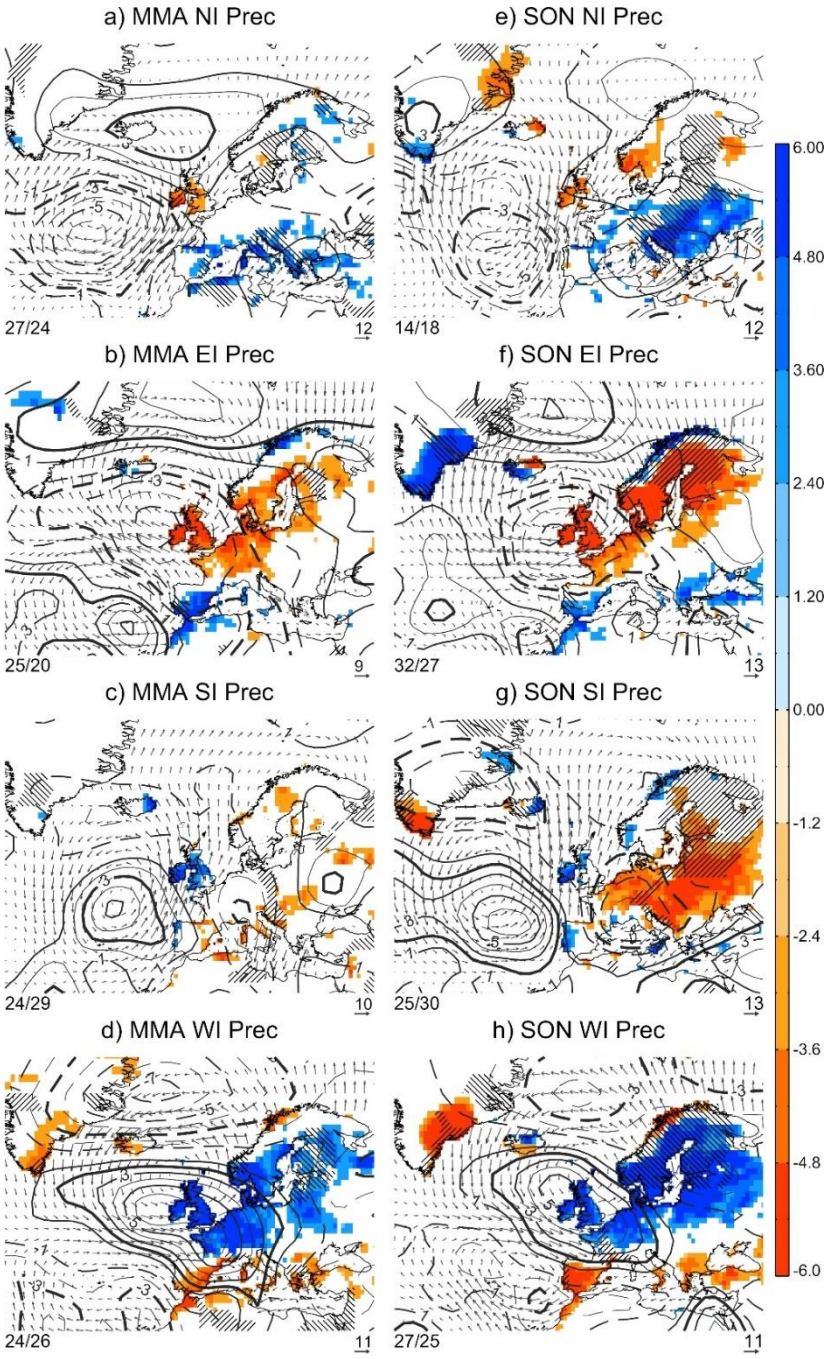

Figure 4.5. As Figure 4.3 but for spring (a-d) and autumn (e-h)

The distinct spatial signatures of the zonal and meridional DIs stresses the added value of integrating their information in order to explain anomalous periods and events. A good example is the hot summer of 2003 (e.g., García-Herrera et al. 2010; Barriopedro et al. 2011), for which the standardized DIs indicate the dominance of southerly and easterly winds ($NI_{2003JJA} = -0.68; EI_{2003JJA} = 0.83; SI_{2003JJA} = 0.31; WI_{2003JJA} = -0.60$) both related to warming in southeastern and northwestern Europe, respectively. Another example

can be found during the winter period 1973-1990, characterized by positive phases of the NAO (e.g., Pinto and Raible 2012; Hanna et al. 2016). The DIs confirm the prevalence of WI over EI but also large SI values ($NI_{1973-1990DJF} = -0.83; EI_{1973-1990DJF} = -0.16; SI_{1973-1990DJF} = 0.53; WI_{1973-1990DJF} = 0.24$). Precisely, the appearance of this southern circulation involves changes in the geographical location of the action centers, adding evidence to the recent shift of the NAO dipole reported in other studies (e.g., Vicente-Serrano and Lopez-Moreno 2008).

Despite the complementary signals of zonal and meridional DIs, the results also indicate some redundancy among them. By construction, the sum of the DIs is constant, and therefore enhanced westerlies (northerlies) tend to be associated with reduced easterlies (southerlies), and vice versa, leading to certain degree of collinearity among them, as further described below. To account for this, we used a SRM (see Section 2.2.3 for further details) to find the combination of DIs that best explains the dependent variable (either temperature or precipitation) at each gridpoint. Figure 4.6 shows the best two predictors of temperature (first two columns) and precipitation (last two columns) for each season (rows). The analysis reveals that in most of Europe there is always at least one DI (and often no more than two DIs) explaining a significant fraction of variance of the dependent variable. In terms of spatial extension, DIs are more skillful indicators in winter (Figure 4.6, first row) than in the rest of the year, and of temperature (Figs. 4.6a-h) than precipitation (Figures 4.6i-p) anomalies, whose signal is more spatially fragmented and commonly well explained by one DI alone. Still, the DIs are able to explain a significant amount of temperature and precipitation variability over large areas of Europe all year-round.

Overall, zonal indices tend to be the best predictors of temperature in central Europe (Figures 4.6a-d), with the exception of summer, and of precipitation in most of Europe (Figures 4.6i-l). In turn, meridional indices are skillful predictors of temperature in western Europe and eastern Mediterranean, and of precipitation in southeastern Europe. We also note that the most skillful combination of DIs can vary seasonally, particularly for temperature. For example, the WI and NI dominate the temperature anomalies over large parts of the continent during winter, spring and autumn (Figures 4.6a, b, d), while EI and SI acquire relatively more importance during summer (Figure 4.6c). In spite of these seasonal variations, there is some coherence, in the sense that the leading DIs of a given season, frequently appear as second predictors in contiguous seasons. On the contrary, for precipitation, the WI appears

as the dominant DI in large areas of Europe, being selected as first predictor all year-round (Figures 4.6i-l). This result strengthens the role of maritime air advection as a major driver of precipitation in Europe (Gimeno et al. 2012). However, there are regions and seasons where other DIs are more important, like southeastern Europe, where meridional indices dominate precipitation variability during the cold seasons (Figures 4.6i, l). Therefore, all DIs are required to achieve the best possible description of temperature and precipitation anomalies over Europe.

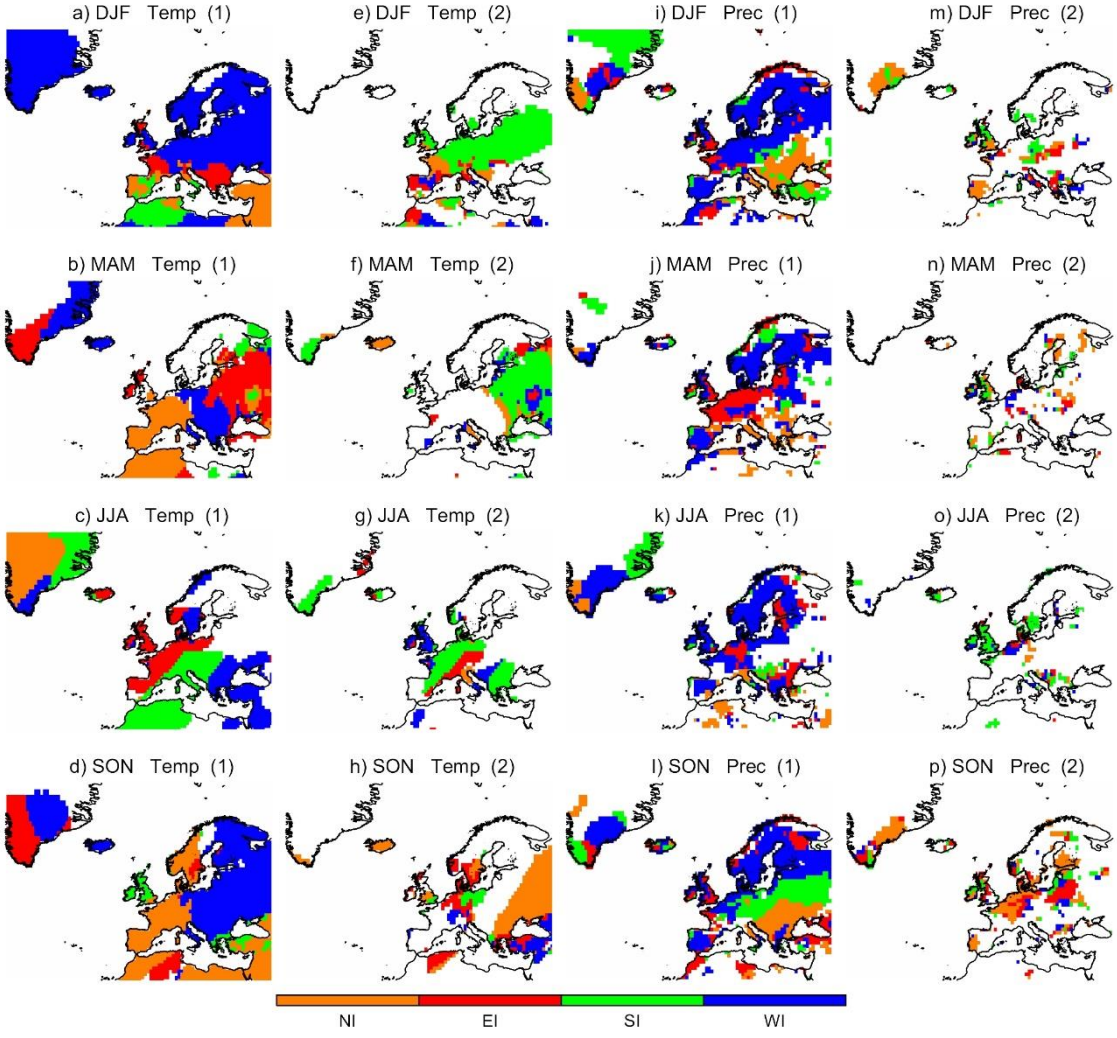

Figure 4.6. Stepwise regression model for the period 1901-2014 showing the best DIs predictors of seasonal: (a-h) temperature and; (i-p) precipitation anomalies. The best predictor of each season is shown in panels (a-d) for temperature and (i-l) for precipitation. Panels (e-h) and (m-p) indicate the second best predictor of temperature and precipitation, respectively. Rows indicate the respective season from winter (DJF, first row) to autumn (SON, last row). Colors represent the DI: NI (orange), EI (red), SI (green) and WI (blue). White areas show regions where none of the DIs is able to explain a significant amount of variance.

The above results stress the added value of integrating the four DIs. This largely results from their completion of the wind rose, which provides a finer picture of the atmospheric circulation than that derived from single zonal indices, such as the WI or the NAO. To further support this, we have compared the skill of DIs as European climate predictors with that of NAO-like indices. To do so, we repeated the SRM of temperature and precipitation against the DIs for the 1901-2014 period (Figure 4.6) but including the NAO as a predictor. We used the summer NAO index defined by Folland et al. (2009) for the high-summer months (July-August) and the monthly NAO index of Jones et al. (1997) for the rest of the year, since the former is fundamentally different from the canonical NAO pattern (see Section 1.5 in Chapter 1). Hence, the NAO will be included in the model as a skillful predictor in areas and seasons for which it improves the results obtained by the DIs. For the DIs+NAO SRM, we can expect NAO-related improvements in two different ways: by explaining variance in some regions where DIs are not skillful predictors or/and by increasing the explained variance already provided by the DIs.

Figure 4.7 shows the variance in temperature and precipitation explained by the SRM with the DIs only (first and third columns) and with the DIs and the NAO (second and fourth columns). The DIs are able to account for up to 70% of the variance of the dependent variable in certain regions and seasons of Europe. The inclusion of the NAO in the model adds some new areas of explained variance around the Nordic countries and Iceland for spring and summer temperature (compare Figures 4.7b, c with Figures 4.7f, g), and in northern and eastern Europe for winter and summer precipitation (cf. Figures 4.7i, k and Figures 4.7m, o). However, these areas are relatively small when compared to those where the DIs are only selected as the most skillful predictors (the rest of Europe throughout the year).

On the other hand, winter is the season when the NAO conveys the largest improvements over the DIs model in terms of the amount of explained variance. In the case of temperature, the DIs+NAO model improves the results of the DIs model in the Mediterranean, particularly over the eastern basin during winter and autumn (Figures 4.7a, d and e, h), being the improvements very small during spring and almost neglectable during summer. In general, the increase of explained variance in precipitation is not as clear as in temperature, with the only exception of winter over central Europe (Figures 4.7i, m). In summary, the results indicate that the DIs are better indicators of the European climate than the NAO alone, improving in most cases the variance accounted for by the NAO. Given the limited record of SLP

observations over the Atlantic, the DIs constitute an excellent outperforming alternative of the NAO to explore the atmospheric circulation over the eastern North Atlantic and European climate variability. The ability of the DIs to provide a finer picture of the Euro-Atlantic atmospheric circulation will further be exploited in Chapters 5 and 6.

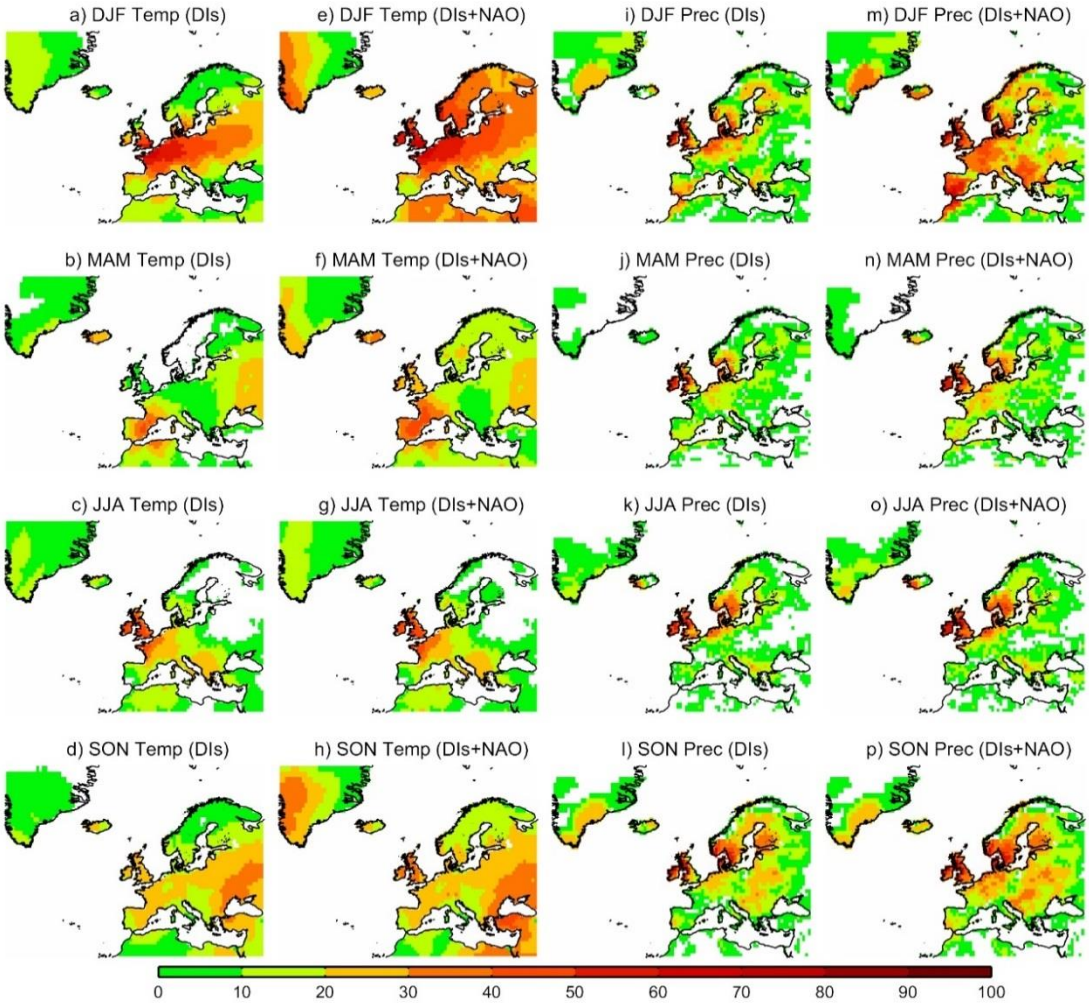

Figure 4.7. Explained variance (in percentage) of seasonal: (a-h) temperature and; (i-p) precipitation anomalies based on Stepwise Regression Models for 1901-2014 using the DIs only (panels (a-d) for temperature and (i-l) for precipitation) and the DIs + NAO ((e-h) for temperature and (m-p) for precipitation) as predictors. White areas denote regions where none of the predictors is able to explain a significant amount of variance.

4.3 European past climate variability

DIs provide a detailed picture of the Euro-Atlantic atmospheric circulation and are useful predictors of the European surface climate variability. Therefore, in this section we show how they help to better understand the European past climate during the period 1685-2014, from multidecadal to seasonal time scales. Due to the high resolution of the DIs, special attention

will be placed on seasonal extremes of the atmospheric circulation, herein defined as DI values above the 95th percentile and below the 5th percentile, respectively.

To interpret in a simple way the temperature and precipitation responses to the DI values recorded during a given period or event, two additional Circulation Indices (CI_T , CI_P) have been constructed, which combine the information provided by the DIs according to their temperature (Figure 4.2) and precipitation (Figure 4.3) signals over Europe, respectively:

$$CI_T = \begin{cases} (SI + WI) - (NI + EI) & (a) \\ (SI + EI) - (NI + WI) & (b) \end{cases} \quad (4.1)$$

$$CI_P = (WI - EI) \quad (4.2)$$

CI_T in Equation 4.1a is designed in order to encapsulate the overall temperature signals of the DIs during the cold half of the year, when enhanced southerlies and westerlies (easterlies and northerlies) are associated with warmer (colder) conditions over large parts of Europe (Figures 4.2a-d and Figure 4.4e-h). Recall that the DIs fingerprints in temperature vary seasonally (Figure 4.2), and hence CI_T is reformulated in the warm half of the year following Equation 4.1b in order to account for the reversed temperature signal of the zonal DIs. Therefore, positive (negative) values of CI_T indicate dynamically-prone warm (cold) conditions on continental scale regardless of the season. Unlike temperature, the precipitation signal shows a consistent response all year-round (Figures 4.3 and 4.5), with zonal DIs explaining a substantial fraction of its variability over central and northern Europe (Figures 4.7i-l). As such, CI_P, as defined in Equation 4.2, is an indicator of the precipitation anomalies that can be expected therein from the atmospheric circulation. Using all this information we have assessed the most relevant features of the atmospheric circulation for the last three centuries on different time scales (from multi-decadal periods to seasonal extremes), and the associated surface conditions over Europe.

Figure 4.8 shows the standardized annual mean DIs for 1685-2014, computed from their monthly values (seasonal time series can be found in the Annex). To complement Figure 4.8, Figure 4.9 presents the decadal frequency of positive minus negative extreme occurrences of each seasonal DI, with reddish (bluish) colors indicating a dominance of extremely positive (negative) DIs. The DIs time series extend back to the later part of the Little Ice Age (LIA,

ca., 1300-1900), thereby including the transition to the present climate characterized by increasing anthropogenic forcing from human activities (Luterbacher et al. 2000). There are only two periods of frequent missing data (light blue bars in Figure 4.8) around 1875 and during the WWII (Figure 2.2b), although some monthly and seasonal values exist for them. On interannual time scales the zonal DIs are significantly anti-correlated ($p<0.01$) for all calendar months of the year, and the same occurs for the meridional DIs. In addition, the annual series of SI and WI show a correlation coefficient of -0.44 ($p<0.05$) due to the predominance of south-westerly winds over the English Channel, which implies that periods with an anomalous frequency of westerlies are partially compensated by opposite changes in the southerlies. These linkages are not so evident, and actually weaken, on longer time scales (orange and green shading in Figure 4.8) and for seasonal extremes (Figure 4.9), as illustrated by the examples described below.

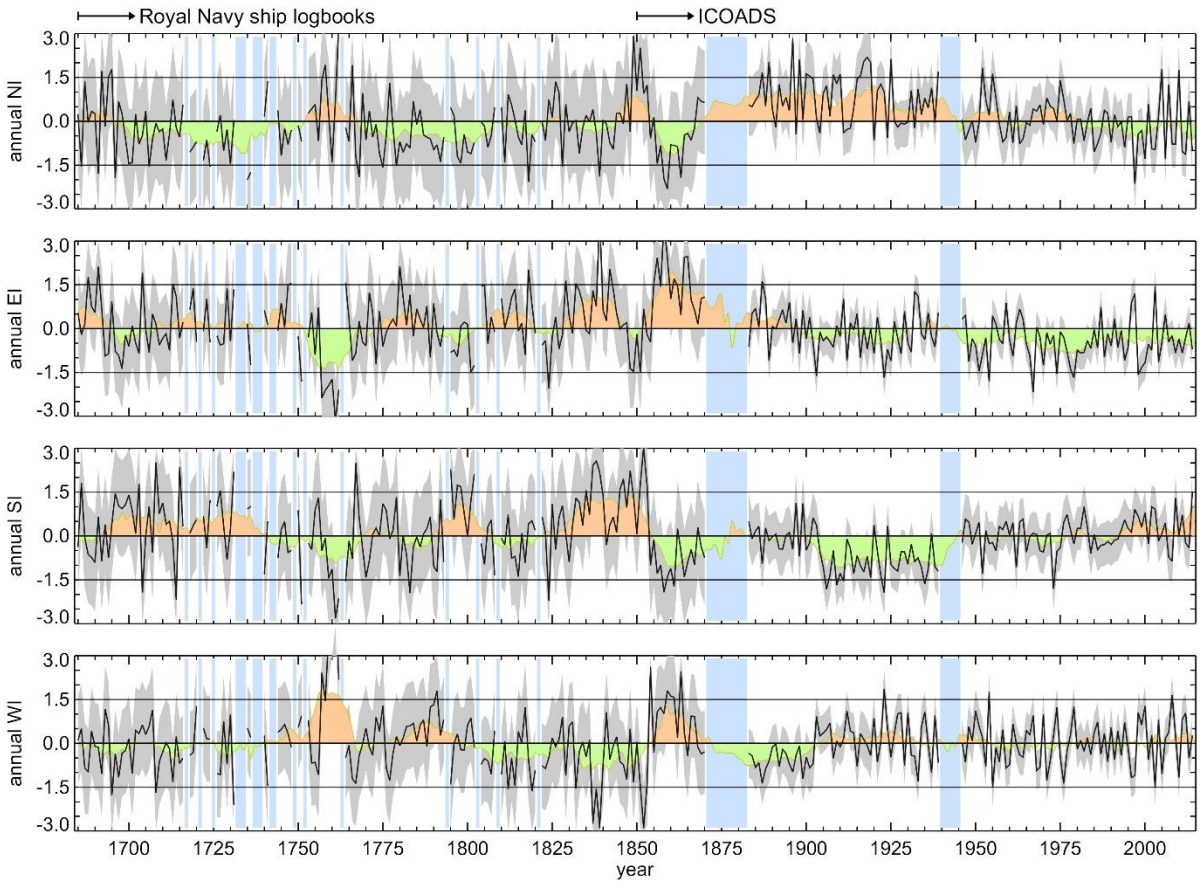

Figure 4.8. Standardized annual series of DIs for 1685-2014 (black line) with the associated uncertainty (grey shading, ± 1 sigma) and an 11-year running mean (grey line) superimposed. Green/orange shading highlights periods above/below the 1685-2014 mean. Horizontal lines indicate ±1.5 sigma relative to the 1685-2014 period. Vertical blue bars indicate years with at least one missing month.

We have first focused on long-term changes by looking for differences between the preindustrial (1685-1869) and industrial (1870-2014) halves of the seasonal DI series. Some differences are statistically significant (95% confidence level). More specifically, when compared with the preindustrial period, the industrial era is characterized by a decline of the annual easterlies (-2.6%), spring and summer southerlies (-2.8% and -8.5%, respectively) and autumn westerlies (-2.4%), as well as an increase of the northerlies in spring and summer (4.5% and 6.5%). Although significant, most of these changes are relatively small (note that a seasonal change of 5% corresponds approximately to ~5 days per season in a ~150-year period) and some of them depend on the periods chosen. The latter highlights substantial variability even on centennial time scales, and hence the reported differences should not necessarily be interpreted as a response to anthropogenic factors. In fact, the mean values of the last decades are not exceptional in the context of the last 330 years. Instead, these results stress that the instrumental record is too short to properly characterize the whole spectrum of atmospheric fluctuations as reported by the DIs, and hence we might be underestimating the range of internal variability, particularly on long time scales.

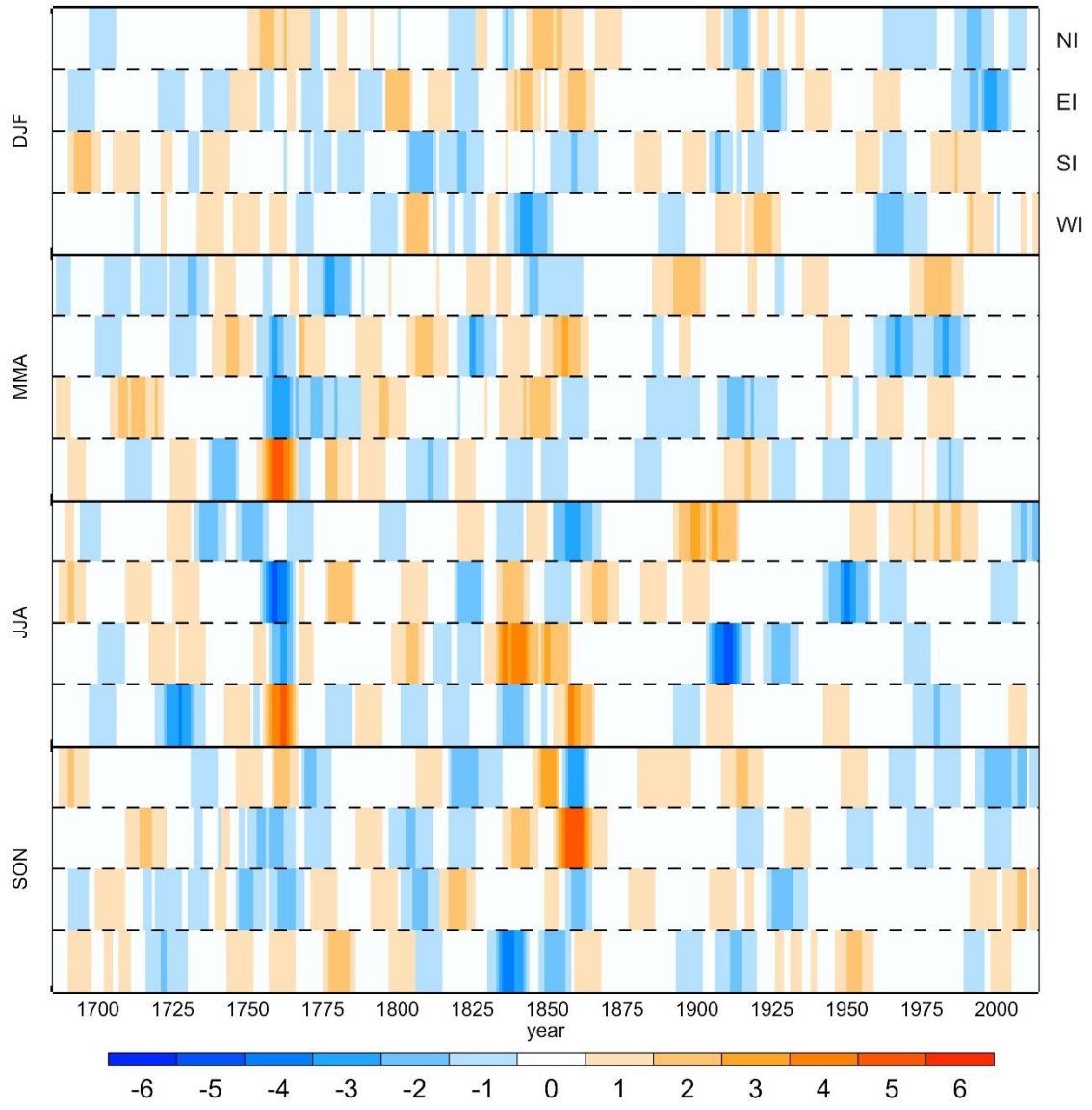

Figure 4.9. Frequency difference of positive minus negative seasonal DIs extremes for running 11-year intervals of the 1685-2014 period (x-axis), with red (blue) shading denoting positive (negative) differences. Positive (negative) DIs extremes are defined as those above the 95th (below the 5th) percentile of their seasonal 1685-2014 distribution. Seasons are displayed from the top (winter, DJF) to the bottom (autumn, SON) in the left y-axis. For each season, the DIs are arranged clockwise from the NI (top of each season) to the WI (bottom of each season), as shown for the winter season in the right y-axis.

On multi-decadal (50 years) time scales, two periods (1701-1750 and 1826-1875) stand out in the annual time series of the DIs (Figure 4.6). The most remarkable circulation signatures of the former ($CI_{P,Annual(1701-1750)} = -0.32$) support the dry conditions reported in Europe during the first half of 18th century (Pauling et al. 2007). The second period displayed similar features ($CI_{P,Annual(1826-1875)} = -0.84$) but is almost unnoticed in the literature, with the exception of Casty et al. (2005), who suggested 1830 as a year of transition

from wet to dry conditions over Europe. Moreover, some shorter intervals within these periods presented CI_P values below -1 SD, indicating the presence of dry extremes (Figure 4.7). This widespread dryness over continental Europe was largely due to the prevalence of EI ($EI_{Annual(1826-1875)} = 0.81$). We note, however, that in both periods SI anomalies were remarkable ($SI_{Annual(1701-1750)} = 0.42$; $SI_{Annual(1826-1875)} = 0.31$), indicating that continental drying should have coexisted with relatively wetter conditions over the UK and the Iberian Peninsula (Figures 4.3b, c, f, g). Supporting this result, previous studies have reported above average rainfall in Lisbon between 1864-1875, as well as unusually wet years in the Iberian Peninsula, including the outstanding year of 1856 (Kutiel and Trigo 2014; Domínguez-Castro et al. 2015).

On the other hand, the 20-year periods of 1760-1780, 1840-1860 and 1905-1925 displayed high frequency of extreme DIs (Figure 4.9). The 1760-1780 period exhibited recurrent positive extremes of WI and negative extremes of SI during the warm half of the year (Figure 4.9), associated with cold conditions over northern and central Europe, respectively (Figures 4.2h, g). Differently, the winters (autumns) of this period (Figure 4.9) showed an alternation of negative and positive extremes in the zonal (meridional) DIs, which agrees with Cornes et al. (2013), who reported a wide range of circulation extremes during the winters of 1760s. On the other hand, the years around the mid-19th century were prone to widespread cooling during the cold seasons, as featured by positive (negative) values of NI and EI (SI and WI). This result agrees with Küttel et al. (2010), who used station pressure series and marine information to conclude that the cold decade of the 1840s was followed by an even colder period. Finally, the beginning of the 20th century (1905-1925) exhibited recurrent negative extremes of SI in all seasons (Figure 4.9), indicating persistent high-pressure systems over the Atlantic throughout the year (Figures 4.2c, g). These were accompanied by positive extremes of WI during winter (Figures 4.9), further enhancing the warm conditions in central and eastern Europe (Figure 4.2d). Both results agree with the strong zonal circulation reported by Slonosky et al. (2001) during 1900-1930 and the warm European conditions described by Küttel et al. (2010) in the 1910s and 1920s.

On decadal scales, there are also outstanding periods in the DIs, mainly during winter. The winters of 1717-1726 and 1730-1739 stand out by the prevalence of SI and WI over EI and NI, and the largest CI_T values on record ($CI_{T,DJF(1717-1726)} = 2.10$; $CI_{T,DJF(1730-1739)} = 2.16$) , thus indicating extraordinary warm conditions. In fact, the multi-proxy reconstruction

of Luterbacher et al. (2004) points the close decade of 1733-1742 as the warmest one of 1500-2000, only surpassed by the end of the 20st century (1989-1998). On the contrary, 1687-1696 and 1810-1819 are ascribed to cold winter conditions according to their CI_T values ($CI_{T,DJF(1687-1696)} = -1.29$; $CI_{T,DJF(1810-1819)} = -1.24$). The first period took place during the Late Maunder Minimum (LMM, ca., 1685-1715) and the so-called 'climax of the LIA' (Luterbacher et al. 2001), which includes some of the most exceptional cold episodes in the CI_T series, such as the 1692 ($CI_{T,DJF(1692)} = -4.31$) and 1695 ($CI_{T,DJF(1695)} = -4.64$) winters, both reported by previous studies (Luterbacher et al. 2000; Slonosky et al. 2001; Casty et al. 2005). Chapter 5 is devoted to this exceptional period, providing a more detailed assessment of the atmospheric circulation during the LMM. On the other hand, the cold winters of the second period (1810-1819) are explained by large positive anomalies in the EI ($EI_{DJF(1810-1819)} = 0.67$) and positive extremes of NI (Figure 4.9), both indicating coldness and dryness. This is in good agreement with previous studies (e.g., Briffa et al. 2000; D'Arrigo et al. 2006), which described the 1813-1822 decade as one of the coldest in the Northern Hemisphere partially due to the role exerted by two strong external forcings (Trigo et al. 2009). Hence, besides several strong volcanic eruptions, this period is also well known as a period characterized by reduced sunspot number since it is embedded within the Dalton minimum (ca.,, 1790-1830). Thus, DIs provide complementary information that helps to a better understanding of all the internal mechanism and external forcings that control this period.

Finally, the resolution of the DIs allows us to examine the atmospheric circulation during extreme episodes on seasonal (actually monthly) time scales and in seasons other than winter. For example, the 1807 summer displayed outstanding values of the meridional indices ($NI_{JJA(1807)} = -1.4$; $SI_{JJA(1807)} = 1.93$), thus indicating warm conditions over central Europe (Figures 4.2e, g; see also Casty et al. 2005). A more recent example can be given for the 1902 summer, the coldest of the last 500 years in the European temperature reconstruction of Luterbacher et al. (2004). This summer was characterized by an extremely positive value of the NI ($NI_{JJA(1902)} = 2.19$), favoring colder temperatures over the Mediterranean basin and Greenland (Figure 4.2e). While other summers of the early 20th century were also characterized by extreme values of the NI (Figure 4.9), the widespread cooling of this summer was likely enhanced by the additional effect of the decreased easterlies ($EI_{JJA(1902)} = -0.8$) over northwestern Europe (Figure 4.2f).

In summary, these results indicate that the DIs are useful indicators of the European climate, being able to capture major anomalies in the European climate reported in previous studies and uncover other less well-documented periods. The former adds evidences of a major control of atmospheric circulation anomalies on near-surface climate, irrespectively of whether they were or not externally forced. The latter provides a deeper knowledge of the Euro-Atlantic atmospheric circulation in the past, shedding light on controversial periods. For example, the DIs bring new insights into the 1760s and 1800s, for which the atmospheric circulation is still far from clear, with discrepancies between reconstructed NAO indices (Luterbacher et al. 2001; Cook et al. 2002; Cornes et al. 2013). The winter DIs display a wide range of extreme values in the four directions (Figure 4.9), including the largest positive value of the WI time series in 1761 ($WI_{DJF1761} = 5.54$). The large anomalies of all DIs reflect that the meridional circulation also played an important role during both periods, which may explain the discrepancies between the different reconstructed NAO indices. This calls for caution when characterizing atmospheric circulation in terms of the NAO alone. This question will be further addressed in Chapter 6.

4.4 Impact of tropical volcanic eruptions

The DIs extend the currently available instrumental record of atmospheric circulation indices by at least 150 years, thus allowing a better characterization of the internal variability and the fingerprints of external forcings in atmospheric circulation. Herein, we exploit this advantage to identify the regional responses to tropical volcanic eruptions. While their effects on European climate during summer and winter have been reported before (e.g., Fischer et al. 2007, Luterbacher et al. 2016), they have been largely inferred from multi-proxy reconstructions of near-surface fields for the last 500 years, even when some of the volcanic signatures are assumed to occur through changes in the atmospheric circulation (Robock 2000) particularly for the largest eruptions such as Tambora in 1815 (e.g., Trigo et al., 2009). Moreover, the regional responses in seasons other than winter and summer are less documented. To the best of our knowledge, this assessment provides the first observational year-round evidence of the Euro-Atlantic circulation response to tropical volcanic eruptions of the last three centuries.

Table 4.1. List of the strongest (VEI>=5) tropical volcanic eruptions of 1685-2014.

Volcanoes	Latitude (ºN)	Longitude (ºE)	Year	Month	VEI	Total SO_2 emission (GT)
Unknown	-7.98	113.34	1808	12	6	35.10
Mount Tambora	-8.25	118.00	1815	4	7	52.00
Galunggung	-7.25	108.06	1822	10	5	1.50
Cosigüina	12.98	271.43	1835	1	5	18.20
Krakatoa	-6.10	105.42	1883	8	6	16.90
Santa Maria	14.76	267.45	1902	10	6	2.48
Mount Agung	-8.34	115.51	1963	2	5	7.50
Chichon	17.36	266.77	1982	4	5	3.70
Pinatubo	15.13	120.35	1991	6	6	18.00

Volcanic eruptions have been obtained from a recently revisited catalogue (Ryan Neely III, personal communication), based on a cross-comparison of multiple evidences from sulfate deposition in ice cores (Sigl et al. 2015; Toohey and Sigl 2017) and the Global Volcanism Program (https://volcano.si.edu/). We selected the nine tropical eruptions from 1685 with a Volcanic Explosivity Index (VEI) equal or larger than 5 (Table 4.1). Superposed Epoch Analyses (SEA) are often employed to explore their seasonal responses, which are expressed as differences with respect to the averaged conditions for the five years before the time of the eruption (year 0). However, different criteria are adopted to determine the seasons of the years 0 and +1 (Robock et al. 2000; Fischer et al. 2007; Luterbacher and Pfister 2015). Herein, year 0 (+1) is defined as the first (second) four-season period occurring after the volcanic eruption (Sigl et al. 2015; Luterbacher and Pfister 2015). For example, for the Tambora' eruption (April 1815), the year 0 is the one that spans from summer 1815 to spring 1816 (i.e., excluding the spring of 1815). As the largest impact may arguably occur in any of them, depending on the timing of the eruption and the large-scale circulation at that time, we take for each DI the largest absolute standardized seasonal anomaly of years 0 and +1. The results are not very sensitive to small changes in these criteria and to the chosen catalogue of volcanic eruptions (not shown).

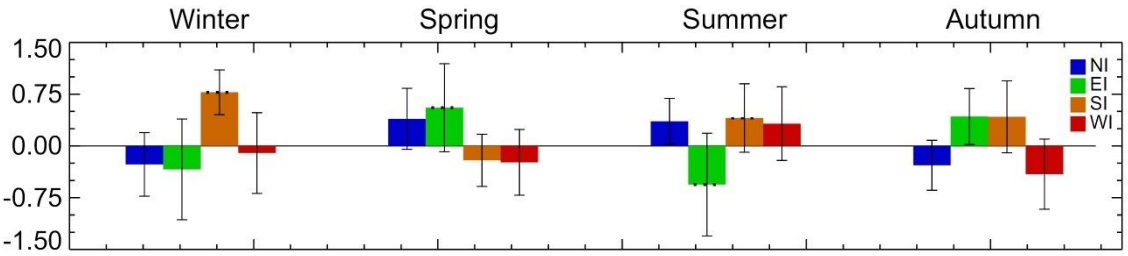

Figure 4.10. Superposed epoch analyses of the seasonal standardized DIs following the strongest (VEI≥5) tropical volcanic eruptions of 1685-2014. For each DI (colored bars, see legend) and season, anomalies are expressed as the difference between the largest standardized anomaly of the years 0 and +1 and the averaged value for the five years preceding each volcanic eruption. Columns with dotted top bars indicate significance at the 90% confidence level after a 5000-trial bootstrap test. Error bars indicate the ±0.5·sigma level.

SEA of the seasonal standardized DIs following explosive tropical volcanic eruptions are shown in Figure 4.10. The significance at the 90% confidence level (dotted top bars in Figure 4.8) is assessed with a bootstrap method of 5000 trials, each one containing the same number and calendar months of volcanic eruptions, but with random years of occurrence. The results are qualitatively similar if we analyze the DIs signals in years 0 and +1 separately, albeit the significance may be affected. All seasons except autumn reveal significant changes in at least one DI. Interestingly, some of the largest responses affect the meridional DIs (Figure 4.10). In particular, the cold half of the year is characterized by a southward veering of the wind, more pronounced in winter, and the summer circulation displays a significant decrease of the EI frequency and an increase of both meridional circulation indices, although only the change in the SI is significant. Differently, the zonal indices seem to play a major role in transitional seasons, which are characterized by increases in EI (only significant in spring though). Surprisingly, there are not significant changes in the WI. This is in disagreement with previous studies, which attributed the post-eruption European winter warming to positive NAO-like phases (e.g., Fischer et al. 2007). On the other hand, the presence of significant DI signals in summer suggests some role of the atmospheric circulation in the European cooling, which had been largely attributed to radiative forcing so far (Fischer et al. 2007; Sigl et al. 2015). However, the large spread associated with the composited values of the DIs (Figure 4.10) points to large case-to-case variability, suggesting that the overall signal could be dominated by a few volcanic eruptions, for which the atmospheric circulation might well reflect internal variability. As an example, the Tambora's eruption (April 1815) that preceded the year without summer (Trigo et al. 2009; Luterbacher and Pfister. 2015) was characterized

by the prevalence of westerlies during the two post-eruption summers and winters, which does not fully agree with the composite picture described above.

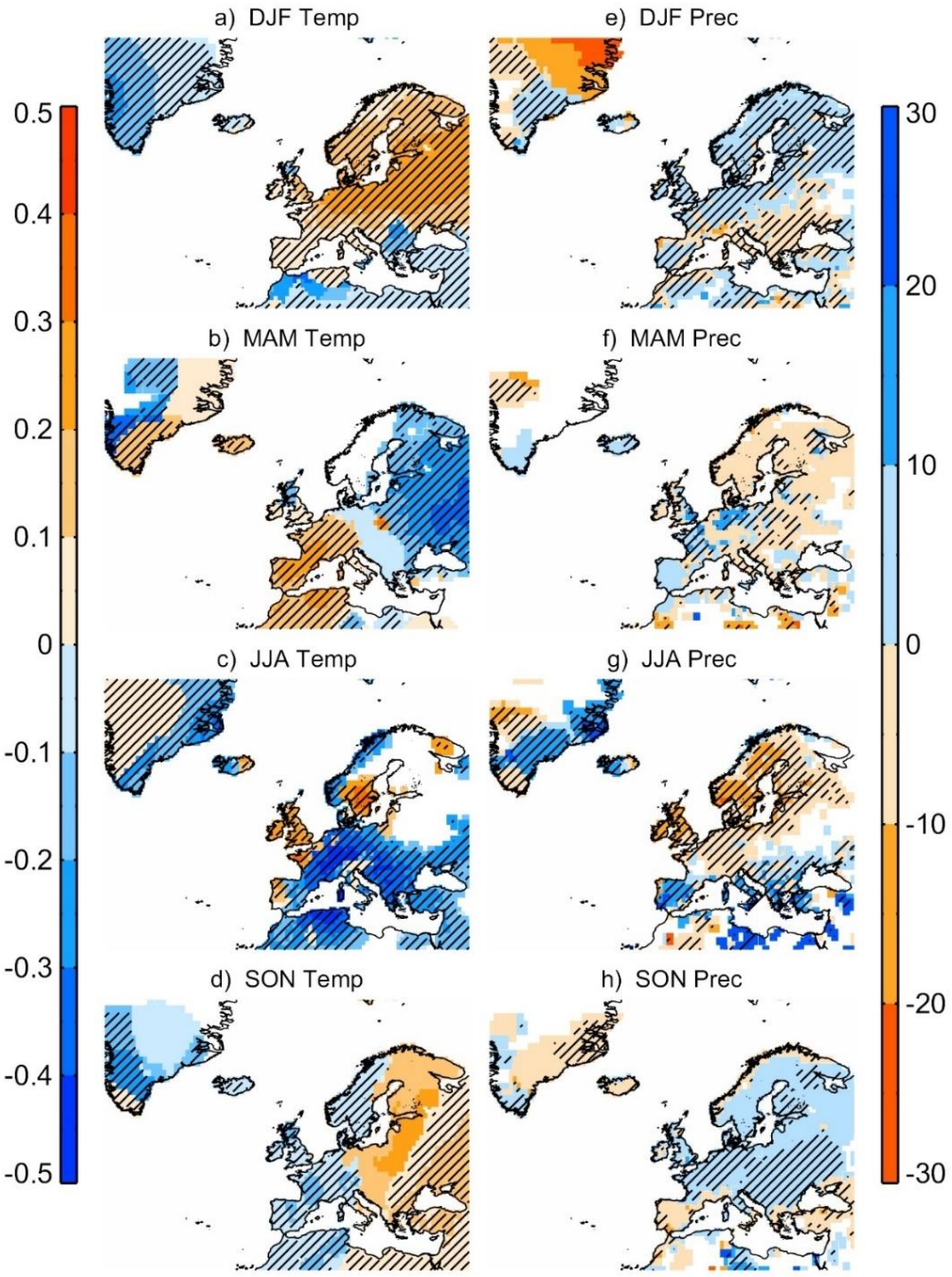

Figure 4.11. Reconstructed mean seasonal anomalies (with respect to 1901-2014) of: (a-d): temperature (ºC) and; (e-h) precipitation (in percentage of normal) following explosive tropical volcanic eruptions of 1685-2014. Red/blue colors indicate positive/negative temperature anomalies and below-/above-normal precipitation. The reconstructed anomalies are derived by applying the Stepwise Regression Model of the DIs series for 1901-2014 to the DIs anomalies recorded after each volcanic eruption. White areas show regions where none of the DIs is able to explain a significant amount of variance. Hatching indicates regions for which 66% of the volcanic eruptions display an anomaly of the same sign. See text for details.

To better frame these results, we reconstructed the near-surface signatures associated with the post-eruption DIs by using the SRM of Section 4.2, which integrates the joint effects of all DIs and interpret them in terms of temperature and precipitation. Figure 4.11 shows the seasonal composites of temperature and precipitation anomalies, as inferred from the DIs following the nine tropical volcanic eruptions. Figure 4.11c (4.11a) confirms that summers (winters) after large tropical eruptions are prone to cold (warm) conditions over central and eastern (central and northeastern) Europe, in agreement with previous studies (Robock 2000; Fischer et al. 2007; Luterbacher et al. 2016). Similarly to Fischer et al. (2007), there are also drier (wetter) conditions over southeastern (northern) Europe in winter (Figure 4.11e), and over parts of northern Europe (the Mediterranean basin) in summer (Figure 4.11h).

While our results are relatively robust (see hatching in Figure 4.11) and qualitatively agree with previous studies, they also indicate that the surface responses induced by the atmospheric circulation cannot be simply interpreted in terms of changes in zonality, as previously suggested. They also uncover circulation responses previously unnoticed in seasons other than winter. Thus, the winter warming can be foreseen by autumn over eastern Europe (Figure 4.11d), along with wetter conditions over central Europe (Figure 4.11h), whereas the summer cooling is already evidenced in spring over the northern and central sectors of Europe (Figure 4.11b).

4.5 Conclusions

This Chapter exploits the value of the DIs to characterize the Euro-Atlantic atmospheric circulation from monthly to multi-decadal time scales, and the associated surface climate variability over Europe. The main conclusions can be summarized as follows:

- The DIs are dominated by substantial variability from interannual to multidecadal and longer time scales, including some differences between industrial (1870-2014) and pre-industrial (1685-1869) periods such as declines in the easterlies, more pronounced during winter, and in the westerlies during autumn. This stresses the limitations of the currently available instrumental record to characterize the whole spectrum of variability of the atmospheric circulation, particularly in the low frequency.

- By covering all principal wind directions, the DIs give a more complete picture of the atmospheric circulation than that provided by zonal indices such as the NAO. In fact,

they shed light on some inconsistencies between NAO indices for specific periods, which can be explained by the presence of a marked meridional circulation. The results emphasize some shortcomings when characterizing the atmospheric circulation with just one circulation index.

- DIs fluctuations are associated with precipitation and temperatures anomalies over large areas of Europe all year-round with zonal and meridional indices often affecting different regions. Precipitation is strongly controlled by moisture advection, mainly associated with the zonal DIs and shows a robust and coherent response throughout the year. Differently, the spatial response in temperature is largely explained by temperature advection and radiative processes. As a consequence, the temperature signal associated with the zonal DIs reverses during the warm half of the year. Statistical models including all DIs are able to explain a considerable amount of European climate variability, improving in most cases that accounted for by the NAO.

- The DIs are able to reproduce the known European climatic history and provide new insights of certain episodes from monthly to multi-decadal time scales, such as the warm winter decade of 1730-1739 or the extremely cold 1902 summer. The results stress the key role of the atmospheric circulation in driving surface climate anomalies, providing a dynamical context to better understand the European climate of the last centuries

- We provide the first instrumental evidences of all year-round Euro-Atlantic circulation signatures and the associated European surface climate anomalies following the strongest tropical volcanic eruptions since 1685. These responses are more complex than previously thought and suggest that the well-reported winter warming and summer cooling can be detected several months in advance.

Chapter 5

5. Euro-Atlantic atmospheric circulation during the Late Maunder Minimum

The Little Ice Age (LIA, ca., 1300-1900); e.g., Wanner et al. 2000) was one of the coldest periods in the last two millennia (e.g., Mann et al. 2009; Ljungqvist et al. 2012; Masson-Delmotte et al. 2013; PAGES 2k Consortium 2013; Nicole et al. 2017). There are evidences from proxy records of both hemispheres (mainly Europe, North America, and eastern China; Chambers et al. 2014) that strongly suggest that the LIA was a global phenomenon (Rhodes et al. 2012). The Maunder Minimum (MM, 1645-1715) is often regarded as the coldest period of the LIA (e.g., Luterbacher et al. 2001) and was concurrent with a low number of sunspots (Vaquero et al. 2016). The coldness reached its climax during the last decades of the MM, often called the LMM (ca.,, 1675–1715; Wanner et al. 1995; Slonosky et al. 2001). The exceptionally low temperatures recorded across Europe make the LMM a period of great interest from a climatic viewpoint (e.g., Wanner et al. 1995; Luterbacher et al. 2001; Slonosky et al. 2001; Xoplaki et al. 2001; Xoplaki et al. 2005). However, there are limited direct evidences of the atmospheric circulation at that time. In this chapter, we exploit the information derived from the wind direction observations presented in Chapter 2 and the DIs constructed in Chapter 3 to provide new instrumental-based evidences of the atmospheric circulation and the related surface climate anomalies during the period 1685-1715, which, for simplicity, will also be referred to as the LMM. Taking advantage of the high-resolution of the DIs, a detailed description and classification of the LMM winters in terms of the atmospheric circulation will also be targeted. The main results of this chapter can be found in Mellado-Cano et al. (2018).

5.1 Wind Roses

Figure 5.1 illustrates the wintertime series of the DIs for the LMM in standardized anomalies with respect to the 1981-2010 period, which contains the same number of years as the LMM and will be used as a reference period in this chapter, unless otherwise stated. As

shown in Chapter 4, this reduced number of indices allows us to interpret easily the synoptic characteristic as well as their associated impacts.

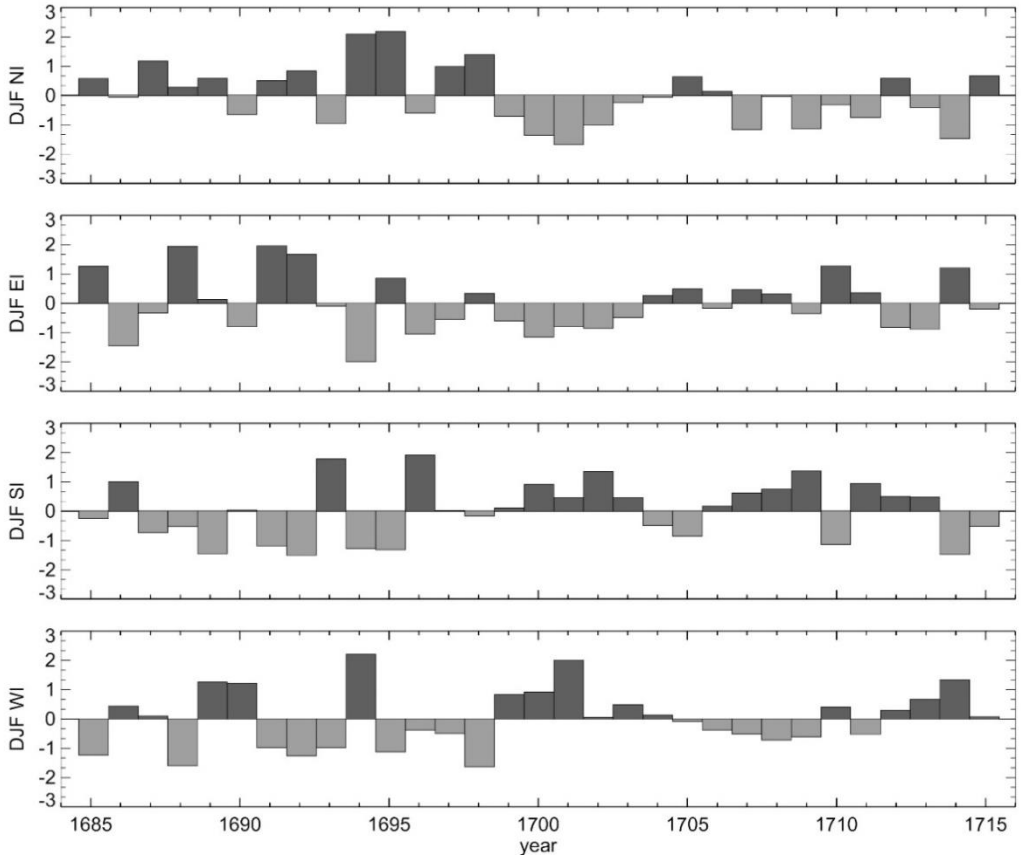

Figure 5.1. Standardized winter DIs time series for the LMM (1685-1715), with dark (light) grey bars highlighting years with values above (below) the 1981-2010 average.

Figure 5.1 reflects that the LMM displayed very dissimilar winters in terms of atmospheric circulation and a generalized cooling cannot be obviously inferred. To provide a more detailed description of the atmospheric circulation during the LMM, in this Chapter we further exploit the wind direction data from ships' logbooks. Thus, in addition to the four DIs, monthly 8-point wind roses are derived for the LMM. For coherence with the DIs, the 8-point wind roses are constructed in 45° sectors starting at 0° such that each DI corresponds to two full bins in the wind rose. As wind direction observations of the LMM period come from ships' logbooks, the wind roses were constructed by simply taking the principal wind direction abstracted for each day. These observations were taken by a 32-point compass, which allows higher resolution wind roses. For comparative purposes with climatological present-day conditions, we also constructed wind roses for the 1981-2010 period. This period

is covered by ICOADs, which includes wind direction observations from 8- to 3600-point compasses, thus limiting the precision of wind roses to 8 points. Regarding this reference period, we are just concerned about its climatological mean wind roses and hence they were constructed by classifying the mean wind direction of each day in the 8-point wind rose. Similar results were obtained from other approaches (not shown). Although the wind roses yield a less manageable number of directional indices than the DIs, they can eventually be useful to provide a better interpretation of extreme events and the underlying dynamics involved in specific episodes. When necessary, they will be employed in the following sections, which explore the mean anomalies and variability on different time-scales of the atmospheric circulation during the LMM.

5.2 Mean atmospheric circulation for the LMM

Figure 5.2 shows the seasonal DIs averaged for the LMM (1685-1715, color bars) and compares them with those of the reference period (1981-2010, grey bars). These anomalies are obtained from the seasonal time series developed in Chapter 4, allowing us to put in context the LMM with respect to present conditions. The frequency of days with meridional circulation (the sum of SI and NI) during the LMM was slightly higher than during the reference period, and the WI presented lower frequencies in the LMM than in the reference period for all seasons.

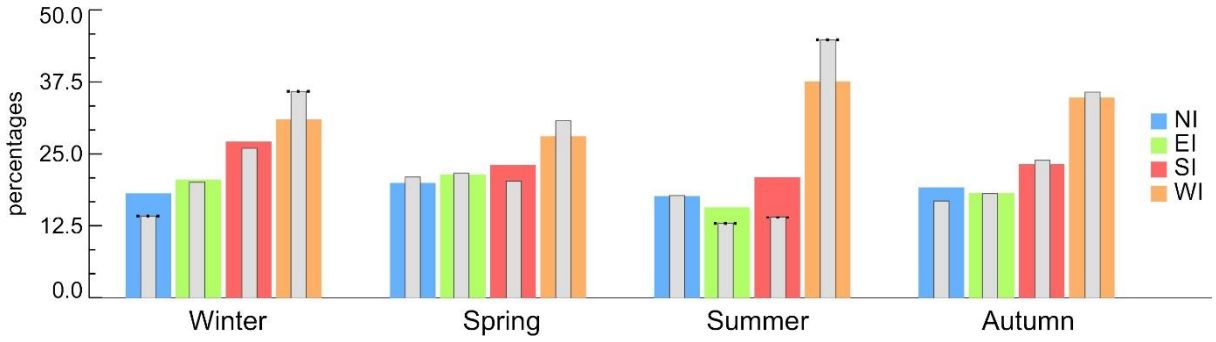

Figure 5.2. Seasonal frequencies of DIs (in percentage of total days) averaged for the LMM (color bars). Grey thin bars indicate the corresponding value for the 1981-2010 reference period. Grey bars with dotted tops indicate significance differences between the two periods at the 90% confidence level after a two-tailed t-test.

As we have seen in Chapter 4, a below-normal persistence of westerlies inhibits the warm oceanic advection over most of Europe during all seasons, except in summer (Figures 4.2 and 4.4), when it is rather associated with high-pressure systems and radiative warming. In terms

of precipitation, the WI is also an optimal indicator of the transport of moisture fluxes to Europe, with decreased westerlies denoting below-average precipitation over large areas of central Europe all year round (Figures 4.3 and 4.5). Accordingly, the reduced frequency of WI in Figure 5.2 indicates a drier and colder LMM compared to present (with the exception of summer), modulated by the remaining DIs, which have also robust temperature responses over large areas of Europe (Figures 4.2 and 4.4).

Seasonally, summer and winter are the seasons of the LMM that show the largest (significant) differences with the reference period (Figure 5.2). Therefore, in the following analyses, we will focus on these seasons. Winters were characterized by a low frequency of westerlies and high values of northerlies, both contributing to a pronounced cooling due to the reduction (intensification) of warm (cold) advection from the ocean (higher latitudes) as shown in Figures 4.2 and 4.4. Differently, LMM summers exhibited low frequency of westerlies and increased of southerlies. Together, these anomalies tend to favor warmer temperatures (Figures 4.2 and 4.4). Note that in both cases, the reduced westerlies lead to exacerbate the continental climate, with enhanced cooling in winter and warming in summer. Hence, on average, the role of the atmospheric circulation on European temperature displayed a clear seasonal contrast: in winter, the dynamics favored cold conditions in Europe, while in summer it promoted warm conditions. However, it is worth noticing that the effects of the atmospheric circulation on European temperatures are weaker in summer than in winter, due to the smaller pressure gradients over the North Atlantic and the higher contribution of regional and thermodynamical processes (Vautard and Yiou 2009). In agreement with that, the temperature fingerprints of the DIs extend over larger European areas in winter than in summer (Section 4.2).

Overall, the values of the DIs during the LMM do not seem exceptional when compared with those of the reference period (1981-2010, Figure 5.2) or the twentieth century (1901-2014, not shown). This contrasts with the extreme temperature character of the LMM. This apparent decoupling between the atmospheric circulation and the surface conditions could be partly explained by an enhanced role of thermodynamical processes associated with changes in the external forcings, such as volcanism and solar activity, similar to what has been reported for the last decades of increasing anthropogenic forcing (Vautard and Yiou 2009). Notwithstanding, many studies stress the necessity to account for the large-scale dynamics when assessing the climatic impact of solar variability (e.g., Barriopedro et al. 2008) or major

volcanic events (Section 4.4), such as the outstanding eruption of Tambora in 1815 (e.g., Trigo et al., 2009; Luterbacher and Pfister, 2015). Changes in atmospheric circulation, either internal or externally forced, are also necessary to explain the spatial heterogeneity and the extreme character of specific events that occurred during the LMM (Alcoforado et al. 2000; Niedźwiedź 2010). In this sense, the results indicate that the atmospheric circulation contributed to the cold European temperatures of the LMM during winter. By contrast, the summer circulation anomalies were prone to mild conditions, and at most they acted to offset any expected radiative cooling that can be attributed to changes in external forcings. This is in agreement with previous studies, which have stressed that the cold conditions of the LMM were essentially confined to winter (e.g., Wanner et al., 1995; Luterbacher et al., 2001; Slonosky et al., 2001). In consequence, in the remainder of the Chapter we will focus on the LMM circulation during winter and the associated temperature responses.

5.3 Intraseasonal and interdecadal changes

Here we carry out a closer inspection of the mean circulation anomalies during the LMM on monthly time scales and for different decadal periods. This allows us to assess whether the moderate seasonal DIs anomalies described in Section 5.2 for the entire LMM actually hide large anomalies on intra-seasonal or inter-decadal scales that may better explain the surface conditions. This analysis will be performed with the 8-point wind roses, which can better uncover the occurrence of wind anomalies in relatively narrow sectors.

To address intraseasonal changes within the LMM, we computed the mean LMM wind roses for each calendar month of the winter season, i.e. December, January and February. Overall, the results are consistent with the behavior shown by the winter DIs in Figures 5.2 (i.e., enhanced NI and reduced WI), and display an overall resemblance during all winter months, indicating sustained anomalies through winter (Figure 5.3). Specifically, LMM winters were characterized by statistically significant increased frequencies in the NE and/or NW directions (orange color bands in Figure 5.3). On the other hand, the SW (green color bands in Figure 5.3) component stands out by its reduced frequency through all winter months. Although the wind roses provide higher resolution than the DIs, still, on average, they do not show exceptional anomalies for any wind direction and month. This suggests that the extremely cold conditions may have arisen from the combined effect of simultaneous anomalies affecting to different wind directions.

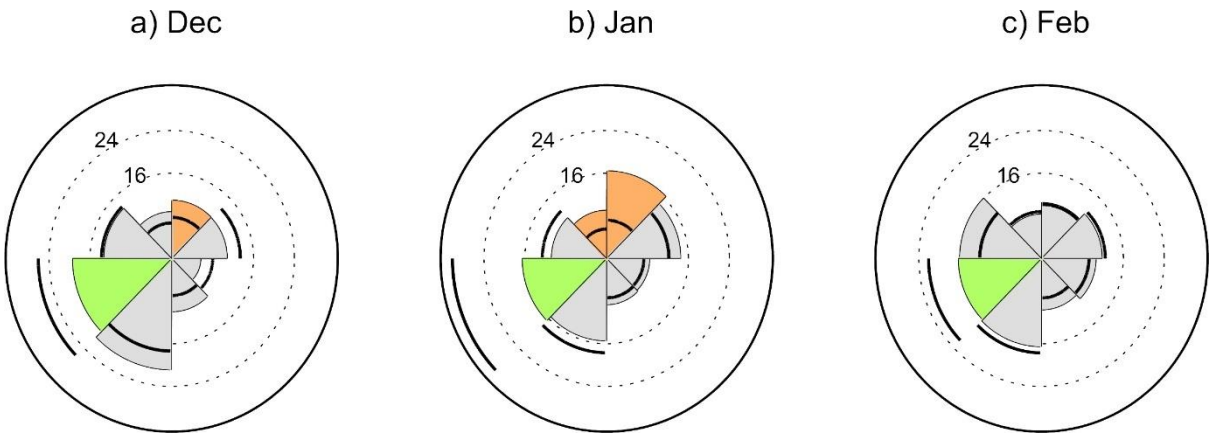

Figure 5.3. Monthly mean 8-point wind-roses for the LMM: a) December; b) February; c) March. The frequencies are expressed in percentage of days (contour interval of 8%) with orange (green) colors highlighting wind directions whose frequency is significantly above (below) that of the 1981-2010 period at the 90% confidence level. The climatology of the 1981-2010 period is shown with thick lines.

With the aim to explore the decadal variability, we divided the winters of the LMM into two subperiods of approximately equal length (1685-1699, first half and 1700-1715, second half). The wind roses of the two halves are superimposed on Figure 5.4, with blue and red shading indicating a larger predominance of that wind direction in the first and second half of the LMM, respectively. The winter wind roses from Figure 5.4 reveal remarkable decadal changes in circulation. The increased frequency of northerly and easterly winds that characterized the first half of the LMM was replaced by opposite anomalies (enhanced southerly and westerly winds) in the second one. In the overall, these interdecadal changes in circulation are observed in all winter months, notably during December and January, and suggest that the first half of the LMM was much colder than the second one.

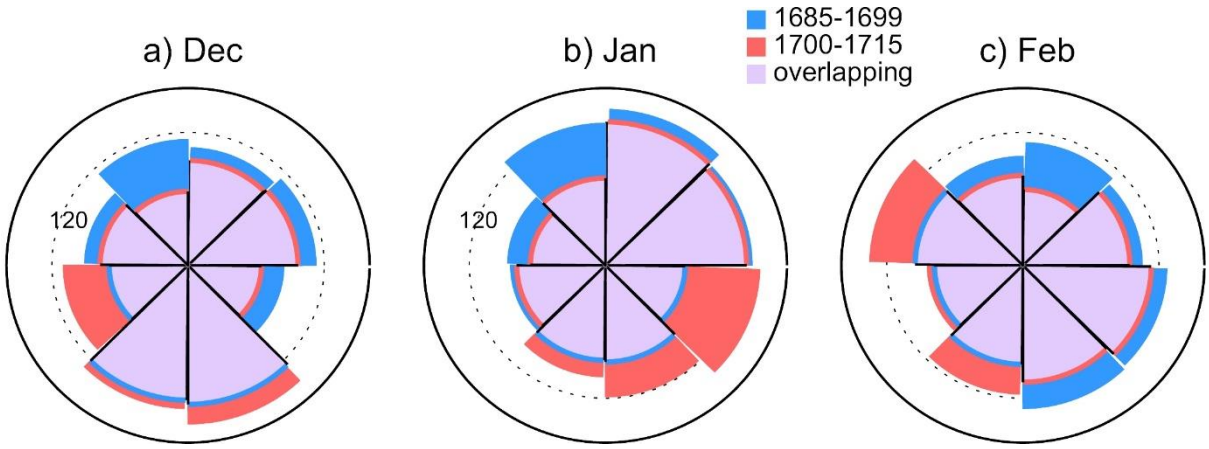

Figure 5.4. Monthly mean 8-point wind roses for the first (1685-1699, blue) and second (1700-1715, red) half of the LMM: a) December; b) January; c) March. Purple indicates the overlapped areas between both subperiods. For a better comparison, the frequency of each bin is expressed in percentage of normals with respect to 1981-2010 (contour interval of 40%).

An example of the substantial decadal winter variability within the LMM is found in the 1690s decade, which, on average, was dominated by increased northerlies and reduced westerlies (standardized DIs anomalies of $\mathrm{NI}_{1690s} = 0.36; \mathrm{EI}_{1690s} = 0.10; \mathrm{SI}_{1690s} = 0.20; \mathrm{WI}_{1690s} = -0.41$). The predominance of the cold advection from northerly and easterly winds over the warm advection associated with westerlies and southerlies confirms the cold conditions reported by previous authors (e.g., Luterbacher et al. 2001; Niedźwiedź 2010). As an exception to this cold decade, the 1699 winter was mild (Luterbacher et al. 2000; Alcoforado et al. 2000; Slonosky et al. 2001; Barriopedro et al. 2014), in agreement with an increased persistence of westerlies and southerlies ($\mathrm{NI}_{1699} = -0.65$; $\mathrm{EI}_{1699} = -0.42$; $\mathrm{SI}_{1699} = 0.46$; $\mathrm{WI}_{1699} = 0.36$). The analysis of the two LMM halves allows us to conclude that the large interdecadal winter variability within the LMM should be taken into account to explain the relatively weak circulation anomalies observed for the entire LMM in Figure 5.2. Moreover, the seasonal DIs are able to capture episodes of shorter duration (e.g., 1699) and hence interannual variations of the atmospheric circulation during the LMM. Therefore, in the remaining, we will focus on characterizing the interannual variability of the LMM and providing a detailed description of the LMM winters.

5.4 Interannual variability

To characterize the interannual variability of the LMM in a more comprehensive way, we synthesized the 4-dimensional information of the DIs by computing a cumulative Circulation

Index (CI, hereafter) that aggregates the standardized values of the four DIs in two components (CI_T, CI_C):

$$CI_T = (SI + WI) - (NI + EI) \quad (5.1)$$

$$CI_C = (NI + SI) - (EI + WI) \quad (5.2)$$

CI_T was first described in Section 4.3 (Equation 4.1a) and is used as an indicator of the European temperature conditions that could be expected from the dynamics, with positive (negative) values of CI_T indicating an overall warming (cooling). CI_C measures the degree of meridional (NI, SI) vs. zonal (WI, EI) circulation, with positive (negative) values indicating a dominance of the former (latter).

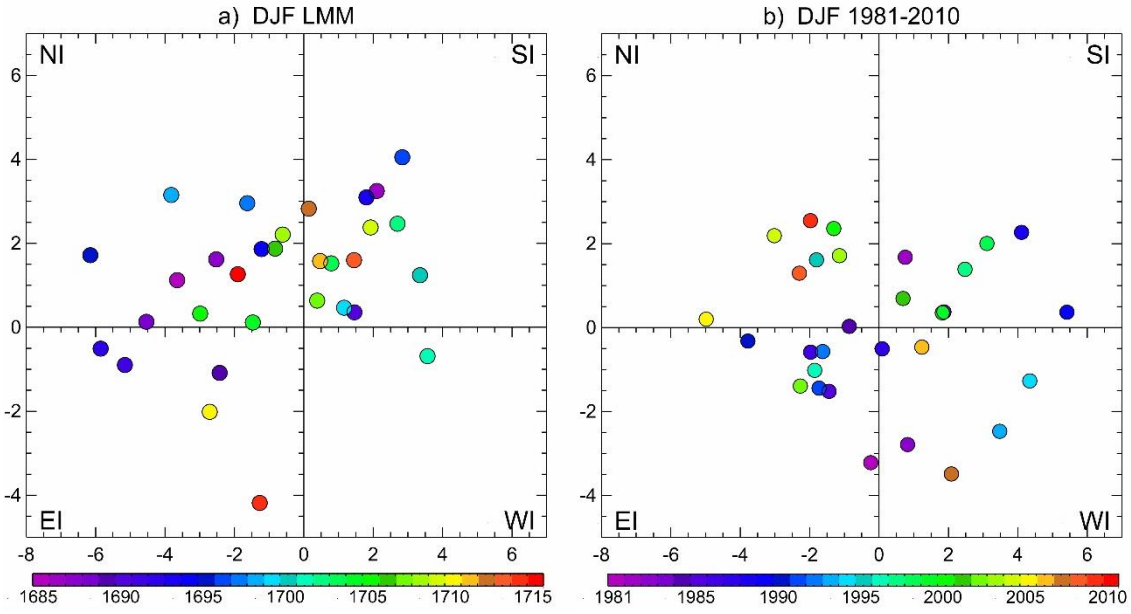

Figure 5.5. Scatter plot of the cumulative index (CI) for: a) the LMM winters; b) winters of the reference period (1981-2010), with colors indicating the year within the LMM. The x-axis (y-axis) represents the CI_T (CI_C) coordinate of the CI.

Figure 5.5a shows the scatter plot of the CI components for the individual winters of the LMM. Overall, the results confirm that the meridional circulation (winters that are above zero in the y-axis, $CI_C > 0$) predominated during the LMM. In fact, only 19% of winters displayed a zonal circulation anomaly (winters below the zero y-axis, $CI_C < 0$). By contrast, about half

of the winters in the 1981-2010 reference period (Figure 5.5b) were dominated by prevailing zonal circulation anomalies.

By construction, the location of each winter along the x-axis of the scatter plot in Figure 5.5 is informative about the balance between wind components that promote cold advection ($CI_T < 0$) from higher latitudes (NI) and the continent (EI), and those associated with warm advection ($CI_T > 0$) from the ocean (WI) and lower latitudes (SI). For example, the 1698 winter, at the upper left corner of Figure 5.5a ($CI_T = -2.74, CI_C = 2.26$) was characterized by the prevalence of meridional (NI+SI) over zonal (WI+EI) flow, and of cold (NI+EI) over warm (WI+SI) advection ($NI_{1698} = 1.10;\ EI_{1698} = 0.44;\ SI_{1698} = 0.20;\ WI_{1698} = -1.40$).

Thus, during winters located at the right x-axis the dynamics is expected to favor warmer conditions due to a predominant southerly and westerly circulation, while winters placed on the left are prone to colder conditions as a result of dominant easterly and northerly winds. Attending to CI_T, the results of Figure 5.5a reveal two different groups of winters, located on the left ($CI_T < 0$) and right ($CI_T > 0$) x-axis, respectively. The color of the symbols in the scatter plot represents the year of each LMM winter, and its distribution indicates that these two groups tend to organize in the first and second half of LMM, respectively. This supports the high decadal variability during the LMM, with a first half colder than the second one.

To confirm that the two groups of winters identified in Figure 5.5a actually display different circulation anomalies in terms of the DIs, we applied a k-means clustering analysis (Section 2.2.4) to the four DIs of the 31 LMM winters. When two clusters are set, it is found that the first cluster represents winters with anomalously high values of NI and EI, as revealed by the DIs values of its centroid ($EI = 0.42, SI = -0.77, WI = -0.41, NI = 0.95$). On the other hand, winters belonging to the second cluster are dominated by positive anomalies of SI (centroid values of $EI = -0.36, SI = 1.17, WI = -0.31, NI = -0.03$). We stress herein that the cluster analysis only takes into account the information of the DIs and hence the resulting classification of winters is based on dynamical arguments. This analysis is also independent of that performed in Figure 5.5 with the CI. However, Figure 5.6 reveals that when the winters of each cluster are displayed in the CI scatter, the clusters tend to group according to CI_T. Accordingly, winters of the first cluster (blue squares in Figure 5.6) are preferably located in the left x-axis ($CI_T < 0$) and coincide fairly well with the cold-prone winters of the first half of the LMM (Figure 5.5a). On the contrary, winters of the second cluster (red

triangles in Figure 5.6) tend to fall into the right side of the scatter plot ($CI_T > 0$), including the majority of the mild-prone winters of the second half of the LMM. Thus, the cluster analysis provides an objective tool to catalogue winters of the LMM according to their circulation signatures, from which the dynamically-driven temperature anomalies can be estimated and contrasted with independent evidences.

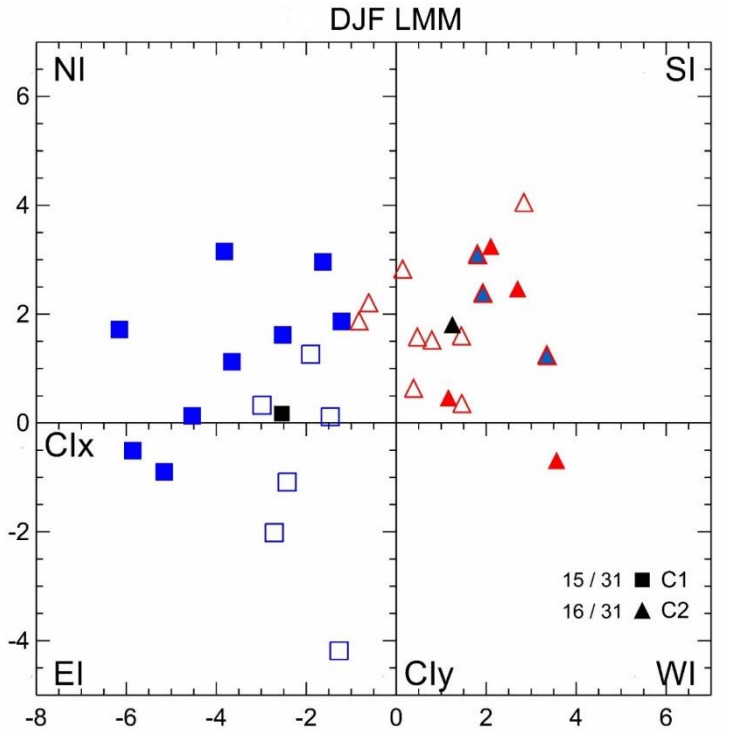

Figure 5.6. As Figure 5.5a but with open blue squares (red triangles) representing winters of the cluster one (two). The number of winters of each cluster is shown in the lower right corner. Black symbols denote the centroid CI values of the cluster one (black square, $CI_T = -2.55, CI_C = 0.17$) and two (black triangle, $CI_T = 1.25, CI_C = 1.81$). Symbols filled with blue (red) in b) represent well documented cold (warm) winters in the literature.

5.5 New catalogue of winters for the LMM

In this section we address how well the temperature conditions inferred from the atmospheric circulation compare with those reported elsewhere in order to evaluate the dynamical contribution to the LMM winter cooling. Filled symbols in Figure 5.6 represent anomalous winters that have been well documented in the literature, based on multiple and independent evidences across Europe (see sources in Table A1 in the Annex). All of them were reported as cold (filled blue), except 1686, 1699, 1701 and 1702, which have been described as warm winters (filled red) in many regions of Europe. Note also that most well

documented cold winters occurred in the first half of the LMM and belong to the first cluster (blue squares in Figure 5.6). On the other hand, the few winters that have been documented as warm in the literature fall in the cluster two (red triangles). This general agreement provides an observational support to previous studies on cold winters, further stressing the major role of the atmospheric circulation in driving the variable conditions within the LMM. For the sake of simplicity, in the following analyses, winters of the first and second cluster will also be referred to as dynamically cold and dynamically mild winters, respectively. However, we stress that this terminology relies on dynamical arguments only.

From Figure 5.6 we also note that a substantial number of LMM winters have not been described in the literature (open symbols), with the exception of some reports for specific locations, such as those by Kington (2010) for London. In this sense, the information provided by the DIs allows us to derive new observational-based evidences about the winter conditions of the LMM. To do so, we have assigned each winter of the LMM to the first (dynamically cold) or the second (dynamically mild) cluster, according to their dynamical signatures (Figure 5.6). We then cross-referenced this catalogue of LMM winters with evidences provided by the literature (Table A1) in order to assess the level of agreement between the temperature anomalies expected from the atmospheric circulation and those reported elsewhere. This comparison has allowed us to identify four groups of winters in the LMM, as shown in the last column of Table A1: i) Group 1 (G1 hereafter): dynamically cold winters cataloged as cold in other studies (1685, 1687, 1688, 1691, 1692, 1694, 1695, 1697 and 1698); ii) Group 2 (G2 hereafter): dynamically cold winters that have not been documented in the literature or whose evidence of cold conditions is spatially and temporally restricted (1689, 1704, 1705, 1710, 1714, and 1715); iii) Group 3 (G3 hereafter): dynamically mild winters that have been either undocumented or reported as mild in the literature (1686, 1690, 1696, 1699, 1701, 1702, 1703, 1706, 1707, 1708, 1711, 1712 and 1713); iv) Group 4 (G4 hereafter): dynamically mild winters that have been described as cold in the literature (1693, 1700 and 1709). Note that G2 and G3 contain mostly winters that have been poorly described or fully unnoticed so far, for which the DIs provide supporting or new observational-based evidence.

In order to confirm the aforementioned heterogeneity of winters, and to explain discrepancies with previous studies, we have inferred the spatial pattern of temperature anomalies from the atmospheric circulation for each winter of the LMM. To do so, we first

searched for the best circulation analogue of each winter of the LMM, among those available for the period 1901-2014. These flow analogues are calculated using the seasonal 8-point wind roses, which provide higher resolution and hence a more detailed information of the atmospheric circulation than the four DIs. The analogue of each LMM winter is the winter of the period 1901-2014 that minimizes the RMSD of their wind roses (see Section 2.2.6). The spatial temperature and geopotential anomaly pattern of each LMM winter is the one corresponding to its analogue of the 1901-2014 period, as obtained from the CRU TS3 and the 20CR v2c, respectively. As we are exclusively interested in the temperature anomalies induced by the atmospheric circulation, the 1901-2014 linear trend of the seasonal temperature series was removed for each grid point before computing the temperature anomaly (with respect to the period 1981-2010). For coherence with the temperature field, we also removed the linear trends of the winter geopotential height. We stress that the analogues method provides the temperature responses due to circulation anomalies, which in turn may have been internally or externally forced, but it does not account for temperature changes associated to other factors (Yiou et al. 2017).

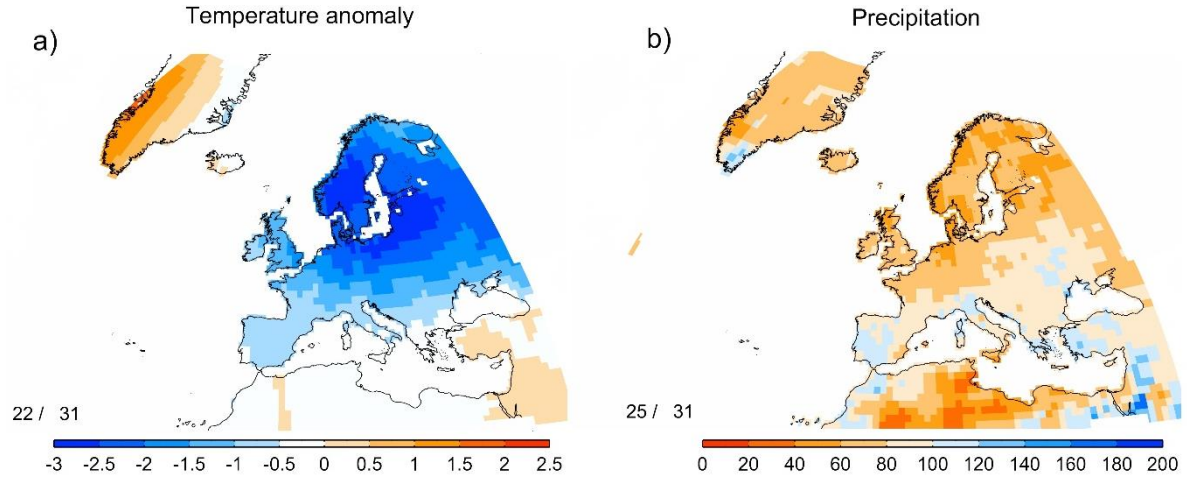

Figure 5.7. LMM mean winter anomalies with respect to 1981-2010, as inferred from circulation analogues of the 1901-2014 period: a) near-surface temperature (in ºC); b) precipitation (in percentage of totals). Numbers at the left bottom of each panel indicate the total number of winters analogues employed in each composite.

Overall, the results from the analogue method indicate that the LMM was cold (see the LMM mean temperature pattern in Figure 5.7a) but displayed substantial variability, both in atmospheric circulation and temperature, as shown next. Taking the analogues as surrogates of the LMM winters, we derived the composite of temperature and geopotential height at 500 hPa anomalies for each group of LMM winters. Figure 5.8 shows the temperature and

geopotential anomaly patterns for the winters of G1, G2 and G3. The composite for G1 (documented cold winters, Figure 5.8a) shows a pronounced and widespread cooling across Europe, supporting the extreme conditions reported by independent sources (Table A1). Using historical series from different European regions, the mean temperature of these winters was 2.3ºC for the Central England Temperature (CET, Manley 1974) and -0.1 ºC in the Netherlands (Van den Dool et al. 1978). The associated circulation displays a strong negative phase of the NAO, Figure 1.10), and shows a large resemblance to the unusual winter of 2009/2010 (Cattiaux et al. 2010, Ouzeau et al. 2011), which has been catalogued as the coldest winter of the last 100 years in some parts of Europe (Prior and Kendon 2011). Using the seasonal NAO index (Hurrell et al. 2003) for the analogue winters of G1, we obtained an average value of -2.21 SD, in agreement with the circulation pattern of Figure 5.8a.

The winters of G2 (dynamically cold winters that have been poorly documented or undocumented) were less extreme than those of G1, especially in central and northern Europe, but still cold throughout most of the continent (Figure 5.8b). The instrumental series of temperature from Central England (the Netherlands) give an average value of 3.6ºC (2.3ºC), which is higher than that obtained for G1 winters. The associated circulation was also characterized by a negative NAO-like pattern. However, and different to G1, the G2 pattern displays a departure of the NAO dipole from zonality with a migration of the centers of action. Interestingly, this "low zonal" NAO dipole reflects the dominant mode of variability during periods of decoupling (i.e., insignificant correlations) between the WI and the NAO, such as 1871-1900 (Barriopedro et al. 2014), while the corresponding pattern of G1 fits well into the "high zonal" NAO pattern, characterized by strong correlations between the WI and the NAO (e.g., 1901-1930). This lack of stationarity in the NAO pattern during the LMM has not been reported before, probably due to the inherent limitations of the proxy-based reconstructions of the NAO, thus reinforcing the added value of the wind direction data. The less extreme cold temperatures associated with the "low zonal" NAO pattern of G2 could be the reason of the unnoticed character of these winters. These results suggest an additional contribution of other dominant modes of Euro-Atlantic atmospheric variability in shaping the G2 pattern and its departure from the canonical NAO. This will be further addressed in Chapter 6.

The composite for G3 (dynamically mild winters that have been poorly documented or undocumented) confirms that these winters were not as cold as those of G1 or G2 (Figure 5.8c). Indeed, the Mediterranean basin was characterized by relatively warm conditions, while a weak cooling signal was confined to northern and eastern European regions. The temperature pattern inferred from the atmospheric circulation is in good agreement with the instrumental series from Central England (the Netherlands), which indicate mean temperatures of 4.3ºC (3.1ºC), higher than those obtained for G1 and G2. The difference between the composites of G3 and G2 (Figure 5.8d) confirms that the winters of G2 were also colder than those of G3, emphasizing the large variability within the LMM. The circulation anomaly during the winters of G3 displays anomalous centers that are displaced southeastward with respect to the NAO, similar to the positive phase of the EA pattern (Figure 1.10). We stress that G3 (and to some extent G2) contains winters that have not been catalogued to date or whose evidence is restricted in spatial or temporal scales. Therefore, our analysis is particularly informative of non-extreme winters (G2 and G3), for which documentary records often do not provide sufficient information.

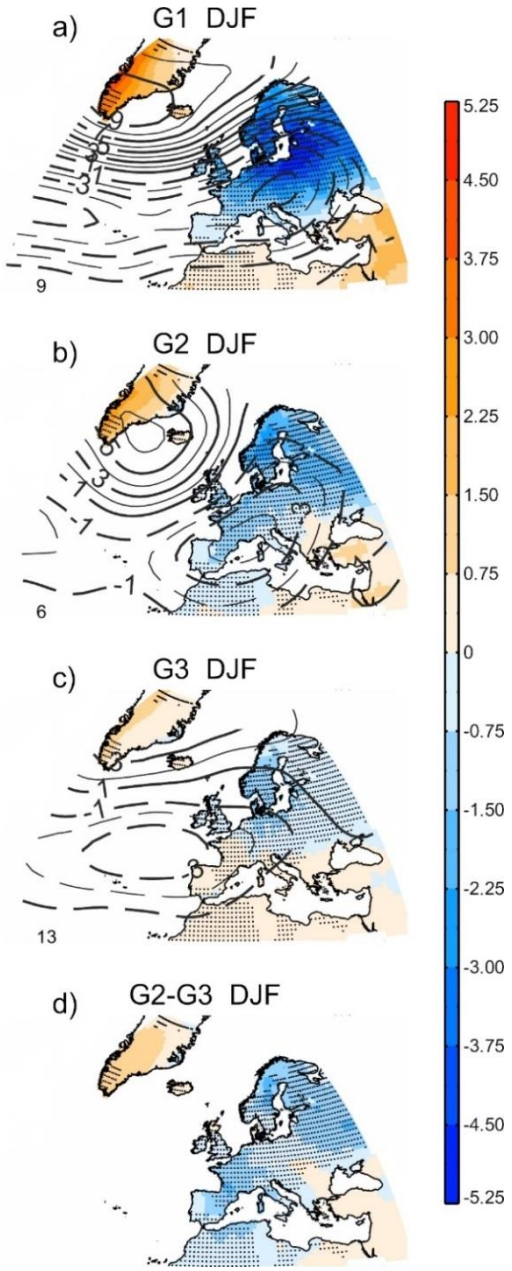

Figure 5.8. Winter composites of near-surface temperature (shading, in ºC) and geopotential height at 500 hPa (contours, in dam) anomalies for the winter analogues of: a) Group 1 (G1); b) Group 2 (G2); c) Group 3 (G3); d) the difference between G2 and G3. Dotted areas highlight those regions where the MSSS is significantly above the climatology at the 90% confidence level. Numbers at the left bottom of each panel indicate the total number of winters of each group.

Finally, we assess the winters of G4 (1693, 1700 and 1709), which are classified as dynamically mild winters herein, but have been documented as cold winters elsewhere. Note that the causes of the discrepancies could lay on the side of the proxies (e.g., evidences confined or biased to specific regions) or the wind indices and the methodology (e.g., inferential approach from a limited sample). However, it could also indicate a reduced control

of the dynamics on temperature (e.g., an enhanced role of external forcings). To clarify these discrepancies, we analyzed in more detail the winters of G4 by evaluating their analogues separately (Figure 5.9). Different to the composite analysis of Figure 5.8, the assessment of individual winters leads to noisier and more extreme fields than those obtained therein. Thus, to account for the range of temperature anomalies that can be obtained under the same atmospheric circulation and to avoid misleading comparisons with Figure 5.8, we selected the analogues of each winter of G4 (up to a maximum of three) that do not double the RMSD of the best analogue, and their average is shown instead. This choice was taken as a compromise between a low number of analogues, which can lead to non-robust patterns, and a high number of analogues, whose averaging can miss the extreme character of the winter.

The wind roses of 1693 and (not shown) reveal higher values of the meridional wind components in both cases. The high frequency of southerly winds explains why these winters are catalogued as dynamically mild, with 1693 (1700) displaying 41% (30%) of days with wind blowing from 135º to 225º. Despite the overall cooling reported in previous studies, there are local evidences of coldness as well as warmness in some parts of Europe, suggesting heterogeneous regional patterns. Thus, the 1693 winter (Figure 5.9a) has been reported as cold and slightly cold in Iberia (Alcoforado et al. 2000) and Hungary (Rácz 1994), respectively. However, warmer or normal conditions were reported in Czech Republic (Brázdil et al. 2008), London (Kington 2010) and Switzerland (Pfister 1992). Based on the historical series of temperature, the 1693 winter was the 11th (7th) warmest winter of the 1685-1715 period in Central England (the Netherlands). On the other hand, the reported cooling of the 1700 winter (Figure 5.9b) is mostly based on local evidences from Czech Republic (Brázdil et al. 2008), the Balkans and Greece (Xoplaki et al. 2001), but there were near normal temperatures in London (Kington 2010) and Switzerland (Pfister 1992), and it was the 3th warmest winter of 1685-1715 in the Netherlands. In agreement with the literature, our results also indicate that the winter of 1693 (1700) was relatively cold in several European regions, including Iberia and Hungary (Czech Republic, Balkans), and warm in Czech Republic (the Netherlands). Regarding the atmospheric circulation, the 1693 winter was dominated by a primary high-pressure center over Scandinavia, resembling a positive phase of the SCA pattern (Figure 1.10), and a low-pressure center over Iberia, which would explain the reported cooling therein. On the other hand, 1700 was characterized by a negative phase of the NAO, but with its centers displaced westward, especially the high-pressure anomaly, which retreated towards Greenland, likely reducing the cold advection over the continent. In

summary, the 1693 and 1700 winters were characterized by a strong meridional circulation (including northerly and southerly components), thus leading to a heterogeneous spatial pattern with regional signals of warming and cooling across Europe, similar to the mild winters of G3 (Figure 5.9b), but still compatible with indirect evidences reporting local or regional cold conditions.

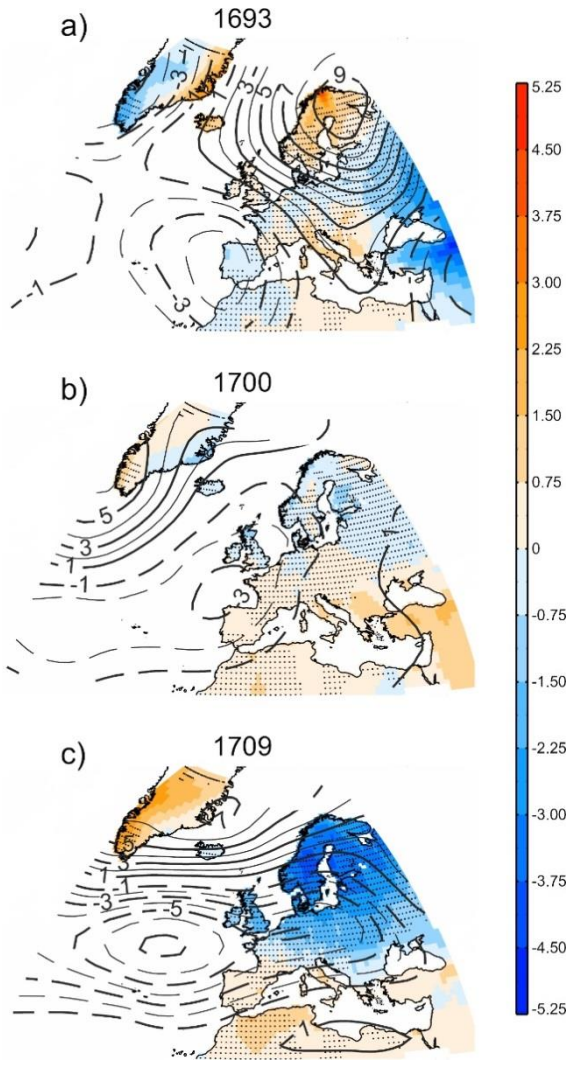

Figure 5.9. As Figure 5.8 but for the average of the best analogues of each winter of Group 4: a) 1693; b) 1700; c) 1709. See text for details.

Similar to the other winters of the G4, the 1709 winter ("The Great Frost", as it was known in England) displayed persistent northerly winds and hence it was actually cold in many areas of Europe (Figure 5.9c). However, different to 1693 and 1700, the coldness of this winter is very well documented across Europe (Table A1). Thus, we investigated thoroughly the circulation of this winter by taking advantage of the daily resolution of wind observations.

We found that December and February of 1709 were characterized by westerlies and southerlies, with the exception of some persistent intrusions of polar and continental winds, mainly in February. Accordingly, our results suggest a near normal December and a cold February, which agree with previous studies (Luterbacher et al. 2004, Kington 2010). January 1709 has been reported as the coldest month of that winter in Europe (e.g., Luterbacher et al. 2004 and references therein), being the main reason of discrepancy with our results. A detailed analysis of the daily wind direction observations revealed a gap in wind data between 5 and 14 of January 1709. This is the only month of the LMM containing a long interval of successive missing days, while still satisfying the minimum threshold of available daily data to consider it as a non-missing month. Unfortunately, this lack of data matches with an extremely cold polar outbreak in Europe, which started between 4 and 6 of January 1709 in England and France, and persisted until the middle of that month (Derham 1708, Maraldi 1710; Monahan 1993; Kington 2010). This period should have coincided with persistent northerly winds, likely changing the temperature character of January 1709 and the entire winter of 1709 to dynamically cold. Therefore, the discrepancy with the reported evidences is attributed to a 10-day spell of missing data that is unique in our record, and hence the winter of 1709 should be reclassified as dynamically cold. In spite of this, the regional cooling reported in Greece and the Balkans (Xoplaki et al. 2001) is confirmed by the results (Figure 5.9c). This result highlights the importance of daily data when explaining extreme events such as the winter of 1709.

We note in closing that wind direction has also significant signals in precipitation across Europe (Section 4.2) and hence the wind roses can also be used to infer the anomalous precipitation patterns associated to the LMM. Accordingly, we have applied the same analysis of analogues to precipitation fields extracted from the GPCC for the 1901-2014 period. The results indicate that the LMM was overall a dry period (Figure 5.7b), partially due to the reduced frequency of westerlies (the DI with the largest precipitation responses). However, the precipitation anomalies and decadal variability were not as large as in the case of temperature. We hypothesize that the reduced frequency of southerlies (easterlies) in the first (second) half of the LMM partially compensated the precipitation deficits induced by the lack of westerlies.

5.6 Conclusions

In this chapter, we have presented a new observational analysis of the LMM (1685-1715) based on direct instrumental evidence of the atmospheric circulation over the eastern Atlantic, as provided by the DIs. The main findings can be summarized as follows:

- The average circulation anomalies during the LMM contributed to relatively cold and dry conditions in most of Europe due to the prevalence of a strong meridional circulation and the absence of westerlies throughout the year, as compared to present (1981–2010).

- The atmospheric circulation during the LMM displayed contrasting seasonal signals. The year-round deficit of westerlies was partially compensated by an increase of northerly and southerly winds in winter and summer, respectively. Therefore, winter circulation contributed the most to the cold conditions.

- Despite the meridional character of the winter circulation during the LMM, this period was not exceptional when compared to more recent periods, due to the presence of significant decadal variability of the North Atlantic atmospheric circulation within the LMM. In particular, there was an increase of northerly winds favoring colder winters in the first half of the LMM, but enhanced southerlies contributing to milder conditions in the second half of the LMM.

- The analysis of the atmospheric circulation allowed us to yield a new and complete classification of LMM winters. The temperature inferred from the atmospheric circulation confirms the majority of extremely cold winters well documented in the literature, while uncovering other less documented cold and mild winters.

- These findings indicate that the LMM in Europe was more heterogeneous than previously thought, displaying contrasting spatial patterns in both circulation and temperature. In particular, we provide evidences of a non-stationarity of the NAO pattern within the LMM, with extremely cold winters being driven by negative phases of a ‘‘high zonal’’ NAO pattern and ‘‘low zonal’’ NAO patterns dominating during moderately cold winters.

These results consolidate the potential of the DIs to study the European past climate and its variability on different time scales, as well as to capture departures from the canonical

NAO pattern. The latter motivated the next Chapter 6, which will further exploit the added value of the DIs as an additional source of information of the Euro-Atlantic atmospheric circulation beyond that provided by the NAO.

Chapter 6

6. Examining the NAO-EA relationship and the jet stream variability since 1685

The limited understanding of the jet stream variability is partially hampered by the short observational record of wind measurements in the historical period, which are mostly constrained to the 20th century (García-Herrera et al. 2018 and references therein). Previous studies have shown that the concomitant state of NAO and EA account for much of the winter North Atlantic eddy-driven jet stream variability. Unfortunately, an integrated assessment of NAO and EA indices to infer the variability of the eddy-driven jet in the historical period is missing because the evolution of the EA before the mid-19th century remains unknown, and the few existing studies considering NAO and EA are limited to the 20th century (Comas-Bru et al. 2016, 2018).

This Chapter will use the DIs to extend current instrumental records of NAO and EA back to the 17th century, analyze their multiple combinations and exploit them to reconstruct the variability of the North Atlantic eddy-driven jet stream since 1685. The analysis will be restricted to the winter (December-February) season, when the NAO and EA account for the largest fraction of variance and are tightly coupled to the jet stream (e.g., Woollings et al. 2010). The main results of this Chapter can be found in Mellado-Cano et al. (2019b) (accepted).

6.1 NAO and EA indices

An SVD analysis (see Section 2.2.5) was applied to the 1685-2014 winter series of the four DIs, retaining the two first singular vectors, which explain 44% and 35% of the total variance, respectively. Similar results were obtained by applying the same analysis to the DIs series of each winter month separately (December: 45%, 34%; January: 43%, 36%; February 44%, 35%). Table 6.1 shows the Pearson correlation coefficients between these singular vectors and different NAO and EA indices for their overlapping periods (see the definition of these indices in Section 2.1.2.3). Regardless of the considered period, all NAO (EA) indices

display significant correlations at p<0.01 with the first (second) singular vector of the DIs and insignificant or very weak correlations with the second (first) one. The series of highest correlation with the first singular vector (0.67) corresponds to the NAO index of Jones et al. (1997) for the common period (1824-2014). High correlation coefficients (0.74) are also obtained between the second singular vector and the EA index of Comas-Bru and Hernández (2018) for the 1950-2014 period. This relationship weakens back in time, arguably due to methodological issues in the definition of that EA index (which involves a multi-reanalysis ensemble mean), a progressive loss of variance in the long reanalyses (i.e., increasing spread across members back in time), the quality or quantity of observations affecting both SLP and wind measurements, as well as non-stationarities in the EA pattern. Still, the correlations observed with the second singular value are of similar magnitude to those obtained between other EA indices for the recent 1950-2014 period (e.g., r=-0.58 for the EA indices of CPC and Valentia SLP series), stressing the differences between its multiple definitions.

Table 6.1. Pearson correlation coefficients between the two first SVD vectors of the DIs and different NAO and EA indices for different periods. The correlation coefficient with the first (SVD1) / second (SVD2) vector is shown in the last column. Significant correlations at p<0.01 are highlighted in bold.

Indices	Overlapping period	SVD1 / SVD2
NAO		
CPC NOAA	1950-2014	**0.60** / -0.2
Hurrell et al. 1995	1901-2014	**0.48** / -0.19
Jones et al. 1997	1824-2014	**0.67** / -0.05
Luterbacher et al. 2002	1685-2001	**0.61** / -0.04
EA		
CPC NOAA	1950-2014	0.32 / **0.55**
Comas-Bru and Hernández (2018)	1950-2014	0.20 / **0.74**
2nd EOF SLP ERA-20C	1901-2010	-0.21 / **0.57**
Comas-Bru and Hernández (2018)	1852-2014	**0.28** / **0.47**

Figure 6.1 shows the composites of CRU temperature, GPCC precipitation and ERA-20C Z500 anomalies associated with the first and second singular vectors of the DIs for the 1901-2010 period. Overall, their signatures agree well with those reported elsewhere for other NAO

(e.g., Trigo et al. 2002) and EA (Comas-Bru and McDermott 2014) indices. Consequently, from now on, these DI-based indices will be referred to as NAO_{DI} and EA_{DI}.

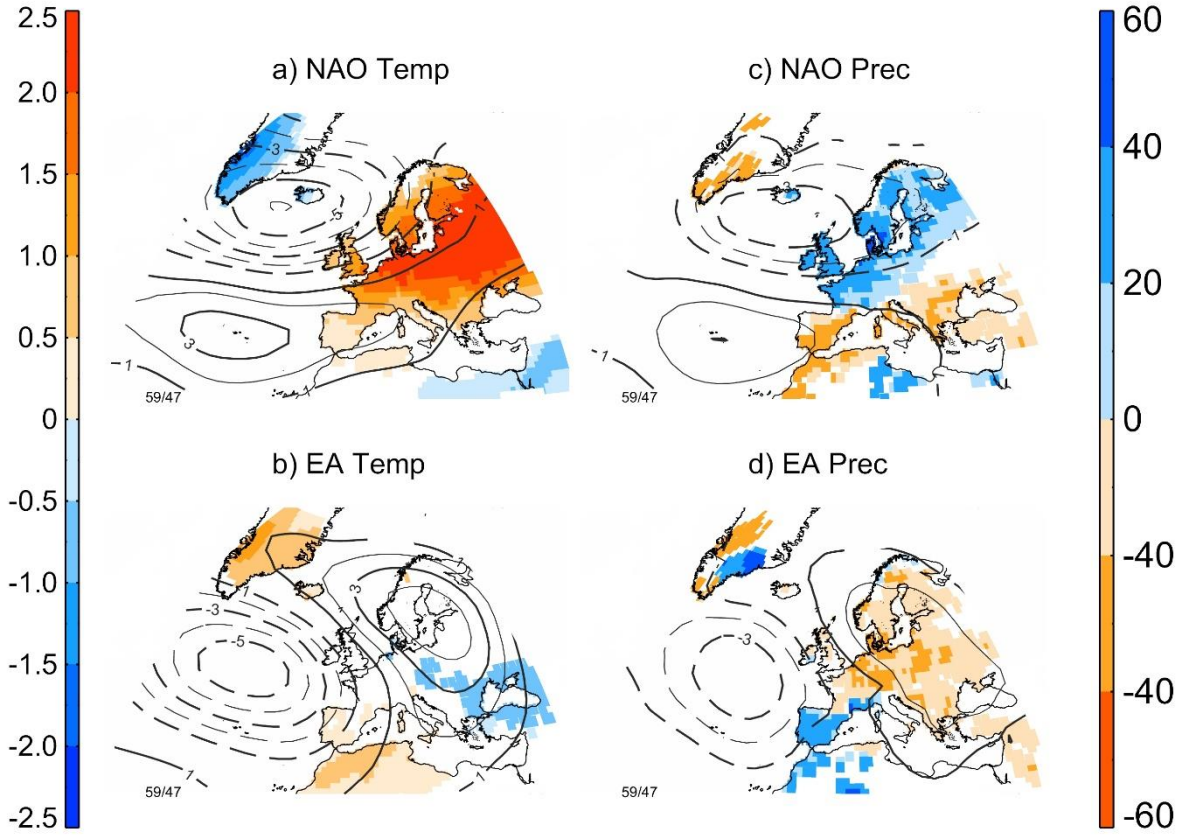

Figure 6.1. Winter composite differences between positive (>0.5 SD) and negative (<-0.5 SD) phases of a, c): NAO_{DI} (upper panel) and b, d): EA_{DI} (lower panel) for 1901-2010: a, b) near-surface temperature (shading, in ºC) and geopotential height at 500 hPa (contours, in dam) anomalies; c, d) precipitation (shading, in percentage of normals) and SLP (contours, hPa) anomalies. Only temperature and precipitation anomalies that are significantly different ($p<0.05$) from the climatology are shown, after a 5000-trial bootstrap test. We used monthly near surface temperature from the CRU TS v3.23 (Harris et al. 2014) and total monthly precipitation from the GPCC (Schamm et al. 2014) on a grid of 1°x1°, as well as geopotential height data at 2.5°x2.5° from the ERA-20C reanalysis (see Section 2.1.2.2).

Figures 6.2a and b show the winter series of NAO_{DI} and EA_{DI} for the last 330 years (black lines), with red (blue) colors indicating 7-year running mean values above (below) zero. NAO_{DI} captures outstanding anomalous periods reported in previous studies, including the dominant positive phases during 1900-1930 and 1970-2000 as well as the persistent negative phases of 1820-1845 and the 1960s (Jones et al. 1997; Visbeck et al. 2001; Slonosky and Yiou 2001; Luterbacher et al. 2002; Trouet et al. 2009; Cornes et al. 2013). The NAO_{DI} series also displays extreme negative values for the well-known cold winters of 1916/17 (NAO_{DI}=-

1.97 SD) and 1962/63 (NAO_{DI}=-2.30 SD) (Cornes et al. 2013; Greatbatch et al. 2015). The same level of agreement applies to the EA_{DI} index, which captures the predominance of positive phases at the end of the 19th century and the subsequent reversal at the beginning of the 20th century (Comas-Bru and Hernández 2018). It also reflects extreme episodes on different time scales, such as the recurrent negative values in the 1950s reported by the CPC EA index or the extreme 2004/05 winter (EA_{DI}=-1.40 SD). Therefore, we are confident that our indices are excellent indicators of the two leading modes of atmospheric variability over the Euro-Atlantic sector. They provide the longest instrumental series of both NAO and EA, extending current records by more than 150 years in the case of EA. Superimposed on the aforementioned signatures, our records also show large variability on very low frequencies (multidecadal and longer). The EA_{DI} negative phase dominated during the 1750-1950 period, while the positive phase prevailed before 1750 and after 1950 (Figure 6.2b). The NAO_{DI} shows a more alternating behavior until 1800, with a certain prevalence of the negative phase along the 19th century (Figure 6.2a).

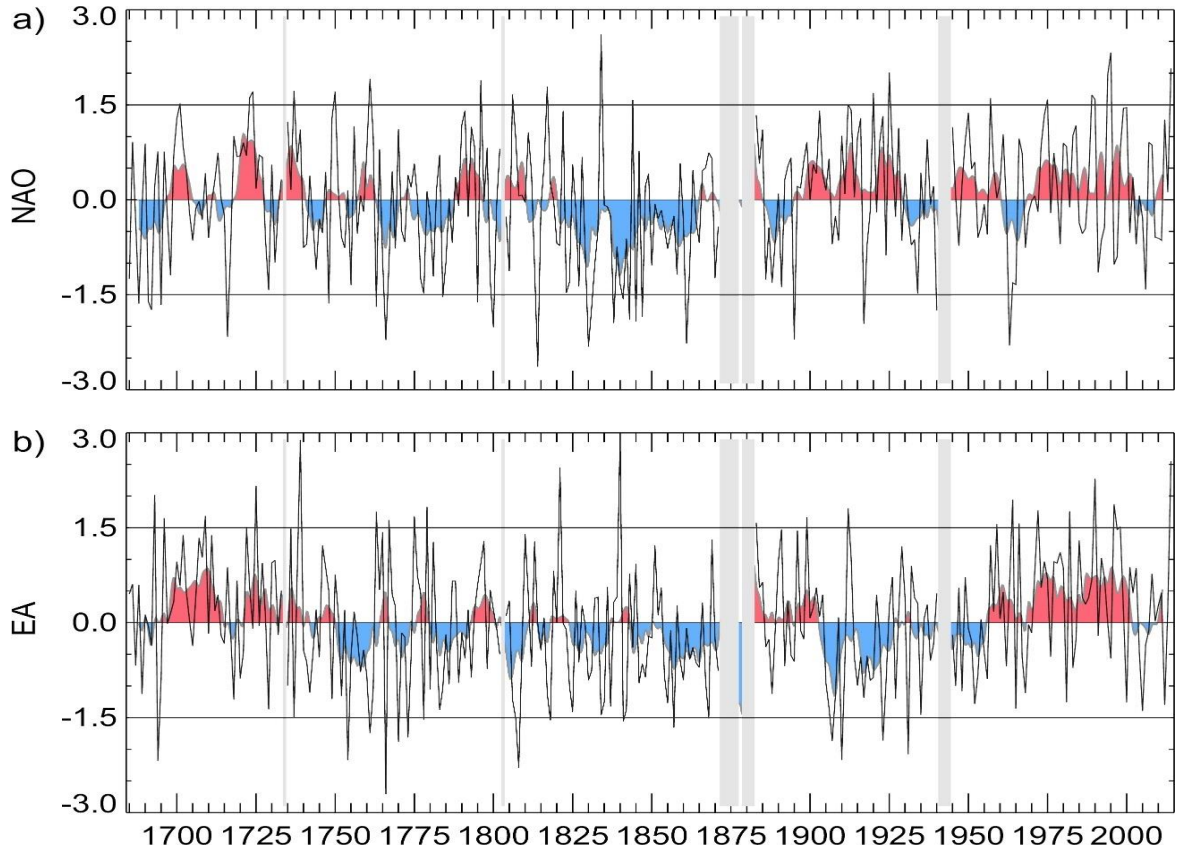

Figure 6.2. Winter standardized series of: a) NAO_{DI}; b) EA_{DI} for 1685-2014 (in SD, black line) and a 7-year running mean (grey line), with red (blue) shading indicating periods above (below) the 1685-2014 mean. Vertical grey shading identifies periods of missing data.

6.2 The combined role of NAO and EA in Euro-Atlantic climate

In order to determine the joint effects of the NAO_{DI} and EA_{DI} on the Euro-Atlantic climate we have partitioned the 2-D NAO_{DI}/EA_{DI} phase space, thus defining four combinations of the NAO_{DI} and EA_{DI} indices attending to their phases: NAO_{DI}+/EA_{DI}+, NAO_{DI}+/EA_{DI}-, NAO_{DI}-/EA_{DI}+ and NAO_{DI}-/EA_{DI}-. This analysis is restricted to the period of available data in the reanalysis and the observational products of temperature and precipitation (1901-2010). These groups only contain winters with absolute values of NAO_{DI} and EA_{DI} larger than 0.5 SD. This criterion provides a balanced and sufficient number of cases (Figure 6.3), excluding winters with weak signals of either NAO_{DI} or EA_{DI}. The resulting composites for each combination are weaker but qualitatively similar if the above threshold is omitted, therefore cataloguing all winters in one of the four groups (not shown). The robustness of the results was further confirmed by repeating the analysis for the NAO and EA indices of the CPC and the period 1950-2014 (Figure 6.4). Our approach is similar to that adopted by Comas-Bru and McDermott (2014), except that they only considered two groups formed by winters with equal and opposite phases of NAO and EA, thus disregarding asymmetric responses between positive and negative phases, as those reported for the NAO (e.g., Cornes et al. 2013).

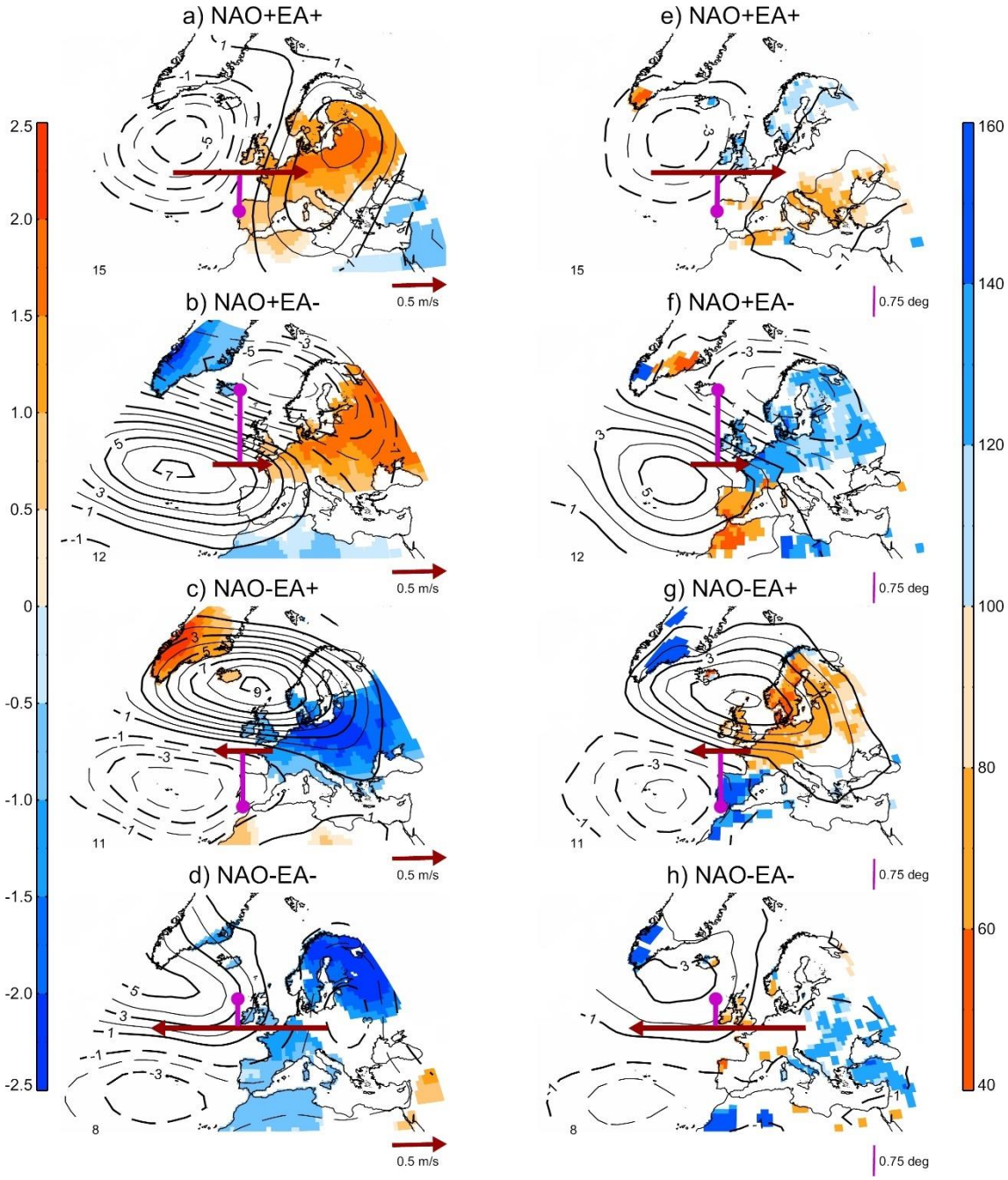

Figure 6.3. Winter composites of: a-d) near-surface temperature (shading, in ºC) and geopotential height at 500 hPa (contours, in dam) anomalies; e-h) precipitation (shading, in percentage of normals) and SLP (contours, hPa) anomalies for different combinations of NAO_{DI} and EA_{DI} indices with absolute values larger than 0.5 SDs: a) NAO_{DI}+/EA_{DI}+; b) NAO_{DI}+/EA_{DI}-; c) NAO_{DI}-/EA_{DI}+; d) NAO_{DI}-/EA_{DI}-. Anomalies are computed with respect to 1901-2010. Numbers in the left bottom corner of each panel represent the number of cases employed in each composite. Only temperature and precipitation anomalies that are significantly different ($p<0.05$) from the climatology are shown, after a 5000-trial bootstrap test. Horizontal red arrows and vertical purple lines summarize the composited winter anomalies of the jet speed and latitude respectively, with the length being proportional to the anomaly. Eastward (westward) red arrows indicate a strengthening (weakening) of the jet. Purple lines pointing upward (downward) indicate a poleward (equatorward) shift of the jet.

Figure 6.3 shows the composites of winter anomalies in atmospheric circulation (Z500 and SLP from ERA-20C, contours) and near-surface (2-m temperature and precipitation from the CRU and GPCC respectively, shading) fields for each combination of indices. Red arrows and purple lines illustrate the composites of the winter mean anomalies in the jet speed and latitude. The winter means were obtained by averaging the corresponding daily parameters of the North Atlantic jet stream, which were diagnosed from zonal wind data of the ERA-20C reanalysis, as explained in Chapter 2 (see Section 2.1.2.4). All NAO_{DI}/EA_{DI} combinations display a pressure dipole, but exhibit differences in the location, intensity and spatial extension of the centers of action. When NAO_{DI} and EA_{DI} are in the same phase (Figures 6.3a, e and d, h), the southern center of action is reinforced and eastward shifted towards Europe, while the northern center retreats towards the Atlantic. As a consequence, the North Atlantic jet stream displays changes in the typical SW-NE tilt. This can occur at expense of the westerlies (i.e., a wavier pattern; Figures 6.3d, h, $NAO_{DI}-/EA_{DI}-$) or be accompanied by a stronger jet (i.e., an enhanced SW-NE tilt of the jet; Figures 6.3a, e, $NAO_{DI}+/EA_{DI}+$). This is supported by the corresponding composites of jet speed anomalies, which show a reinforced jet for $NAO_{DI}+/EA_{DI}+$ and the opposite for $NAO_{DI}-/EA_{DI}-$ (horizontal red arrows in Figures 6.3a, d), with relatively weaker anomalies in the jet latitude. On the other hand, when the NAO_{DI} and EA_{DI} have opposite phases (Figures 6.3b, f and c, g) the northern and southern centers of the resulting dipole shift towards Europe and the Atlantic, respectively. In this case the anomalies in the jet latitude are larger than those obtained when both indices are in the same phase, with a poleward shift of the jet for $NAO_{DI}+/EA_{DI}-$ (vertical red arrows in Figures 6.3b, f) and equatorward migrations for $NAO_{DI}-/EA_{DI}+$ (Figures 6.3d, h).

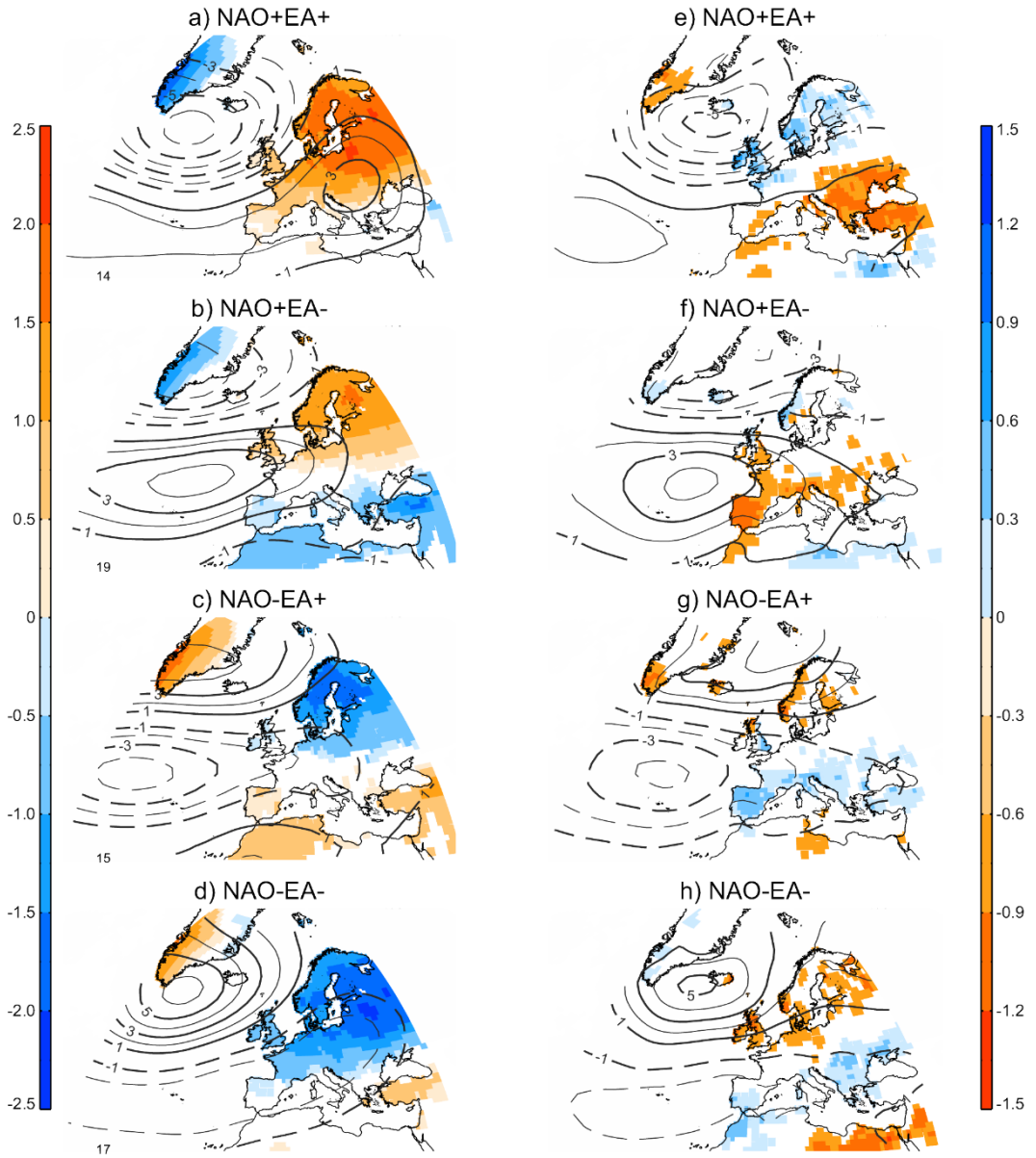

Figure 6.4. As Figure 6.3 but for the NAO and EA indices of the Climate Prediction Center (NOAA) and the 1950-2010 period. Groups are defined without demanding a minimum threshold to the indices so that all winters are included in the composites. Anomalies are relative to 1950-2010.

Overall, our results indicate that NAO_{DI} and EA_{DI} induce anomalies of the same sign in the jet speed but have opposite effects in the jet latitude. Woollings and Blackburn (2012) found that meridional shifts of the jet are largely due to the NAO, while NAO and EA are of roughly equal importance in describing jet speed anomalies. These discrepancies with our results could be due to model biases in the jet, differences between our indices and those considered therein and/or non-stationary influences of NAO and EA on the jet. From our results the role of EA_{DI} in modulating the jet responses to the NAO_{DI} seems to occur through

the tilt of the jet, with the positive phase favoring a stronger and reinforced SW-NE tilt (i.e., southward displacements in the North Atlantic and the opposite in the exit region of Europe). Using daily data, Woollings et al. (2010) identified three nodal locations for the North Atlantic jet stream in northern, central and southern latitudes. According to our results, winters with a central jet position tend to occur when NAO_{DI} and EA_{DI} display the same sign, while meridional displacements dominate in winters of opposite phases, being poleward (equatorward) for NAO_{DI}+/EA_{DI}- (NAO_{DI}-/EA_{DI}+).

We next turn attention to the composites of surface climate anomalies for the different partitions of the NAO_{DI}/EA_{DI} phase space. The sign of the temperature anomalies is largely determined by the NAO_{DI}, with warmer winters in most of continental Europe for all combinations with positive NAO_{DI} phases (Figures 6.3a, b) and approximately the opposite pattern for winters of negative NAO_{DI} (Figures 6.3c, d). However, the EA_{DI} shapes this overall picture by modulating the regions where the largest temperature anomalies occur, which shift from central to northeastern Europe when the EA_{DI} changes from positive (Figures 6.3a, c) to negative (Figures 6.3b, d) phases. Analogously, Greenland exhibits larger anomalies when the EA_{DI} phase is opposite to that of NAO_{DI}. In addition, there are areas where the additional role of one of the indices is able to alter the expected temperature response to the other. For example, under NAO_{DI}+, the Iberian Peninsula exhibits warming if EA_{DI} is in a positive phase (Figure 6.3a), but no significant signals for EA_{DI}- (Figure 6.3b). Therefore, the reported influence of EA in Iberian winter temperature (Sáenz et al., 2001; Toreti et al. 2010; Hernández et al. 2015; Sánchez-López et al. 2016) is modulated by the NAO. Similarly, Greenland warming, typically associated with pervasive blocking conditions under negative NAO phases (Davini et al. 2012; Hanna et al 2016), is more pronounced for EA_{DI}+ (Figure 6.3c) but substantially damped and even reversed under EA_{DI}- (Figure 6.3d).

On the other hand, precipitation anomalies (Figure 6.3, right panels) are overall more sensitive to the concomitant state of NAO_{DI} and EA_{DI} than those in temperature, although the areas displaying significant responses are comparatively reduced. Widespread precipitation responses occur in winters with opposite phases of NAO_{DI} and EA_{DI} (Figures 6.3f, g), since these combinations reflect the largest anomalies in the jet latitude, which largely controls the trajectories of the moisture transport into Europe. As such, the EA_{DI} exerts a strong modulation on the NAO_{DI} precipitation responses. For example, NAO_{DI}-/EA_{DI}+ (Figure 6.3g) and NAO_{DI}-/EA_{DI}- (Figure 6.3h) are the only combinations leading to above-normal

precipitation in the Iberian Peninsula and central-eastern Mediterranean, respectively. Surprisingly, the former region is among the areas with the strongest responses to the NAO (e.g., Trigo et al. 2002), meaning that the EA_{DI} also modulates the canonical fingerprints of the NAO. These unexpected results are in agreement with the opposite effects of NAO_{DI} and EA_{DI} on the jet latitude. During NAO_{DI}-/EA_{DI}+ both modes contribute to a southward shift of the jet and enhanced storminess in southern Europe (Figure 6.3g). However, the high-pressure systems over the North Atlantic and central Europe associated with NAO_{DI}- and EA_{DI}+ merge, obstructing the progression of storm-tracks into eastern Mediterranean. Differently, the NAO_{DI}-/EA_{DI}- combination is less efficient in displacing the jet, due to their competing effects in the jet latitude (Figures 6.3d, h). In this case, positive pressure anomalies are confined to eastern Atlantic mid-latitudes, impeding the entrance of storm tracks to the westernmost sector of southern Europe. The resulting weaker and wavier jet allows storm tracks to be diverted northward or southward of the high-pressure center (not shown). This configuration leaves a corridor of low pressure through northern Africa towards eastern Mediterranean (Figures 6.3d) that has also been associated with anomalies in the African jet (Gaetani et al. 2011). These results indicate that the Mediterranean precipitation responses in NAO- composites arise from mixing winters with precipitation signals in either western or eastern Mediterranean, which are influenced by the additional role of EA. A similar behavior is found for positive NAO_{DI} phases (Figures 6.3e, f). As such, the canonical precipitation signature attributed to NAO in southwestern Europe mainly occurs when EA is in the opposite phase. If EA is in phase with the NAO, the signal shifts eastward leading to weaker precipitation responses in that region (see also Figure 6.4). This west-east EA modulation of the NAO signal may explain the reported anti-correlation in drought severity between western (Iberia) and eastern (Turkey) Mediterranean for the 20th century (Sousa et al. 2011).

6.3 NAO, EA and jet stream since 1685

In the previous section we have reported how different combinations of NAO_{DI} and EA_{DI} have profound implications in the Euro-Atlantic climate variability through their effects in the latitude and speed of the eddy-driven jet. Herein, we explore the whole 1685-2014 record to address the relative frequencies of NAO_{DI}/EA_{DI} combinations and their relevance to explain anomalous periods of the last three centuries. To further exploit the complementary information of these indices on the jet stream, we performed a SRM for the 1901-2010 period, using either the latitude or speed of the jet as the dependent variable and the NAO_{DI} and EA_{DI}

as the predictors (see Section 3.2.3 for further details). The regression coefficients of the selected predictors are then used to reconstruct the latitude and speed of the jet stream for the 1685-2014 period. The SRM (Table 6.2) is able to explain a significant amount of the jet variance, being more skillful for the jet speed (r=0.71) than for the jet latitude (r=0.40). For both jet parameters, the NAO_{DI} and EA_{DI} enter in the SRM, confirming their independent influences on the jet. As inferred from the regression coefficients of the SRM, NAO_{DI} and EA_{DI} have opposite (equally signed) effects on the jet latitude (speed), but with different loadings.

Table 6.2. Stepwise Regression Model of the jet speed (top) and latitude (bottom) standardized anomalies onto the NAO_{DI} and EA_{DI} indices for 1901-2010. For each jet parameter, the first two rows indicate the regression coefficients for each index with their p-values in parentheses (based on a t-test with null hypothesis of zero coefficient). The last row shows the multiple correlation coefficient (i.e., explained variance) with the p-value of the goodness-of-fit F-statistic in parentheses.

Predictor	Inference (p-value)
Jet speed	
NAO_{DI}	0.74 (<0.01)
EA_{DI}	0.18 (<0.01)
NAO_{DI} & EA_{DI}	0.71 (<0.01)
Jet latitude	
NAO_{DI}	0.19 (0.02)
EA_{DI}	-0.37 (<0.01)
NAO_{DI} & EA_{DI}	0.40 (<0.01)

Figure 6.5a shows the frequency of the dominant NAO_{DI}/EA_{DI} combination for each 7-year overlapping interval of the 1685-2014 period, with the color identifying the specific pair: $NAO_{DI}+/EA_{DI}+$, $NAO_{DI}+/EA_{DI}-$, $NAO_{DI}-/EA_{DI}+$ or $NAO_{DI}-/EA_{DI}-$. Herein, all winters are catalogued in one of these four groups based on the sign of the indices. Moreover, Figure 6.5b displays the 7-year running mean standardized anomalies of the jet latitude reconstructed from NAO_{DI} and EA_{DI}, with orange (blue) colors indicating strengthening (weakening) of the jet for the same 7-year mean periods. When the whole period is considered, there is a balanced frequency of NAO_{DI}/EA_{DI} combinations, with $NAO_{DI}-/EA_{DI}+$ displaying slightly lower frequencies (22.4%) than the rest. Independently of the combination considered, it is observed that NAO_{DI} and EA_{DI} show the largest absolute values in nearly 50% of the winters

indicating that the last three centuries cannot be properly described by the state of the NAO_{DI} alone. Accordingly, the jet displayed substantial variability from interannual to centennial time scales, both in terms of intensity and latitudinal location (Figure 6.5b). In spite of this, there are no hints of long-term trends or exceptional values for the last decades in the context of the last 330 years.

In addition, there are some periods that stand out from the dominance of a given NAO_{DI}/EA_{DI} combination. For example, 1720-1740 was characterized by recurrent positive phases of NAO_{DI} and EA_{DI} (Figure 6.5a) as well as large anomalies in the jet (i.e., a stronger and mostly equatorward shifted jet, Figure 6.5b), suggesting warm (cold) winters in central Europe (Greenland and eastern Mediterranean basin), as well as dry (wet) conditions over Mediterranean (northern European) regions. This result provides a dynamical evidence of the reported shift towards increased precipitation in northern Europe (Jacobeit et al. 2003, Pauling et al. 2006) as well as the drought 1700-1715 period in the south (Domínguez-Castro et al. 2008). Our time series also allow explaining individual extreme years. For example, the winter of 1783/84 that followed the Laki's eruption was extremely cold around the circum-North Atlantic. D'Arrigo et al. (2011) suggested that the unusual conditions were caused by a negative NAO phase and a warm ENSO event. Our results confirm the former (NAO_{DI}=-1.54 SD) event but also uncover a key role of the EA_{DI}, which was also in its negative phase (-1.04 SD), both contributing to an extreme weakening of the jet.

Now, we turn attention to periods of contrasting phases between the NAO_{DI} and EA_{DI} which are those displaying the largest displacements of the jet stream. There were recurrent periods of NAO_{DI}-/EA_{DI}+ through 1685-2014 characterized by southward excursions of the jet stream (Figure 6.5b), including some decades of the LMM (Chapter 5). Although the period 1825-1875 was mostly dominated by negatives phases of NAO_{DI} and EA_{DI}, the EA_{DI} was in a positive phase during the 1840s (blue shading in Figure 6.5a). Interestingly, Cornes et al. (2013) and Luterbacher et al. (2001) reported negative phases of the NAO during the 1830s, but their indices disagree on the 1840s. Our results indicate that a shift in the phase of the EA_{DI} prompted changes in the NAO_{DI} dipole (similar to those observed from Figures 6.3d to c), which are not captured in the same way by different NAO indices. On the other hand, Santos et al. (2013) described two recent exceptional winters in the North Atlantic sector (2009/10 and 2011/12) with a contrasting behavior in the jet stream. In addition to the

extreme negative (positive) NAO phase reported therein, our series evidence a measurable influence of EA_{DI}+ (EA_{DI}-) in the southwardly (northwardly) shifted jet of 2009/10 (2011/12).

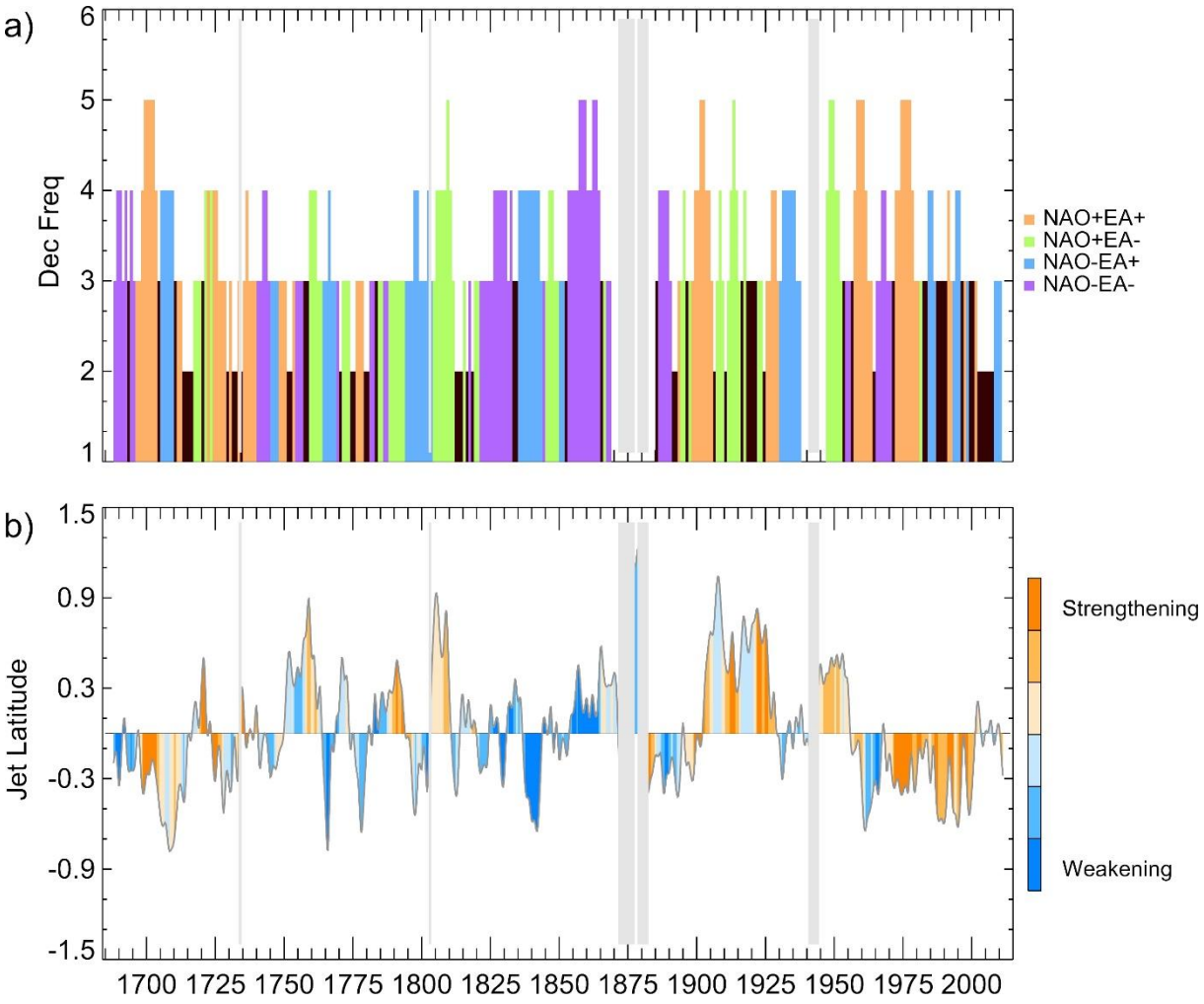

Figure 6.5. a) Frequency and type of the dominant winter NAO_{DI}/EA_{DI} combination for each 7-year overlapping interval of the 1685-2014 period, with the black color indicating intervals without a dominant combination. The highest values (columns) imply that 5 out of 7 years are dominated by that NAO_{DI}/EA_{DI} combination. Vertical grey shading identifies periods of missing data; b) Reconstructed jet latitude anomaly (in SD with respect to 1685-2014) with a 7-year running mean (grey line). The corresponding 7-year running mean of the jet speed anomalies are shown in color, with orange (blue) colors shading denoting a strengthening (weakening) of the jet.

On the other hand, the combination NAO_{DI}+/EA_{DI}- dominated several intervals of the 1685-2014 period, most notably the beginning of the 20th century (Figure 6.5a), which was characterized by poleward excursions of the jet stream (Figure 6.5b). This was followed by a strengthening and more frequent southward migrations of the jet at the end of the 20th century, coinciding with a transition towards EA_{DI}+ winters during 1975-2000. This shift from EA_{DI}- to EA_{DI}+ (Figures 6.3e, f) is timely with the well-reported migration of the NAO action

centers (e.g., Jung et al. 2003; Vicente-Serrano and Lopez-Moreno 2008). Similar transitions have been recurrent in the last three centuries (e.g., from $NAO_{DI}+/EA_{DI}+$ to $NAO_{DI}+/EA_{DI}-$ at the beginning of the 20th century, or from $NAO_{DI}-/EA_{DI}+$ to $NAO_{DI}-/EA_{DI}-$ in the mid-19th century). Therefore, our results stress that the non-stationarities of the NAO can to a large extent be explained by the prevailing phase and strength of the EA and that relatively long-periods dominated by different combinations of these indices have occurred frequently in the last three centuries.

6.4 Conclusions

In this Chapter we present the longest (1685-2014) instrumental records of winter NAO and EA indices, as well as estimates of the North Atlantic eddy-driven jet stream for the same period derived from the DIs. The main findings can be summarized as follows:

- The new DIs-based indices are optimal indicators of instrumental NAO and EA series, also capturing their main signatures on European temperature and precipitation. For the 1685-2014 period, they display large variability from interannual to multidecadal time scales, with e.g. positive EA phases dominating before 1750 and after 1950, and negative NAO phases prevailing during much of the 19th century.

- By identifying winters with different combinations of NAO and EA indices in the 20th century NAO/EA phase space, our results highlight the role of EA in shaping the North Atlantic action centers and the European climate responses to NAO. The EA modulation of the NAO signal is stronger in precipitation than in temperature and affects areas with strong responses to NAO such as Greenland and western Mediterranean. These NAO/EA combinations have occurred frequently during the 1685-2014 period, indicating that the past atmospheric circulation cannot be properly described by the state of the NAO alone.

- The combined influence of these indices on the Euro-Atlantic climate is explained by additive (canceling) effects of NAO and EA on the speed (latitude) of the North Atlantic jet stream and their different degrees of influence. Therefore, much of the North Atlantic jet stream variability through the 20th century can be explained by the NAO and EA. These relationships have been used to reconstruct the jet speed and latitude for the 1685-2018 period. This reconstruction has been assessed using a SRM

model which suffer from some limitations (Harrell 2001) and consequently the results should be interpret with caution, particularly for the jet latitude for which the explained variance by model is much lower than for the jet speed.

- The so-inferred anomalies of the jet stream are related to transitions in the NAO/EA phase space, which have been recurrent and explain non-stationary NAO signatures, such as the displacement of the NAO action centers in the late 20th century, as well as some disagreements between instrumental NAO indices. The last three centuries uncover substantial interannual to centennial variability in the North Atlantic jet stream, thus providing new evidences of the dynamics behind some anomalous periods.

In summary, by extending back the instrumental records of the NAO and EA indices, we provide the first observational evidences of the North Atlantic jet stream for the last three centuries. This supposes a step forward to achieve a full picture of the past Euro-Atlantic atmospheric circulation, overcoming some limitations of current estimates that are mainly based on the NAO alone.

Chapter 7

7. Summary and discussion

This Chapter summarizes and discusses the main conclusions of this Thesis (Section 7.1) and presents insight into future studies and applications (Section 7.2).

7.1 Main conclusions

This Thesis presents new instrumental indices of the atmospheric circulation over the eastern North Atlantic based on daily wind direction observations from the English Channel for 1685-2014. They provide an excellent framework to study the European climate from monthly to centennial time scales, emphasizing the added value of ships' logbooks as an instrumental source to characterize the atmospheric circulation all year-round, its forced and internal variability and the associated fingerprints on surface climate. This represents a substantial step forward since the current knowledge of the European climate for the last centuries strongly relies on multi-proxy reconstructions, which are often biased towards the summer season and suffer from various other caveats. The main conclusions can be summarized as follows:

1. Ships observations from ICOADS (1850-2014) have been extended back to 1685 by using more than 70.000 wind direction records abstracted from ships' logbooks. A robust methodology has been designed to obtain the monthly persistence of the wind in the four cardinal directions (i.e., the Northerly, Easterly, Southerly and Westerly Indices, NI, EI, SI and WI), as well as the uncertainties associated with sampling issues and changes in the number of observations. These Directional Indices (DIs) are the longest and highest resolution instrumental indices of atmospheric circulation over the North Atlantic currently available.

2. The DIs reveal substantial variability from interannual to multidecadal and even longer time scales, including some differences between industrial and pre-industrial periods. The latter may reflect: 1) a dynamical response to external forcings; 2) a previously unnoticed multicentennial variability; 3) other issues not addressed herein. This result can be informative for future projections but with very different implications: while the

first interpretation could provide guidance on potential dynamical responses to increasing anthropogenic forcing, the second one would mean that we may be underestimating the range of internal variability, at least on very low frequencies. Future modeling studies are required to further evaluate these hypotheses.

3. The DIs reflect synoptic-to-large-scale changes in the atmospheric circulation, affecting the mid-latitudes of northeastern Atlantic and Western Europe, providing an appropriate framework for modulating the thermal advection and moisture fluxes into the continent. As such, fluctuations in the DIs are associated with precipitation and temperature anomalies over large areas of Europe in all seasons. The climatic signals of the DIs are spatially complementary, with zonal (WI and EI) and meridional (NI and SI) indices frequently affecting different areas. Precipitation is strongly controlled by zonal DIs all year-round through moisture advection, while the spatial temperature response to the DIs is more complex and can vary with the season as it depends on temperature advection and radiative processes. In summary, the combined information of the four DIs captures all year-round climatic signals in terms of temperature and precipitation, making them excellent benchmarks for proxy calibrations.

4. The long record of the DIs allows us to better constrain the regional responses to some of the external forcings of the climate system. Thus, the assessment of the atmospheric circulation signatures following the strongest tropical volcanic eruptions since 1685 supports the well-reported winter warming over Europe, but also shows that the associated atmospheric circulation signals are complex, involving changes in the meridional flow and substantial case-to-case variability. The atmospheric circulation may also play a role in the post-eruption European summer cooling, which had previously been attributed to radiative factors alone. Besides, the DIs provide new evidences for the less documented transitional seasons, with hints of cooling before summer and warming prior to winter. These results support the idea that explosive tropical eruptions can induce measurable changes in the atmospheric circulation throughout the year. Similar analyses could be applied to explore the circulation responses to other natural external forcings (e.g., grand solar maxima and minima).

5. The surface signals of the DIs also allow us to infer anomalous conditions driven by atmospheric circulation, thus providing new insights into the European climate since

1685. For example, the 1717-1727 and 1687-1697 winters, as well as the 1835-1839 and 1757-1762 summers, stand out as some of the warmest and coldest periods before the 20th century. On longer time scales, the first half of 18th century and the 1825-1875 period were relatively dry during all months. While the identification of these periods is based on dynamical arguments only, the so-inferred anomalies could be compared with the "actual" conditions reported from historical records in order to quantify the role of non-dynamical processes, opening new opportunities to explore and understand past anomalous periods.

6. In this sense, the analysis of the Late Maunder Minimum (LMM, 1685-1715) reveals that it was characterized by a strong meridional circulation, with a generalized frequency reduction of the westerlies all year-round, contributing to relatively cold and dry conditions in Europe. Nevertheless, this overall picture hides important variations on seasonal and decadal time scales. Winter and summer were the seasons with the largest circulation anomalies but displayed contrasting signals, with winter circulation contributing the most to the LMM cooling. In spite of this, the winter DIs were not exceptional, partially due to the presence of large decadal variability. As such, the reduced frequency of westerlies was compensated by an increase of northerly winds (favoring colder winters) in the first half of the LMM, but was also accompanied by enhanced southerlies (contributing to milder conditions) in the second half of the LMM.

7. Based on dynamical arguments, the DIs yield a new and complete catalogue of winters for the LMM. The results indicate that the LMM in Europe was more heterogeneous than previously thought, displaying contrasting spatial patterns in both circulation and temperature. The temperature anomalies inferred by the DIs confirm the majority of extremely cold winters well documented in the literature (e.g., 1692, 1694, 1695), while uncovering other less documented cold (e.g., 1704, 1710) and mild (e.g., 1686, 1690) winters. In addition, some of the winters classified as cold in Europe (e.g., 1693, 1700) may rather have displayed complex spatial patterns, with regional signals of warming and cooling. The results call for caution when generalizing to European scales the temperature anomalies obtained from local records, and also highlight the added value of daily records when dealing with extreme events.

8. By covering all principal wind directions, the DIs give a more complete picture of the atmospheric circulation than that provided by zonal indices such as the North Atlantic Oscillation (NAO). In fact, they often improve the variance accounted for by the NAO on temperature and precipitation. They also shed light on some inconsistencies between NAO indices for specific periods of the past, which can be explained by non-stationary NAO patterns, frequently associated with the presence of a marked meridional circulation. As an example, the DIs suggest that during the LMM, the extremely cold winters documented in the literature were dominated by a negative phase of the NAO. However, other relatively cold but less extreme winters were rather characterized by a departure of the NAO dipole from zonality, probably explaining the largely unnoticed cold behavior of these winters. Consequently, the DIs arise as a powerful tool to explore the complexities of the Euro-Atlantic atmospheric circulation, including non-stationary signatures of the NAO and their climatic implications.

9. Based on the DIs, we present an almost continuous record of instrumental winter NAO and East Atlantic (EA) indices for the last 330 years. The exploration of the 20th century evidences an important role of EA in modulating the spatial pattern of the NAO and the geographical location of the North Atlantic action centers: when both indices are in the same phase the resulting southern action center strengthens and extends towards Europe, while winters of opposite phases are characterized by the westward retreat of the southern node. Preferred NAO/EA states can persist for decadal time scales, with temporary transitions explaining recent changes in the Euro-Atlantic circulation such as the displacement of the NAO centers during the last decades of the 20th century. Similar transitions have been recurrent in the last three centuries, explaining some disagreements between long-term NAO indices and pointing the EA as an important source of non-stationary signatures of the NAO.

10. The EA also alters substantially the canonical signatures of the NAO on the European surface climate: it modulates the spatial pattern of the temperature response to NAO, and can dampen and even reverse the NAO-related precipitation signal. For example, the canonical NAO precipitation signal in western Mediterranean is mainly confined to winters with an out-of-phase EA, but it weakens when EA is in phase with the NAO due to an eastward shift of the precipitation response towards eastern Mediterranean. The results have important implications for NAO reconstructions based on proxy

records, whose climatic signals are calibrated against the NAO alone, therefore assuming stationary relationships. As the climatic signals are often affected by the concomitant state of NAO and EA (even in canonical spots of the NAO), the blurring effect of EA can lead to weak and sometimes misleading NAO-proxy relationships, affecting the skill of the NAO reconstruction. Thus, a better calibration and improved reconstructions of the atmospheric circulation would be obtained by considering the joint effects of these indices.

11. Winter NAO and EA have significant fingerprints in the North Atlantic jet stream for the 20th century: NAO and EA have an additive influence on the jet speed, dominating the role of the NAO over the EA, while NAO and EA have opposite influences in the jet latitude, being both of comparable importance. As such, the largest departures in jet speed (latitude) tend to occur in winters with equal signed (opposite) phases of NAO and EA. Thus, an additional effort to deep further into the past evolution of the EA (in addition to that of the NAO) is necessary to better pin down the long-term variability of the North Atlantic jet stream. Taking advantage of the NAO and EA indices derived from the DIs, we provide the first reconstruction of the North Atlantic jet stream since the 17th century. The results unveil substantial interannual to centennial variability in jet speed and latitude, providing a dynamical interpretation for some anomalous periods and extreme episodes. Further studies are required to disentangle the internal variability of the jet from externally forced responses. These prospective studies should also distinguish changes in jet speed and latitude, which are independent and may thus respond differently to changes in external forcings. This gains special relevance in the context of the ongoing climate change and the large uncertainty in future climate change projections of the jet stream**.**

Based on all the topics mentioned above I am confident to state that the promising results of this Thesis put into evidence the added value of the DIs. Their instrumental nature, high-temporal resolution and marine origin make them informative of the atmospheric circulation over regions that are poorly covered by other observational records, being excellent candidates to improve current European climate reconstructions.

7.2 Outlook

This Thesis illustrates some of the DIs' applications, but they can be further exploited in order to deep into some findings reported herein that deserve further investigation as well as to identify new opportunities. In this Section a few of them are listed and shortly discussed:

- Reconstructions of SLP over large geographical areas provide internally consistent and spatially coherent patterns that allow further insights into climate variability than univariate circulation indices (e.g., NAO, EA). There exist several published reconstructions of Euro-Atlantic SLP fields beyond the industrial era (e.g., Jones et al. 1999; Luterbacher et al. 2002), but they are exclusively based on instrumental series or proxy information from land. In this sense, SLP reconstructions lack data from the ocean. The longest SLP reconstruction including ocean data information covers the period since 1750 and was developed in the last decade by Küttel et al. (2010). They used a multivariate principal component regression that became very popular at the beginning of the 21st century (e.g., Jones et al., 1999; Luterbacher et al., 2002; Gallego et al., 2005; Pauling et al., 2006). Over the last few years, further research has been conducted on testing and improving different reconstruction techniques (e.g., Lee et al. 2008; Tingley and Huybers 2010). For example, Bayesian inference of hierarchical models is a powerful method where a likelihood function is combined with a prior probability density function to yield a posterior distribution for the fields and parameters (e.g., Gelman et al. 2003). Taking advantage of this, Tingley and Huybers (2010a) developed a Bayesian Algorithm for Reconstructing Climate Anomalies in Space and Time (BARCAST) and applied it to surface air temperatures. Werner et al. (2013) found that this method outperformed models based on regressions. It has also been applied to reconstruct the European summer temperatures of the last 2000 years (Luterbacher et al. 2014). The DIs offer the opportunity to retrieve a new land-ocean combined BARCAST reconstruction of SLP since 1685, extending the largest instrumental land-only SLP reconstruction currently available and superseding the only land-ocean combined reconstruction of Küttel et al. (2010) in terms of the amount of assimilated data and method performance.

- In the context of climate change, there is a requirement from users and policy-makers to reduce uncertainties of future climate projections. In addition to uncertainties related

to the chosen scenario, a large amount of the model spread can be attributed to future atmospheric circulation changes, which exert a strong control on regional projections (e.g., Zappa and Shepherd 2017). In this sense, there are key weather systems of the Euro-Atlantic atmospheric circulation with short records (mostly confined to the reanalysis period) that could be extended back with the aid of the DIs. For example, high pressure systems such as blocking and subtropical ridges are major contributors to the intra-seasonal variability, causing outstanding impacts on Europe at monthly and seasonal time scales. They also display uncertain climate change responses and controversy links with recent sea-ice extent decline and Arctic Amplification (e.g. Woollings et al. 2018 and references therein). These uncertainties are difficult to cope with, because these weather systems are not well represented in state-of-the-art climate models, and the observational record is too short to characterize their forced responses (e.g., Trigo et al.2 2004; Barriopedro et al. 2006, Sousa et al. 2016, 2018). As these weather systems have fingerprints in the lower tropospheric circulation, prospective studies of the DIs should aim to reconstruct their past monthly frequency and variability, providing a long temporal context to interpret some of the aforementioned issues (e.g., links with polar regions; Ayre et al. 2015).

- The DIs evidence that the Euro-Atlantic atmospheric circulation over the last three centuries has experienced large variability from seasonal to multi-decadal or even centennial time scales. The sources of this variability include internal fluctuations, but also forced responses to external factors (e.g. explosive volcanic eruptions). To further elucidate the range of internal variability and to better constrain the forced responses in the atmospheric circulation the use of model simulations is encouraged in future studies. There are ongoing initiatives which provide model data for specific anomalous periods of the past (e.g., VolMIP, Zanchettin et al. 2016), or the last millennium (e.g. the Paleoclimate Modeling Intercomparison Project), herein including large ensembles of single- and full-forcing simulations (e.g., the Community Earth System Model Last Millennium Ensemble, CESM-LME, Otto-Bliesner et al. 2016). Using daily wind data from the lower troposphere (e.g. at 10 m) over the English Channel and applying the methodology developed herein, DIs can be constructed in the model world, which provides a surrogated reality in which different hypotheses and results of this Thesis can be tested. They include the forced responses to external factors, the sources of non-stationary NAO signals, the drivers of LMM-

like decadal variability of the DIs, the recurrent transitions of NAO/EA states, and their linkages with the North Atlantic eddy-driven jet stream.

- As shown in this Thesis, instrumental ships' logbooks provide precise and reliable information of the past climate. Figure 7.1 shows ships' logbooks observations prior to 1857. With the exception of projects like CLIWOC or ICOADS there is still an uncountable number of logbooks from different countries that have not been digitalized, including many from Portugal. Even more, already abstracted ships' logbooks provide enough number of wind observations (Figure 7.1) to yield nearly continuous time series of any particular wind direction in unexplored areas such as the east coast of the United States or the Pacific Ocean. The former could be used to characterize extratropical cyclones and to better constrain the North Atlantic jet stream, while the latter could be indicative of the past evolution of ENSO. Hence the promising results of this Thesis will hopefully stimulate future developments of such kind of indices as well as of ships' logbooks recovery in international projects.

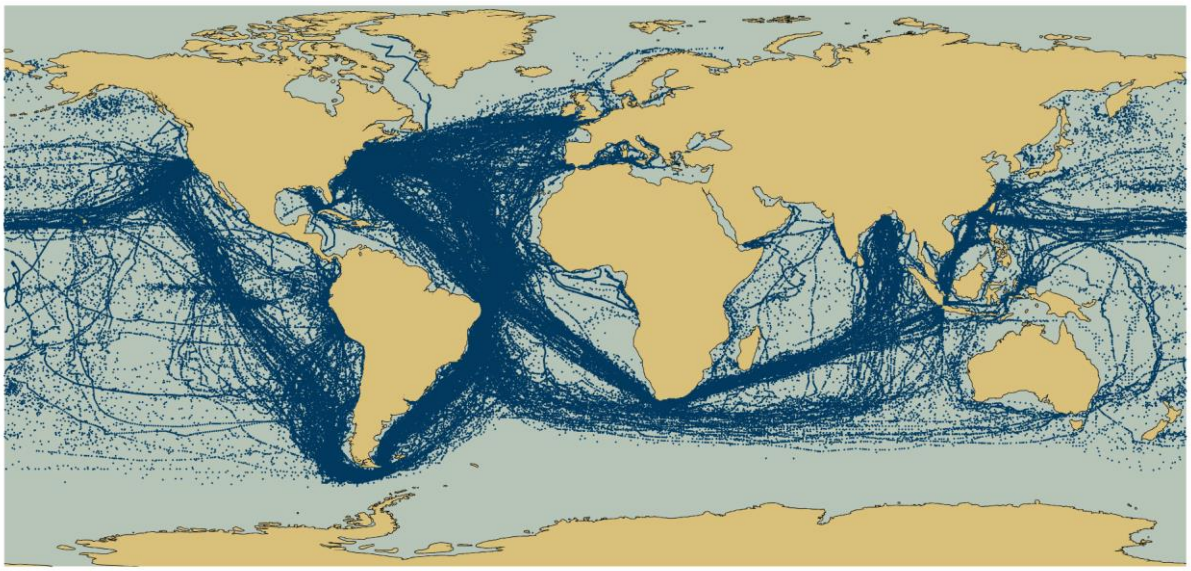

Figure 7.1. Wind direction observations from ICOADS for the period 1663-1857 in blue dots.

Publications

Mellado-Cano, J., D. Barriopedro, R. García-Herrera, R. M. Trigo, and M.C. Álvarez-Castro, 2018: Euro-Atlantic Atmospheric Circulation during the Late Maunder Minimum. J. Climate, 31, 3849–3863, https://doi.org/10.1175/JCLI-D-17-0261.1

Mellado-Cano, J., D. Barriopedro, R. García-Herrera, and R. M. Trigo, 2018: New instrumental insights into the atmospheric circulation over the Euro-Atlantic sector since 1685. Climate Dynamics (under review).

Mellado-Cano, J., D. Barriopedro, R. García-Herrera, R. M. Trigo, 2019: Examining the NAO-EA relationship and the jet variability since 1685. Journal of Climate (accepted).

García-Herrera, R., D. Barriopedro, D. Gallego, **J. Mellado-Cano**, D. Wheeler, and C. Wilkinson, 2018: Understanding weather and climate of the last 300 years from ships' logbooks. Wires Climate Change, doi: 10.1002/wcc.54

García-Herrera, R., D. Gallego, D. Barriopedro, **J. Mellado-Cano**, 2017: Ship log books help to understand climate variability. In: Ducruet, C. (Ed.), Advances in Shipping Data Analysis and Modeling: Tracking and Mapping Maritime Flows in the Age of Bid Data. Routledge, New York, NY, pp. 189–205.

References

AchutaRao, K., and K. Sperber, 2006: ENSO simulations in coupled ocean-atmosphere models: Are the current models better? Climate Dynamics, 27, 1–16.

Alcoforado, M. J., M. de F. Nunes, J. C. Garcia, and J. P. Taborda, 2000: Temperature and precipitation reconstruction in southern Portugal during the late Maunder Minimum (AD 1675–1715). The Holocene, 10, 333–340, doi:10.1191/095968300674442959

Alcoforado, M. J., J. M. Vaquero, R. M. Trigo, and J. P. Taborda, 2012: Climate of the Past Early Portuguese meteorological measurements (18th century). Climate of the Past, 8. 353-371, doi:10.5194/cp-8-353-2012

Alexandersson, H., 1986: A homogeneity test applied to precipitation data. Journal of Climatology 6: 661–675.

Alexandersson, H., and A. Moberg, 1997: Homogenization of Swedish temperature data. Part I: homogeneity test for linear trends. International Journal of Climatology, 17: 25–34.

Allen, M. R., O. P. Dube, W. Solecki, F. Aragon-Durand, W. Cramer, S. Humphreys, M. Kainuma, J. Kala, N. Mahowald, Y. Mulugetta, R. Perez, M. Wairiu, and K. Zickfeld, 2018: Framing and Context. In: Global Warming of 1.5°C. An IPCC Special Report on the impacts of global warming of 1.5°C above pre-industrial levels and related global greenhouse gas emission pathways, in the context of strengthening the global response to the threat of climate change, sustainable development, and efforts to eradicate poverty [Masson-Delmotte, V., P. Zhai, H.-O. Portner, D. Roberts, J. Skea, P.R. Shukla, A. Pirani, W. Moufouma-Okia, C. Pean, R. Pidcock, S. Connors, J.B.R. Matthews, Y. Chen, X. Zhou, M.I. Gomis, E. Lonnoy, T. Maycock, M. Tignor, and T. Waterfield (eds.)]. In Press.

Andres, H. J., and W. R. Peltier, 2016: Regional influences of natural external forcings on the transition from the medieval climate anomaly to the little ice age. Journal of Climate, 29, 5779–5800, doi: 10.1175/JCLI-D-15-0599.1

Athanasiadis, P. J., J. M. Wallace, and J. J. Wettstein, 2010: Patterns of Wintertime Jet Stream Variability and Their Relation to the Storm Tracks. Journal of Atmospheric Science, 67, 1361–1381, https://doi.org/10.1175/2009JAS3270.1

Ayre, M., J. Nicholls, C. Ward, and D. Wheeler, 2015: Ships' logbooks from the Arctic in the pre-instrumental period. Geoscience Data Journal, 2(2), 53–62, https://doi.org/10.1002/gdj3.27

Barboza, L., B. Li, M. P. Tingley, and F. G. Viens, 2014: Reconstructing past temperatures from natural proxies and estimated climate forcings using short-and long-memory models. Annals of Applied Statistics, 8, 1966–2001, doi:10.1214/14-AOAS785

Barnston, A. G., and R. E. Livezey, 1987: Classification, seasonality and persistence of low-frequency atmospheric circulation patterns. Monthly Weather Review, 115, 1083-1126, doi:10.1175/1520-0493(1987)115<1083:CSAPOL>2.0.CO;2

Barnes, E.A., and D.L. Hartmann, 2010: Influence of eddy-driven jet latitude on North Atlantic jet persistence and blocking frequency in CMIP3 integrations. Geophysical Research Letters, 37, https://doi.org/10.1029/2010GL045700

Barnes, E.A., and L. Polvani, 2013: Response of the midlatitude jets, and of their variability, to increased greenhouse gases in the CMIP5 models. Journal of Climate, 26, 7117–7135, https://doi.org/10.1175/JCLI-D-12-00536.1

Barnett, P. T., R. W. Preisendorfer, 1978: Multifield Analog Prediction of Short-Term Climate Fluctuations Using a Climate State vector. Journal of Atmospheric Sciences. 35. 1771-1787. 10.1175/1520-0469(1978)035<1771:MAPOST>2.0.CO;2

Barriendos, M., 1997: Climatic variations in the Iberian Peninsula during the late Maunder Minimum (AD 1675-1715): an analysis of data from rogation ceremonies. The Holocene, 7, 1, p. 105-111.

Barriopedro, D., R. García-Herrera, and R. Huth, 2008: Solar modulation of Northern Hemisphere winter blocking. Journal of Geophysical Research, 113, D14118, doi:10.1029/2008JD009789

Barriopedro, D., E. M. Fischer, J. Luterbacher, R. Trigo, and R. García-Herrera, 2011: The hot summer of 2010: Redrawing the temperature record map of Europe. Science, 332, 220–224.

Barriopedro, D., D. Gallego, M. C. Álvarez-Castro, R. García-Herrera, D. Wheeler, C. Peña-Ortiz, and S. M. Barbosa, 2014: Witnessing North Atlantic westerlies variability from ships'

logbooks (1685–2008). Climate Dynamics, 43, 939–955, https://doi.org/10.1007/s00382-013-1957-8

Bastos, A., I. Janssens, C. Gouveia, R. M. Trigo, P. Ciais, F. Chevallier, J. Penuelas, C. Rodenbeck, S. Piao, P. Friedlingstein, and S. W. Running, 2016: European land CO2 sink influenced by NAO and East-Atlantic Pattern coupling. Nature Communication, 7, doi:10.1038/ncomms10315

Bladé I., B. Liebmann, D. Fortuny, and G. van Oldenborgh, 2012: Observed and simulated impacts of the summer NAO in Europe: implications for projected drying in the Mediterranean region. Climate Dynamics. 39: 709–727, doi: 10.1007/s00382-011-1195-x

Borisenkov, Y. P., 1994: Climatic and other natural extremes in the European territory of Russia in the late Maunder Minimum (1675-1715). In: B. Frenzel (Editor), Climatic trends and anomalies in Europe 1675-1715, Paläoklimaforschung, Gustav Fischer Verlag, Stuttgart Jena New York, pp. 83-94.

Braconnot, P., S. Harrison, M. Kageyama, P. Bartlein, V. Masson-Delmotte, A. Abe-Ouchi, B. Otto-Bliesner, and Y. Zhao, 2012: Evaluation of climate models using palaeoclimate data. Nature Climate Change, 2, 417-424, doi:10.1038/NCLIMATE1456

Bradley, R. S., 2011: High-resolution paleoclimatology. In: M. K. Hughes, T. W. Swetnam and H. F. Diaz (eds). Dendroclimatology: Progress and Prospects. Developments in Paleoenvironmental Research 11, Springer, Berlin, 3-15.

Brázdil, R., P. Dobrovonlý, B. Chocholác, and J. Munzar, 1994: 'Reconstruction of the Climate of Bohemia and Moravia in the Period of 1675 to 1715 on the Basis of Written Sources', in Climatic Trends and Anomalies in Europe 1675–1715, G. Fischer, Stuttgart, pp. 109–121.

Brázdil, R., T. Černušák, and L. Řezníčková, 2008: "Weather Information in the Diaries of the Premonstratensian Abbey at Hradisko, in the Czech Republic, 1693-1783". Weather, 63 (7): 201-7, doi:10.1002/wea.264

Brázdil, R, A. Kiss, J. Luterbacher, D. J. Nash, and L. Řezníčková, 2018: Documentary data and the study of past droughts: A global state of the art. Climate of the Past, 14, 1915-1960, doi:10.5194/cp-14-1915-2018

Bretherton, C. S., C. Smith, and J.M. Wallace, 1992: An Intercomparison of Methods for Finding Coupled Patterns in Climate Data. Journal of Climate, 5, 541–560, https://doi.org/10.1175/1520-0442(1992)005<0541:AIOMFF>2.0.CO;2

Briffa, K. R., 2000: Annual climate variability in the Holocene: interpreting the message of ancient trees. Quaternary Science Reviews, 19, 87-105.

Brohan, P., R. Allan, J. E. Freeman, A. M. Waple, D. Wheeler, C. Wilkinson, and S. Woodruff, 2009: Marine observations of old weather. Bulletin of the American Meteorological Society 90: 219 – 230, doi: 10.1175/2008BAMS2522.1

Brown T. J., and B. L. Hall, 1999: The use of t values in climatological composite analyses. Journal of Climate, 12:2941-2944.

Bruce, P., and A. Bruce, 2017: Practical statistics for data scientists: 50 essential concepts. Sebastopol: O'Reilly Media.

Bunel, M., F. Bahoken, C. Ducruet, C. Lagesse, B. Marnot, E. Mermet, and S. Petit, 2017: Geovisualizing the sail-to-steam transition through vessel movement data. In: Ducruet, C. (Ed.), Advances in Shipping Data Analysis and Modeling: Tracking and Mapping Maritime Flows in the Age of Bid Data. Routledge, New York, NY, pp. 189–205.

Camuffo, D. and S. Enzi, 1994: The climate of Italy from 1675-1715. In: B. Frenzel (Editor), Climatic trends and anomalies in Europe 1675-1715, Paläoklimaforschung, Gustav Fischer Verlag, Stuttgart Jena New York, pp. 43-50.

Camuffo, D, C. Bertolin, M. Barriendos, F. Domínguez-Castro, C. Cocheo, S. Enzi, M. Sghedoni, A. D. Valle, E. Garnier, M. J. Alcoforado, E. Xoplaki, J. Luterbacher, N. Diodato, M. Maugeri, M. Nunes, and R. Rodriguez, 2010: 500-Year temperature reconstruction in the Mediterranean Basin by means of documentary data and instrumental observations. Climatic Change, 101, 169-199, doi:10.1007/s10584-010-9815-8

Cao, L. J., and Z. W. Yan, 2012: Progress in research on homogenization of climate data. Advance Climate Change Research, 3(2), doi: 10.3724/SP.J.1248.2012.00059

Casado, M. J., M. A. Pastor, and F. J. Doblas-Reyes, 2009: Euro-Atlantic circulation types and modes of variability in winter. Theoretical and Applied Climatology, 96(1): 17–29, https://doi.org/10.1007/s00704-008-0036-2

Casty, C., H. Wanner, J. Luterbacher, J. Esper, and R. Böhm, 2005: Temperature and precipitation variability in the European Alps since 1500. International Journal of Climatology, 25, 1855–1880, doi:10.1002/joc.1216

Cattiaux, J., R. Vautard, C. Cassou, P. Yiou, V. Masson-Delmotte, and F. Codron, 2010: Winter 2010 in Europe: A cold extreme in a warming climate. Geophysical Research Letters, 37, L20704, doi:10.1029/2010GL044613

Chambers, F. M., S. A. Brain, D. Mauquoy, J. McCarroll, and T. Daley, 2014: The "Little Ice Age" in the Southern Hemisphere in the context of the last 3000 years: Peat-based proxy-climate data from Tierra del Fuego. The Holocene, 8, doi:10.1177/0959683614551232

Christensen, J. H., K. Krishna Kumar, E. Aldrian, S. I. An, I. F. A. Cavalcanti, M. de Castro, W. Dong, P. Goswami, A. Hall, J. K. Kanyanga, A. Kitoh, J. Kossin, N. C. Lau, J. Renwick, D.B. Stephenson, S. P. Xie and T. Zhou, 2013: Climate Phenomena and their Relevance for Future Regional Climate Change. In: Climate Change 2013: The Physical Science Basis. Contribution of Working Group I to the Fifth Assessment Report of the Intergovernmental Panel on Climate Change [Stocker, T. F., D. Qin, G. K. Plattner, M. Tignor, S. K. Allen, J. Boschung, A. Nauels, Y. Xia, V. Bex and P. M. Midgley (eds.)]. Cambridge University Press, Cambridge, United Kingdom and New York, NY, USA

Comas-Bru, L., and F. McDermott, 2014: Impacts of the EA and SCA patterns on the European twentieth century NAO–winter climate relationship. Quarterly Journal of the Royal Meteorological Society, 140: 354-363, doi:10.1002/qj.2158

Comas-Bru, L., and A. Hernández, 2018: Reconciling North Atlantic climate modes: revised monthly indices for the East Atlantic and the Scandinavian patterns beyond the 20th century. Earth System Science Data, https://doi.org/10.5194/essd-10-2329-2018

Compo, G. P., J. S. Whitaker, P. D. Sardeshmukh, N. Matsui, R. J. Allan, X. Yin, B. E. Gleason, R. S. Vose, G. Rutledge, P. Bessemoulin, S. Brönnimann, M. Brunet, R. I. Crouthamel, A. N. Grant, P. Y. Groisman, P. D. Jones, M. C. Kruk, A. C. Kruger,G. J. Marshall, M. Maugeri, H.

Y. Mok, Ø. Nordli, T. F. Ross, R. M. Trigo, X. L. Wang, S. D. Woodruff, and S. J. Worley, 2011: The Twentieth Century Reanalysis Project. Quaterly Journal of the Royal Meteorological Society, 137, 1–28, https://doi.org/10.1002/qj.776

Cook, E. R., R. D. D'Arrigo, and M. E. Mann, 2002: A Well-Verified, Multiproxy Reconstruction of the Winter North Atlantic Oscillation Index since A.D. 1400. Journal of Climate, 15: 1754–1764, doi: 10.1175/1520-0442(2002)015<1754:AWVMRO>2.0.CO;2

Cornes, R. C., P. D. Jones, K. R. Briffa, and T. J. Osborn, 2013: Estimates of the North Atlantic Oscillation back to 1692 using a Paris–London westerly index. International Journal of Climatology, 33: 228-248, doi:10.1002/joc.3416

Costa, A., and A. Soares, 2009: Homogenization of Climate Data: Review and New Perspectives Using Geostatistics. Mathematical Geosciences, 41, 291-305, doi:10.1007/s11004-008-9203-3

Crowley T. J., W. Hyde, and W. Peltier, 2001: CO2 levels required for deglaciation of a "Near-Snowball" Earth. Geophysical Research Letters – Geophysical Research Letter, 28, doi:10.1029/2000GL011836

Crowley, T. J., and M. B. Unterman, 2013: Technical details concerning development of a 1200–year proxy index for global volcanism. Earth System Science Data, 5, 187–197.

Cubasch, U., D. Wuebbles, D. Chen, M.C. Facchini, D. Frame, N. Mahowald, and J. G. Winther, 2013: Introduction. In: Climate Change 2013: The Physical Science Basis. Contribution of Working Group I to the Fifth Assessment Report of the Intergovernmental Panel on Climate Change [Stocker, T. F., D. Qin, G. K. Plattner, M. Tignor, S. K. Allen, J. Boschung, A. Nauels, Y. Xia, V. Bex and P. M. Midgley (eds.)]. Cambridge University Press, Cambridge, United Kingdom and New York, NY, USA.

D'Arrigo, R., R. Wilson, and G. Jacoby, 2006: On the long-term context for late twentieth century warming. Journal of Geophysical Research: Atmosphere, 111, 1–12, doi:10.1029/2005JD006352

D'Arrigo, R., R. Seager, J. E. Smerdon, A. N. LeGrande and E. R. Cook, 2011: The anomalous winter of 1783–1784: Was the Laki eruption or an analog of the 2009–2010 winter to blame? Geophysical Research Letters, 38, L05706, doi:10.1029/2011GL046696

Davini P., C. Cagnazzo, R. Neale and J. Tribbia, 2012: Coupling between Greenland blocking and the North Atlantic Oscillation pattern. Geophysical Research Letters, 39, L14701 doi:10.1029/2012GL052315

Deser C., A. Phillips, V. Bourdette, and H. Teng, 2012: Uncertainty in climate change projections: the role of internal variability. Climate Dynamics, 38, 527–546, doi: 10.1007/s00382-010-0977-x

Delworth T., and F. Zeng, 2012: Multicentennial variability of the Atlantic Meridional Overturning Circulation and its climatic influence in a 4000 year simulation of the GFDL CM2.1 climate model. Geophysical Research Letters, 39, 13702, doi: 10.1029/2012GL052107

Derham, W., 1708: "The History of the Great Frost in the Last Winter 1703 and 1708/9." Philosophical Transactions of the Royal Society 26: 454-78.

Domínguez-Castro, F., J. I. Santisteban, M. Barriendos, and R. Mediavilla, 2008: Reconstruction of drought episodes for central Spain from rogation ceremonies recorded at Toledo Cathedral from 1506 to 1900: A methodological approach, Global Planet. Change, 63, 230–242.

Domínguez-Castro, F., P. Ribera, R. García-Herrera, J. Vaquero, M. Barriendos, J. Cuadrat, and J. M. Moreno, 2012: Assessing extreme droughts in the Iberian Peninsula during 1750-1850 from rogation ceremonies. Climate of the Past Discussions, 7. 4037-4072. 10.5194/cpd-7-4037-2011.

Domínguez-Castro, F., A.M. Ramos, R. García-Herrera, and R.M. Trigo, 2015: Iberian extreme precipitation 1855/1856: an analysis from early instrumental observations and documentary sources, International Journal of Climatology, 35, 142-153, doi: 10.1002/joc.3973

Emile-Geay, J., and M. Tingley, 2016: Inferring climate variability from nonlinear proxies: application to palaeo-ENSO studies. Climate of the Past, 12, 31-50, https://doi.org/10.5194/cp-12-31-2016

Farrona, A.M.M., R. M. Trigo, M. C. Gallego, and J. M. Vaquero, 2012: The meteorological observations of Bento Sanches Dorta, Brazil: 1781 – 1788. Climatic Change, 115: 579 – 595, doi: 10.1007/s10584-012-0467-8

Fernández-Donado, L., J. F. González Rouco, C. Raible, C. Ammann, D. Barriopedro, E. Garcia Bustamante, J. H. Jungclaus, S. J. Lorenz, J. Luterbacher, S. J. Phipps, J. Servonnat, D. Swingedouw, S. Tett, S. Wagner, P. Yiou, and E. Zorita, 2013: Large-scale temperature response to external forcing in simulations and reconstructions of the last millennium. Climate of the Past, 9, 393-421, doi: 10.5194/cp-9-393-2013

Fernández-Fernández, M., M. C. Gallego, F. Domínguez-Castro, R. Trigo, and J. M. Vaquero, 2015: The climate in Zafra from 1750 to 1840: precipitation. Climatic Change, 129, doi:10.1007/s10584-014-1315-9

Fischer, E. M., J. Luterbacher, E. Zorita, S. F. B. Tett, C. Casty, and H. Wanner, 2007: European climate response to tropical volcanic eruptions over the last half millennium. Geophysical Research Letter, 34, L05707, doi:10.1029/2006GL027992.

Flato, G., 2011: Earth system models: an overview. Wiley Interdisciplinary Reviews, Climate Change, 2, 783–800.

Flato, G., J. Marotzke, B. Abiodun, P. Braconnot, S. C. Chou, W. Collins, P. Cox, F. Driouech, S. Emori, V. Eyring, C. Forest, P. Gleckler, E. Guilyardi, C. Jakob, V. Kattsov, C. Reason, and M. Rummukainen, 2013: Evaluation of climate models. In Climate Change 2013: The Physical Science Basis. Contribution of Working Group I to the Fifth Assessment Report of the Intergovernmental Panel on Climate Change. T.F. Stocker, D. Qin, G. K. Plattner, M. Tignor, S. K. Allen, J. Doschung, A. Nauels, Y. Xia, V. Bex, and P. M. Midgley, Eds. Cambridge University Press, pp. 741-882, doi:10.1017/CBO9781107415324.020.

Folland, C., T. R. Karl, and M. Salinger, 2006: Observed climate variability and change. Weather, 57, 269 – 278, doi:10.1256/004316502320517353

Folland, C. K., J. Knight, H. W. Linderholm, D. Fereday, S. Ineson, and J. W. Hurrell, 2009:The Summer North Atlantic Oscillation: Past, Present, and Future. Journal of Climate, 022, 1082–1103, https://doi.org/10.1175/2008JCLI2459.1

Francis, J. A., and S. J. Vavrus, 2012: Evidence linking Arctic amplification to extreme weather in mid-latitudes. Geophysical Research Letter, 39, L06801, doi:10.1029/2012GL051000

Freitas, C., O. M. Dedekind, and E. B. Brill, 2014: A Reanalysis of Long-Term Surface Air Temperature Trends in New Zealand. Environmental Modeling and Assessment, 20, doi:10.1007/s10666-014-9429-z

Freeman, J., S. Woodruff, S. J. Worley, S. J. Lubker, E. Kent, W. Angel, D. Berry, P. Brohan, R. Eastman, L. Gates, W. Gloeden, Z. Ji, J. Lawrimore, N. A. Rayner, G. Rosenhagen, and S. R. Smith, 2017: ICOADS Release 3.0: A major update to the historical marine climate record. International Journal of Climatology, 37, 2211–2232, doi:10.1002/joc.4775

Gaetani, M., B. Pohl, H. Douville, and B. Fontaine, 2011: West African Monsoon influence on the summer Euro-Atlantic circulation, Geophysical Research Letters, 38, L09705, doi:10.1029/2011GL047150

Gallego, D., R. García-Herrera, N. Calvo, and P. Ribera, 2007: A new meteorological record for Cádiz (Spain) 1806-1852: Implications for climatic reconstructions. Journal of Geophysical Research: Atmosphere, 112, 1–9, doi:10.1029/2007JD008517

Gallego, D., P. Ordóñez, P. Ribera, C. Peña-Ortiz, and R. García-Herrera, 2015: An instrumental index of the West African Monsoon back to the nineteenth century. Quarterly Journal of the Royal Meteorological Society, 141, 3166–3176, doi:10.1002/qj.2601.

Gallego, D., R. García-Herrera, C. Peña-Ortiz, and P. Ribera, 2017: The steady enhancement of the Australian Summer Monsoon in the last 200 years. Nature, https://doi.org/ 10.1038/s41598-017-16414-1

Garcia, R., H. Diaz, R. García-Herrera, J. Eischeid, M. Prieto, E. Hernández, L. Gimeno, F. Rubio Durán, and A. María Bascary, 2001: Atmospheric Circulation Changes in the Tropical Pacific Inferred from the Voyages of the Manila Galleons in the Sixteenth-Eighteenth Centuries. Bulletin of The American Meteorological Society - Bulletin of the American Meteorological Society, 82, 2435-2456, doi: 10.1175/1520-0477(2001)082<2435:ACCITT>2.3.CO;2

García-Herrera R., C. Wilkinson, F. B. Koek, M.R. Prieto, N. Calvo, and E. Hernández, 2005a: Description and general background to ships' logbooks as a source of climatic data. Climatic Change, 73, 13 - 36.

García-Herrera R., G. Können, D. Wheeler, M.R. Prieto, P. Jones, and F. Koek, 2005b: A climatological database for the world's oceans 1750-1854. Climatic Change, 73, 1 - 12.

García-Herrera, R., P. Können, A. Gunther, D. Wheeler, M. Prieto, P. Jones, and F. Koek ,2006: Ship Logbooks Help Analyze Pre-instrumental Climate. Eos, Transactions American Geophysical Union, 87, doi:10.1029/2006EO180002

García-Herrera, R., J. Díaz, R. M. Trigo, J. Luterbacher, and E. M. Fischer, 2010: A Review of the European Summer Heat Wave of 2003, Critical Reviews in Environmental Science and Technology, 40:4,267-306, doi:10.1080/10643380802238137

García-Herrera, R., D. Gallego, D. Barriopedro, J. Mellado-Cano, 2017: Ship log books help to understand climate variability. In: Ducruet, C. (Ed.), Advances in Shipping Data Analysis and Modeling: Tracking and Mapping Maritime Flows in the Age of Bid Data. Routledge, New York, NY, pp. 189–205.

García-Herrera, R., and D. Barriopedro, 2018: Climate of the Mediterranean Region. Oxford Research Encyclopedia of Climate Science. doi: 10.1093/acrefore/9780190228620.013.509

García-Herrera, R., D. Barriopedro, D. Gallego, J. Mellado-Cano, D. Wheeler, and C. Wilkinson, 2018: Understanding weather and climate of the last 300 years from ships' logbooks. Wires Climate Change, doi: 10.1002/wcc.54

Gimeno, L., A. Stohl, R. M. Trigo, F. Dominguez, K. Yoshimura, L. Yu, A. Drumond, A. M. Durán-Quesada, and R. Nieto, 2012: Oceanic and terrestrial sources of continental precipitation, Review Geophysical, 50, RG4003, doi:10.1029/2012RG000389

Gillett, N. P., and J. C. Fyfe, 2013: Annular mode changes in the CMIP5 simulations, Geophysical Research Letter, 40,1189–1193, doi:10.1002/grl.50249

Gómez-Delgado, F. P., D. Gallego, C. Peña-Ortiz, I. Vega, P. Ribera, and R. García-Herrera, 2019: Long term variability of the northerly winds over the Eastern Mediterranean as seen from historical wind observations. Global and Planetary Change, 172, 355–364, doi: 10.1016/j.gloplacha.2018.10.008

Goosse, H., E. Crespin, S. Dubinkina, M. F. Loutre, M. E. Mann, H. Renssen, Y. Sallaz-Damaz, and D. Shindell, 2012: The role of forcing and internal dynamics in explaining the "Medieval Climate Anomaly." Climate Dynamics, 39, 2847–2866, doi:10.1007/s00382-012-1297-0

Greatbatch, R. J., G. Gollan, T. Jung, and T. Kunz, 2015: Tropical origin of the severe European winter of 1962/1963. Quarterly Journal of the Royal Meteorological Society, 141: 153-165, doi:10.1002/qj.2346

Joel, G., H. Wu, W. Jiang, and Y. L. Luo, 2011: East Asian Monsoon and Paleoclimatic Data Analysis, doi:10.1201/b12226-18.

Hanna, E., T. E. Cropper, R. J. Hall, and J. Cappelen, 2016: Greenland Blocking Index 1851–2015: a regional climate change signal. International Journal of Climatology, 36: 4847-4861, doi:10.1002/joc.4673

Harrell, F., 2001: Regression Modeling Strategies: With Applications to Linear Models, Logistic Regression, and Survival Analysis. Chapter 5: Resampling, Validating, and Simplifying the Model. 3. 88-103.

Harris, I., P. D. Jones, T. J. Osborn, and D. H. Lister, 2014: Updated high-resolution grids of monthly climatic observations— The CRU TS3.10 dataset. International Journal of Climatology, 34, 623–642, https://doi.org/10.1002/joc.3711.

Hawkins, E. and R. Sutton, 2009: The Potential to Narrow Uncertainty in Regional Climate Predictions. Bulletin of the American Meteorological Society, 90, 1095–1108, https://doi.org/10.1175/2009BAMS2607.1

Hegerl, G. C., T. J. Crowley, M. Allen, W. T. Hyde, H. N. Pollack, J. Smerdon, and E. Zorita, 2007: Detection of Human Influence on a New, Validated 1500-Year Temperature Reconstruction. Journal of Climate, 20, 650–666, https://doi.org/10.1175/JCLI4011.1

Hegerl, G., J. Luterbacher, F. González-Rouco, S. F. B. Tett, T. Crowley, and E. Xoplaki, 2011: Influence of human and natural forcing on European seasonal temperatures. Nature Geoscience, 4, 99–103, doi:10.1038/ngeo1057.

Hughes, M. K., T. W. Swetnam, H. F. Diaz, 2011: *Dendroclimatology: Progress and Prospects.* Dordrecht: Springer Science+Business Media B.V.

Howe, S., and T. Webb, 1983: Calibrating pollen data in climatic terms: improving the methods. Quaternary Science Reviews, 2, 17-51

Hurrell, J.W., 1995: Decadal trends in the North Atlantic Oscillation and relationships to regional temperature and Precipitation. Science 269:676–679, doi: 10.1126/science.269.5224.676.

Hurrell, J., Y. Kushnir, G. Ottersen, and M. Visbeck, 2003: An overview of the North Atlantic Oscillation. pages 1–35. American Geophysical Union, Washington, D.C

Jackson, A., A. R. T. Jonkers, and M. R. Walker, 2000: Four centuries of geomagnetic secular variation from historical records. Philosophical Transactions of the Royal Society A: Mathematical, Physical and Engineering Sciences., 358, 957–990, doi:10.1098/rsta.2000.0569

Jackson, S. T., and J. W. Williams, 2004: Modern analogs in quaternary paleoecology. Annual Review of Earth and Planetary Sciences, 32:1, 495-537.

Jacobeit, J., H. Wanner, J. Luterbacher, C. Beck, A. Philipp, and K. Sturm, 2003: Atmospheric circulation variability in the North-Atlantic-European area since the mid-seventeenth century. Climate Dynamics, 20, 341-352, doi:10.1007/s00382-002-0278-0

Jacobeit, J., M. Homann, A. Philipp, and C. Beck, 2017: Atmospheric circulation types and extreme areal precipitation in southern central Europe. Advances in Science and Research. 14. 71-75. 10.5194/asr-14-71-2017.

Jerez S., and R. M. Trigo, 2013: Time-scale and extent at which large-scale circulation modes determine the wind and solar potential in the Iberian Peninsula, Environmental Research Letters, 8, 044035, doi:10.1088/1748-9326/8/4/044035

Jerome, S., P. Yiou, M. Khodri, D. Swingedouw, S. Denvil, 2010: Influence of solar variability, CO 2 and orbital forcing between 1000 and 1850 AD in the IPSLCM4 model. Climate of the Past, 6, doi:10.5194/cp-6-445-2010

Jones, P. D., T. Jonsson, and D. Wheeler, 1997: Extension to the North Atlantic oscillation using early instrumental pressure observations from Gibraltar and south-west Iceland. International Journal of Climatology, 17, 1433–1450, doi:10.1002/(SICI)1097-0088(19971115)17:13<1433::AID-JOC203>3.0.CO;2-P

Jones, P. D., T. J. Osborn, and K. R. Briffa, 2001:The evolution of climate over the last millennium, Science, 292, 662–667.

Jones, P. D., and M. E. Mann, 2004: Climate Over Past Millennia, Reviews of Geophysics, 42, RG2002, doi: 10.1029/2003RG000143

Jones, P. D., and M. Salmon, 2005: Preliminary reconstructions of the North Atlantic Oscillation and the Southern Oscillation Index from measures of wind strength and direction taken during the CLIWOC period. Climate Change, 73:131-154, doi: 10.1007/s10584-005-6948-2

Jones, P. D., K. R. Briffa, T. J. Osborn, J. M. Lough, T. D. van Ommen, B. M. Vinther, J. Luterbacher, E. R. Wahl, F. W. Zwiers, M. E. Mann, G. A. Schmidt, C. M. Ammann, B. M. Buckley, K. M. Cobb, J. Esper, H. Goosse, N. Graham, E. Jansen, T. Kiefer, C. Kull, M. Küttel, E. Mosley-Thompson, J. T. Overpeck, N. Riedwyl, M. Schulz, A. W. Tudhope, R. Villalba, H. Wanner, E. Wolff, and E. Xoplaki, 2009: High-resolution paleoclimatology of the last millennium: A review of current status and future prospects. The Holocene, 19, 3-49, doi:10.1177/0959683608098952

Jones, P. D., C. Harpham, and B. M. Vinther, 2014: Winter-responding proxy temperature reconstructions and the North Atlantic Oscillation, Journal of Geophysical Research: Atmosphere, 119, 6497–6505, doi:10.1002/2014JD021561

Jung, T., M. Hilmer, E. Ruprecht, S. Kleppek, S. Gulev, and O. Zolina, 2003: Characteristics of the recent eastward shift of interannual NAO variability. Journal of Climate, 16 (20), 3371–3382.

Kalnay, E., M. Kanamitsu, R. Kistler, W. Collins, D. DEAVEN, L.S. Gandin, M. Iredell, S. Saha, G. White, J. Wollen, Y. Zhu, M. Chelliah, W. Ebisuzaki, W. Higgins, J. Janowiak, K. C. Mo, C. Ropelewski, J. Wang, and A. Leetmaa, 1996: The NMC/NCAR 40-year reanalysis project. Bulletin of the American Meteorological Society, 77, doi:10.1175/1520-0477(1996)077<0437:TNYRP>2.0.CO;2

Kidston, J., A. A. Scaife, S. C. Hardiman, D. M. Mitchell, N. Butchart, M. P. Baldwin, and L. J. Gray, 2015: Stratospheric influence on tropospheric jet streams, storm tracks and surface weather. Nature Geoscience, 8, 433–440, doi:10.1038/ngeo2424

Kington, J., 1995: The severe winter of 1694/95. Weather 50: 160–163.

Kington, J., 1997: The severe winter of 1696/97. Weather 52: 386–391.

Kington, J., 1998: The great storm of 1-2 October 1697. Weather 53, 424-27.

Kington, J.,1999: The severe winter of 1697/98. Weather 54: 43–49.

Kington, J., 2010: Climate and weather. Published by Harper Collins Publishers, United Kingdom, 484 pp., SBN, doi:10: 0007395949

Knutti, R., 2008: Why are climate models reproducing the observed global surface warming so well? Geophysical Research Letters, 35, L18704.

Knutti, R., R. Furrer, C. Tebaldi, J. Cermak, and G. A. Meehl, 2010: Challenges in combining projections from multiple climate models. Journal of Climate, 23, 2739–2758.

Können, P. G., and F. Koek, 2005: Description of the CLIWOC database. Climatic Change, 73, 117-130, doi:10.1007/s10584-005-6946-4

Kruizinga, S., and A. H. Murphy, 1983: Use of an Analogue Procedure to Formulate Objective Probabilistic Temperature Forecasts in The Netherlands. Monthly Weather Review – Monthly Weather Review, 111, doi: 10.1175/1520-0493(1983)111<2244:UOAAPT>2.0.CO;2

Kutiel, H., and R. M. Trigo, 2014: The rainfall regime in Lisbon in the last 150 years. Theoretical and Applied Climatology, doi: 10.1007/s00704-013-1066-y

Küttel, M., E. Xoplaki, D. Gallego, J. Luterbacher, R. García-Herrera, R. Allan, M. Barriendos, P. Jones, D. Wheeler, and H. Wanner, 2010: The importance of ship log data: Reconstructing North Atlantic, European and Mediterranean sea level pressure fields back to 1750. Climate Dynamics, 34, 1115-1128, doi:10.1007/s00382-009-0577-9

Küttel, M., J. Luterbacher, and H. Wanner, 2011: Multidecadal changes in winter circulation-climate relationship in Europe: Frequency variations, within-type modifications, and long-term trends. Climate Dynamics, 36, 957–972, https://doi.org/10.1007/s00382-009-0737-y

Lamb, H. H., 1972: British Isles Weather types and a register of daily sequence of circulation patterns, 1861-1971. Geophysical Memoir 116, HMSO, London, 85pp.

Lamb, H. H., 1977: Climate, Present, Past and Future Volume: 2 . Climatic History and the future. Methuen: London; 835.

Lamb, H. H., 1982: Climate, History and the Modern World. Methuen: London.

Landrum, L., B. L. Otto-Bliesner, E. R. Wahl, A. Conley, P. J. Lawrence, N. Rosenbloom, and H. Teng, 2013: Last millennium climate and its variability in CCSM4. Journal of Climate, 26, 1085–1111, doi:10.1175/JCLI-D-11-00326.1

Lawrimore, J. H., M. J. Menne, B. E. Gleason, C. N. Williams, D. B. Wuertz, R. S. Vose, and J. Rennie, 2011: An overview of the Global Historical Climatology Network monthly mean temperature data set, version 3. Journal of Geophysical Research: Atmosphere, 116, 1–18, doi:10.1029/2011JD016187.

Lehner, F., A. Born, C. C. Raible, and T. F. Stocker, 2013: Amplified inception of European little Ice Age by sea ice-ocean-atmosphere feedbacks. Journal of Climate, 26, 7586–7602, doi:10.1175/JCLI-D-12-00690.1

Lehner, F., F. Joos, C. Raible, J. Mignot, A. Born, K. Keller, and T. Stocker, 2015: Climate and carbon cycle dynamics in a CESM simulation from 850–2100 CE. Earth System Dynamics Discussions, 6, doi:10.5194/esdd-6-351-2015

Li, B., D. W. Nychka, and C. M. Amman, 2010: The value of multi-proxy reconstructing of past climate. Under review at the Journal of the American Statistical Association, http://www.image.ucar.edu/ nychka/manuscripts/JASALiPaleo.pdf

Ljungqvist, F. C., P. J. Krusic, G. Brattstrom, and H. S. Sundqvist, 2012: Northern Hemisphere temperature patterns in the last 12 centuries. Climate of the Past, 8, 227–249, doi:10.5419/cp-8-227-2012

Lorenz, E. N., 1969: The predictability of a flow which possesses many scales of motion. Tellus, 21: 289-307, doi:10.1111/j.2153-3490.1969.tb00444.x

Luterbacher, J., C. Schmutz, D. Gyalistras, E. Xoplaki, and H. Wanner, 1999: Reconstruction of monthly NAO and EU indices back to A.D. 1675. Geophysical Research Letters, 26, 2745–2748, doi:10.1029/1999GL900576

Luterbacher, J., R. Rickli, C. Tinguely, E. Xoplaki, E. Schuepbach, D. Dietrich, J. Huesler, Ambühl, C. Pfister, P. Beeli, U. Dietrich, A. Dannecker, T. D. Davies, P. Jones, V. Slonosky, A. E. J. Ogilvie, P. Maheras, F. Kolyva-Machera, J. Martin-Vide, and H. Wanner, 2000: Monthly mean pressure reconstruction for the Late Maunder Minimum Period (AD 1675-1715). International Journal of Climatolog, 20, 1049-1066, doi: 10.1002/1097-0088(200008)20:10<1049::AID-JOC521>3.0.CO;2-6

Luterbacher, J., R. Rickli, E. Xoplaki, C. Tinguely, C. Beck, C. Pfister, and H. Wanner, 2001: The Late Maunder Minimum (1675–1715)–A Key Period for Studying Decadal Scale Climatic Change in Europe. Climate Change, 49, 441–462, doi: 10.1023/A:1010667524422.

Luterbacher, J., E. Xoplaki, D. Dietrich, P. Jones, T. D. Davies, D. Portis, J. F. González Rouco, H. Von Storch, D. Gyalistras, C. Casty, and H. Wanner, 2002: Extending North Atlantic Oscillation Reconstructions Back to 1500. Atmospheric Science Letters, 2, 114-124, doi:10.1006/asle.2001.0044

Luterbacher, J., D. Dietrich, E. Xoplaki, M. Grosjean, and H. Wanner, 2004: European seasonal and annual temperature variability, trends, and extremes since 1500. Science, 303, 1499–1503, https://doi.org/10.1126/science.1093877

Luterbacher, J., and C. Pfister, 2015: The year without a summer. Nature Geoscience, 8, 246–248, https://doi.org/10.1038/ngeo2404

Luterbacher, J., J. Werner, J. E. Smerdon, L. Fernández-Donado, J. F. González Rouco, D. Barriopedro, F. Ljungqvist, U. Büntgen, E. Zorita, S. Wagner, J. Esper, D. Mccarroll, A. Toreti, D. Frank, J. H. Jungclaus, M. Barriendos, C. Bertolin, O. Bothe, R. Brázdil, and C. Zerefos, 2016: European summer temperatures since Roman times. Environmental Research Letters, 11, doi:10.1088/1748-9326/11/2/024001

McShane B. B., and A. Wyner, 2011: A Statistical Analysis of Multiple Temperature Proxies: Are Reconstructions of Surface Temperatures Over the Last 1000 Years Reliable?. The Annals of Applied Statistics. 5. 10.1214/10-AOAS398.

Mahlstein, I., R. W. Portmann, J. S. Daniel, S. Solomon, and R. Knutti, 2012: Perceptible changes in regional precipitation in a future climate. Geophysical Research Letters, 39, L05701, doi:10.1029/2011GL050738.

Manley, G., 1974: Central England temperatures: monthly means 1659 to 1973. Quarterly Journal of the Royal Meteorological Society 100: 389–405.

Mann, M. E., 2002: The Value of Multiple Proxies, Science, 297, 1481-1482.

Mann, M. E., S. Rutherford, E. R. Wahl, and C. Ammann, 2005: Testing the fidelity of methods used in proxy-based reconstructions of past climate. Journal of Climate 18: 4097-4107.

Mann, M. E., S. Rutherford, E. R. Wahl, and C. Ammann, 2007: Robustness of proxybased climate field reconstruction methods. Journal Geophysical Research, 112, D12109.

Mann, M., Z. Zhang, S. Rutherford, R. Bradley, M. K Hughes, D. Shindell, C. Ammann, G. Faluvegi, and F. Ni, 2009: Global Signatures and Dynamical Origins of the Little Ice Age and Medieval Climate Anomaly. Science (New York, N.Y.), 326, 1256-60, doi: 10.1126/science.1177303

Manzini, E., Y. A. Karpechko, J. A. Anstey, M. P. Baldwin, R. X. Black, C. Cagnazzo, N. Calvo, A. Charlton-Perez, B. Christiansen, P. Davini, E. P. Gerber, M. Giorgetta, L. J. Gray, S. C. Hardiman, Y. Y. Lee, D. R. Marsh, B. A. McDaniel, A. Purich, A. A. Scaife, and G. Zappa, 2014: Northern winter climate change: Assessment of uncertainty in CMIP5 projections related to stratosphere-troposphere coupling: stratosphere-troposphere climate change. Journal of Geophysical Research: Atmospheres, 119, doi:10.1002/2013JD021403

Maraldi, J. P., 1710: "Sur Les Arbres Morts Par La Gelee de 1709." Histoire de l'Academie Royale Des Sciences, 59-61.

Marcos, M., and A. Amores, 2014: Quantifying anthropogenic and natural contributions to thermosteric sea level rise, Geophysical Research Letter, 41, 2502– 2507, doi:10.1002/2014GL059766

Masson-Delmotte, V., M. Schulz, A. Abe-Ouchi, J. Beer, A. Ganopolski, J. F. González Rouco, E. Jansen, K. Lambeck, J. Luterbacher, T. Naish, T. Osborn, B. Otto-Bliesner, T. Quinn, R. Ramesh, M. Rojas, X. Shao and A. Timmermann, 2013: Information from Paleoclimate Archives. In: Climate Change 2013: The Physical Science Basis. Contribution of Working Group I to the Fifth Assessment Report of the Intergovernmental Panel on Climate Change [Stocker, T. F., D. Qin, G. K. Plattner, M. Tignor, S. K. Allen, J. Boschung, A. Nauels, Y.

Xia, V. Bex and P. M. Midgley (eds.)]. Cambridge University Press, Cambridge, United Kingdom and New York, NY, USA.

Mbengue, C. and T. Schneider, 2013: Storm Track Shifts under Climate Change: What Can Be Learned from Large-Scale Dry Dynamics. Journal of Climate, 26, 9923–9930, https://doi.org/10.1175/JCLI-D-13-00404.1

McShane, B. B., and A. J. Wyner, 2011: A statistical analysis of multiple temperature proxies: Are reconstructions of surface temperatures over the last 1000 years reliable? The annals of Applied Statistics, 5, 5–44, doi:10.1214/10-AOAS398

Menne, M. J., I. Durre, R. S. Vose, B. E. Gleason, and T. G. Houston, 2012: An overview of the global historical climatology network-daily database. Journal of Atmospheric and Oceanic Technology, 29, 897–910, doi:10.1175/JTECH-D-11-00103.1

Michel, S., D. Swingedouw, M. Chavent, P. Ortega, J. Mignot, and M. Khodri, 2019: Reconstructing climatic modes of variability from proxy records: sensitivity to the methodological approach, Geoscience Model Development.

Moberg, A., D. M. Sonechkin, K. Holmgren, N.M. Datsenko, and W. Karlén, 2005: Highly variable northern hemisphere temperatures reconstructed from low- and high-resolution proxy data. Nature, 433: 613-617.

Monahan, W. G., 1993: "Year of Sorrows: The Great Famine of 1709 in Lyon."

Moore, G. W. K., R. S. Pickart, and I. A. Renfrew, 2011: Complexities in the climate of the subpolar North Atlantic: A case study from the winter of 2007. Quarterly Journal of the Royal Meteorological Society, 137, 757 – 767, doi.10.1002/qj.778

Moore, G. W. K., and I. A. Renfrew, 2012: Cold European winters: interplay between the NAO and the East Atlantic mode. Atmospheric Science Letters, 13, 1-8, doi:10.10025/asl.356

Moore, G. W. K., I. A. Renfrew, and R. S. Pickart, 2013: Multidecadal Mobility of the North Atlantic Oscillation. Journal of Climate, 26, 8, 2453-2466, doi:10.1175/jcli-d-12-00023.1

Morrill, C., A. N. LeGrande, H. Renssen, P. Bakker, and B. L. Otto-Bliesner, 2013: Model sensitivity to North Atlantic freshwater forcing at 8.2 ka. Climate of the Past, 9, 955-968, doi:10.5194/cp-9-955-2013

Myhre, G., D. Shindell, F. M. Bréon, W. Collins, J. Fuglestvedt, J. Huang, D. Koch, J.-F. Lamarque, D. Lee, B. Mendoza, T. Nakajima, A. Robock, G. Stephens, T. Takemura, and H. Zhang, 2013: Anthropogenic and natural radiative forcing. In Climate Change 2013: The Physical Science Basis. Contribution of Working Group I to the Fifth Assessment Report of the Intergovernmental Panel on Climate Change. T. F. Stocker, D. Qin, G. K. Plattner, M. Tignor, S. K. Allen, J. Doschung, A. Nauels, Y. Xia, V. Bex, and P.M. Midgley, Eds. Cambridge University Press, pp. 659-740, doi:10.1017/CBO9781107415324.018

Neukom, R., A. P. Schurer, N. J. Steiger, and G. Hegerl, 2018: Possible causes of data model discrepancy in the temperature history of the last Millennium. Scientific Reports. 8. 10.1038/s41598-018-25862-2

Neuwirth, B., F. H. Schweingruber, and M. Winiger, 2007: *Spatial patterns of central European pointer years from 1901 to 1971*, Dendrochronologia 24, 79–89.

Nicolle, M., M. Debret, N. Massei, C. Colin, A. de Vernal, D. Divine, J. Werner, A. Hormes, A. Korhola, and H. Linderholm, 2017: Climate variability in subarctic area for the last two millennia. Climate of the Past Discussions, 1-24, doi: 10.5194/cp-2017-33

Niedźwiedź, T., 2010: The polish climate in the European context: An historical overview. Polish Climate, 1–535, doi:10.1007/978-90-481-3167-9

Ordonez, P., D. Gallego, P. Ribera, C. Pena-Ortiz, and R. García-Herrera, 2016: Tracking the Indian Summer Monsoon onset back to the pre-instrumental period. Journal of Climate, JCLI-D-15-0788.1, doi:10.1175/JCLI-D-15-0788.1

Ortega, P., F. Lehner, D. Swingedouw, V. Masson-Delmotte, C. Raible, M. Casado, and P. Yiou, 2015: A model-tested North Atlantic Oscillation reconstruction for the past millennium. Nature, 523. 71-74, doi:10.1038/nature14518

Otterå, O. H., M. Bentsen, H. Drange, and L. Suo, 2010: External forcing as a metronome for Atlantic multidecadal variability. Nature Geoscience, 3, 688-694, doi: 10.1038/ngeo955

Otto-Bliesner, B. L., E.C. Brady, J. Fasullollollo, A. Jahn, L. Landrum, S. Stevenson, N. Rosenbloom, A. Mai, and G. Strand, 2016: Climate variability and change since 850 CE: An Ensemble Approach with the Community Earth System Model. Bulletin of the American Meteorological Society, 735-754, http://dx.doi.org/10.1175/BAMS-D-14-00233.1

Overpeck, J., I. Prentice, and W. L. Thompson, 1985: Quantitative interpretation of fossil pollen spectra: dissimilarity coefficients and the method of modern analogs for pollen data. Quaternary Research, 23, 87-108, doi:10.1016/0033-5894(85)90074-2

Ouzeau, G., J. Cattiaux, H. Douville, A. Ribes, and D. Saint-Martin, 2011: European cold winter 2009-2010: How unusual in the instrumental record and how reproducible in the ARPEGE-Climat model? Geophysical Research Letters, 38, 1–6, doi:10.1029/2011GL047667

PAGES2k Consortium, 2013: Continental-scale temperature variability during the last two millennia. Nature Geoscience, 6 339–46.

PAGES2k Consortium, 2014: PAGES2k—a framework for community-driven climate reconstructions during the past two millennia EOS95 361–3.

Parker, G., 2013: Global Crisis: War, Climate Change and Catastrophe in the Seventeenth Century. New Haven; London: Yale University Press. 884 pp. Retrieved from http://www.jstor.org/stable/j.ctt32bksk

Pauling, A., J. Luterbacher, C. Casty, and H. Wanner, 2006: Five hundred years of gridded high-resolution precipitation reconstructions over Europe and the connection to large-scale circulation. Climate Dynamics, 26, 387–405, doi:10.1007/s00382-005-0090-8

Peings, Y., J. Cattiaux, S. Vavrus, and G. Magnusdottir, 2018: Projected squeezing of the wintertime North-Atlantic jet. Environmental Research Letters, 13, doi: 10.1088/1748-9326/aacc79

Pfister, C., 1992: Monthly temperature and precipitation in central Europe from 1525-1979: quantifying documentary evidence on weather and its effect. In: R. Bradley and T.C. Johns (Editors), Climate since A.D. 1500, Routledge, London, pp. 118-142.

Pinto, J., U. Ulbrich, G. C. Leckebusch, T. Spangehl, M. Reyers, and S. Zacharias, 2007: Changes in storm track and cyclone activity in three SRES ensemble experiments with the

ECHAM5/MPI-OM1 GCM. Climate Dynamics, 29, 195-210, doi:10.1007/s00382-007-0230-4

Pinto, J. G., and C. C. Raible, 2012: Past and recent changes in the North Atlantic oscillation. Wires Climate Change, 3: 79-90. doi:10.1002/wcc.150

Poli, P., H. Hersbach, D. Dee, P. Berrisford, A. J. Simmons, F. Vitart, P. Laloyaux, D. G. H. Tan, C. Peubey, J. N. Thépaut, Y. Tremolet, E. V. Hólm, M. Bonavita, L. Isaksen, and M. Fischer, 2016: ERA-20C: An atmospheric reanalysis of the 20th century. Journal of Climate, 29, 160308090852005, doi:10.1175/JCLI-D-15-0556.1

Prieto M.R., D. Gallego, R. García-Herrera, N. Calvo, 2005: Deriving wind force terms from nautical reports through content analysis. The Spanish and French cases. Climatic Change, 73, 37 - 75.

Prior, J., and M. Kendon, 2011: The UK winter of 2009/2010 compared with severe winters of the last 100 years. Weather, 66, 4–10, doi:10.1002/wea.735

Racz, L., 1994: The climate of Hungary during the late Maunder Minimum (1675-1715). In: B. Frenzel (Editor), Climatic trends and anomalies in Europe 1675-1715, Paläoklimaforschung, Gustav Fischer Verlag, Stuttgart Jena New York, pp. 43-50

Rácz, L., 1999: Climate History of Hungary since 16th Century: Past, Present and Future.Pécs, p. 160.

Raible, C. C., F. Lehner, J. F. Gonzalez-Rouco, and L. Fernandez-Donado, 2014: Changing correlation structures of the Northern Hemisphere atmospheric circulation from 1000 to 2100 AD, Climate of the Past, 10, 537-550. doi:10.5194/cp-10-537-2014

Rhoades, D., and M. Salinger, 1993: Adjustment of temperature and rainfall records for site changes. International Journal of Climatology, 13, 899 – 913, doi:10.1002/joc.3370130807

Rhodes, R. H., N. A. N. Bertler, J. A. Baker, H. C. Steen-Larsen, S. B. Sneed, U. Morgenstern, and S. J. Johnsen, 2012: Little Ice Age climate and oceanic conditions of the Ross Sea, Antarctica from a coastal ice core record. Climate of the Past, 8, 1223–1238, doi:10.5194/cp-8-1223-2012

Robock, A., 2000: Volcanic eruptions and climate. Review of Geophysics, 38:191–219.

Röthlisberger, M., S. Pfahl, and O. Martius, 2016: Regional-scale jet waviness modulates the occurrence of midlatitude weather extremes, Geophysical Research Letters, 43, 10,989–10,997, doi:10.1002/2016GL070944

Sáenz, J., J. Zubillaga, and C. Rodriguez-Puebla, 2001: Interannual variability of winter precipitation in Northern Iberian Peninsula. International Journal of Climatology, 21, 1503 – 1513, doi: 10.1002/joc.69

Santos, J. A., T. Woollings, and J. G. Pinto, 2013: Are the winters 2010 and 2012 archetypes exhibiting extreme opposite behavior of the North Atlantic jet stream?. Monthly Weather Review, 141(10), 3626–3640, doi:10.1175/mwr-d-13-00024.1

Schamm, K., M. Ziese, A. Becker, P. Finger, A. Meyer-Christoffer, U. Schneider, M. Schröder, and P. Stender, 2014: Global gridded precipitation over land: A description of the new GPCC First Guess Daily product. Earth System Science Data, 6, 49–60, https://doi.org/10.5194/essd-6-49-2014

Schimanke, S., H. E. M. Meier, E. Kjellström, G. Strandberg, and R. Hordoir, 2012: The climate in the Baltic Sea region during the last millennium. Climate of the Past 8, 1419–1433, http://dx.doi.org/10.5194/cp-8-1419-2012

Schmutz, C., J. Luterbacher, D. Gyalistras, E. Xoplaki, and H. Wanner, 2000: Can we trust proxy-based NAO index reconstructions?. Geophysical Research Letters, 27, doi:10.1029/1999GL011045.

Schultz, J., C. Beck, G. Menz, B. Neuwirth, C. Ohlwein, and A. Philipp, 2015: Sensitivity of proxies on non-linear interactions in the climate system. Scientific Reports, 5, 18560, doi:10.1038/srep18560

Schurer, A. P., G. C. Hegerl, M. E. Mann, S. F. B. Tett, and S. J. Phipps, 2013: Separating 715 forced from chaotic climate variability over the past millennium. Journal of Climate, 26, 716 6954–6973, doi:10.1175/JCLI-D-12-00826.1

Shepherd, T. G., 2014: Atmospheric circulation as a source of uncertainty in climate change projections. Nature Geoscience, 7, 703-708.

Siglm M., M. Winstrup, J. R. McConnell, K. C. Welten, G. Plunkett, F. Ludlow, U. Büntgen, M. Caffee, N. Chellman, D. Dhal-Jensen, H. Fischer, S. Kipfstuhl, C. Kostick, O. J. Maselli, F. Mekhaldi, R. Mulvaney, R. Muscheler, D. R. Pasteris, J. R. Pilcher, M. Salzer, S. Schüpbach , J. P. Steffensen, B. M. Vinther, and T. E. Woodruff, 2015: Timing and climate forcing of volcanic eruptions for the past 2,500 years. Nature, 523 543–9

Sigmond, M. and F. J. Scinocca, 2010: The Influence of Basic State on the Northern Hemisphere Circulation Response to Climate Change. Journal of Climate, 23, doi:10.1175/2009JCLI3167.1

Sjolte, J., C. Sturm, F. Adolphi, B. M. Vinther, M. Werner, G. Lohmann, and R. Muscheler, 2018: Solar and volcanic forcing of North Atlantic climate inferred from a process-based reconstruction, Climate of the Past, 14, 1179-1194, https://doi.org/10.5194/cp-14-1179-2018

Slonosky, V., and P. Yiou, 2001: The North Atlantic Oscillation and its relationship with near surface temperature. Geophysical Research Letter, 28, 807-810, doi: 28. 807-810. 10.1029/2000GL012063

Slonosky, V., P. Jones, and T. Davies, 2001: Instrumental pressure observations and atmospheric circulation from the 17th and 18th centuries: London and Paris. International Journal of Climatology, 21, 285–298, doi:10.1002/joc.611

Smerdon, J. E., 2012: Climate models as a test bed for climate reconstruction methods: pseudoproxy experiments. Wires Climate Change, 3, 63–77.

Smith, I., 2004: An assessment of recent trends in Australian rainfall. Aust. Meteorol. Mag. 53, 163–173.

Stott, P. A., and C. E. Forest, 2007: Ensemble climate predictions using climate models and observational constraints. Philos. R. Soc. London A, 365, 2029–2052.

Stott, P. A., N. Christidis, F. E. Otto, Y. Sun, J. Vanderlinden, G. J. van Oldenborgh, R. Vautard, H. von Storch, P. Walton, P. Yiou, and F. W. Zwiers, 2016: Attribution of extreme weather and climate-related events. Wires Climate Change, 7: 23-41, doi:10.1002/wcc.380

Stryhal, J. and R. Huth, 2017: Classifications of Winter Euro-Atlantic Circulation Patterns: An Intercomparison of Five Atmospheric Reanalyses. Journal of Climate, 30, 7847–7861, https://doi.org/10.1175/JCLI-D-17-0059.1

Sousa, P. M., R. M. Trigo, P. Aizpurua, R. Nieto, L. Gimeno, and R. García-Herrera , 2011: Trends and extremes of drought indices throughout the 20th century in the Mediterranean, Natural Hazards and Earth System Science, 11, 33-51, https://doi.org/10.5194/nhess-11-33-2011

Taschetto, A. S. and M. H. England, 2009: An analysis of late twentieth century trends in Australian rainfall. International Journal of Climatology, 29, 791–807, https://doi.org/10.1002/joc.1736

Teisserenc de Bort, M.M, 1883: 'E´ tude sur l'hiver de 1879–80 et recherches sur l'influence de la position des grands centres d'action de l'atmosphère dans les hivers anormaux', Ann. Soc. Meteor. France, 31, 70–79

Thébault, E., C. Finlay, P. Alken, C. D. Beggan, E. Daix Canet, A. Chulliat, B. Langlais, V. Lesur, F. Lowes, C. Manoj, M. Rother, and R. Schachtschneider, 2015: Evaluation of candidate geomagnetic field models for IGRF-12. Earth Planets and Space. 67, doi:10.1186/s40623-015-0273-4

Tomé, A., and P. M. A. Miranda, 2004: Piecewise linear fitting and trend changing points of climate parameters. Geophysical Research Letter, 31, L02207, doi:10.1029/2003GL019100

Toohey, M. and M. Sigl, 2017: Volcanic stratospheric sulfur injections and aerosol optical depth from 500 BCE to 1900 CE, Earth System Science Data, 9, 809-831, https://doi.org/10.5194/essd-9-809-2017

Toreti, A., E. Xoplaki, D. Maraun, F. G. Kuglitsch, H. Wanner, and J. Luterbacher, 2010: Characterisation of extreme winter precipitation in Mediterranean coastal sites and associated anomalous atmospheric circulation patterns. Natural Hazards and Earth System Sciences, 10:1037–1050, doi:10.5194/nhess-10-1037-2010

Trigo, R., T. Osborn, and J. Corte-Real, 2002: The North Atlantic Oscillation influence on Europe: Climate impacts and associated physical mechanisms. Climate Research, 20(1), 9-17.

Trigo, R. M., I. M. Trigo, C. C. DaCamara, and T. J. Osborn, 2004: "Winter blocking episodes in the European-Atlantic sector: climate impacts and associated physical mechanisms in the Reanalysis". Climate Dynamics, 23, 17-28.

Trigo, R. M., M. A. Valente, I. F. Trigo, M. Miranda, A. M. Ramos, D. Paredes, and R. García-Herrera, 2008: North Atlantic wind and cyclone trends and their impact in the European precipitation and Atlantic significant wave height. Annals of the New York Academy of Sciences, 1146, 212–234, doi: 10.1196/annals.1446.014

Trigo, R. M., J. M., Vaquero, M. J. Alcoforado, M. Barriendos, J. Taborda, R. García-Herrera, and J. Luterbacher, 2009: Iberia in 1816, the year without a summer, International Journal of Climatology, 29, 99–115, doi:10.1002/joc.1693, 2009

Trouet, V., J. Esper, N. E. Graham, A. Baker, J. Scourse, and D. Frank, 2009: Persistent Positive North Atlantic Oscillation Mode Dominated the Medieval Climate Anomaly. Science. 324. 78-80, doi: 10.1126/science.1166349

Van den Dool, H. M., H. J. Krijnen and J. E. Schuurmans, 1978: Average Winter Temperatures at the De Bilt (the Netherlands): 1634-1977. Climatic Change, 1, 319-330.

Van Den Dool, H. M.,1994: Searching for analogues, how long must we wait?. Tellus A, 46: 314-324, doi:10.1034/j.1600-0870.1994.t01-2-00006.x

Vaquero, J. M., R. M. Trigo and M. C. Gallego, 2005: A "lost" sunspot observation in 1785. Astronomische Nachrichten, 326(2),112-114, doi:10.1001/asna.200410343

Vaquero, J. M., L. Svalgaard, V. Carrasco, F. Clette, L Lefèvre, M. C. Gallego, R. Arlt, A. Aparicio, J. G. Richard, and R. Howe, 2016: A Revised Collection of Sunspot Group Numbers. Solar Physics, 291, 1-14, doi:10.1007/s11207-016-0982-2

Vautard, R., and P. Yiou, 2009: Control of recent European surface climate change by atmospheric flow. Geophysical Research Letters, 36, 6–11, doi:10.1029/2009GL040480

Vega, I., D. Gallego, P. Ribera, F. P. Gómez-Delgado, R. García-Herrera, and C. Peña-Ortiz, 2018: Reconstructing the Western North Pacific Summer Monsoon since the Late Nineteenth Century. Journal of Climate, 31, 355–368, https://doi.org/10.1175/JCLI-D-17-0336.1

Vicente-Serrano, S. M., and J. I. López-Moreno, 2008: Nonstationary influence of the North Atlantic Oscillation on European precipitation. Journal of Geophysical Research, 113, D20120, doi:10.1029/2008JD010382

Vicente-Serrano, S. M., R. García-Herrera, D. Barriopedro, C. Azorin-Molina, J. I. López-Moreno, N. Martín-Hernández, M. Tomas-Burguera, L. Gimeno, R. Nieto, 2016: The Westerly Index as complementary indicator of the North Atlantic oscillation in explaining drought variability across Europe. Climate Dynamics, doi:10.1007/s00382-015-2875-8

Vicente-Serrano, S. M., D. G. Miralles, F. Domínguez-Castro, C. Azorin-Molina, A. El Kenawy, T. R. McVicar, M. Tomás-Burguera, S. Beguería, M. Maneta, and M. Peña-Gallardo, 2018:Global Assessment of the Standardized Evapotranspiration Deficit Index (SEDI) for Drought Analysis and Monitoring. Journal of Climate, 31, 5371–5393, https://doi.org/10.1175/JCLI-D-17-0775.1

Visbeck, M., J. W. Hurrell, L. Polvani, and H. Cullen, 2001: The North Atlantic oscillation: Past, Present, and Future. Proceedings of the National Academy of Sciences, 98, 12876-12877, doi:10.1073/pnas.231391598

Von Storch, H., 2010: Climate models and modeling: an editorial essay. Wires Climate Change, 1: 305-310, doi:10.1002/wcc.12

Walker, G. T., 1924: Correlation in seasonal variations in weather IX: A further study of world weather. Mem. Indian Meteor. Dep., 24, 275–332.

Wallace, J. M. and D. S. Gutzler, 1981: Teleconnections in the Geopotential Height Field during the Northern Hemisphere Winter, Monthly Weather Review, 109, 784-812

Wang, B. and LinHo, 2002: Rainy Season of the Asian–Pacific Summer Monsoon. Journal of Climate, 15, 386–398, https://doi.org/10.1175/1520-0442(2002)015<0386:RSOTAP>2.0.CO;2

Wang, P. X., B. Wang, H. Cheng, J. Fasullo, Z. T. Guo, T. Kiefer, and Z. Y. Liu, 2014: The global monsoon across timescales: Coherent variability of regional monsoons. Climate of the Past, 10, 2007–2052, https://doi.org/10.5194/cp-10-2007-2014

Wanner, H., C. Pfister, and R. Brázdil, 1995: Wintertime European circulation patterns during the late Maunder Minimum cooling period (1675-1704). Theor. Appl. Climatol., 51, 167–175, doi:10.1007/BF00867443.

Wanner, H., H. P. Holzhauser, C. Pfister, and H. Zumbühl, 2000: 'Interannual to Century Scale Climate Variability in the European Alps', Erdkunde 54, 62–69.

Wheeler, D., 1996: A climatic reconstruction of the Battle of Quiberon Bay, 20 November 1759. Weather, 50: 230-238.

Wheeler, D., 2005: British Naval Logbooks from the Late Seventeenth Century: New climatic information from old sources. 2, 133–146.

Wheeler, D. and C. Wilkinson, 2005: The Determination of Logbook Wind Force and Weather Terms: The English Case. Climatic Change, 73, 57-77, doi: 10.1007/s10584-005-6949-1.

Wheeler, D., and R. García-Herrera, 2008: Ships' logbooks in climatological research. Ann. Annals of the New York Academy of Sciences., 1146, 1–15, doi: 10.1196/annals.1446.006

Wheeler, D., R. García-Herrera, C. W. Wilkinson, and C. Ward, 2010: Atmospheric circulation and storminess derived from Royal Navy logbooks: 1685 to 1750. Climatic Change, 101, 257–280, doi: 10.1007/s10584-009-9732-x

Wheeler, D., 2014: Hubert Lamb's 'treasure trove': ships' logbooks in climate research. Weather, 69: 133-139, doi:10.1002/wea.2284

Wilks, D. S., 2011: Statistical Methods in the 874 Atmospheric Sciences.3rd ed. Elsevier, 704 pp.

Wilkinson, C., S. Woodruff, P. Brohan, S. Claesson, J. Freeman, F. Koek, S. J. Lubker, C. Marzin, D. Wheeler, 2011: RECovery of logbooks and international marine data: the RECLAIM project. International Journal of Climatology, 31, 968 – 979, doi: 10.1002/joc.2102.

Williams, C. J. R., R. P. Allan, and D. R. Kniveton, 2012: Diagnosing atmosphere-land feedbacks in CMIP5 climate models. Environmental Research Letters, 7, 044003.

Wilmshurst, J., M. Mcglone, J. R. Leathwick, and R. Newnham, 2007: A pre-deforestation pollen-climate calibration model for New Zealand and quatitative temperature reconstructions

for the past 18 000 years BP. Journal of Quaternary Science. 22. 535 – 547, doi:10.1002/jqs.1135

Winton, M., 2011: Do climate models underestimate the sensitivity of Northern Hemisphere sea ice cover? Journal of Climate, 24, 3924–3934

Wood, C. A., 1992: Climatic effects of the 1783 Laki eruption, in The Year Without a Summer: World Climate in 1816, edited by C. R. Harrington, pp. 58–77, Can. Mus. of Nat., Ottawa

Woollings T, A. Hannachi, and B. Hoskins, 2010: Variability of the North Atlantic eddy-driven jet stream. Quarterly Journal of the Royal Meteorological Society, 649: 856–868.

Woollings T, and M. Blackburn, 2012: The North Atlantic jet stream under climate change, as described by the NAO and EA patterns. Journal of Climate 25: 886–902.

Woollings, T., E. Barnes, B. Hoskins, Y. O. Kwon, R. W. Lee, C. Li, E. Madonna, M. McGraw, T. Parker, R. Rodrigues, C. Spensberger, and K. Williams, 2018: Daily to Decadal Modulation of Jet Variability. Journal of Climate,31,1297–1314, https://doi.org/10.1175/JCLI-D-17-0286.1

Xoplaki, E., P. Maheras, and J. Luterbacher, 2001: Variability of Climate in Meridional Balkans. Climatic Change, 48, 581–615, doi:10.1023/A:1005616424463

Xoplaki, E., J. Luterbacher, H. Paeth, D. Dietrich, N. Steiner, M. Grosjean, and H. Wanner, 2005: European spring and autumn temperature variability and change of extremes over the last half millennium, Geophysical Research Letters, http://doi.wiley.com/10.1029/2005GL023424

Xu, T., Z. Shi, and Z. An, 2018: Responses of ENSO and NAO to the external radiative forcing during the last millennium: Results from CCSM4 and MPI-ESM-P simulations. Quaternary International, doi: 10.1016/j.quaint.2017.12.038

Yiou, P., T. Salameh, P. Drobinski, L. Menut, R. Vautard, and M. Vrac, 2013: Ensemble reconstruction of the atmospheric column from surface pressure using analogues, Climate Dynamics, 41: 1333, doi:10.1007/s00382-012-1626-3

Zanchettin, D., M. Khodri, C. Timmreck, M. Toohey, A. Schmidt, E. P. Gerber, G. Hegerl, Robock, F. S. R. Pausata, W. T. Ball, S. E. Bauer, S. Bekki, S. S. Dhomse, A. N. LeGrande,

G. W. Mann, L. , Marshall, M. Mills, M. Marchand, U. Niemeier, V. Poulain, E. Rozanov, A. Rubino, A. Stenke, K. Tsigaridis, and F. Tummon, 2016: The Model Intercomparison Project on the climatic response to Volcanic forcing (VolMIP): experimental design and forcing input data for CMIP6, Geoscientific Model Development, 9, 2701-2719, https://doi.org/10.5194/gmd-9-2701-2016

Zappa, G. and T. G. Shepherd,2017:Storylines of Atmospheric Circulation Change for European Regional Climate Impact Assessment. Journal of Climate, 30, 6561–6577, https://doi.org/10.1175/JCLI-D-16-0807.1

Annex

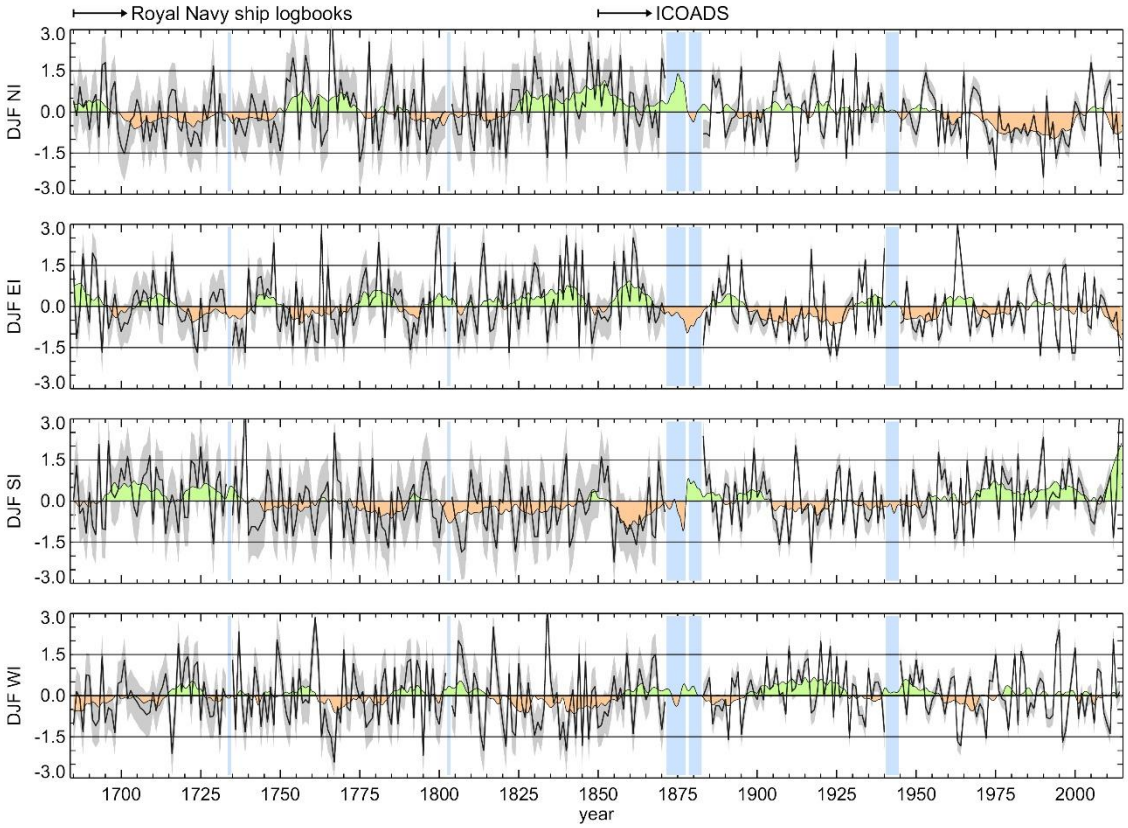

Figure A1. As Figure 4.8 but for winter (December-to-February, DJF)

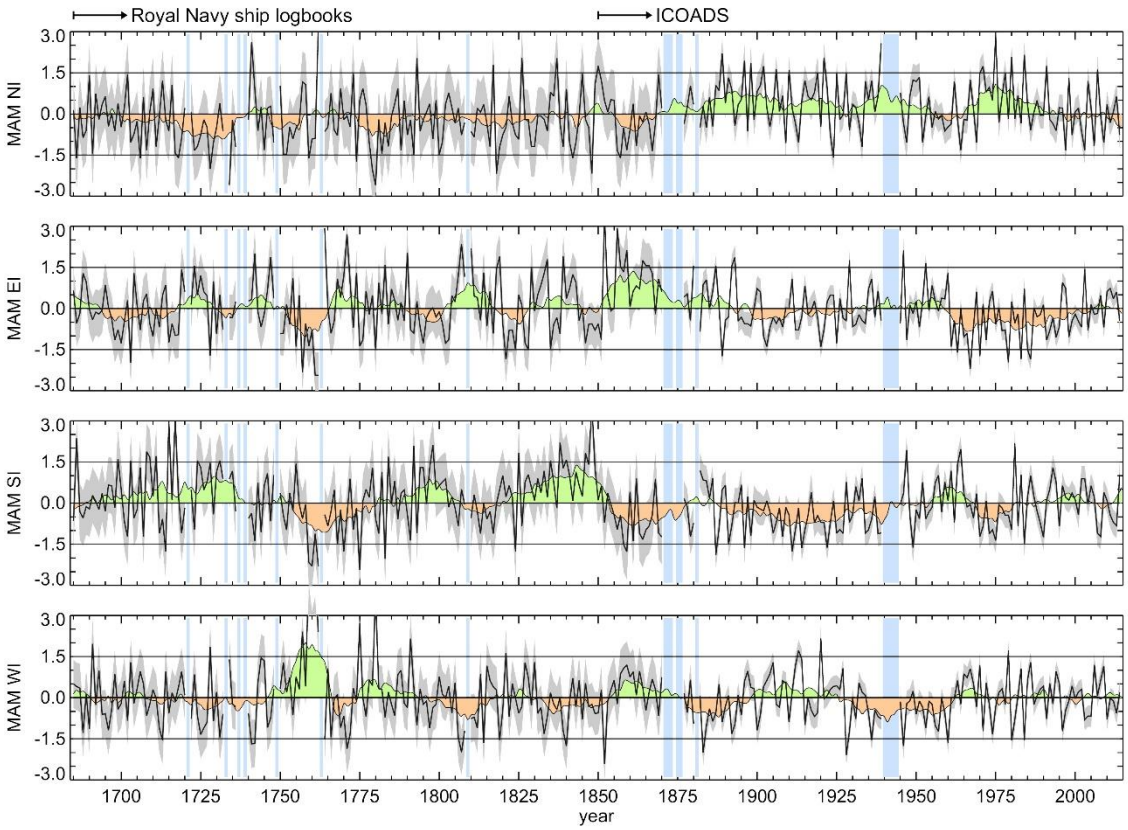

Figure A2. As Figure 4.8 but for spring (March-to-April, MMA)

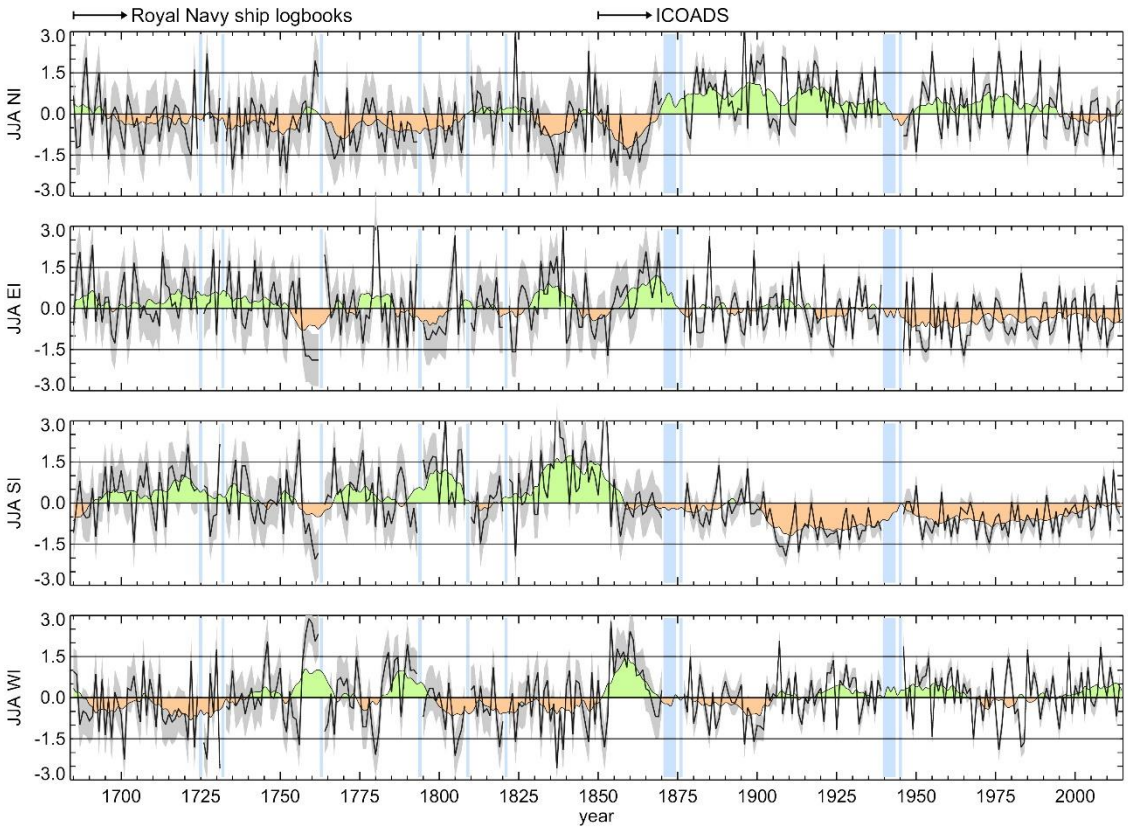

Figure A3. As Figure 4.8 but for summer (June-to-August, JJA)

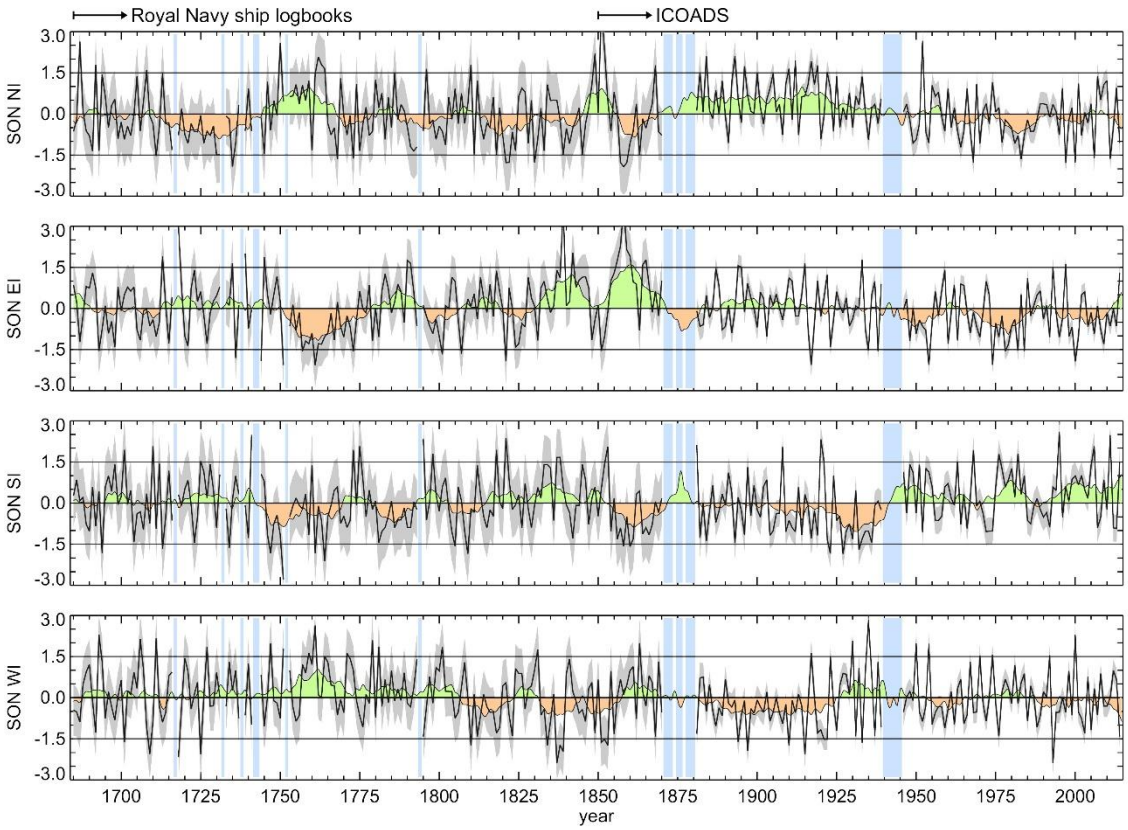

Figure A4. As Figure 4.8 but for autumn (September-to-November, SON)

Table A1. Assessment of the temperature conditions for each winter of the LMM. Columns indicate the evidence found for each winter, including the temporal resolution, the affected region and the description provided by the bibliography. The sources are represented by 1 (2) if they are based on historical (multiproxy) evidences. The last column classifies all winters in four groups: G1 (dynamically cold winters cataloged as cold in other studies); G2 (dynamically cold winters that have not been documented in the literature or whose evidence of cold conditions is spatially and temporally restricted); G3 (dynamically mild winters that have been either undocumented or reported as mild in the literature); G4 (dynamically mild winters that have been described as cold in the literature).

Year	Scale	Description	Region	Source	Bibliography	Assessment
1685	Seasonal	Cold	Italy	1	Camuffo and Enzi (1994)	G1
	Seasonal	Cold and dry	London	1	Kington (2010)	
	Seasonal	Severest winter in the thermometer. Cold	Switzerland, North Europe and England.	1	Lam (1982)	
	Seasonal	2.7ºC	Midlands region in England	1	Manley (1974)	
	Seasonal	Very cold	Switzerland	1	Pfister (1992)	
	Seasonal	Very cold	Hungary	1	Rácz (1994)	
	Seasonal	1.2ºC	Netherlands	1	Van den Dool et al. 1978	
	Seasonal	Very cold. Location of 'blocking' anticyclones close to the British Isles.	Europe	1	Wheeler et al. 2010	
	Seasonal	Great northerly and easterly winds. Inferred cold	Europe	1	Wheeler et al. 2010	
	Seasonal	Cold	Greece	2	Xoplaki et al. 2001	
Year	Scale	Description	Region	Source	Bibliography	Assessment
1686	Seasonal	Mild	London	1	Kington (2010)	G3
	Seasonal	Mild winter	England	1	Lamb (1982)	
	Seasonal	Warm	Over wide parts of Europe	2	Luterbacher et al 2001	
	Seasonal	6.3ºC	Midlands region in England	1	Manley (1974)	
	Seasonal	Mild	Switzerland	1	Pfister (1992)	

	Seasonal	4.2ºC	Netherlands	1	Van den Dool et al. 1978	
Year	Scale	Description	Region	Source	Bibliography	Assessment
1687	Seasonal	Mild	London	1	Kington (2010)	G1
	Seasonal	4.7ºC	Midlands region in England	1	Manley (1974)	
	Seasonal	This winter was severe to a degree that had not been seen in a very long time. For fifty days, the roads were closed and people could not go outside. (cold and snow)	Istanbul	1	Parke (2013)	
	Seasonal	Very cold	Switzerland	1	Pfister (1992)	
	Seasonal	Cold	Hungary	1	Rácz (1994)	
	Seasonal	2.2ºC	Netherlands	1	Van den Dool et al. 1978	
	Seasonal	Experienced severe cold and heavy snow	Greece	1	Xoplaki et al.2001	
Year	Scale	Description	Region	Source	Bibliography	Assessment
1688	Seasonal	Cold	Portugal	1	Alcoforado et al. (2000)	G1
	Seasonal	Cold	Iberia	1	Alcoforado et al. 2000	
	Annual	Very cold	Europe	1	Casty et al.2005	
	Seasonal	Normal temperatures	London	1	Kington (2010)	
	Seasonal	3.7ºC	Midlands region in England	1	Manley (1974)	
	Seasonal	Cold	Switzerland	1	Pfister (1992)	
	Seasonal	1.5ºC	Netherlands	1	Van den Dool et al. 1978	
Year	Scale	Description	Region	Source	Bibliography	Assessment
1689	Seasonal	Very cold	London	1	Kington (2010)	G2

	Seasonal	2.7ºC	Midlands region in England	1	Manley (1974)	
	Seasonal	Normal temperatures	Switzerland	1	Pfister (1992)	
	Seasonal	Cold	Hungary	1	Rácz (1994)	
	Seasonal	1ºC	Netherlands	1	Van den Dool et al. 1978	
Year	Scale	Description	Region	Source	Bibliography	Assessment
1690	Seasonal	Mild	London	1	Kington (2010)	G3
	Seasonal	4.3ºC	Midlands region in England	1	Manley (1974)	
	Seasonal	Mild	Switzerland	1	Pfister (1992)	
	Seasonal	2.4ºC	Netherlands	1	Van den Dool et al. 1978	
Year	Scale	Description	Region	Source	Bibliography	Assessment
1691	Seasonal	Cold	Italy	1	Camuffo and Enzi (1994)	G1
	Seasonal	Cold	Alps	1	Casty et al 2005	
	Seasonal	Cold	England	1	Kington (1998)	
	Seasonal	Cold and dry	London	1	Kington (2010)	
	Seasonal	2.2ºC	Midlands region in England	1	Manley (1974)	
	Seasonal	Very cold	Switzerland	1	Pfister (1992)	
	Seasonal	Cold	Hungary	1	Rácz (1994)	
	Seasonal	-1.3ºC	Netherlands	1	Van den Dool et al. 1978	
Year	Scale	Description	Region	Source	Bibliography	Assessment
1692	Annual	Temperature extremes exceeding the 2 standard deviations of the twentieth century mean.	Alps	1	Casty et al. 2005	G1
	Seasonal	Very cold winter	London	1	Kington (2010)	

	Seasonal	Cold. (with mean temperature below + 3°C (December, January and February) in central England)	England	1	Lamb (1977)	
	Seasonal	1.8ºC	Midlands region in England	1	Manley (1974)	
	Seasonal	Very cold	Switzerland	1	Pfister (1992)	
	Seasonal	Very cold	Hungary	1	Rácz (1994)	
	Seasonal	Cold	England	1	Slonosky et al 2001	
	Seasonal	-1.3ºC	Netherlands	1	Van den Dool et al. 1978	
Year	Scale	Description	Region	Source	Bibliography	Assessment
1693	Seasonal	Severe winter, Cold extreme	Iberia	1	Alcoforado et al 2000	G4
	January	Normal temperatures	Czech Republic	1	Brázdil et al. 2008	
	February	Warm	Czech Republic	1	Brázdil et al. 2008	
	Seasonal	Average winter temperatures	London	1	Kington (2010)	
	Annual	Cold	Central Europe	2	Luterbacher et al.2001	
	Seasonal	3.8ºC	Midlands region in England	1	Manley (1974)	
	Seasonal	Normal temperatures	Switzerland	1	Pfister (1992)	
	Seasonal	Slightly cold	Hungary	1	Rácz (1994)	
	Seasonal	3.3ºC	Netherlands	1	Van den Dool et al. 1978	
Year	Scale	Description	Region	Source	Bibliography	Assessment
1694	Seasonal	Cold	Portugal	1	Alcoforado et al. (2000)	G1
	Seasonal	Severe cold spells. Droughts	Iberia and central Europe	1	Alcoforado et al. 2000	
	December	Cold	Czech	1	Brázdil et	

			Republic		al.2008	
	January	Very cold	Czech Republic	1	Brázdil et al.2008	
	Seasonal	Cold	Italy	1	Camuffo and Enzi (1994)	
	Seasonal	Cold	England	1	Kington (1998)	
	Seasonal	Cold	London	1	Kington (2010)	
	Seasonal	Average temperatures over December, January and February in the seven coldest winters in central England between 1659 and 1979. (0.7C)	England	1	Lamb (1982)	
	Seasonal	2.7ºC	Midlands region in England	1	Manley (1974)	
	Seasonal	Cold	Switzerland	1	Pfister (1992)	
	Seasonal	Cold	Hungary	1	Rácz (1994)	
	Annual	Coldest year	England	1	Slonosky et al. 2001	
	Seasonal	1.9ºC	Netherlands	1	Van den Dool et al. 1978	
Year	Scale	Description	Region	Source	Bibliography	Assessment
1695	January	Extremely Cold	Czech Republic	1	Brázdil et al.2008	G1
	February	Very cold	Czech Republic	1	Brázdil et al.2008	
	Seasonal	Temperature extremes exceeding the - 2 standard deviations of the twentieth century mean.	Alps	1	Casty et al. 2005	

	Seasonal	During the winter of 1694/95 there was frequent blocking. cold continental airstreams being advected westward over the British Isles. The severe conditions continued until spring	England	1	Kington (1995)	
	Seasonal	Cold	England	1	Kington (1998)	
	Seasonal	Very cold	London	1	Kington (2010)	
	Seasonal	Cold. (with mean temperature below + 3°C (December, January and February) in central England)	England	1	Lamb (1977)	
	Annual	Coldest year	England. Europe	1	Lamb (1982)	
	Seasonal	Coldest winter in century	Western Europe	2	Lamb (1982)	
	Seasonal	Cold winter	Russia	2	Luterbacher et al. 2000	
	Seasonal	Most severe winter. Extreme coldness and dryness	Europe (especially alps)	2	Luterbacher et al. 2001	
	Seasonal	0.7ºC	Midlands region in England	1	Manley (1974)	
	Seasonal	Very cold	Switzerland	1	Pfister (1992)	
	Seasonal	Very cold	Hungary	1	Rácz (1994)	
	Seasonal	Second coldest year	England	1	Slonosky et al. 2001	
	Seasonal	-1.7ºC	Netherlands	1	Van den Dool et al. 1978	
	Seasonal	Cold	Europe	2	Wanner et al.1995	

	Seasonal	Great northerly and easterly winds. Inferred cold	Europe	1	Wheeler et al. 2010	
	Seasonal	Dry period	Balkans	2	Xoplaki et al .2001	
Year	Scale	Description	Region	Source	Bibliography	Assessment
1696	December	Cold	Czech Republic	1	Brázdil et al.2008	G3
	January	Warm	Czech Republic	1	Brázdil et al.2008	
	February	Very warm	Czech Republic	1	Brázdil et al.2008	
	December	Cold	London	1	Kington (2010)	
	January	Mild and wet	London	1	Kington (2010)	
	February	Mild and wet	London	1	Kington (2010)	
	Seasonal	4.7ºC	Midlands region in England	1	Manley (1974)	
	Seasonal	Mild	Switzerland	1	Pfister (1992)	
	Seasonal	2.8ºC	Netherlands	1	Van den Dool et al. 1978	
Year	Scale	Description	Region	Source	Bibliography	Assessment
1697	Seasonal	Slightly cold	Portugal	1	Alcoforado et al. (2000)	G1
	December	Very cold	Czech Republic	1	Brázdil et al.2008	
	January	Very cold	Czech Republic	1	Brázdil et al.2008	
	February	Cold	Czech Republic	1	Brázdil et al.2008	
	Seasonal	Temperature extremes exceeding the -2 standard deviations of the twentieth century mean.	Alps	1	Casty et al. 2005	
	Seasonal	Cold	England	1	Kington (1997)	
	Seasonal	Very cold	London	1	Kington (2010)	
	Seasonal	Cold	Russia	2	Luterbacher et al. 2000	

	Seasonal	1.3ºC	Midlands region in England	1	Manley (1974)	
	Seasonal	Very cold	Switzerland	1	Pfister (1992)	
	Seasonal	Cold	Hungary	1	Rácz (1994)	
	Seasonal	-2.5ºC	Netherlands	1	Van den Dool et al. 1978	
	Seasonal	Great northerly and easterly winds. Inferred cold	Europe	1	Wheeler et al. 2010	
Year	Scale	Description	Region	Source	Bibliography	Assessment
1698	December	Cold	Czech Republic	1	Brázdil et al.2008	G1
	January	Very cold	Czech Republic	1	Brázdil et al.2008	
	February	Cold	Czech Republic	1	Brázdil et al.2008	
	Annual	Cold	Alps	1	Casty et al. 2005	
	Seasonal	Cold	England	1	Kington (1998)	
	Seasonal	Very cold	London	1	Kington (2010)	
	Seasonal	Cold. (with mean temperature below + 3°C (December, January and February) in central England)	England	1	Lamb (1982)	
	Annual	Cold	Europe	2	Luterbacher et al. 2001	
	Seasonal	1ºC	Midlands region in England	1	Manley (1974)	
	Seasonal	Cold	Switzerland	1	Pfister (1992)	
	Seasonal	Very cold	Hungary	1	Rácz (1994)	
	Seasonal	-1.5ºC	Netherlands	1	Van den Dool et al. 1978	
	Seasonal	Great northerly and easterly winds. Inferred cold	Europe	1	Wheeler et al. 2010	

Year	Scale	Description	Region	Source	Bibliography	Assessment
1699	Seasonal	Warm	Portugal	1	Alcoforado et al. (2000)	G3
	Seasonal	Warm	Iberia	1	Alcoforado et al. 2000	
	Seasonal	Warm	Europe	1	Barriopedro et al. 2014	
	December	Normal temperatures	Czech Republic	1	Brázdil et al.2008	
	January	Very warm	Czech Republic	1	Brázdil et al.2008	
	February	Very cold	Czech Republic	1	Brázdil et al.2008	
	Seasonal	Cold	Italy	1	Camuffo and Enzi (1994)	
	Seasonal	First half cold and wet and second warm and dry	London	1	Kington (2010)	
	Seasonal	Warm	England	2	Luterbacher et al. 2000	
	Seasonal	3.4ºC	Midlands region in England	1	Manley (1974)	
	Seasonal	Normal temperatures	Switzerland	1	Pfister (1992)	
	Seasonal	Mild winter	Europe	1	Slonosky et al. 2001	
	Seasonal	4.2ºC	Netherlands	1	Van den Dool et al. 1978	
Year	Scale	Description	Region	Source	Bibliography	Assessment
1700	Seasonal	Very cold	Bohemia and Moravia	1	Brázdil et al 1994	G4
	January	Cold	Czech Republic	1	Brázdil et al.2008	
	February	Cold	Czech Republic	1	Brázdil et al.2008	
	Seasonal	Mild	London	1	Kington (2010)	
	Seasonal	3.3ºC	Midlands region in England	1	Manley (1974)	
	Seasonal	Normal	Switzerland	1	Pfister (1992)	

		temperatures				
	Seasonal	Very cold	Hungary	1	Rácz (1999)	
	Seasonal	4.2ºC	Netherlands	1	Van den Dool et al. 1978	
	Seasonal	Very cold, with continuous snowfall that lasted more than two months.	Balkans and Greece	1	Xoplaki et al. 2001	
Year	Scale	Description	Region	Source	Bibliography	Assessment
1701	Seasonal	Slightly cold	Portugal	1	Alcoforado et al. 2000	G3
	Seasonal	Mild	Russia	1	Borisenkov (1994)	
	January	Normal temperatures	Czech Republic	1	Brázdil et al.2008	
	February	Normal temperatures	Czech Republic	1	Brázdil et al.2008	
	Seasonal	Averages winter temperatures	London	1	Kington (2010)	
	Seasonal	3.2ºC	Midlands region in England	1	Manley (1974)	
	Seasonal	Mild	Switzerland	1	Pfister (1992)	
	Seasonal	Very cold	Hungary	1	Rácz (1994)	
	Seasonal	3.2ºC	Netherlands	1	Van den Dool et al. 1978	
Year	Scale	Description	Region	Source	Bibliography	Assessment
1702	Seasonal	Slightly cold	Portugal	1	Alcoforado et al. 2000	G3
	Seasonal	Mild	Russia	1	Borisenkov (1994)	
	Seasonal	Warm	Italy	1	Camuffo and Enzi (1994)	
	Seasonal	Mild wet	London	1	Kington (2010)	
	Seasonal	5.2ºC	Midlands region in England	1	Manley (1974)	
	Seasonal	Mild	Switzerland	1	Pfister (1992)	
	Seasonal	Warm	Hungary	1	Rácz (1994)	
	Seasonal	3.8ºC	Netherlands	1	Van den Dool et al. 1978	

Year	Scale	Description	Region	Source	Bibliography	Assessment
1703	January	Snowfall	Lisbon	1	Alcoforado et al. 2000	G3
	Seasonal	Normal temperatures. Drought	Russia	1	Borisenkov (1994)	
	Seasonal	Very mild winter, wet	London	1	Kington (2010)	
	Seasonal	3.5ºC	Midlands region in England	1	Manley (1974)	
	Seasonal	Normal temperatures	Switzerland	1	Pfister (1992)	
	Seasonal	3.1ºC	Netherlands	1	Van den Dool et al. 1978	
Year	Scale	Description	Region	Source	Bibliography	Assessment
1704	January	Snowfall	Lisbon	1	Alcoforado et al. 2000	G2
	Seasonal	Average winter temperatures	London	1	Kington (2010)	
	Seasonal	3.5ºC	Midlands region in England	1	Manley (1974)	
	Seasonal	Cold	Switzerland	1	Pfister (1992)	
	Seasonal	Cold	Hungary	1	Rácz (1994)	
	Seasonal	2.6ºC	Netherlands	1	Van den Dool et al. 1978	
Year	Scale	Description	Region	Source	Bibliography	Assessment
1705	Seasonal	Cold and dry	London	1	Kington (2010)	G2
	Seasonal	3.4ºC	Midlands region in England	1	Manley (1974)	
	Seasonal	Very Cold	Switzerland	1	Pfister (1992)	
	Seasonal	Very Cold	Hungary	1	Rácz (1994)	
	Seasonal	3ºC	Netherlands	1	Van den Dool et al. 1978	
Year	Scale	Description	Region	Source	Bibliography	Assessment
1706	Seasonal	Mainly mild	London	1	Kington (2010)	G3
	Seasonal	3.8ºC	Midlands region in England	1	Manley (1974)	

	Seasonal	2.3ºC	Netherlands	1	Van den Dool et al. 1978	
Year	Scale	Description	Region	Source	Bibliography	Assessment
1707	Seasonal	Mild winter	Iberia	1	Alcoforado et al. 2000	G3
	Seasonal	Average winter temperatures	London	1	Kington (2010)	
	Seasonal	3.7ºC	Midlands region in England	1	Manley (1974)	
	Seasonal	3.3ºC	Netherlands	1	Van den Dool et al. 1978	
Year	Scale	Description	Region	Source	Bibliography	Assessment
1708	Seasonal	Mild wet	London	1	Kington (2010)	G3
	Seasonal	4.5ºC	Midlands region in England	1	Manley (1974)	
	Annual	Cold year	Upminster (England)	1	Slonosky et al. 2001	
	Seasonal	2.3ºC	Netherlands	1	Van den Dool et al. 1978	
Year	Scale	Description	Region	Source	Bibliography	Assessment
1709	Seasonal	Cold.Temperature extremes exceeding the 2 standard deviations of the twentieth century mean.	Alps	1	Casty et al. 2005	G4*
	Seasonal	Very cold and wet	London	1	Kington (2010)	
	Seasonal	Cold	Europe (Especially alps)	2	Luterbacher et al. 2000	
	Annual	Extremely cold	Russia	2	Luterbacher et al. 2000	
	Seasonal	Coldest winter since 1500	Europe	2	Luterbacher et al. 2004	
	Seasonal	1.2ºC	Midlands region in England	1	Manley (1974)	
	Seasonal	Cold	France	1	Maraldi (1710)	

	Seasonal	Cold	France	1	Monahan (1993)	
	December	Mild	London	1	Slonosky et al. 2001	
	Seasonal	Cold	England	1	Slonosky et al. 2001	
	Seasonal	-2.3ºC	Netherlands	1	Van den Dool et al. 1978	
	Seasonal	Severe cold	Serbia	1	Xoplaki et al. 2001	
Year	Scale	Description	Region	Source	Bibliography	Assessment
1710	Seasonal	Average winter temperatures	London	1	Kington (2010)	G2
	Seasonal	3.2ºC	Midlands region in England	1	Manley (1974)	
	Seasonal	2.7ºC	Netherlands	1	Van den Dool et al. 1978	
Year	Scale	Description	Region	Source	Bibliography	Assessment
1711	Seasonal	Very mild winter	London	1	Kington (2010)	G3
	Seasonal	4.8ºC	Midlands region in England	1	Manley (1974)	
	Seasonal	2.8ºC	Netherlands	1	Van den Dool et al. 1978	
Year	Scale	Description	Region	Source	Bibliography	Assessment
1712	Seasonal	Mild and dry	London	1	Kington (2010)	G3
	Seasonal	3.8ºC	Midlands region in England	1	Manley (1974)	
	Seasonal	2.4ºC	Netherlands	1	Van den Dool et al. 1978	
Year	Scale	Description	Region	Source	Bibliography	Assessment
1713	Seasonal	Mild wet	London	1	Kington (2010)	G3
	Seasonal	4.2ºC	Midlands region in England	1	Manley (1974)	
	Seasonal	1.4ºC	Netherlands	1	Van den Dool et al. 1978	
Year	Scale	Description	Region	Source	Bibliography	Assessment
1714	Seasonal	Cold and dry	London	1	Kington (2010)	G2

	Seasonal	4.5ºC	Midlands region in England	1	Manley (1974)	
	Seasonal	1.8ºC	Netherlands	1	Van den Dool et al. 1978	
	Seasonal	Cold	Serbia and northern Greece	2	Xoplaki et al. 2001	
Year	Scale	Description	Region	Source	Bibliography	Assessment
1715	Seasonal	Mild	London	1	Kington (2010)	G2
	Seasonal	4.3ºC	Midlands region in England	1	Manley (1974)	
	Seasonal	2.8ºC	Netherlands	1	Van den Dool et al. 1978	

*There was a 10-day missing period of wind observations coinciding with an extreme cold spell and hence the dynamical classification of this winter should be taken with caution.